STRENGTH OF THE EPOXY BONDED STEEL CONNECTION IN GLUE LAMINATED TIMBER

A thesis
submitted in partial fulfilment
of the requirements for the Degree
of
Doctor of Philosophy in Civil Engineering
at the
University of Canterbury

by

Xixian Deng

University of Canterbury
Christchurch
New Zealand

1996

To My Dear Wife Yan Feng

TABLE OF CONTENTS

ABSTRACT xi

ACKNOWLEDGEMENTS xiii

NOTATION xv

CHAPTER ONE

INTRODUCTION 1

1.1 BACKGROUND 1
1.2 OBJECTIVES 2
1.3 STUDY DESIGN 2

CHAPTER TWO

LITERATURE REVIEW 5

2.1 VARIOUS CONNECTIONS IN TIMBER STRUCTURES 5
2.2 ADHESIVE BONDED STEEL CONNECTIONS IN TIMBER STRUCTURE 7
2.3 APPLICATION OF ADHESIVE BONDED STEEL CONNECTIONS 8
2.4 PREVIOUS STUDIES OF ADHESIVE BONDED STEEL CONNECTIONS 13
2.4.1 Strength Properties of the Connection 13
2.4.2 Fire Resistance 19
2.4.3 Load Duration and Environment Effects 19
2.5 BRIEF REVIEW OF ADHESION THEORY 20
2.6 ADHESIVES AND ADHESIVE BONDING 21
2.6.1 Basic Characteristics of Epoxy Resin Adhesives 22
2.6.2 Epoxy Bonding to the Wood 23
2.7 CHARACTERISTICS OF WOOD AS AN ADHEREND RELATED TO ADHESIVE BONDING 25
2.7.1 Surface Roughness 25
2.7.2 Time Dependent Behaviour 26
2.7.3 Environmental Effects 28
2.8 APPLICATIONS OF ANALYTICAL TOOLS 30
2.9 SUMMARY 30

CHAPTER THREE

SHORT DURATION EXPERIMENTS 33

3.1 OBJECTIVES AND SCOPE 33
3.2 DESIGN OF THE EXPERIMENTS 34
3.2.1 Design Principles 34
3.2.2 Factors Influencing the Strength of the Connection 34
3.2.3 General Considerations 35
3.2.4 Design of Experiment One 36
3.2.5 Design of Experiment Two 38
3.2.6 Design of Experiment Four 38
3.3 MATERIALS 39
3.3.1 Timber 39
3.3.2 Epoxy 40
3.3.3 Steel Rods 42
3.4 SPECIMEN PREPARATION 43
3.4.1 Cutting Scheme of Glulam Timber 43
3.4.2 Steel Rod Placement 48
3.4.3 Epoxy Injection Procedure 49
3.5 TESTING EQUIPMENT AND INSTRUMENTATION 49
3.5.1 Loading System 49
3.5.2 Data Acquisition System 49
3.5.3 Tensile Load Measurement 50
3.5.4 Measurement of Displacement 50
3.5.5 Software 50
3.6 DRY AND WET CYCLING ENVIRONMENT 51
3.7 EXPERIMENT PROCEDURE 53
3.8 RESULTS OF THE SHORT DURATION EXPERIMENTS 54
3.8.1 Experiment One 54
3.8.2 Experiment Two 55
3.8.3 Experiment Four 55

CHAPTER FOUR

ANALYSIS OF SHORT DURATION EXPERIMENTS 63

4.1 FAILURE MODES 63
4.1.1 Definitions and Descriptions 63
4.1.2 Distribution of Failure Modes in the Experiments 67
4.1.3 Analysis of Failure Modes 70

4.2 INFLUENCE FACTORS 73
4.2.1 Environmental Effects 73
4.2.2 Effect of Steel Rod Surface Geometry 74
4.2.3. Effects from Using Different Epoxies 75
4.2.4 Effect of Different Embedment Length 77
4.2.5 Effect of Different Bar Diameters 81
4.2.6 Effect of Edge Distance 84
4.2.7 Effect of Different Hole Diameters 86
4.2.8 Effect of Connection Reinforcement 87
4.3 AN EMPIRICAL MODEL 88
4.4 ESTIMATION OF THE EMPIRICAL MODEL 92
4.4.1 Comparison of the Short Duration Experiment Result and the Model Prediction 92
4.4.2 Application to Multiple Bar Connections 95
4.4.3 Comparison of the Empirical Model with the European Formula 97
4.5 DISCUSSION AND CONCLUSIONS 100

CHAPTER FIVE

STRESS DISTRIBUTION IN THE CONNECTION: THEORETICAL MODEL 103

5.1 BACKGROUND 103
5.2 OBJECTIVES AND SCOPE 104
5.3 FINITE ELEMENT MODEL 105
5.3.1 Parameters of the Model 105
5.3.2 Basic Assumptions and Material Properties 106
5.3.3 The Finite Element Model 109

CHAPTER SIX

STRESS DISTRIBUTION IN THE CONNECTION: EXPERIMENTAL VERIFICATION AND MODEL PREDICTION 115

6.1 OBJECTIVES AND SCOPE 115
6.2 DESIGN OF THE EXPERIMENT 115
6.3 MATERIALS 122
6.4 SPECIMEN PREPARATION 122
6.5 EXPERIMENTAL PROCEDURE 124
6.6 RESULTS OF THE EXPERIMENT 125
6.7 CORRELATION OF EXPERIMENTAL AND THEORETICAL RESULTS 129
6.8 STRESS DISTRIBUTION PREDICTED IN THE MODEL 135
6.8.1 Some Considerations Concerning the Stress Distribution Analysis 135

6.8.2 Simplifying Presentation 136
6.8.3 Shear Stress Distribution 138
6.8.4 Tensile Stress Distribution 138
6.8.5 Tangential Stress Distribution 139
6.8.6 The Radial Stress Distribution 141
6.9 DISCUSSION 141
6.9.1 Experimental Results and the Finite Element Model 141
6.9.2 Stress Concentrations and Failure Modes 142
6.9.3 Effect of Geometry Change to Stress Distribution 143
6.10 CONCLUSIONS 143

CHAPTER SEVEN

STRESS DISTRIBUTION IN THE CONNECTION: A PARAMETRIC STUDY 145

7.1 OBJECTIVE 145
7.2 DESIGN OF THE PARAMETRIC STUDY 145
7.2.1 The Reference Model and Parameters 145
7.2.2 Non-dimensionalized Stress 146
7.2.3 Non-dimensionalized Coordinates 147
7.3 PRESENTATION OF THE RESULTS 149
7.3.1 Scope of Presentation 149
7.3.2 Shear Stress 152
7.3.3 Tensile Stress 155
7.3.4 Transverse Stress 162
7.4 DISCUSSION AND CONCLUSION 169
7.4.1 Discussion on the Shear Stress 169
7.4.2 Discussion on the Tensile Stress 170
7.4.3 Discussion on the Transverse Stress 170
7.4.4 General Discussions 170
7.4.5 Concluding Remarks 171

CHAPTER EIGHT

LONG DURATION LOAD AND ENVIRONMENT EFFECTS 173

8.1 INTRODUCTION 173
8.2 OBJECTIVES AND SCOPE 173
8.3 TEST PROGRAMME OF EXPERIMENT THREE 174
8.3.1 Design of the Experiment 174
8.3.2 Materials 176

8.3.3 Construction of Loading Frames 176
8.3.4 Testing Sites and Irrigation System 180
8.3.5 Instrumentation 182
8.3.6 Specimen Preparation 185
8.3.7 Experiment Set-up 187
8.3.8 Experimental Procedure 187
8.4 RESULTS OF EXPERIMENT THREE 189
8.4.1 Moisture Content Fluctuations 189
8.4.2 Sustained Tensile Load in the Specimens 190
8.4.3 Failed Specimens and Failure Mode 191
8.4.4 Typical Results Among Different Environmental Conditions 194
8.4.5 Typical Results Under Two Different Load Levels 198
8.5 MEASUREMENT OF MOISTURE CONTENT AND SHRINKAGE IN SITU 199
8.5.1 Test Programme 199
8.5.2 Measurement Set-up and Procedure 206
8.6 RESULTS OF MOISTURE CONTENT AND SHRINKAGE MEASUREMENT 206
8.7 DISCUSSION 211
8.7.1 Discussion of Experiment Three 211
8.7.2 Discussion of Moisture and Shrinkage of Glulam Timber 216
8.8 CONCLUSIONS 218

CHAPTER NINE

SUMMARY, CONCLUSIONS AND RECOMMENDATIONS 219

9.1 SUMMARY OF THE RESEARCH 219
9.2 CONCLUSIONS 220
9.2.1 Strength and Failure Characteristics of the Connection Subjected to Short Duration Tensile Load 220
9.2.2 Strength and Failure Characteristics of the Connection Subjected to Long Duration Tensile Load 221
9.2.3 The Theoretical Model 222
9.2.4 The Parametric Studies 223
9.3 RECOMMENDATIONS FOR FURTHER STUDY 224
9.3.1 Further Experimental Studies 224
9.3.2 Further Theoretical Studies 225

REFERENCES 227

APPENDICES 239

ABSTRACT

In New Zealand, there has been little use of epoxy bonded steel connections in the timber construction industry due to the lack of knowledge and experiences about the performance. A research was carried out both experimentally and theoretically to study the epoxy bonded steel connections in glue laminated timber. This research provides a better understanding of the mechanical and physical properties of such connections in tension, subjected to short and long duration load, with variables of embedment length, bar diameter, edge distance, hole diameter, moisture content, steel bar type and epoxy type.

In the study, five different failure modes were identified. A theoretical three dimensional model was established using a finite element method. The characteristics of the connection, the three dimensional stress distributions and the effect of the variables in the connections were studied using this model. The study shows that there is a strong correlation between the failure modes and the stress concentrations. It is possible to optimise the design of the connections by developing a better geometry.

The study also shows that the connections can be used safely in timber structures provided the moisture content of wood does not exceeding 22%.

Empirical equations were developed to predict the axial capacity of the connection in tension or compression.

ACKNOWLEDGEMENTS

I should like to thank my supervisors Dr. A.H. Buchanan and Dr. J.C.F. Walker for their invaluable advice and consistent encouragement throughout this project.

Acknowledgements are also made to the New Zealand Timber Industry Federation who funded part of this research and to Associate Professors Peter Moss and Richard Woolons who assisted the project.

My thanks to Mr. M. Stuard-Jones for his technical support and assistance in preparing the test specimens and test facilities for the experiments, also Messrs D. Macpherson, P.A. Murphy, Gavin Hill, J.H. Maley and P.F. Fuller for their helpful technical assistance particularly during the preparation of the specimens, the long duration experiment test frames and the test facilities.

My thanks also to Mr G.E. Hill for his excellent technical support and to Mr. R.N. Allen for his willing assistance in workshop and the test site setup for the long duration experiment. Thanks are also due to Messrs M. Griffin, P.J. Coursey, S. Cockburn and B. Hutchinson for their support with the computer facilities.

A grateful acknowledgement is made to NUPLEX Industries Ltd of Auckland and Adhesive Technologies Ltd of Auckland for their generous donation of epoxy resins.

I would also like thank my fellow postgraduate students: Dr. J.I. Restrepo-Posada, Mr. R.H. Fairweather, Mr W. Munro, Ms S Gaskin, Mr. G. Thomas, Mr X.R. Li and Mr. B. Li for their friendship, enthusiasm and the many helpful comments made during the course of discussions on my project.

Finally, a special acknowledgement is given to my wife for her continuous support, encouragement, love and patience during the entire period of this research.

NOTATION

a = short edge of the cross-section of the specimen (mm)

A = cross-section area of the specimen (mm^2)

A_s = cross section area of the steel rod (mm^2)

A_w = net area of wood cross section (mm^2)

b = long edge of the cross-section of the specimen (mm)

d = nominal steel rod diameter (mm)

d_h = inner end hole diameter of the steel rod (mm)

d_r = diameter of the steel rod for transverse reinforcement in the connection (mm)

d_s = diameter of the circumference where the strain gauges are located (mm)

$d\alpha/dt$ = time rate of damage accumulation

e = edge distance of the specimen measured from the centre of the steel rod (mm)

E = modulus of elasticity of material (GPa)

E_a = modulus of elasticity of the epoxy (GPa)

E_L = modulus of elasticity of glulam timber in longitudinal direction (GPa)

E_R = modulus of elasticity of glulam timber in radial direction (GPa)

E_s = modulus of elasticity of the steel (GPa)

E_T = modulus of elasticity of glulam timber in tangential direction (GPa)

E_w = modulus of elasticity of the wood (GPa)

f = general function defining the cumulative damage function

F = pullout force in the short duration experiments - ultimate tensile load (kN)

f_t = characteristic tensile strength of glulam timber (MPa)

f_y = characteristic yield strength of steel (MPa)

G = shear modulus (GPa)

G_{LR} = modulus of rigidity in glulam timber at the associated plane (GPa)

G_{LT} = modulus of rigidity in glulam timber at the associated plane(GPa)

G_{RT} = modulus of rigidity in glulam timber at the associated plane(GPa)

h = embedment hole diameter (mm)

h_r = hole diameter of the transverse reinforcement in the connection (mm)

K = constant

k_b = bar type factor

k_e = epoxy type factor

k_m = moisture influence factor

k_w = stress concentration factor

k_1 = duration of load factor in NZS3603:1993

l = embedment length of the specimen (mm)

L = length of the glulam timber in the specimen (mm)

L_f = length of loading frame for Experiment Three (mm)

l_h = depth of the hole at the inner end of the steel rod (mm)

l_m = distance between two inner embedment ends (mm)

l_s = embedment length at the support end of the specimen (mm)

l_t = embedment length at the test end of the specimen (mm)

M = moisture content (%)

n = number of steel rod

n_1 = number of the observations in the first sample of the experiment

n_2 = number of the observations in the second sample of the experiment

N^* = design axial force produced by the strength limit state design loads (N)

P = applied tensile force in the finite element model (N)

P_s = sustained tensile load in long duration test (kN)

Q_n = norminal axial strength of the connection

R = equivalent radius of the cross-section of the finite element model (mm)

r^2 = coefficient of simple determination ($0 \leq r^2 \leq 1$)

r_e = ratio of the edge distance to steel rod diameter

r_h = ratio of the embedment hole diameter to steel rod diameter

RH = average relative humidity

r_{ss} = stress ratio in steel

r_{sw} = stress ratio in wood

s_1^2 = standard deviation of the observations in the first sample

s_2^2 = standard deviation of the observations in the second sample

t = a certain time period

T = average temperature

t_e = epoxy thickness (mm)

u_x = displacement in the direction parallel to the x-axis of the finite element model

u_y = displacement in the direction parallel to the y-axis of the finite element model

u_z = displacement in the direction parallel to the z-axis of the finite element model

W_s = ratio of wood to steel in the cross-section of the finite element model

x = variable in the finite element model

x_1 = mean of observations in the first sample

x_2 = mean of observations in the second sample

y = variable in the finite element model

z = variable in the finite element model

α = damage parameter

γ_{LV} = surface tension at the interface of the liquid phase and vapour phase

γ_{SL} = surface tension at the interface of the solid phase and liquid phase

γ_{SV} = surface tension at the interface of the solid phase and vapour phase

ΔP = difference of tensile force over a small length Δz (N)

Δz = length of the small region between the strain gauges (mm)

ε = tensile strain

ν = Poisson's ratio

ν_{LR} = Poisson's ratio for the passive strain in radial direction and the active strain in longitudinal direction of glulam timber

ν_{LT} = Poisson's ratio for the passive strain in tangential direction and the active strain in longitudinal direction of glulam timber

ν_{RL} = Poisson's ratio for the passive strain in longitudinal direction and the active strain in radial direction of glulam timber

ν_{RT} = Poisson's ratio for the passive strain in tangential direction and the active strain in radial direction of glulam timber

ν_{TL} = Poisson's ratio for the passive strain in longitudinal direction and the active strain in tangential direction of glulam timber

ν_{TR} = Poisson's ratio for the passive strain in radial direction and the active strain in tangential direction of glulam timber

σ = stress (MPa)

σ_i = average applied stress ratio within the interval of time Δt_i

σ_{nz} = nominal tensile stress of the reference model (MPa)

σ_r = stress ratio in the damage accumulation model

σ_x = tensile stress in x direction of the model coordinate (MPa)

σ_y = tensile stress in y direction of the model coordinate (MPa)

σ_z = tensile stress in z direction of the model coordinate (MPa)

τ = average shear stress along the embedment length (MPa)

τ_{nyz} = nominal shear stress of the reference model at the y-z plane of the model coordinate (MPa)

τ_{xy} = shear stress in x-y plane of the model space (MPa)

τ_{xz} = shear stress in x-z plane of the model space (MPa)

τ_{yz} = shear stress in y-z plane of the model space (MPa)

ϕ = strength reduction factor

ϕQ_n = design strength of the connection

CHAPTER ONE

INTRODUCTION

1.1 BACKGROUND

Timber building structures are widely used in many countries around the world. In New Zealand, they are not only used dominantly in residential houses but also in large industrial and commercial buildings.

In timber structures, connections play an important role in load transformation. Developing strong and reliable connections is the key to ensure the safety of structures. There are many types of connections used in timber structures. This study will focus only on the epoxy bonded steel connection.

The epoxy bonded steel connection is the connection of the timber members by placing a threaded or deformed reinforcing steel bar into predrilled holes in the timber members and bonding with epoxy resin. This connection has been used in Europe for over twenty years. In New Zealand, there has been little use of this connection in the timber construction industry; an early use was in the construction of timber classroom buildings (McIntosh, 1989). Two of recent uses include the swimming pool building (Buchanan and Fletcher, 1989) and space frame roof (NZ Journal of Timber Construction, 1986). The lack of use of the epoxy bonded steel connection in New Zealand arise out of lack of knowledge and experience about performance.

The epoxy bonded steel connection has many advantages over other types of connections: (1) the embedded steel bar with the epoxy bonding agent allows a strong connection to be made with increased stiffness of the joint; (2) the epoxy adhesive can provide a bond stronger than the timber so that the full strength of the timber can be utilised; (3) the steel components are protected from corrosion by the timber member; and (4) the structure can still retain its excellent aesthetic appeal.

The first study on the adhesive bonded steel connection in glulam timber was carried out by Riberholt in the 1970's (1986, 1988a). Although the connection has been used for quite a long time, the performance, the stress distribution, the rheological properties, the effect of load duration, environmental conditions, etc. are neither theoretically nor empirically fully understood.

1.2 OBJECTIVES

The objectives of this study are:

1. To experimentally study the mechanical and physical properties of the epoxy bonded steel connection subjected to short or long duration tensile load under different environmental conditions.

2. To study the failure modes with different load duration and environmental conditions in the experiments.

3. To develop an equation to predict the strength of the connection.

4. To establish a theoretical model of the connection using the finite element method and carry out a parametric study based on the model to better understand the connection mechanism and geometry influences.

1.3 STUDY DESIGN

In order to achieve the above objectives, the study was designed and outlined as follows:

1. Conduct experiments to understand the failure mode and tensile strength of the connection subjected to short duration tensile load.

2. Carry out a long duration experiment to understand the failure mode, the effect of load duration, rheological behaviour and environment effects of the connection.

3. Study the *in situ* shrinkage of glulam timber columns with changes in moisture content.

The experimental work includes five individual experiments and shows in Table 1.1

Table 1.1 The summary of the experiments carried out in this study

Experiment	Load Duration	Brief Description	Number of Specimens
Experiment One	short	2^7 factorial experiment to investigate the strength and failure mode of the connection, including seven parameters.	128
Experiment Two	short	3^4 factorial experiment to further study the strength and failure mode, including four parameters.	81
Experiment Three	long	The specimens are subjected to sustained tensile loading with wet-cycling or dry environmental condition to study the effect of load duration, rheological behaviour and environment effects.	48
Experiment Four	short	Study the effect of transverse reinforcement to avoid wood splitting around the connection.	8
in situ Measurement	long	Measurement of moisture content and shrinkage in glulam columns in a swimming pool building.	14

4. Analyse the results from the short duration tensile load experiments and develop an empirical equation to calculate the capacity of the connection.

5. Analyse the results of the long duration experiment.

6.. Establish a theoretical model using finite element method and verify it with the experiment.

7. Conduct a parametric study using the finite element model.

The study is described in detail in the following chapters.

CHAPTER TWO

LITERATURE REVIEW

2.1 VARIOUS CONNECTIONS IN TIMBER STRUCTURES

An understanding of the connection behaviour of structural materials, in particular timber, is of great importance. The connection is the key to the successful design of timber structures. Often, a major constraint on design can be difficulty in making good connections, especially moment resisting connections. Several standard connections are used in moment-resisting timber frame buildings, including nailed connections (nailed gusset plates made from steel or plywood or a combination of the two), bolted connections (the steel bolts by themselves or combined with tooth plates, split rings and shear plates), dowel connections, glued connections and adhesive bonded steel connections.

Nailed gusset connections are a common method for making moment-resisting joints in industrial buildings as shown in Figure 2.1(a), (b), (c) and (d). A wide range of moment resisting nailed connections have been used (Batchelar and Hunt, 1991) and the design methods are described by Walford (1989). Various nailed connections are discussed and compared in detail by Buchanan and Fairweather (1993). The connections are easy to construct, but have poor aesthetic appearance and fire resistance if they are not covered by a suitable material (Fairweather, 1992).

Using steel bolts and shear fasteners, the timber or glulam members also can be assembled to make a moment-resisting joint. A large variety of these connections exist and many have been reviewed recently by several authors (Fairweather 1992, Crews 1992, 1993).

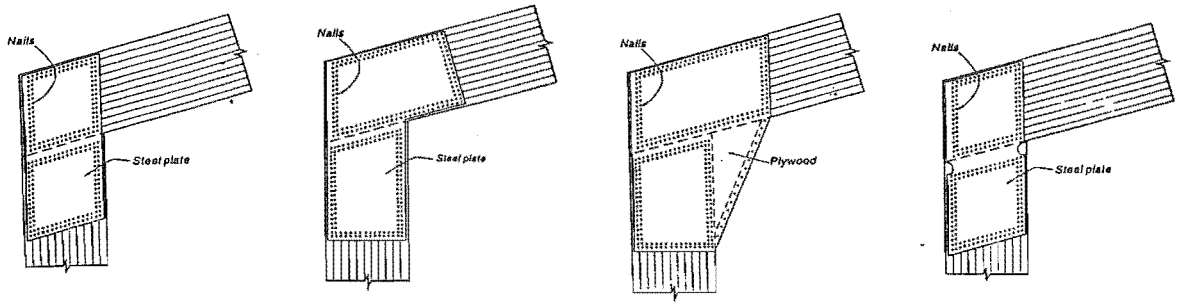

(a) (b) (c) (d)

Figure 2.1 Nailed portal frame knee joint connections (Buchanan and Fairweather, 1993)

Dowel connections as shown in Figure 2.2 are a popular type of connection in Europe. These connections are attractive and easily assembled. The tests conducted by Ceccotti and Vignoli (1988) in Italy showed excellent ductile behaviour. Similar connections with a steel plate in a central slot were tested in Japan (Komatsu et al., 1991) as shown in Figure 2.3. However, it is difficult to utilise the full strength of the members using this type of connections and problems with splitting failures in service have been reported.

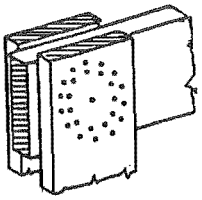

Figure 2.2 Types of dowel joints (Ceccotti and Vignoli, 1988)

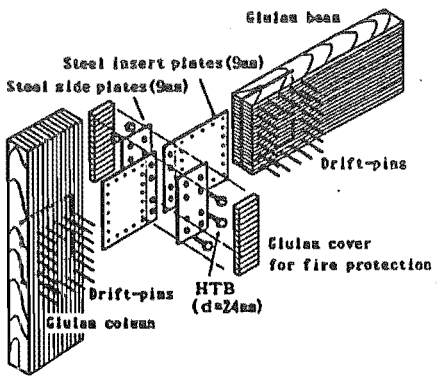

Figure 2.3 Modified moment-resisting joint (Komatsu et al. 1991)

A glued connection is one of the early methods used in timber structures (McIntosh, 1989). This kind of connection can be used to make strong rigid connections between glulam members such as the cross-lapped portal frame joint as shown in Figure 2.4 (a) and the mitred finger jointed connection in Figure 2.4 (b). The connections are widely used in Europe. They have good fire resistance and are

attractive, but require very high quality control and must be manufactured in the factory, resulting in transportation problems. The connections have poor ductility in terms of seismic design (Buchanan and Fairweather, 1993).

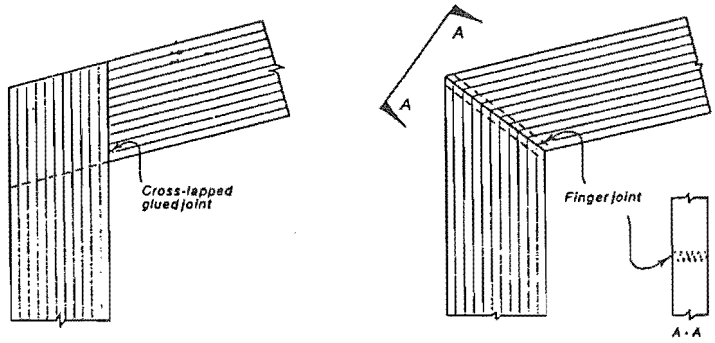

(a) (b)

Figure 2.4 Glued moment-resisting glulam connection (McIntosh, 1989)

2.2 ADHESIVE BONDED STEEL CONNECTIONS IN TIMBER STRUCTURE

A number of recently developed adhesives, now provide the opportunity for adhesive bonded steel connections in timber or glulam. In broad terms, Wake (1986) explained why and in what situations adhesive bonding should be used rather than mechanical bonding. One of the most important structural advantages is the reduction of peak stresses or stress concentrations. With proper design of adhesive joints a more uniform stress distribution throughout the structure can be achieved. However, this requires a larger bonding surface area compared to the mechanical bonding methods. A small bonding area would result in high stress value over the area which would exceed the adhesive bonding strength.

According Townsend (1990), the major advantages of using adhesive bonded steel connection can be summarised as follows:

- excellent aesthetic appearance
- ductile behaviour for seismic design

- corrosion resistance
- excellent performance and high strength

The connection can be formed by two techniques (Syme, 1987). In the first technique, a slightly undersized hole (1 to 2 mm smaller than the threaded rod diameter) is used. After half filling the hole with glue, the threaded rod is screwed into the hole leaving 10 mm clearance at the end of the hole. With this technique, the amount of the glue must be predetermined in order to allow sufficient flow to take place around the embedded portion and permit relief of hydrostatic pressure. The disadvantage is that splitting can easily occur in timber members as the threaded rod is screwed into the holes. In addition, the quality of the connection is very difficult to control because it is almost impossible to monitor whether the glue has been properly distributed. In the second technique, developed by Riberholt (1986), the rod is placed in an oversized hole (1 to 2 mm larger than the threaded rod diameter). Adhesive is injected through an "injection hole" into the embedment hole. An "air hole" at the other end of the embedment ensures that the adhesive can flow readily around the rod and completely fill the embedment hole. It is assumed that an adequate amount of glue has been injected once the glue starts being extruded from the "air hole". This technique provides much better quality control of the connection.

2.3 APPLICATION OF ADHESIVE BONDED STEEL CONNECTIONS

Initially, adhesive bonded steel connections were used mainly for the purpose of repairing damaged structures. Gopu (1981) studied the behaviour of cracked pitch cambered beams that had been repaired using epoxied radial reinforcement. The results of the test program indicate that radial tension stresses in the wood are reduced by about 45% if reinforcement is utilised, and reinforcing the broken beam can restore the original load capacity to that of the unreinforced beam. Law and Yttrup (1989) carried out a similar study on the repair of curved glulam beams as shown in Figure 2.5. The methods to repair curved beams is similar to the method described by Gopu (1981). They found that epoxy bonded bolts are stiffer and stronger than bolts alone and have no initial slip. Furthermore, the stiffness and strength of the steel bolt bonded with epoxy

increases as the epoxy thickness increases. Turkovsky (1991) reported that the use of glued-in bars for restoring delaminated beams increased the strength of members through the external reinforcement.

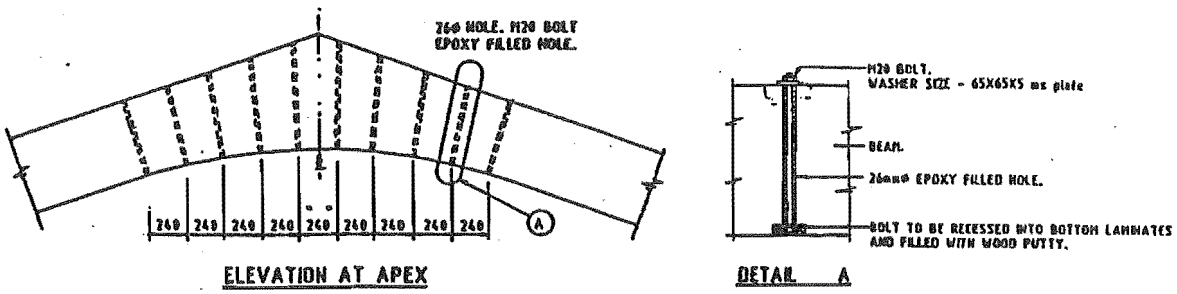

Figure 2.5 Repair of a curved glulam beam with epoxied steel dowels (Law and Yttrup, 1989)

During the 1960s, an early use of the adhesive bonded connections in New Zealand was in the construction of timber classroom buildings. A simple and robust solution, the adhesive bonded threaded steel rod beam-column connection (Figure 2.6) was used in glulam structures to meet the demand for new school buildings. The connection was formed with a 24 mm diameter threaded steel rod glued into the top of the glulam column and, through a hole in the beam. The steel rod was fastened by a nut on the top surface of the beam (McIntosh, 1989).

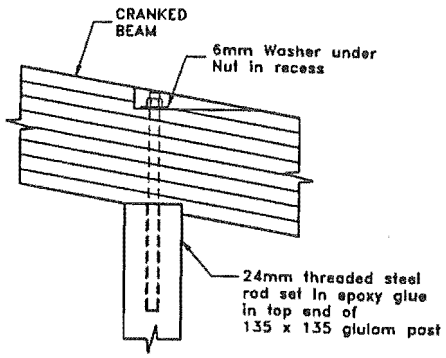

Figure 2.6 Beam-column connection used in timber classrooms (McIntosh, 1989)

Turkovsky (1991) described the Russian application of this kind of connection which has been in use since 1975. A modification was made to skew the connection at an angle to the grain of wood, so that the stress can be distributed through several laminates and gluelines, rather than concentrating the stresses in one laminate or along one glueline. The procedure to manufacture the connection is that the inclined holes were drilled 4 to 5 mm larger than the bar diameters and the epoxy cement was injected into the holes after the bars were placed into the holes. The system has been widely used in the former USSR as shown in Figure 2.7 and Figure 2.8, including a 100m continuous multispan beam in the roof of a public centre and the column-foundation connections for a 50m span sports hall.

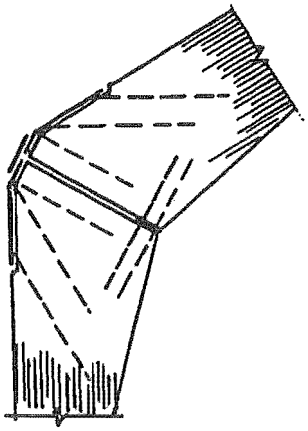

Figure 2.7 Knee joint connection (Turkovsky, 1991)

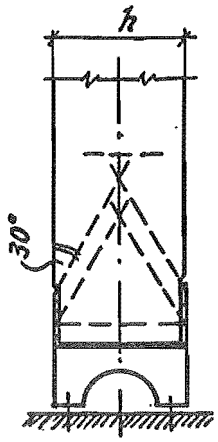

Figure 2.8 Column-foundation connection (Turkovsky, 1991)

Recent examples of application of this connection in New Zealand are described by Buchanan and Fletcher (1989) as shown in Figure 2.9 and Figures 2.10. Epoxy bonded steel connections were constructed in a sports stadium glulam structures so that the requirement of aesthetic appearance and corrosion resistance of the structures could be achieved.

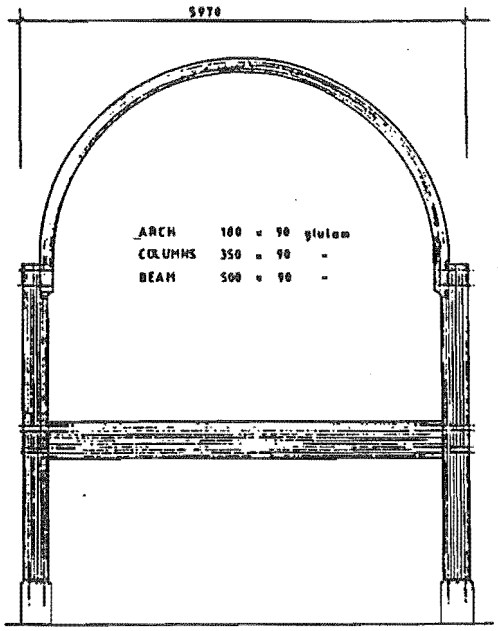

Figure 2.9 Epoxied steel connections used in the entry hall of the sports centre (Buchanan and Fletcher, 1989)

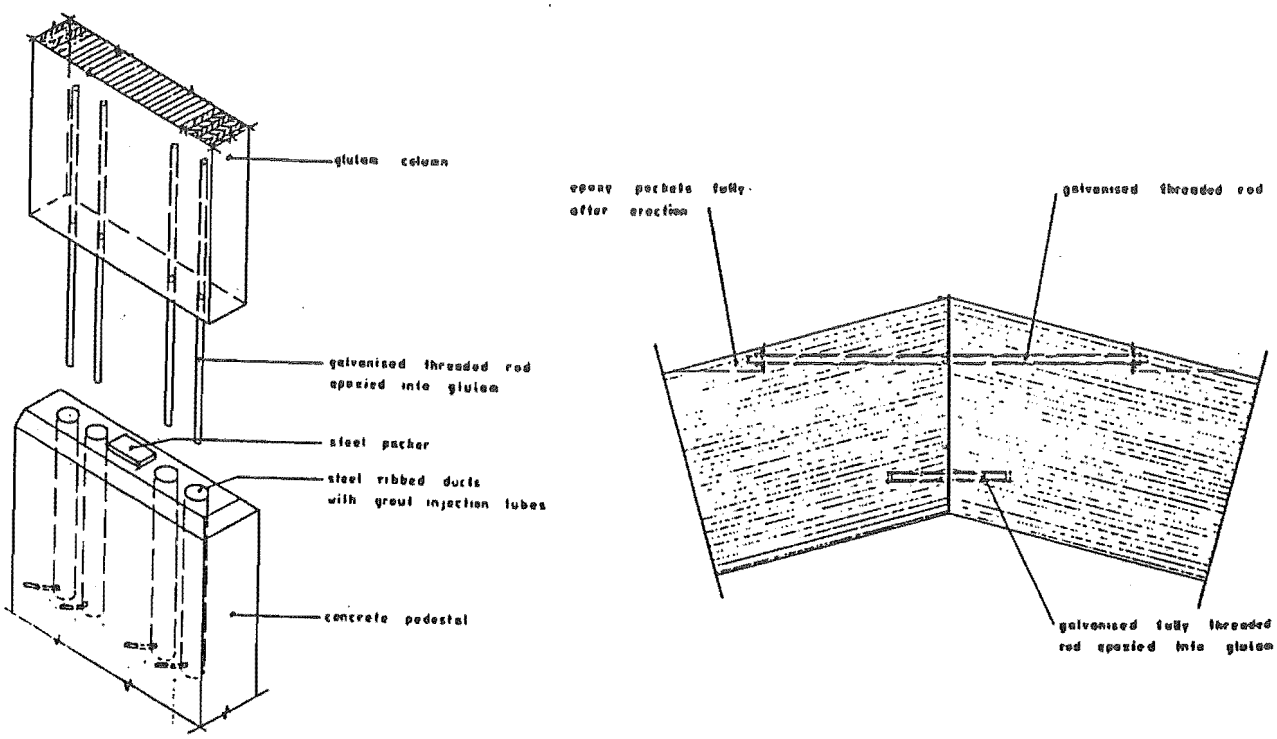

(a) Portal base connection (b) Portal apex connection

Figure 2.10 Applications of the epoxy bonded steel connections (Buchanan and Fletcher, 1989)

Similar connections have been used in Germany and summarised by Gerold (1992). In addition, equations to calculate the strength of the connection were proposed.

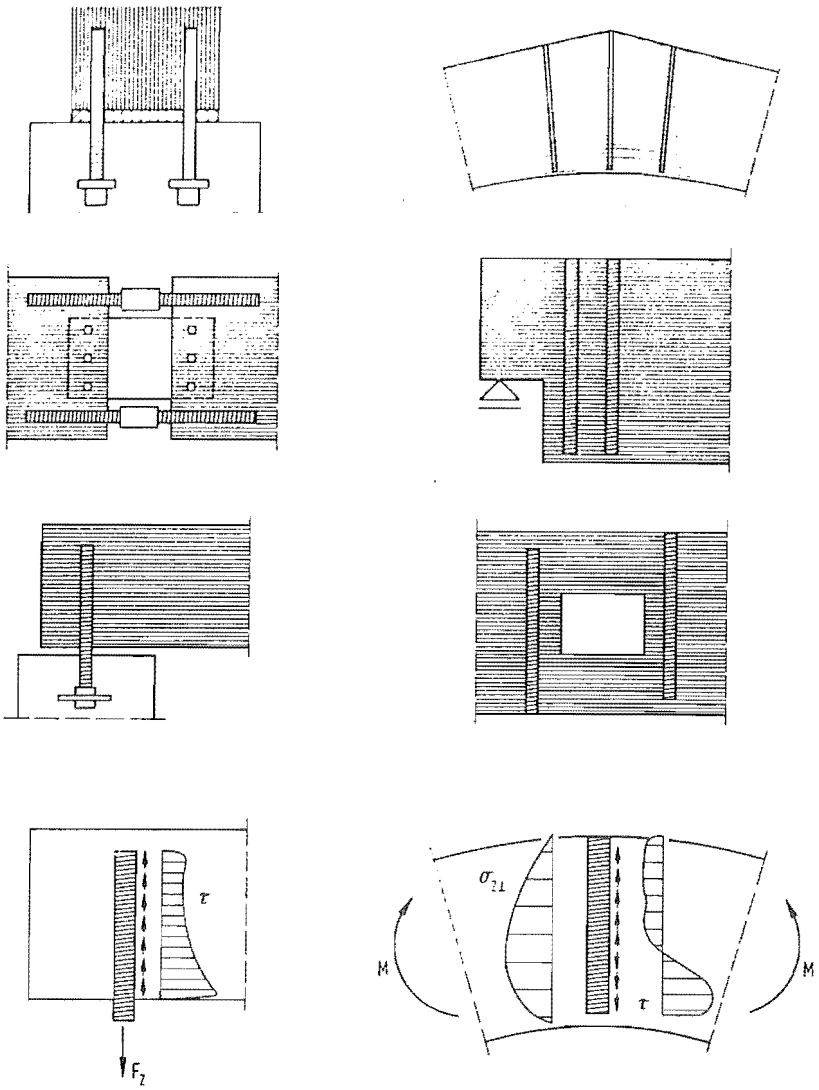

Figure 2.11 Various applications of glued-in bolts (Gerold, 1992)

Another application was in a steel reinforced glulam timber structure developed by Gardner (1989). In this application, epoxy bonded steel reinforcing rods were embedded into the upper and lower position of the beam to form a "composite" beam section (Figure 2.12). This system improved the strength and stiffness of the glulam members and reduced long duration creep.

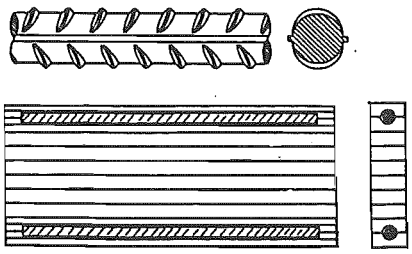

Figure 2.12 Reinforced glulam timber system (Gardner, 1989)

2.4 PREVIOUS STUDIES OF ADHESIVE BONDED STEEL CONNECTIONS

2.4.1 Strength Properties of the Connection

Riberholt (1986) studied adhesive bonded steel connections in glulam timber. His studies included axial short-duration and long-duration loading tests, lateral loading tests and some moment resisting tests. The major experiment was concentrated on axial short duration loading test. A sketch of the test specimen is shown in Figure 2.13. Four major factors were investigated, including glue type, edge distance (b/2 in Figure 2.13), embedment length (l_g) and steel rod diameter (d). Two type of glues were used, one a polyurethane glue, the other araldite AQ 139.

Riberholt found that tensile strength was higher in the connection using polyurethane glue than using araldite AW139. For different edge distance, the results showed that tension failure in the wood occurred frequently in 1.5d edge distance, but not the case for edge distance 2d and above. Riberholt then conducted a regression analysis in terms of the embedment length, wood density and steel rod diameter, and two equations were derived:

1. For two-component polyurethane and other ductile glues,

$$F_{ax,est} = 0.784\rho d\sqrt{l_g} \qquad (2.1)$$

2. For two-component epoxy, phenol-resorcinol and other brittle glues,

$$F_{ax,est} = 0.627\rho d\sqrt{l_g} \qquad (2.2)$$

Where, $F_{ax,est}$ = estimated pullout force of the connection (N)

d = the bolt diameter (mm)

l_g = the embedment length of the bolt (mm)

ρ = the density of the wood (kg/m^3)

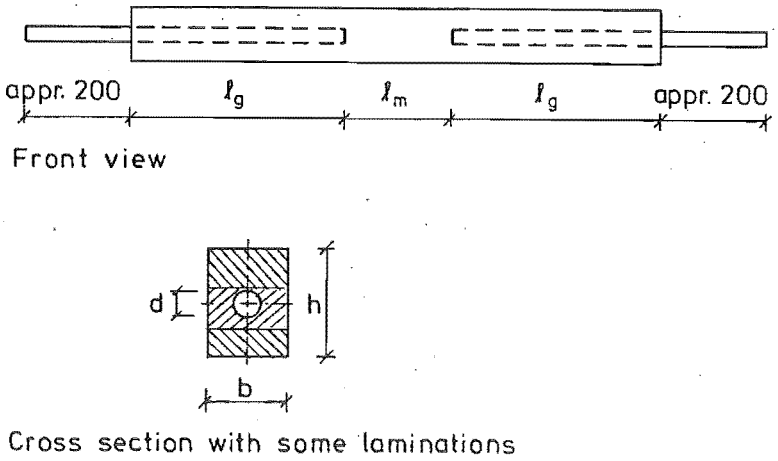

Figure 2.13 Test specimen of glued bolts in glulam (Riberholt, 1986)

Riberholt found that the equations are suitable for $l_g \geq 200$ mm. However, for shorter embedment lengths, the equations tend to overestimate the axial bolt strength. Riberholt (1988a) carried out a similar axial test for another polyurethane glue (Cascobond 1852 with hardener 1853). The test results showed that the axial strength was similar for two different polyurethane glues. Riberholt's work resulted a proposal for the CIB Code on glued bolt in glulam (Riberholt, 1988b). Two different design equations were suggested to correspond to different ranges of the embedment length. The design equations for the characteristic axial capacity in tension and compression are given by:

$$R_{ax,k} = f_{ws}\rho_k d\sqrt{l_g} \quad (l_g \geq 200 \text{ mm}) \qquad (2.3)$$

$$R_{ax,k} = f_{wl}\rho_k d\, l_g \quad (l_g < 200 \text{ mm}) \qquad (2.4)$$

where

$R_{ax,k}$ = characteristic axial capacity in tension or compression (N)

f_{ws} = strength parameter for equation 2.3 ($N/mm^{1.5}$). For brittle glues (phenol-resorcinol and epoxy), the value is 0.520. For non-brittle glues (two-component polyurethane), the value is 0.650.

f_{wl} = strength parameter for equation 2.4 (N/mm). For brittle glues, the value is 0.037. For non-brittle glues, the value is 0.046.

d = maximum of hole or bolt diameter (mm)

l_g = the embedment length of the bolt (mm)

ρ = the characteristic density of the wood (kg/m^3)

Riberholt also suggested the minimum edge distance and minimum distance between two bolts for using the equations 2.3 and 2.4. The values are shown in Figure 2.14.

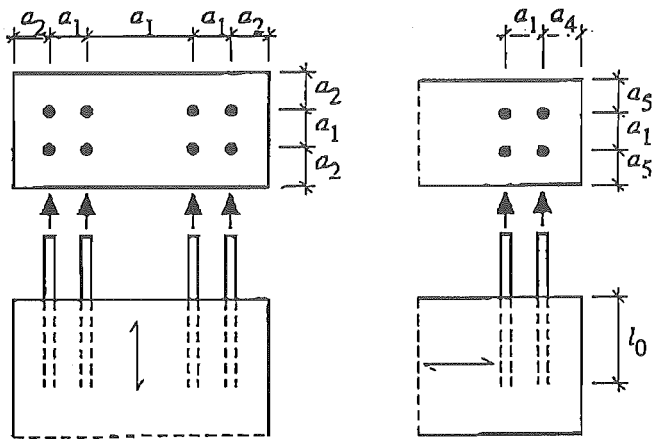

Minimum distance	
a_1	2d
a_2	1.5d
a_4	2d
a_5	2.5d

Figure 2.14 Minimum distances for axially loaded bolts (Riberholt, 1988b)

Townsend (1990) carried out a study with epoxy bonded single bar test specimens loaded parallel to the wood grain in tension. The intention of the study was to adapt the Danish technology to New Zealand conditions. Five parameters were

considered. The parameters included steel bar diameter, embedment length, edge distance, hole diameter and glue type. The pullout forces were studied and an equation was derived:

$$F = 9.2dl(r_d)^2(r_e)^{0.5} \qquad (2.5)$$

where F = average pullout force (N)

d = bar diameter (mm)

l = embedment length (mm)

r_d = ratio of hole diameter to bar diameter

r_e = ratio of edge distance to bar diameter, where the edge distance is measured from the bar centre line

This equation was deduced from the connections using deformed reinforcing bar with Araldite K-2005 epoxy. From the study, it was found that the connections using threaded rod had higher pullout strengths than deformed reinforcing bar connections. However, because only a few threaded rod connections were tested, it was difficult to quantify the difference.

Townsend (1990) also studied the mechanical properties of the full size beam with connection spliced using high strength deformed bars. The splices were either connected at mid-span or offset from the beam mid-span point. In both cases, the beams were loaded at the mid-span (Figure 2.15). It was concluded that with careful formulation and injection process, full strength splices can be achieved in straight glulam beams using deformed reinforcing bars epoxied into the glulam members.

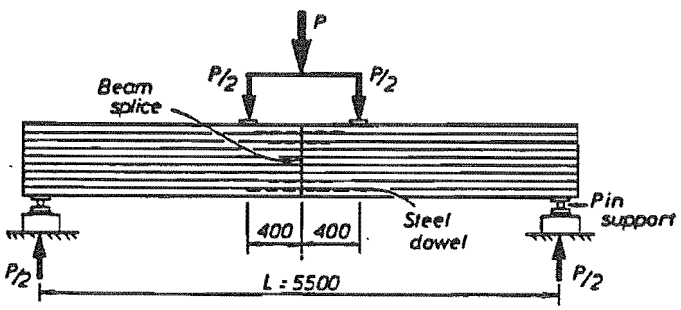

Figure 2.15 Beam splice testing (Townsend, 1990)

Gerold (1992) analysed a large number of test results and concluded that:

1. The strength of the connection loaded in tension and compression is the same.
2. Strain measurements along the glued-in bolts confirm that the shear stress distribution corresponds with the Volkersen theory (1953, see Figure 2.16).
3. The axial bolt strength to some extent depends on the wood density.
4. In general, the axial strength is somewhat higher for bolts glued-in perpendicular to the grain direction than parallel to the grain direction.

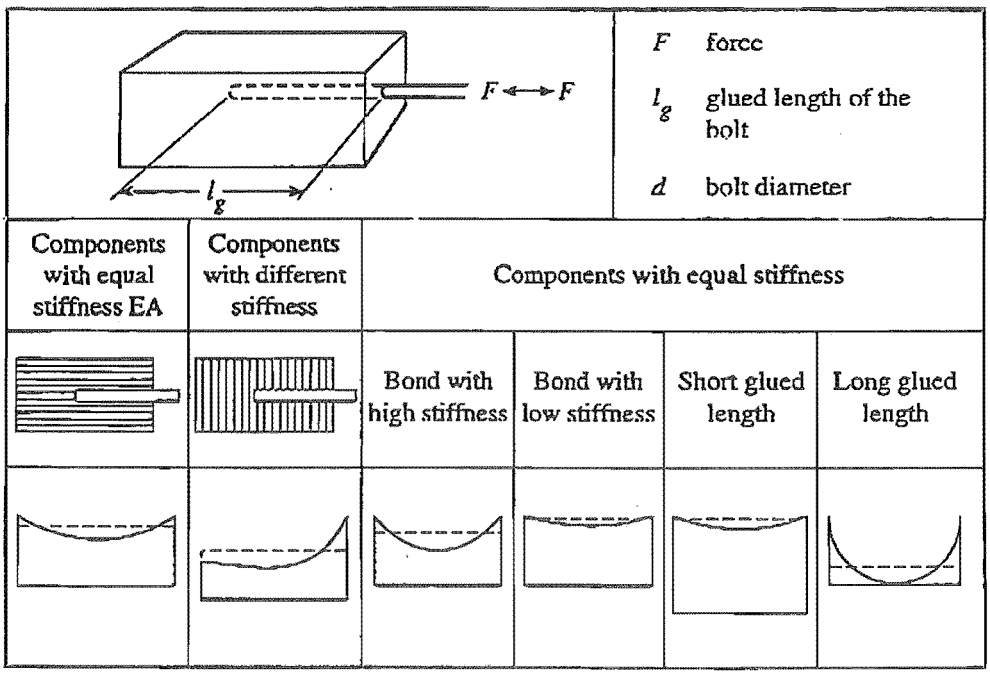

Figure 2.16 Shear stress distribution in a adhesive joint assuming linear elastic behaviour of all materials according to the Volkersen (1953) theory (Gerold 1992)

Crews (1993) carried out a research program on epoxy bonded steel connections. In the program, short duration tests of spliced connections bonded with Araldite K80 epoxy were conducted under a constant bending moment. Crews found that with Araldite K80 epoxy the pullout strength was approximately 15 percent higher than using Araldite K2005 epoxy. Based on the equation 2.5, Crews developed a modified form for the Araldite K80 epoxy:

$$F = 10.6dl(r_d)^2(r_e)^{0.5} \qquad (2.6)$$

Fairweather (1992) undertook a project to develop and improve beam-column connections using epoxy bonded steel rod for multistorey timber construction. Four different types of beam-column connections were tested as shown in Figure 2.17 (a), (b), (c) and (d). A quasi-static cyclic load in the horizontal direction was applied at the top of the column in each specimen to simulate lateral loads on a building due to wind or earthquakes. This work indicated that strong and stiff moment resisting connections can be made using epoxy bonded steel rods in a variety of different geometries. Excellent ductile behaviour can be obtained by preventing brittle fracture of wood. Fairweather also found that a single layer of bars at the column centre-line is better than two layers because there is less weakening of the column which could lead to premature failure. Based on this study, it was concluded that in order to achieve ductility in moment resisting connections between glulam members, the steel components must have sufficient ductile yielding and proper design procedure must be used to ensure no failure would occur in the wood, adhesive or other non-ductile component.

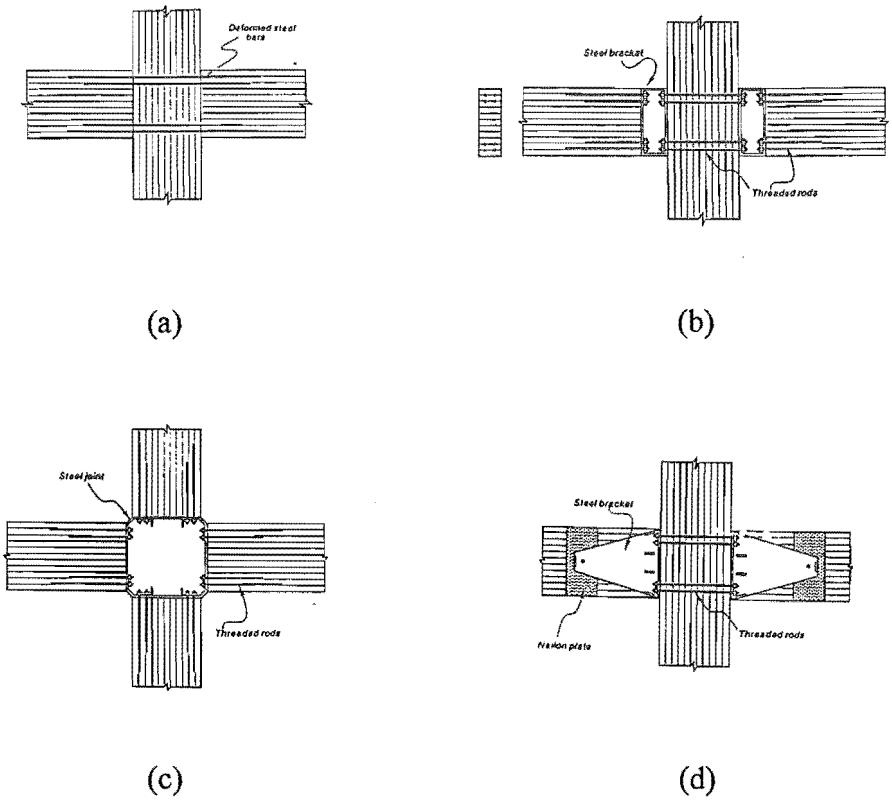

Figure 2.17 Four types of connections (Fairweather, 1992)

2.4.2 Fire Resistance

A study on the fire resistance performance of epoxy bonded steel connection was carried out by Barber (1994). The study investigated how full-size connections would behave at elevated temperatures. Computer modelling was used to analyse heat transfer through the charring wood and was validated by two series of tests. In both series, the connections were loaded in tension parallel to the wood grain. The first series was tested with elevated temperatures (40°C to 90°C) by heating the connections in an oven. The second was tested in a furnace using full-size members exposed to standard fire conditions. The results showed that both West System and Araldite K-80 epoxies had a critical temperature of approximately 50°C and the strength decreased rapidly once this temperature was reached. The connections failed by pull out due to shear failure within the epoxy or loss of bond at the wood epoxy interface as the temperature increased. By contrast, the connections failed by tension failure in wood or by loss of confinement when they were tested at ambient temperature.

2.4.3 Load Duration and Environment Effects

Riberholt (1986) has conducted an on-going long duration experiment commencing in 1977. The specimens were tested either under indoor controlled conditions or under outdoor climate conditions. The test arrangement for the outdoor specimens is shown in Figure 2.18. Riberholt found that the connection bonded with the polyurethane appeared to be superior to the connections bonded with araldite for sustained constant moment. For polyurethane glued bolts the connections exhibited creep deformation, which was at least equal to the initial deformation. The axial pull-out strength of the connection subjected to long duration load under the outdoor climate condition was approximately half of the strength compared to that of the dry specimens tested in short duration loading. Riberholt's long duration test results indicated that provision of adequate control of moisture content in the timber members was essential for long duration loading in harsh environments.

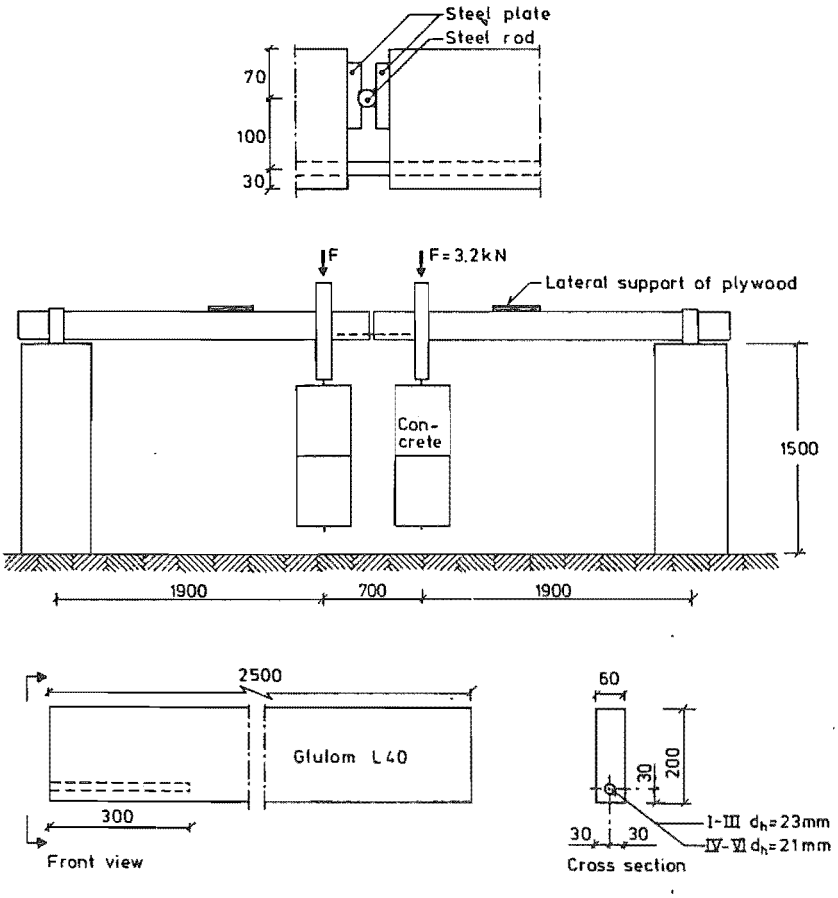

Figure 2.18 Sketch of outdoor specimens for long duration axial loading test (Riberholt, 1986)

2.5 BRIEF REVIEW OF ADHESION THEORY

It is beyond the scope of this study to review in detail the various fundamental adhesion theories, but some theories will be reviewed briefly to provide some background. There are four basic theories on adhesion relevant to the adhesive bonding mechanism (Wake, 1982):

1. The mechanical theory.
2. The diffusion theory.
3. The electrostatic theory.
4. The adsorption theory.

The mechanical theory states that the adhesive fills the microcavities on the surface, hardens and forms a mechanical interlocking interface between the adhesive and adherent. The diffusion theory ascribes that the intrinsic adhesion of high polymers to themselves, and to each other, are due to mutual diffusion of polymer molecules across the interface. The electrostatic theory suggests that the electrostatic forces arising from such contact or junction potentials may contribute significantly to the intrinsic adhesion. Finally, the adsorption theory indicates that adhesion is produced from molecular contact between the adhesive and adherent in the interface. Based on this theory, surface forces are involved in the adhesion, and moreover, where polar molecules or groups are used, they are oriented at the interface (Wake, 1982).

The above four theories are different approaches to explain the adhesion process, but it is likely that only one theory dominates the adhesion process depending on the technology and material used for adhesive and adherents. Zisman (1963) believed that intermolecular force phenomena at the adhesion interface are important and fundamental to all adhesive jointing. Bikerman (1968), on the other hand, suggested that the manifestation of molecular forces and interactions at the interface are not of primary importance. He grouped adhesive joints into three categories, proper joints, improper joints and hooking joints. For proper and improper joints, the joints are normally formed without significant interpenetration of adhesive into adherent. For hooking joints, adhesive acts as a multiple hook after it is fully cured. From Bikerman's perspective it is likely that wood belongs to this category and its adhesion is unlikely to involve atomic and molecular forces. Therefore, the molecular forces and interactions at the interfaces would not be the primary interests. Only the geometry of the connection, the texture of the adherents, and other macroscopic and mechanical factors need to be considered.

2.6 ADHESIVES AND ADHESIVE BONDING

There are many types of adhesives available in the market place, which can be classified into three categories according to their rheological properties: thermoplastic,

elastomeric and thermosetting adhesives (Houwink and Salomon, 1965). However, in this study, only one of thermosetting adhesives - epoxy resin adhesive is of primary interest since it has been widely used in civil engineering and has promising potential. The following discussion of adhesive and adhesive bonding is concentrated on epoxy resin adhesive.

2.6.1 Basic Characteristics of Epoxy Resin Adhesives

Olson and Blomquist (1962) described: "The term 'epoxy resin' is a broad one, referring to any resin system containing the characteristic single oxygen atom linked directly to each of two adjacent carbon atoms on a chain, as in ethylene oxide." Epoxy resin forms bond between adherents by curing, which is the chemical joining together of small molecules to form large ones. The curing process forms crosslinked polymer structures with better heat and mechanical resistance than hot melt or solvent-type adhesive systems. The curing process is an irreversible reaction that results in a thermoset resin. This reaction does not involve condensation polymerisation, therefore no low-molecular-weight substance, such as water, is produced during the curing process (Houwink and Salomon,1965). For this reason, the shrinkage that takes place during cure is slight, and this is one of the properties that makes epoxy resins especially valuable as adhesives. For adhesive bonded connections in timber or glulam, it is essential to avoid the shrinkage of glue.

There are many reasons which make the epoxy adhesives popular. Preiswerk (1950) described major advantages as follows:

1. A minimum of shrinkage during hardening.
2. High adhesion to most materials.
3. Practically no elimination of fugitive materials.
4. High mechanical strength.
5. Resistance to most common chemicals.
6. Good dielectric properties.

Furthermore, Kinloch (1983) also described some properties in favour of epoxy resins:

1. Epoxy resin normally has a sufficiently low viscosity to flow over a substrate surface without the need to employ solvents.
2. Its polar material characteristics assist in removing atmospheric contamination on the surface of substrate and increase the degree of intrinsic adhesion.
3. Various curing agents can be used to give a wide range of possible times and temperatures for the curing reaction.
4. Low thermal contraction on curing.
5. Ability to bond dissimilar materials.

2.6.2 Epoxy Bonding to the Wood

Williamson and Nearn (1958) studied the relationship of wood species to the effectiveness of an epoxy adhesive wood-to-wood bond, measured as the load capable of being sustaining in tension perpendicular to the glue line. Four adhesives and nine species were used for the experiment. One of adhesives was a resorcinol resin used for control specimens. For each combination of adhesive and species, two temperatures were used. The major findings from the experiment are listed as follows:

1. One of three epoxy formulations proved unsuitable for use as a wood adhesive.
2. There is no well-defined species preference among these adhesives when used to bond woods of high strength (Redwood, a low-strength timber, is a possible exception).
3. An increase in the curing temperature does not cause a significant improvement in the bond strength. In some instances, the bond strengths of these epoxy formulations decreased as a result of an increase in curing temperature.
4. The water resistance of the bond is improved with an increase in the curing temperature. However, the epoxies used are not water resistant when cured at room temperature.

Olson and Blomquist (1962) developed epoxy formulations, including Forest Products Laboratory (FPL) Formula 16, that appeared capable of withstanding severe exposure condition, as determined from preliminary 120-h-boil and soak-dry test.

Excellent strength remained after 120 hours in boiling water for plywood test specimens glued with epoxy adhesive using diethylenetriamine as the hardener at the room temperature. The timber used was yellow birch.

Caster (1980) described that wood specimens bonded with two epoxy adhesives performed comparably to solid-wood specimens. The epoxy bonded specimens performed even better than specimens bonded with phenol-resorcinol-formaldehyde and phenol-formaldehyde adhesives during both accelerated ageing in the automatic boil test, and in 11 years of exterior exposure in Mississippi, California, and Washington.

Vick and his co-workers (1995) carried out a study to explore chemical primers as a means of improving the durability of epoxy bonds to wood. Their work led to the discovery of an hydroxymethylated resorcinol (HMR) coupling agent that appears to bond chemically to both epoxy adhesive and lignocellulosics of wood. They reported that epoxy adhesive diluted with benzyl alcohol developed structural bonds on the HMR-primed lumber that met the 5% delamination requirement of ASTM Specification D 2559.

These various researches confirm that epoxy resin as an adhesive can provide outstanding performance in durability, mechanical strength and resistance to chemicals when compared with most other adhesives. This is the reason why it has become the first choice of adhesive for structural applications in civil engineering.

It is emphasised that not every epoxy formulation is suitable as a wood adhesive, and tests may be required to obtain adequate information. The properties of an epoxy adhesive in a glued joint, as well as the adhesion to a particular adherent depend on the whole adhesive composition, viz. the type of resin, the curing agent, fillers and modifiers. Equally, the properties of adhesives become meaningful only when related to a particular adherend in a particular use. "Bond strength" data is of limited value unless accompanied by complete data such as type of species of wood, type of joint, curing temperature etc.

2.7 CHARACTERISTICS OF WOOD AS AN ADHERENT RELATED TO ADHESIVE BONDING

Many chemical and physical properties of adherents relate to the strength of adhesive bonding. However, only a few of such properties will have major influence to the strength of adhesive bonding in the connection. The chemical adhesive bond in the interface of steel and epoxy is not critical since a "threaded-nut-like" mechanical connection can be formed when the epoxy adhesive is fully cured. Therefore, the properties of steel with regard to adhesive bonding are not of critical interest to this thesis. Some wood properties relevant to adhesive bonding, such as surface roughness, time-dependent behaviour, and environmental effects will be discussed below.

2.7.1 Surface Roughness

Marian and co-workers (1958) defined three degrees of surface texture of wood:

1. A surface formed only by anatomic structure - first degree texture.
2. A surface resulting from the action of different cutting (machining) characteristics of wood components and of machining variables - second degree texture.
3. A texture resulting from incidental machine variables, some uncontrollable factors, such as vibrations - third degree texture.

The investigation of surface roughness of five types of machined surface was conducted using the electrical stylus-tracer procedure. The five types of surfaces representing increasing degrees of roughness were tested in terms of the strength of butt and scarf joints. The roughest surfaces gave the strongest adhesive bonding and joint strength increases with surface roughness until a point is reached that simultaneously decreasing strength and increasing porosity cause the wood to fail.

2.7.2 Time Dependent Behaviour

The time dependent behaviour of wood has been widely observed and studied (Bodig and Jayne, 1982). This time dependent behaviour of wood can be explained by its viscoelastic nature. Like many other viscoelastic materials, wood exhibits both elastic and viscous behaviour when subjected to load. Rheology is the study of time dependent deformation and flow of material resulting from the application of deforming forces (Pentoney and Davidson, 1962). From the mechanical point of view, the influence of time on the stress-strain characteristics of a viscoelastic material can be reflected in the three dimensional stress-strain-time diagram (Bodig and Jayne, 1982). The rheological of wood may be characterised by linear viscoelastic behaviour in which the elastic effects obey Hooke's Law and viscous effects are Newtonian. During creep the total deformation (or total creep) δ_t can be expressed by the sum of three components, based on linear viscoelastic theory: an elastic part δ_e, a delayed elastic part δ_{de}, and a viscous component δ_v:

$$\delta_t = \delta_e + \delta_{de} + \delta_v \qquad (2.7)$$

The elastic deformation component δ_e is an instantaneous deformation upon loading and is recoverable. The delayed elastic deformation δ_{de} is time-dependent and is recoverable with time, while the viscous deformation is permanent and irrecoverable. Stress relaxation is governed by the same time dependent characteristics of the material as creep. While the total deformation during stress relaxation is kept constant, the magnitude of the elastic, delayed elastic and viscous components alters as time progresses. Initially all the deformation is elastic. With elapsing time, the elastic deformation subsides as the delayed elastic and viscous components respond. At any particular time, however, the sum of the three deformation components is constant. Removal of the residual forces reduces instantaneously the elastic deformation to zero.

Several different approaches have been developed to model creep rupture phenomena of wood. The fracture mechanics approach has been particularly successful in analysing the fracture process where dominant features, such as a pre-existing crack, can be identified.

Damage accumulation theory offers a popular approach to describe load duration characteristics. The general form of the damage accumulation theory can be written as follows (Hwang and Han, 1986):

$$\frac{d\alpha}{dt} = f(\sigma_r, T, M, ...) \qquad (2.8)$$

where α is a damage parameter, $d\alpha/dt$ reflects the rate of damage accumulation, f is the general function defining $d\alpha/dt$ in terms of stress ratio σ_r, temperature T, moisture M, and any other factors that may influence failure. The damage parameter α is defined between 0 to 1. 0 implies no damage, 1 indicates total failure.

The cumulative damage theory has been adapted to analyse creep rapture by several researchers (Barrett and Foschi, 1978a, 1978b; Foschi and Barrett, 1982; Fridley et al., 1991; Gerhards, 1979; Gerhards and Link, 1987; Nielsen and Kousholt, 1980). These previous researches indicate that it is possible to model the rheological behaviour of wood and predict the duration of load using the cumulative damage theory. However, creep in wood is an extremely complex physical phenomenon and is affected by many variables including moisture, temperature, species, grain direction, loading conditions and wood natural variability. Some understanding of this phenomenon and the cumulative damage theory would certainly be of benefit to the study of the adhesive bonded connection, but intensive study of time dependent behaviour of wood, in addition to adhesive bonding, is beyond the scope of this study.

Much of the existing data for long duration behaviour of wood was collected from bending tests; these results seem to represent member and structural behaviour rather than material characteristics. Bending tests tend to mask the true time dependent material behaviour because the stresses and strains vary throughout the cross section of the specimen (Holzer et al., 1989). Furthermore, the time dependent behaviour of timber structures could be investigated at several levels, including polymer, microstructure, continuum, structural element and structure levels. "Failure to consider any one of these levels is likely to leave an imperfect understanding of how to predict long-term behaviour. These levels are important building blocks for developing a rational approach to structural design with wood".

Creep behaviour in the connection would be more complicated than wood itself due to the large number of influencing factors, such as the connection geometry and material characteristics (including wood, adhesive and steel). Few information was available on study the time dependent behaviour of the connection. With his long term experiment, Reberholt (1986) found that no noticeable time dependant displacements were observed in the specimens under indoor conditions where the humidity and environmental conditions were relatively controlled. However, the outdoor specimens indicated creep in the resin with failures occurring within 4 years of sustained load. The load level was about 50% of tensile strength of the connection subjected to short term tensile load.

Previous studies show that time dependant behaviour could have major influence to the strength of the connection and the creep of the connection is likely depend on the environmental condition.

2.7.3 Environmental Effects

There are many environmental factors that adversely affect the durability and performance of adhesive bonds. Moisture is a hostile environment for adhesive bonding, and the rate of environmental attack is greater if the temperature is relatively high or the adhesive bond is subjected to stress. Comyn in Kinloch (1983) summarise the mechanisms by which water enters the adhesive joint as follows:

Moisture can be enter the joint by

1. Diffusion through the adhesive
2. Transport along the interface.
3. Capillary action through cracks and crazes in the adhesive.
4. Diffusion through the adherent.

When moisture has entered a joint, the mechanism for the decrease in the strength of the adhesive bond can be described as follows:

1. Water may alter the properties of the adhesive in a reversible manner to weaken the strength, such as plasticisation or swelling of the adhesive.
2. Water can also alter the properties of the adhesive in an irreversible manner which induces chemical and physical ageing. This category includes hydrolysis, cracks and crazing.
3. Water may attack the interface either by displacing the adhesive or by hydrating the metal or metal oxide surface of the adherend.
4. Water may induce swelling stresses in the adhesive joint.

While these generalised statements by Comyn are broadly applicable, they are mostly relevant to the epoxy bonded steel connection in glulam timber. Changes in moisture content also adversely affect the durability and performance of adhesive bonds. Effects of the interaction of moisture movement (drying and wetting) with the mechanical behaviour of wood were discussed by Schniewind (1968), Bodig (1982) and Bodig and Jayne (1982).

In addition, moisture is a major influence on the time dependent behaviour of wood. Creep increases with increasing moisture content (Bodig and Jayne 1982; Schniewind 1968), affecting the strength of the connection. Fridley et al. (1991) carried out a study on moisture effects on load-duration behaviour of lumber. It was concluded that moisture effects on the load-duration behaviour were significant and the likely time-to-failure appears shorter at higher moisture contents when subjected to equal mechanical stress ratios.

Schniewind and Lyon (1973) found that the creep rate was always lower in larger specimens than in smaller specimens, which suggests that the larger specimens are less affected by changing moisture content than the smaller ones. Based on the comparison of the results from different moisture cycling environments (Schniewind 1967; Schniewind and Lyon 1973) and constant environment (Wood 1951), Barrett (1982) concluded that there would be little or no effect due to moisture cycling influence on the behaviour of large timber and glulam members. Bodig (1982) stated that large wooden members are less sensitive to moisture cycling than small wood specimens; but the influence of environmental cycling can be significant and should be considered in design when the members are exposed to cyclic moisture conditions. The

moisture movement and moisture level in the connection should be considered as well as the specimen size.

There are many environmental factors besides water which could affect the durability and performance of adhesive bonding, such as temperature, exposure to the sun, applied stress and other environmental effects. None of these is discussed in detail in this study.

2.8 APPLICATIONS OF ANALYTICAL TOOLS

For all adhesive bonded joints, it is necessary to carry out some form of quantitative analysis so that experimental data can be interpreted and strength predictions made. There are two commonly used methods. The first is to set up a series of differential equations to describe the state of stress and strain in a joint, and to find solutions using algebraic functions. This method is commonly called as the closed-form solution. Technically, with this method it is very difficult or impossible to reach a solution because of non-linearities and complicated geometry. The second is the finite element method, which is very powerful and efficient, especially when using small elements in regions with large stress gradients. Adams (1986) claimed that despite substantial computing power requirements, there is no substitute to the finite element method for understanding the mechanics of real adhesive bonded joints. No other modelling technique can accurately represent the distribution of the strains or the stresses and be used to predict the strengths and failure modes of the joints.

2.9 SUMMARY

Mays (1985) claimed four main prerequisites to realise a successful adhesive bond:

1. Careful selection of a suitable adhesive.

2. Adequate surface preparation.
3. Good joint design.
4. Long duration durability.

This chapter has reviewed many aspects related to the strength of the adhesive bonded connection to provide a broad general background.

CHAPTER THREE

SHORT DURATION EXPERIMENTS

3.1 OBJECTIVES AND SCOPE

The objectives of the short duration experiments were to investigate the tensile strength and the failure mode of the single epoxy bonded steel rod connection for a wide range of materials and geometry, in order to understand the physical and mechanical characteristics of the connection and to develop an empirical formula to calculate the strength of the connection. These experiments also allowed an investigation of the effects of reinforcement of the connection to obtain a technique of preventing wood splitting.

Only a single steel rod connection was investigated and subjected to tensile load. Similar capacity is expected when the connection is subjected to compression load (Gerold, 1992). In the experiments only a single species of wood, *Pinus Radiata*, was used.

For designers, these short duration experiments will be of direct benefit when using this type of connection in real structures, and of indirect benefit for assessing similar connections involving other different loading configurations and multiple steel rod connections.

3.2 DESIGN OF THE EXPERIMENTS

3.2.1 Design Principles

A test for an epoxy adhesive joint should be simple to set up and carry out. It has to be repeatable and representative of the loading condition and the environment found in service. Adams (1990) summarised several test methods, including single lap joint test, double lap joint test, butt joint tests and peel test. He concluded that the best test for determining the mechanical properties of an adhesive is to make specimens from bulk samples. To achieve the above requirement, the specimens with a single epoxy bonded connection were fabricated and tested under tensile load parallel to the steel rod axis and wood grain.

3.2.2 Factors Influencing the Strength of the Connection

There are many factors which may influence the connection strength. They can be classified into three major categories: the physical and mechanical properties of the materials, the geometry of the connection and the connection reinforcement.

The properties of wood include wood species, moisture content, modulus of elasticity, strength and density, etc. The properties of epoxy involved for this study are epoxy type and quality. The strength of the steel bar and its surface cleanliness also affect the strength of the connection.

The geometry of the connection include steel rod diameter, embedment length, edge distance, geometry of the steel rod surface, hole diameter, geometry of inner end of the steel rod, hole roughness.

The connection reinforcement is also a influence factor which will be considered in this study. The transverse reinforcement of the connection may provide a method to prevent the wood splitting around the connection.

3.2.3 General Considerations

Three individual experiments were designed: a 2^7 random factorial experiment as Experiment One, a 3^4 random factorial experiment as Experiment Two and an experiment to investigate the effect of reinforcement as Experiment Four. Experiment One was a general investigation of the strength and failure characteristics of the connection, considering as many factors as practically possible. Experiment One has 7 factors with 2 levels for each factor. It consists of 128 specimens with a single replication. Experiment Two was designed to refine the data from Experiment One to get further information. Experiment Two has four factors with 3 levels for each factor. It consists of 81 specimens with a single replication. The random factorial designs in Experiment One and Two provide more efficiency than one-factor-at-a-time experimental design. In the factorial design, all data are used in computing the factors and the interaction among the factors. Furthermore, the design is to eliminate the financial and material resource limitation as single replication was used in the experiments. However, while the design with single replications of the specimens can obtain reasonable good indication, it will not give an accurate indication of the variability. Experiment Four was designed specifically to study the effect of connection reinforcement. It has 8 specimens with only one factor considered.

The determination of a particular specimen geometry was based on the preliminary trials for the short duration experiments and the empirical formula from Crews (1993) shown as follows:

$$F = 10.6dl\,(r_h)^2\,(r_e)^{0.5} \qquad (3.1)$$

where, F = average pull-out force (N)

d = steel rod diameter (mm)

l = embedment length (mm)

r_h = ratio of hole diameter to steel rod diameter

r_e = ratio of edge distance (from steel rod centre line) to rod diameter

This formula is based on the use of Araldite K-80 epoxy resin and the deformed reinforcing bar.

3.2.4 Design of Experiment One

Based on previous researches (Crews, 1993; Riberholt, 1986, 1988a; Townsend, 1990) and the author's preliminary experiments, seven factors were chosen for Experiment One. They are moisture content, epoxy type, steel rod type, embedment length, steel rod diameter, hole diameter and edge distance.

The design procedures for Experiment One are described as follows:

1. Selection of steel rod type and diameter: The high strength threaded rod (tensile strength 850 MPa, yield 680 MPa) and high strength deformed reinforcing bar (HD430 grade) were used. Rod diameters of 16 mm and 24 mm were chosen since they are commonly used and within the capacity of the Instron Universal Testing Machine. The high strength steel rods were used to avoid the probability of steel yielding so that the tensile strength of the connection can be reached before the steel rod yielded.

2. Choice of edge distance and hole diameter: Considering previous test results, available glulam timber material and its tensile strength, 1.5d and 2.25d were chosen as edge distances. 1.15d and 1.4d were chosen as hole diameter (d is the steel rod diameter).

3. Selection of embedment length: Using Crew's formula (Equation 3.1), the embedment length associated with yielding of the steel rods was calculated as shown in Table 3.1, where the maximum values were calculated from the lower values of ratio r_h and r_e, and the minimum values were from upper ratios of r_h and r_e. Based on the calculation, the embedment lengths selected were as 5d and 10d. The selected embedment lengths were significantly lower than the values shown in Table 3.1. This is to avoid the steel rod yielding and ensure that the pullout failure is the major dominant failure mode.

4. Selection of wood cross section: The shape of the wood cross section was selected to provide the specific edge distance, yet be large enough to prevent tensile failure of the wood.

The finalised design details for Experiment One are listed in Table 3.2.

Table 3.1 The embedment length associated with the yield capacity of the steel rod

Bar Diameter (mm)	Embedment Length (mm)	
	Maximum	Minimum
16	367 (22.9d)	202 (12.6d)
24	549 (22.9d)	302 (12.6d)

Table 3.2 Design for Experiment One

Level	Epoxy Type	Steel Rod Type	d (mm)	l (mm)	e (mm)	h (mm)	MC (%)
1	West System	Threaded	16	5d	1.5d	1.15d	10-16
2	K-80	Deformed	24	10d	2.25d	1.4d	22-30

Note: d = steel rod diameter (mm).

l = embedment length (mm).

e = edge distance (mm).

h = embedment hole diameter (mm).

MC = moisture content in wood (refer Section 3.6).

3.2.5 Design of Experiment Two

Four factors were selected for Experiment Two based on the results of Experiment One. They include epoxy type, steel rod diameter, embedment length and edge distance. These factors made a greater contribution to the strength of the epoxied steel connection than the others in Experiment One.

Unlike Experiment One, the embedment length and edge distance were not directly proportional to the different diameters of the steel rod in Experiment Two. Same embedment lengths and similar edge distances were used for all of different diameters of the steel rod. The design for Experiment Two is shown in Table 3.3.

Table 3.3 Design of Experiment Two

Levels	Epoxy Type	d (mm)	l (mm)	e (mm)
1	K-80	16	80	d/2+20
2	West System	20	160	d/2+30
3	Z-2005	24	240	d/2+40

Note: 1. d = steel rod diameter.
l = embedment length.
e = edge distance.

2. Only threaded rod and dry specimens were used.

3. The hole diameter for all specimens was (d+4)mm.

3.2.6 Design of Experiment Four

Experiment Four was designed to investigate the effect of transverse reinforcement in the connection. The design of Experiment Four was based on the results from Experiments One and Two. The experiment was designed to form four pairs of specimens.

Each pair of specimens included one control specimen without reinforcement and one with transverse reinforcement. The geometry of the connections was arranged to be identical within each pair. Similar material properties were selected for each pair of specimens. The design was to obtain wood splitting around the connection in the test end therefore the small edge distance was used. This experiment as a pilot study was to investigate the potential benefits of the connection reinforcement. The design parameters are listed in Table 3.4.

Table 3.4 Design parameters of Experiment Four

Wood member dimension (mm)			Reinforcing rod dimension (mm)		Embedment length (mm)	
Length	Width	Depth	Length	Diameter	l_t	l_s
700	70	140	135	4	200	350

Epoxy type	Steel rod diameter (mm)	Embedment hole diameter (mm)	Reinforcement hole diameter (mm)
West System	20	26	6

Note: 1. l_t = the embedment length at the test end.

2. l_s = the embedment length at the support end.

3.3 MATERIALS

3.3.1 Timber

Pinus Radiata glue laminated timber from Hunter Laminates Ltd. was used for these experiments. The glulam timber, using 45 mm laminates of No.1 framing grade timber and treated with CCA preservative, were fabricated in 1984 as glulam beams for the roof of an indoor ice skating rink in Christchurch. The test specimens were cut out of the beams when the building was re-built in 1992 after the roof was collapsed due to the

heavy snow. The beams were carefully selected. The collapsed beam was excluded. All of selected beams were remain intact and in good condition. All of the specimens for the experiments were randomly selected. The average moisture content was 12.8% for Experiment One (Appendix A), 12.9% for Experiment Two (Appendix C) and 12.1 for Experiment Four (Table 3.11). The moisture content readings were measured by the electric moisture meter (Timber Master Model D184T, Protimeter Ltd.) with the Hammer Electrode.

The modulus of elasticity for timber blocks using in all experiments were measured with a Stress Wave Timer (Metriguard Model 239A, Metriguard, Inc. 1990). This is to obtain wood properties at the region where the steel rod is embedded. It seems to be the only method available during the experiments to measure the modulus of elasticity for the centre lamination of the glulam timber blocks. However, the data obtained from the Stress Wave Timer were not adequately reliable and have great variation. In some case, the measurement was not repeatable and out of range. It is due to the inhomogeneity or interruption along the path of stress wave with any wood defects and finger joints. Therefore, the data measured from the Stress Wave Timer are not included in the analysis.

The timber blocks used in Experiment Four were chosen and sorted by cross-section arrangement and modulus of elasticity to give matching pairs of test specimens. The modulus of elasticity was measured using a 3 point bending test on the 100 kN AVERY Universal Testing Machine and presented in Table 3.11.

3.3.2 Epoxy

The hardener used to cure the resin affects the properties of the cured resin because it completely enters into the final reaction. Each resin-hardener combination will yield a cured adhesive with different properties. It is beyond the scope of this investigation to test all the epoxy adhesives which are available in the market and only three commonly used epoxy resins were used in the experiments. Two types of epoxy were used in Experiment One. One was K-80 (NUPLEX Industries Ltd), the other was West System (Adhesive Technologies Ltd). For Experiment Two, three types of epoxy were used: K-80, West

System and Araldite 2005 (NUPLEX Industries Ltd). For Experiment Four, only the West System epoxy was used.

Typical properties of these epoxies are listed in Table 3.5, with data from the manufacturer's publications.

Table 3.5 The mechanical properties of the epoxies

Epoxy	Compress -ive Strength (MPa)	Tensile Strength (MPa)	Shear Strength (MPa)	Modulus of Elasticity (GPa)	Maximum Operating Temperature (°C)	Cure Time[5] (hours)
K-80	120-130	30-40	10-12[1]	17	75	winter: 6 summer: 12
West System	55.1[2]	50.5[3]	--	3.2	--	Z205: 5-7 Z206: 9
2005	--	--	27[4]	2.0	80	24

Note: 1. The data are from aluminium lap joint test without surface sand filler.

2. ASTM D-695.

3. ASTM D-638

4. The shear strength value relates to mild steel lap joints cured at 20°C for 24 hours and tested at 23°C to BS 5350 Part C5 1976.

5. Cure times are measured at 20°C for West System and Araldite 2005, 25°C for K-80.

K-80:

Araldite K-80 is designed as an all purpose structural grout to bond new to old concrete as well as grouting bolts in concrete. K-80 has desirable properties such as nil shrinkage, low creep, and excellent adhesion to wet concrete, fibreglass, ceramics and timber. It consists two components: resin and hardener. The resin is dark grey, high viscosity, like peanut butter. Two types of hardener were available: summer type and

winter type. Both of them are clear, light-amber, low viscosity hardeners. The summer hardener was mixed with the resin in a 10 part resin to 1 part hardener ratio by weight and give about 30 to 40 minutes pot life. The mixture ratio for winter hardener was 100:12 resin to hardener by weight and it had a pot life of 15 to 20 minutes. The K-80 epoxy mixture had a viscosity similar to motor oil. The summer hardener was used in the experiments (CIBA-GEIGY, 1989a).

West System:

This is a two component epoxy: Z105 and Z205/Z206 hardener. The West System epoxy is designed for use with wood. The Z105 resin is a clear, light-amber, low viscosity, 100% reactive solvent-free resin which cures clear over a wide range of temperatures. Two types of hardener were available for Z105 resin; the Z205 fast hardener and Z206 slow hardener. Both could be mixed with Z105 resin in a five part resin to one part hardener ratio by volume or by weight. In most circumstances, the Z205 can be used to produce a rapid cure that develops its physical properties quickly. It consists of a formulated mixture of medium viscosity polyamine and when mixed with Z105 the pot life is 15 to 20 minutes and hard cure time is 5 to 7 hours at 20°C. The maximum strength is reached after several days at room temperature. The Z206 consists of a low viscosity polyamine mixture and when mixed with Z105, the pot life is 30 to 40 minutes and the hard cure time is approximately nine hours at 20°C. The maximum strength is not reached for at least a week under normal conditions. The Z105 resin and Z206 harder were used in the experiments (Adhesive Technologies Ltd., 1992).

Araldite 2005:

This is a two component epoxy: resin Part A and hardener Part B. The mixing ratio is 2:1 by volume. The mixture of this epoxy has a viscosity a little thicker than liquid honey. Araldite 2005 epoxy has properties such as high shear and peel strength, negligible shrinkage, good heat resistance, resistance to water and to a wide range of chemicals. It has a 20 - 100°C wide curing range. Araldite 2005 is a solvent-free cold-setting epoxy adhesive used for bonding most structural materials such as non-porous metals, ceramics, glass, plastics, porous wood, dry concrete and ferrite (CIBA-GEIGY, 1989 b).

3.3.3 Steel Rods

Two types of steel rod were used in Experiment One: One was high strength threaded rod, the other was high strength deformed reinforcing bars (HD430). For Experiment Two and Four, the high strength threaded rod only was used. The mechanical properties given by the manufacturers are listed in Table 3.6.

Table 3.6 The mechanical properties of the steel rod

Mechanical properties	Bar type	
	Threaded rod (AISI 4140)	Reinforcing bar (HD430)
Tensile strength (MPa)	850	580-620
Yield strength (MPa)	680	475

4 mm diameter threaded steel rod was used for transverse reinforcement in Experiment Four. The rod was mild steel with ISO metric 4.6 grade, tensile strength 400 MPa and yield strength 240 MPa.

3.4 SPECIMEN PREPARATION

3.4.1 Cutting Scheme of Glulam Timber

The glulam timber blocks were selected randomly and cut to the required dimensions for each specimen. The dimensions of the specimens in Experiments One, Two and Four are listed in Table 3.7 (a), (b) and (c) respectively. A hand saw and a bench saw were used; no surface finishing was required.

Table 3.7(a) The dimensions of the glulam timber used in Experiment One

Number of specimens	Dimensions (mm)						
	L	l_t	l_s	l_m	a	b	h
8	440	80	160	200	48	108	18.4
8	440	80	160	200	72	72	18.4
8	600	160	240	200	48	108	18.4
8	600	160	240	200	72	72	18.4
8	440	80	160	2020	48	108	22.4
8	440	80	160	200	72	72	22.4
8	600	160	240	200	48	108	22.4
8	600	160	240	200	72	72	22.4
8	560	120	240	200	72	162	27.6
8	560	120	240	200	108	108	27.6
8	800	240	360	200	72	162	27.6
8	800	240	360	200	108	108	27.6
8	560	120	240	200	72	162	33.6
8	560	120	240	200	108	108	33.6
8	800	240	360	200	72	162	33.6
8	800	240	360	200	108	108	33.6

Table 3.7 (b) The dimensions of the glulam timber used in Experiment Two

Number of specimens	Dimensions (mm)						
	L	l_t	l_s	l_m	a	b	h
3	410	80	130	200	56	111	20
3	410	80	130	200	76	82	20
3	410	80	130	200	96	96	20
3	570	160	210	200	56	111	20
3	570	160	210	200	76	82	20
3	570	160	210	200	96	96	20
3	730	240	290	200	56	111	20
3	730	240	290	200	76	82	20
3	730	240	290	200	96	96	20
3	410	80	130	200	60	161	24
3	410	80	130	200	80	121	24
3	410	80	130	200	100	100	24
3	570	160	210	200	60	161	24
3	570	160	210	200	80	121	24
3	570	160	210	200	100	100	24
3	730	240	290	200	60	161	24
3	730	240	290	200	80	121	24
3	730	240	290	200	100	100	24
3	410	80	130	200	64	218	28
3	410	80	130	200	84	166	28
3	410	80	130	200	104	134	28
3	570	160	210	200	64	218	28
3	570	160	210	200	84	166	28
3	570	160	210	200	104	134	28
3	730	240	290	200	64	218	28
3	730	240	290	200	84	166	28
3	730	240	290	200	104	134	28

Table 3.7 (c) Geometry of glulam timber used in Experiment Four

Number of Specimens	Code	Sketch of Cross-section	Dimensions (mm)							
			L	l_t	l_s	h	a	b	h_r	l_r
2	4001 4003		700	200	350	26	70	140	-	-
2	4002 4004	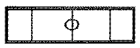	700	200	350	26	70	140	6	135
2	4005 4007	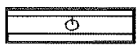	700	200	350	26	70	140	-	-
2	4006 4008	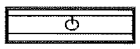	700	200	350	26	70	140	6	135

Note:

L = overall length of the specimen (mm)

l_t = embedment length of the connection at the testing end (mm)

l_s = embedment length at the non-testing end (mm)

l_m = distance between two inner ends of the rods (mm)

h = embedment hole diameter (mm)

e = edge distance (mm)

a = shorter edge of cross-section (a = 2e) (mm)

b = longer edge of cross-section (mm)

h_r = reinforcement hole diameter (mm)

l_r = reinforcement steel rod length (mm)

As shown in Figure 3.1, holes for embedding the steel rods were drilled by an air drill after the glulam timber blocks were cut to the dimensions. Two 8 mm diameter holes were drilled perpendicular to each embedment hole: one was used for epoxy injection, the other was an air hole. For Experiment Four, two extra holes of 6 mm diameter were drilled near the end of the specimens for the transverse reinforcement. The location and depth of the holes are shown in Figure 3.3.

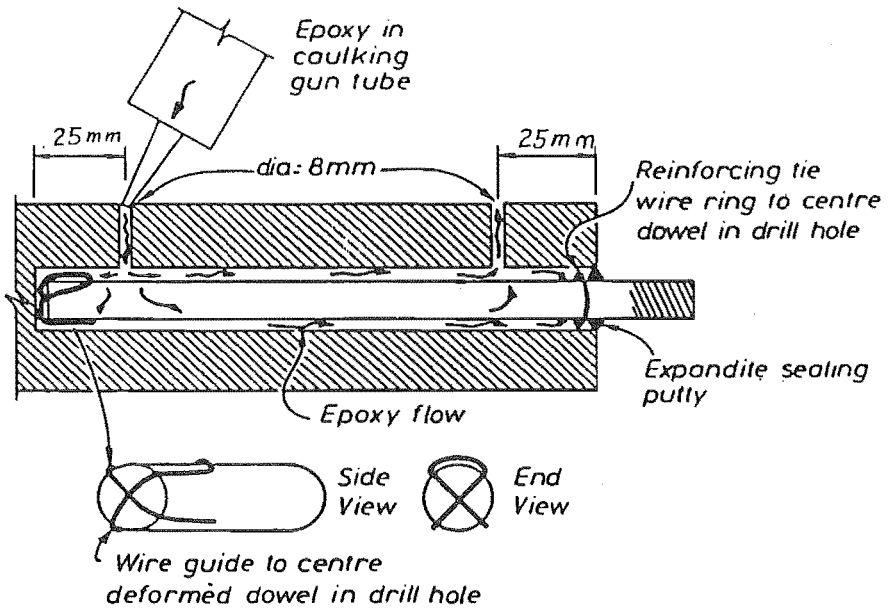

Figure 3.1 Details of the connection

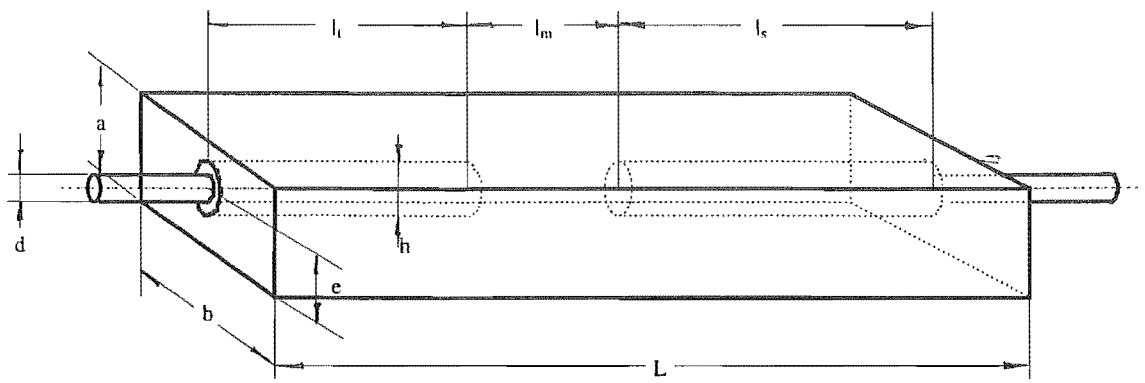

Figure 3.2 Geometry of the specimen for Experiment One and Two

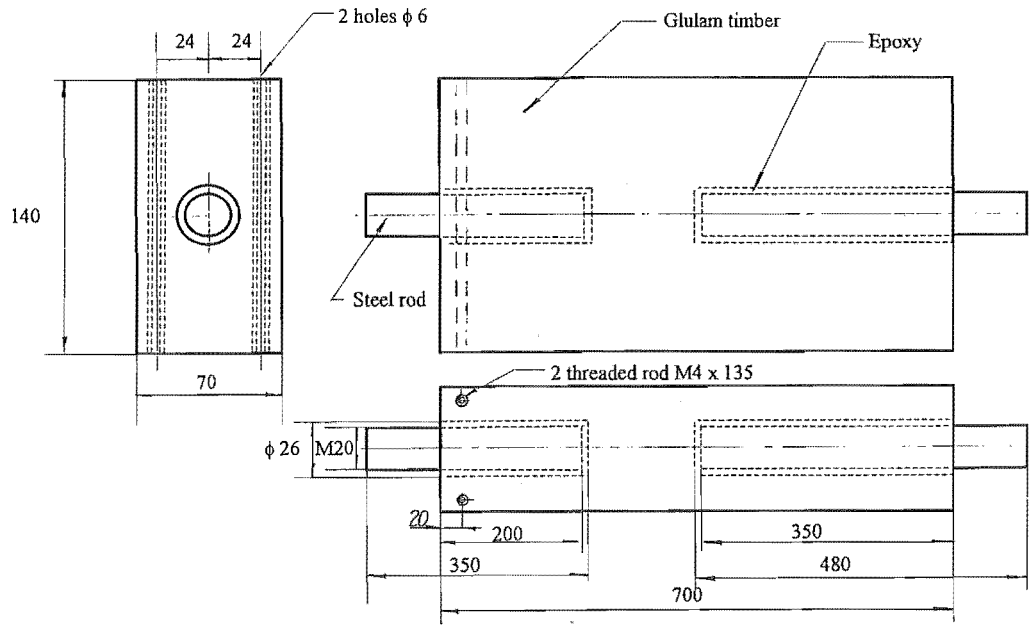

Figure 3.3 Sketch of specimen of Experiment Four

3.4.2 Steel Rod Placement

The threaded rods were cut to the required length, viz. the embedment length plus 120 mm. The deformed bars were supplied in the required length with one end threaded to make a connection between the specimen and the test machine.

A short length of steel wire was tightly wrapped around the end of each rod as shown in Figure 3.1 so that they could be located centrally within the holes. Steel rods were placed at the both ends of the specimens as shown in Figure 3.2. Sealing putty was used to seal the end of the hole. For Experiment Four, 4 mm diameter steel rods were placed into 6 mm diameter holes as shown in Figure 3.3.

3.4.3 Epoxy Injection Procedure

For each type of epoxy, the resin and hardener were mixed manually according to the ratio suggested by the manufacturers. The resin and hardener were weighed on a digital electronic scale. The mixture was stirred quickly and thoroughly to ensure a smooth texture without streaks and to avoid air bubbles, then immediately poured into an empty 328 ml caulking tube, and injected into the injection hole with a caulking gun.

The epoxy preparation and injection were carried out at normal room temperature of about 20°C. The procedure of the epoxy mixing and injecting was undertaken carefully to ensure that the embedment hole was fully filled. After injection of the epoxy, the specimens were stored about one week in a normal laboratory environment to ensure that the maximum strength of the connections was reached before testing.

3.5 TESTING EQUIPMENT AND INSTRUMENTATION

3.5.1 Loading System

The Instron Universal Testing Machine (Model 1116) with 25,000 kg capacity was used as the loading system. The test machine was driven by a stepping motor control unit. The tensile load subjected to the test specimen is displacement dependent. The loading rate for the short duration experiments was 0.1 mm/min.

3.5.2 Data Acquisition System

Three transducers were used in the experiments. One was the 250 kN load cell, installed in the movable head of the Instron Universal Testing Machine. The other two were identical high resolution potentiometers attached to the test specimen, connected to a

Burr-Brown amplifier which supplied the individual input voltages and pre-amplified the signal.

An analogue to digital converter (Dash 16G1 A/D board, Mitrobite) was connected to one of the expansion slots of an IBM compatible personal computer to convert the signals from the Burr-Brown amplifier. Data acquisition software recorded the digital signal from the Dash 16G1 into the computer.

3.5.3 Tensile Load Measurement

The tensile load was measured by the 250 kN load cell, which consisted of a high strength steel hollow cylinder with two independent full bridge (Poisson) circuits. One of the circuits was connected to the Burr-Brown amplifier and the other connected to a digital strain indicator (Measurements Group P-3500). The load cell was calibrated in the Avery Universal Testing Machine (Avery 100T) using the circuit connected to the digital strain indicator. This calibration was reproduced later in the Instron Testing Machine to calibrate the data acquisition system.

3.5.4 Measurement of Displacement

The displacement of the steel rod at the end of the specimen along the loading direction was measured with two potentiometers. The displacement was the average readings from the two potentiometers located at the opposite sides of test end of the specimen.

3.5.5 Software

Data acquisition software was used in the experiments. It was programmed in such manner that the signal would be triggered by whichever came first: either the tensile load increasing by 0.5 kN since last recording or 0.1 mm displacement occurring. The tensile load and the displacement at the connection were recorded during the experiment and stored by the computer after the test was concluded. The sketch of set-up for the

experiments is shown in Figure 3.4. Figure 3.5 shows a overview of a specimen under the short duration tensile test.

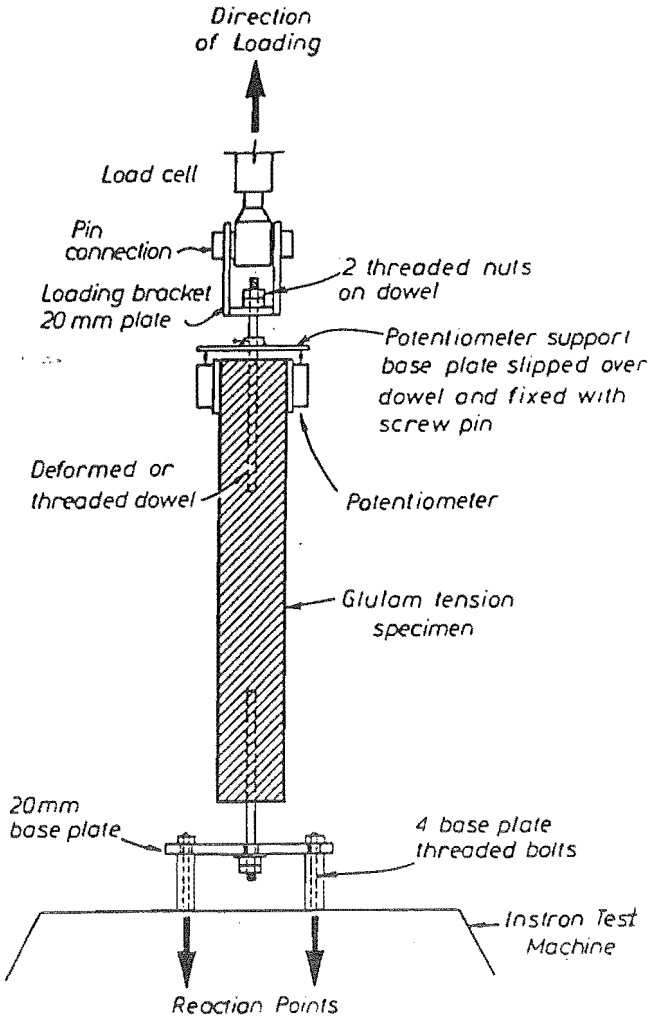

Figure 3.4 Sketch of the set-up for the short duration experiments

3.6 DRY AND WET CYCLING ENVIRONMENT

The specimens in Experiment One were subjected to two different environmental conditions (Table 3.2). One half of the 128 specimens (the control specimens) were tested under the normal indoor laboratory environment without being conditioned under the dry-wet cycling environment. The average moisture content in the specimens was 12.8%

(Appendix A). The other half of the specimens were subjected to a series of dry-wet cycling environmental conditions.

Table 3.8 The scheme of dry-wet cycling for the wet specimens of Experiment One

Cycles		Time periods (days)	Environmental condition	Moisture content (%)
1	dry	cycle starts	-	15
	wet	15	RH = 96% T = 20°C	20.5
2	dry	12	RH = 65% T = 19°C	17
	wet	15	RH = 98% T = 20°C	28
3	dry	12	RH = 62% T = 21°C	17.3
	wet	15	RH = 98% T = 20°C	28
4	dry	12	RH = 65% T = 20°C	16.5
	wet	15	RH = 98% T = 20°C	28
5	dry	12	RH = 65% T = 21°C	17
	wet	15	RH = 98% T = 20°C	28
6	dry	12	RH = 67% T = 18°C	17.6
	wet	15	RH = 98% T = 20°C	28

NOTE:
1. RH = average relative humidity (%) in the specific cycle
   T = average temperature (°C) with the cycle
2. Moisture content is the average value for the moisture content test samples measured by the electric moisture meter (Appendix B).

Six dry-wet cycles were carried out before the specimens were tested. These specimens were tested at the end of the sixth wet cycle while the average moisture content was about 28%. Each dry cycle was undertaken in a normal indoor laboratory condition

with 65% average relative humidity and 20°C in temperature. An electric fan was used to provide air circulation. The wet cycle was carried out in the fog room at the Department of Civil Engineering, University of Canterbury, with 98% relative humidity and 20°C in temperature. The scheme of six dry-wet cycles is shown in Table 3.8.

3.7 EXPERIMENTAL PROCEDURE

The same procedure was used for all of the short term experiments. Two potentiometers were mounted at the test end of the specimen as shown in Figure 3.4, the potentiometer support base being fitted through the steel rod and fixed. The specimen was fixed into the Instron Universal Testing Machine by the loading bracket and the base plate using threaded nuts.

Each specimen was loaded in tension and the speed of the crosshead of the machine was 0.1 mm/min. The computer programme ran once the test machine was started to record the test load and displacement of the connection, data being plotted and displayed on the screen of the computer. The test was continued until the specimen failed; the test time for each specimen was measured by a stop watch.

For Experiment Four, a clamp was used in the region near the outer end of the embedment at the support end of specimen 4008 to prevent the splitting and force the failure to occur in the test end. Figure 3.5 shows a general view of a short duration experimental specimen under test.

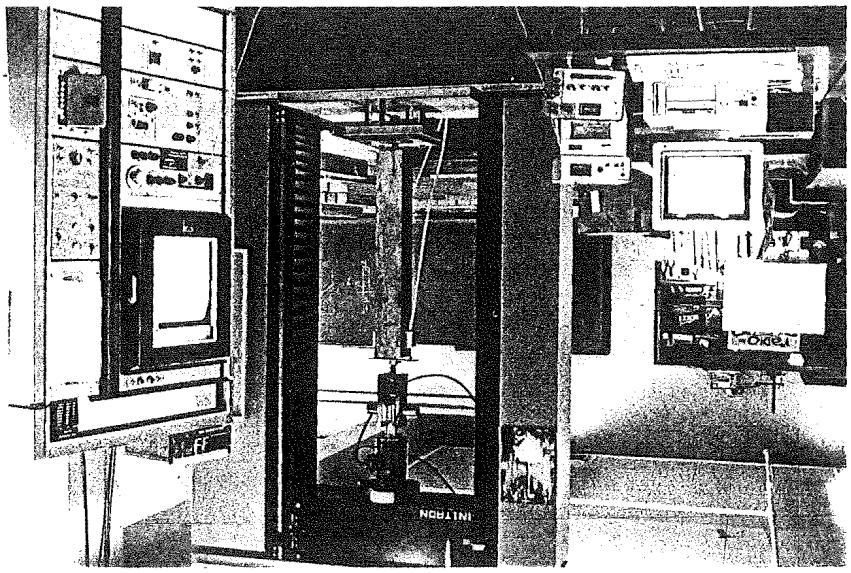

Figure 3.5 General view of a specimen under the short duration tensile test

3.8 RESULTS OF THE SHORT DURATION EXPERIMENTS

3.8.1 Experiment One

The test results for the 128 specimens are listed in Table 3.9. Column 3 in the table shows the two different moisture conditions used in Experiment One:

1. Dry specimens:

   The specimens were prepared and tested under a normal indoor laboratory condition. The moisture content in the specimens did not exceed 16% (Appendix A).

2. Wet specimens:

   The specimens were prepared under a normal indoor laboratory condition with the average moisture content of 12.8%. These specimens were tested while the average moisture content was about 28% after the specimens were subjected to six dry-wet cycles.

The last column in the table records the ultimate tensile load (UTL) for each specimen, that is the maximum tensile load during the test. Column 10 shows the failure mode. Further explanation and discussion of the failure mode are made in Chapter Four.

The load displacement information is presented in Appendix D. This information would be useful to identify secondary effects such as bending of the specimen and yielding of the steel bar.

3.8.2 Experiment Two

The results of Experiment Two are listed in Table 3.10. Experiment Two is a continuation and refinement of Experiment One.

3.8.3 Experiment Four

Table 3.11 shows the results of Experiment Four.

Table 3.9 The results of Experiment One

CODE	BAR TYPE	MC	EPOXY TYPE	d (mm)	l (mm)	e (mm)	b (mm)	h (mm)	FAILURE MODE	UTL mea. (kN)
1001	thread	dry	West	16	80	24	108	18.4	2	30.8
1002	thread	dry	West	16	80	36	72	18.4	2	43.1
1003	thread	dry	West	16	160	24	108	18.4	2	56.4
1004	thread	dry	West	16	160	36	72	18.4	2	87.0
1005	thread	dry	West	16	80	24	108	22.4	2	38.5
1006	thread	dry	West	16	80	36	72	22.4	2	56.8
1007	thread	dry	West	16	160	24	108	22.4	3	68.0
1008	thread	dry	West	16	160	36	72	22.4	2	75.5
1009	thread	dry	West	24	120	36	162	27.6	2	54.2
1010	thread	dry	West	24	120	54	108	27.6	2	97.0
1011	thread	dry	West	24	240	36	162	27.6	2	86.4
1012	thread	dry	West	24	240	54	108	27.6	3	139.5
1013	thread	dry	West	24	120	36	162	33.6	2	78.3
1014	thread	dry	West	24	120	54	108	33.6	2	92.6
1015	thread	dry	West	24	240	36	162	33.6	2	154.9
1016	thread	dry	West	24	240	54	108	33.6	2	175.6
1017	thread	dry	K-80	16	80	24	108	18.4	2	34.3
1018	thread	dry	K-80	16	80	36	72	18.4	2	37.7
1019	thread	dry	K-80	16	160	24	108	18.4	2	70.7
1020	thread	dry	K-80	16	160	36	72	18.4	2	92.1
1021	thread	dry	K-80	16	80	24	108	22.4	2	50.4
1022	thread	dry	K-80	16	80	36	72	22.4	2	55.6
1023	thread	dry	K-80	16	160	24	108	22.4	2	82.7
1024	thread	dry	K-80	16	160	36	72	22.4	3	106.7
1025	thread	dry	K-80	24	120	36	162	27.6	2	81.4
1026	thread	dry	K-80	24	120	54	108	27.6	2	83.2
1027	thread	dry	K-80	24	240	36	162	27.6	3	136.3
1028	thread	dry	K-80	24	240	54	108	27.6	4	176.0
1029	thread	dry	K-80	24	120	36	162	33.6	2	89.7
1030	thread	dry	K-80	24	120	54	108	33.6	2	105.8
1031	thread	dry	K-80	24	240	36	162	33.6	2	112.5
1032	thread	dry	K-80	24	240	54	108	33.6	2	228.0
1033	thread	wet	West	16	80	24	108	18.4	2	32.7
1034	thread	wet	West	16	80	36	72	18.4	2	34.2
1035	thread	wet	West	16	160	24	108	18.4	3	49.1
1036	thread	wet	West	16	160	36	72	18.4	1	67.4
1037	thread	wet	West	16	80	24	108	22.4	2	27.5
1038	thread	wet	West	16	80	36	72	22.4	2	41.1
1039	thread	wet	West	16	160	24	108	22.4	3	35.9
1040	thread	wet	West	16	160	36	72	22.4	3	57.5
1041	thread	wet	West	24	120	36	162	27.6	2	58.4
1042	thread	wet	West	24	120	54	108	27.6	1	75.3
1043	thread	wet	West	24	240	36	162	27.6	3	90.8

Table 3.9 The results of Experiment One - cont.

CODE	BAR TYPE	MC	EPOXY TYPE	d (mm)	l (mm)	e (mm)	b (mm)	h (mm)	FAILURE MODE	UTL mea. (kN)
1044	thread	wet	West	24	240	54	108	27.6	2	131.8
1045	thread	wet	West	24	120	36	162	33.6	2	68.2
1046	thread	wet	West	24	120	54	108	33.6	2	82.8
1047	thread	wet	West	24	240	36	162	33.6	3	102.7
1048	thread	wet	West	24	240	54	108	33.6	2	110.7
1049	thread	wet	K-80	16	80	24	108	18.4	2	29.1
1050	thread	wet	K-80	16	80	36	72	18.4	1	28.5
1051	thread	wet	K-80	16	160	24	108	18.4	2	51.8
1052	thread	wet	K-80	16	160	36	72	18.4	2	62.8
1053	thread	wet	K-80	16	80	24	108	22.4	2	35.8
1054	thread	wet	K-80	16	80	36	72	22.4	1	39.0
1055	thread	wet	K-80	16	160	24	108	22.4	2	43.8
1056	thread	wet	K-80	16	160	36	72	22.4	2	59.8
1057	thread	wet	K-80	24	120	36	162	27.6	2	46.7
1058	thread	wet	K-80	24	120	54	108	27.6	2	71.6
1059	thread	wet	K-80	24	240	36	162	27.6	2	92.9
1060	thread	wet	K-80	24	240	54	108	27.6	2	134.9
1061	thread	wet	K-80	24	120	36	162	33.6	2	58.2
1062	thread	wet	K-80	24	120	54	108	33.6	1	83.7
1063	thread	wet	K-80	24	240	36	162	33.6	5	114.4
1064	thread	wet	K-80	24	240	54	108	33.6	3	140.1
1065	deform	dry	West	16	80	24	108	18.4	2	29.4
1066	deform	dry	West	16	80	36	72	18.4	2	28.9
1067	deform	dry	West	16	160	24	108	18.4	2	43.9
1068	deform	dry	West	16	160	36	72	18.4	2	49.0
1069	deform	dry	West	16	80	24	108	22.4	2	24.9
1070	deform	dry	West	16	80	36	72	22.4	2	31.4
1071	deform	dry	West	16	160	24	108	22.4	2	41.3
1072	deform	dry	West	16	160	36	72	22.4	2	61.7
1073	deform	dry	West	24	120	36	162	27.6	2	48.0
1074	deform	dry	West	24	120	54	108	27.6	2	68.7
1075	deform	dry	West	24	240	36	162	27.6	2	135.1
1076	deform	dry	West	24	240	54	108	27.6	2	106.1
1077	deform	dry	West	24	120	36	162	33.6	2	62.8
1078	deform	dry	West	24	120	54	108	33.6	2	65.8
1079	deform	dry	West	24	240	36	162	33.6	2	117.8
1080	deform	dry	West	24	240	54	108	33.6	2	114.7
1081	deform	dry	K-80	16	80	24	108	18.4	2	40.2
1082	deform	dry	K-80	16	80	36	72	18.4	2	27.5
1083	deform	dry	K-80	16	160	24	108	18.4	2	46.6
1084	deform	dry	K-80	16	160	36	72	18.4	2	52.9
1085	deform	dry	K-80	16	80	24	108	22.4	2	51.0
1086	deform	dry	K-80	16	80	36	72	22.4	2	31.2

Table 3.9 The results of Experiment One - cont.

CODE	BAR TYPE	MC	EPOXY TYPE	d (mm)	l (mm)	e (mm)	b (mm)	h (mm)	FAILURE MODE	UTL mea. (kN)
1087	deform	dry	K-80	16	160	24	108	22.4	2	57.2
1088	deform	dry	K-80	16	160	36	72	22.4	2	79.0
1089	deform	dry	K-80	24	120	36	162	27.6	2	75.7
1090	deform	dry	K-80	24	120	54	108	27.6	2	62.6
1091	deform	dry	K-80	24	240	36	162	27.6	2	92.2
1092	deform	dry	K-80	24	240	54	108	27.6	2	165.3
1093	deform	dry	K-80	24	120	36	162	33.6	2	93.3
1094	deform	dry	K-80	24	120	54	108	33.6	2	95.7
1095	deform	dry	K-80	24	240	36	162	33.6	2	150.6
1096	deform	dry	K-80	24	240	54	108	33.6	2	132.0
1097	deform	wet	West	16	80	24	108	18.4	2	15.4
1098	deform	wet	West	16	80	36	72	18.4	1	5.7
1099	deform	wet	West	16	160	24	108	18.4	1	26.4
1100	deform	wet	West	16	160	36	72	18.4	5	43.7
1101	deform	wet	West	16	80	24	108	22.4	2	22.2
1102	deform	wet	West	16	80	36	72	22.4	1	27.0
1103	deform	wet	West	16	160	24	108	22.4	3	48.1
1104	deform	wet	West	16	160	36	72	22.4	2	44.7
1105	deform	wet	West	24	120	36	162	27.6	2	43.1
1106	deform	wet	West	24	120	54	108	27.6	2	56.9
1107	deform	wet	West	24	240	36	162	27.6	2	105.1
1108	deform	wet	West	24	240	54	108	27.6	2	101.4
1109	deform	wet	West	24	120	36	162	33.6	2	44.2
1110	deform	wet	West	24	120	54	108	33.6	2	45.9
1111	deform	wet	West	24	240	36	162	33.6	3	106.0
1112	deform	wet	West	24	240	54	108	33.6	2	109.3
1113	deform	wet	K-80	16	80	24	108	18.4	1	17.3
1114	deform	wet	K-80	16	80	36	72	18.4	2	24.8
1115	deform	wet	K-80	16	160	24	108	18.4	1	23.5
1116	deform	wet	K-80	16	160	36	72	18.4	2	55.7
1117	deform	wet	K-80	16	80	24	108	22.4	2	26.1
1118	deform	wet	K-80	16	80	36	72	22.4	1	28.7
1119	deform	wet	K-80	16	160	24	108	22.4	3	41.5
1120	deform	wet	K-80	16	160	36	72	22.4	2	55.9
1121	deform	wet	K-80	24	120	36	162	27.6	2	49.2
1122	deform	wet	K-80	24	120	54	108	27.6	1	37.6
1123	deform	wet	K-80	24	240	36	162	27.6	3	116.9
1124	deform	wet	K-80	24	240	54	108	27.6	2	128.4
1125	deform	wet	K-80	24	120	36	162	33.6	1	66.3
1126	deform	wet	K-80	24	120	54	108	33.6	2	53.9
1127	deform	wet	K-80	24	240	36	162	33.6	3	90.4
1128	deform	wet	K-80	24	240	54	108	33.6	4	112.8

Table 3.9 The results of Experiment One - cont.

Note:

1. Bar type: thread = threaded steel rod
   deform = deformed reinforcing bar
2. MC: Moisture content in the specimens
   dry = specimens without any treatment and tested with moisture content below 16%
   wet = specimens subjected to six dry-wet cycles and tested after the sixth wet cycle.
3. Epoxy type: West = West System epoxy
   K-80 = Araldite K-80 epoxy
4. Specimen geometry:
   d = steel rod diameter (mm)
   l = embedment length (mm)
   e = edge distance (mm), e = a / 2
   a = shorter edge of the cross-section (mm)
   b = longer edge of the cross-section (mm)
   h = embedment hole diameter (mm)
5. $UTL_{mea.}$: Test values of ultimate tensile load (kN)
6. Failure mode: 1 = Type 1 Failure Mode
   2 = Type 2 Failure Mode
   3 = Type 3 Failure Mode
   4 = Type 4 Failure Mode
   5 = Type 5 Failure Mode

Table 3.10 The results of Experiment Two

CODE	EPOXY TYPE	d (mm)	l (mm)	e (mm)	b (mm)	FAILURE MODE	UTL mea. (kN)
2001	K-80	16	80	28	111	2	32.6
2002	K-80	16	80	38	82	2	44.9
2003	K-80	16	80	48	96	2	51.2
2004	K-80	16	160	28	111	2	70.4
2005	K-80	16	160	38	82	2	98.0
2006	K-80	16	160	48	96	2	102.5
2007	K-80	16	240	28	111	2	107.0
2008	K-80	16	240	38	82	4	128.0
2009	K-80	16	240	48	96	2	129.0
2010	K-80	20	80	30	161	2	48.8
2011	K-80	20	80	40	121	2	61.7
2012	K-80	20	80	50	100	2	65.1
2013	K-80	20	160	30	161	2	80.2
2014	K-80	20	160	40	121	2	94.0
2015	K-80	20	160	50	100	2	109.9
2016	K-80	20	240	30	161	5	140.0
2017	K-80	20	240	40	121	4	141.0
2018	K-80	20	240	50	100	2	145.1
2019	K-80	24	80	32	218	2	55.2
2020	K-80	24	80	42	166	2	60.0
2021	K-80	24	80	52	134	2	57.6
2022	K-80	24	160	32	218	2	91.4
2023	K-80	24	160	42	166	2	121.5
2024	K-80	24	160	52	134	2	142.0
2025	K-80	24	240	32	218	5	147.5
2026	K-80	24	240	42	166	2	158.0
2027	K-80	24	240	52	134	2	167.0
2028	West	16	80	28	111	2	37.0
2029	West	16	80	38	82	2	41.0
2030	West	16	80	48	96	2	50.4
2031	West	16	160	28	111	2	70.4
2032	West	16	160	38	82	2	78.1
2033	West	16	160	48	96	2	93.5
2034	West	16	240	28	111	2	87.1
2035	West	16	240	38	82	3	97.5
2036	West	16	240	48	96	5	117.5
2037	West	20	80	30	161	2	43.9
2038	West	20	80	40	121	2	48.6
2039	West	20	80	50	100	2	41.5
2040	West	20	160	30	161	3	69.5

Table 3.10 The results of Experiment Two (cont.)

CODE	EPOXY TYPE	d (mm)	l (mm)	e (mm)	b (mm)	FAILURE MODE	UTL mea. (kN)
2041	West	20	160	40	121	2	88.3
2042	West	20	160	50	100	2	108.5
2043	West	20	240	30	161	2	104.1
2044	West	20	240	40	121	2	111.4
2045	West	20	240	50	100	2	156.2
2046	West	24	80	32	218	2	46.6
2047	West	24	80	42	166	2	47.1
2048	West	24	80	52	134	2	48.6
2049	West	24	160	32	218	2	72.3
2050	West	24	160	42	166	2	87.6
2051	West	24	160	52	134	2	135.9
2052	West	24	240	32	218	2	121.4
2053	West	24	240	42	166	2	128.0
2054	West	24	240	52	134	2	171.3
2055	2005	16	80	28	111	2	57.4
2056	2005	16	80	38	82	2	60.0
2057	2005	16	80	48	96	1	50.4
2058	2005	16	160	28	111	2	76.3
2059	2005	16	160	38	82	4	101.0
2060	2005	16	160	48	96	5	124.6
2061	2005	16	240	28	111	2	115.8
2062	2005	16	240	38	82	2	132.0
2063	2005	16	240	48	96	5	154.0
2064	2005	20	80	30	161	2	60.2
2065	2005	20	80	40	121	2	59.7
2066	2005	20	80	50	100	2	79.4
2067	2005	20	160	30	161	2	137.0
2068	2005	20	160	40	121	2	104.8
2069	2005	20	160	50	100	2	169.0
2070	2005	20	240	30	161	2	138.0
2071	2005	20	240	40	121	5	147.0
2072	2005	20	240	50	100	2	175.0
2073	2005	24	80	32	218	1	62.6
2074	2005	24	80	42	166	1	63.7
2075	2005	24	80	52	134	1	60.5
2076	2005	24	160	32	218	3	133.1
2077	2005	24	160	42	166	3	130.5
2078	2005	24	160	52	134	2	170.7
2079	2005	24	240	32	218	3	154.0
2080	2005	24	240	42	166	4	179.4
2081	2005	24	240	52	134	2	206.2

Table 3.11 Summary of the result for Experiment Four

Code	Connection Type	UTL (kN)	Failure mode	Deflection (mm)	MC (%)	Density (kg/m^3)	MOE (GPa)
4001	control	113.0	S-P/T	0.258	12.1	501	5.54
4002	reinforced	120.4	S-P/Spt.	0.276	12.3	496	5.74
4003	control	102.0	S-P/T	0.206	11.9	481	6.11
4004	reinforced	116.5	S-P/Spt.	0.268	12.0	505	6.32
4005	control	106.6	S-P/T	0.217	12.4	496	4.73
4006	reinforced	137.3	S-P/Spt.	0.35	12.2	509	6.50
4007	control	136.8	S-P/T	0.331	11.8	484	7.15
4008	reinforced	155.9	S-P/T/Lo	0.541	12.0	485	7.54
Avg.	-	123.6	-	0.306	12.1	495	6.20

Note: 1. UTL = test value of ultimate tensile load (kN).

2. All of the specimens in Experiment Four failed with splitting in the timber around the connection and the steel rod pulling out. The failures are classified as follows:

   S-P = Type 2 failure mode, wood split around the connection and the steel rod pull out.

   T = fail at the test end.

   Spt. = fail at the support end.

   Lo = wood splits across the long edge.

3. MC = moisture content in the specimens.

CHAPTER FOUR

ANALYSIS OF SHORT DURATION EXPERIMENTS

4.1 FAILURE MODES

4.1.1 Definitions and Descriptions

Although each specimen ruptured differently in the short duration experiments, all of the specimens can be classified into five different failure modes defined as follows:

Type 1 failure mode: The steel bar pulls out without any obvious splitting in the glulam timber. This failure occurs in the epoxy-wood interface mainly caused by shear failure of the wood. The bond between steel and epoxy is intact (Figure 4.1).

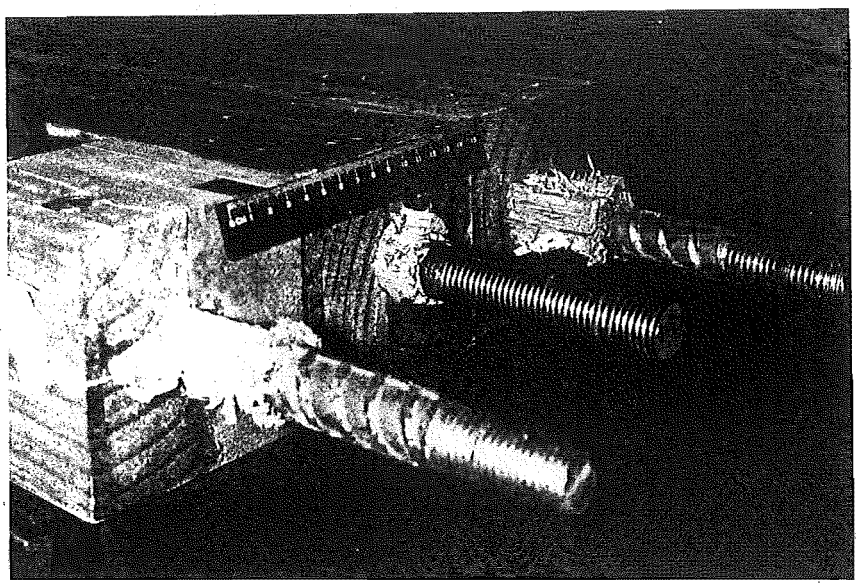

Figure 4.1 (a) Type 1 failure mode in wet specimens

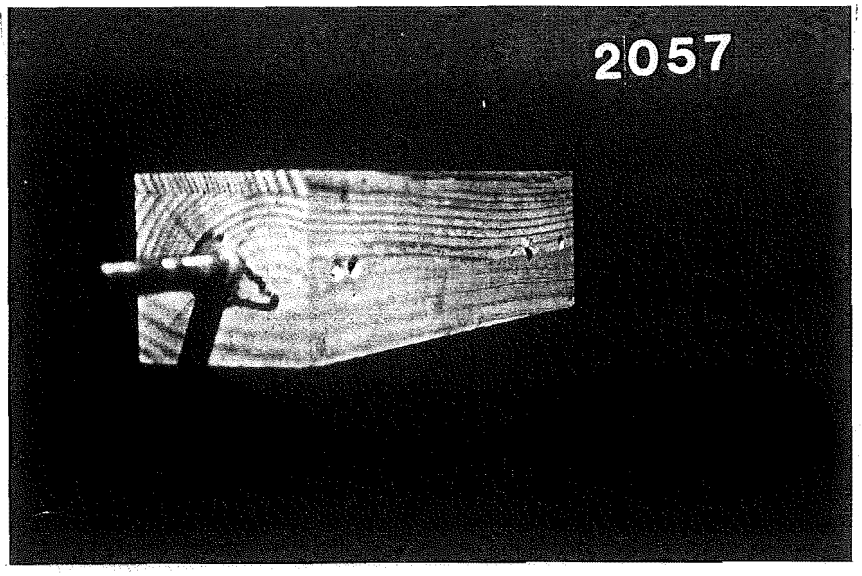

Figure 4.1 (b) Type 1 failure mode in the specimens with Araldite 2005 epoxy

Type 2 failure mode: The glulam timber around the connection splits and the steel bar pulls out from the epoxy confinement (Figure 4.2).

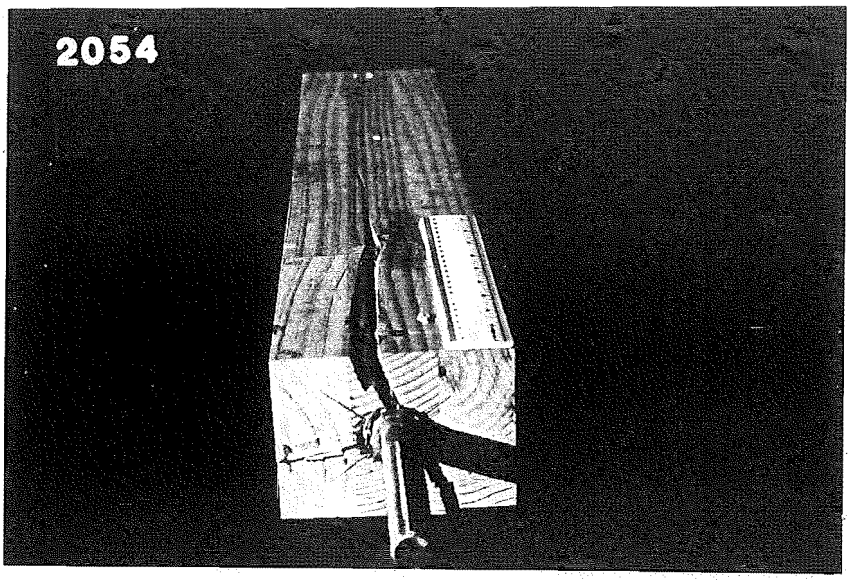

Figure 4.2 (a)Type 2 failure mode in a dry specimen

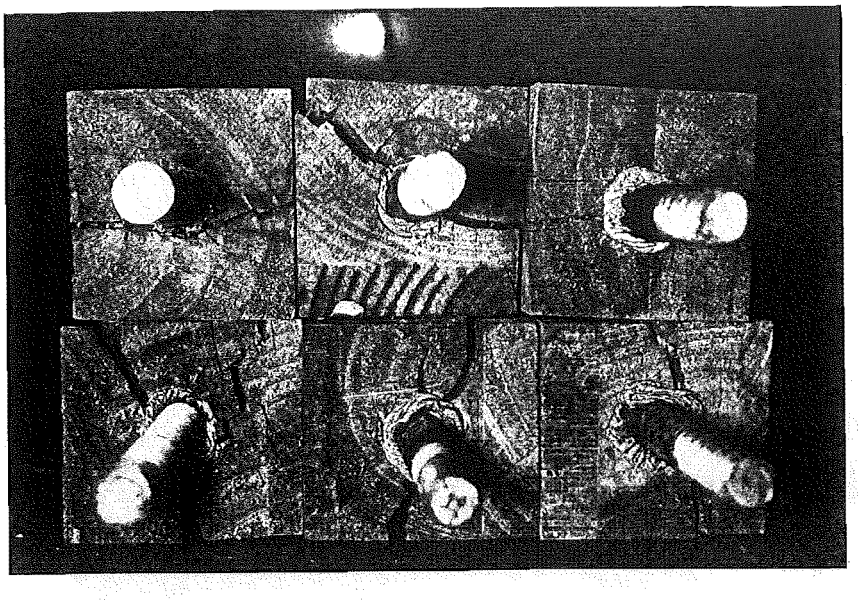

Figure 4.2 (b) Type 2 failure mode in wet specimens

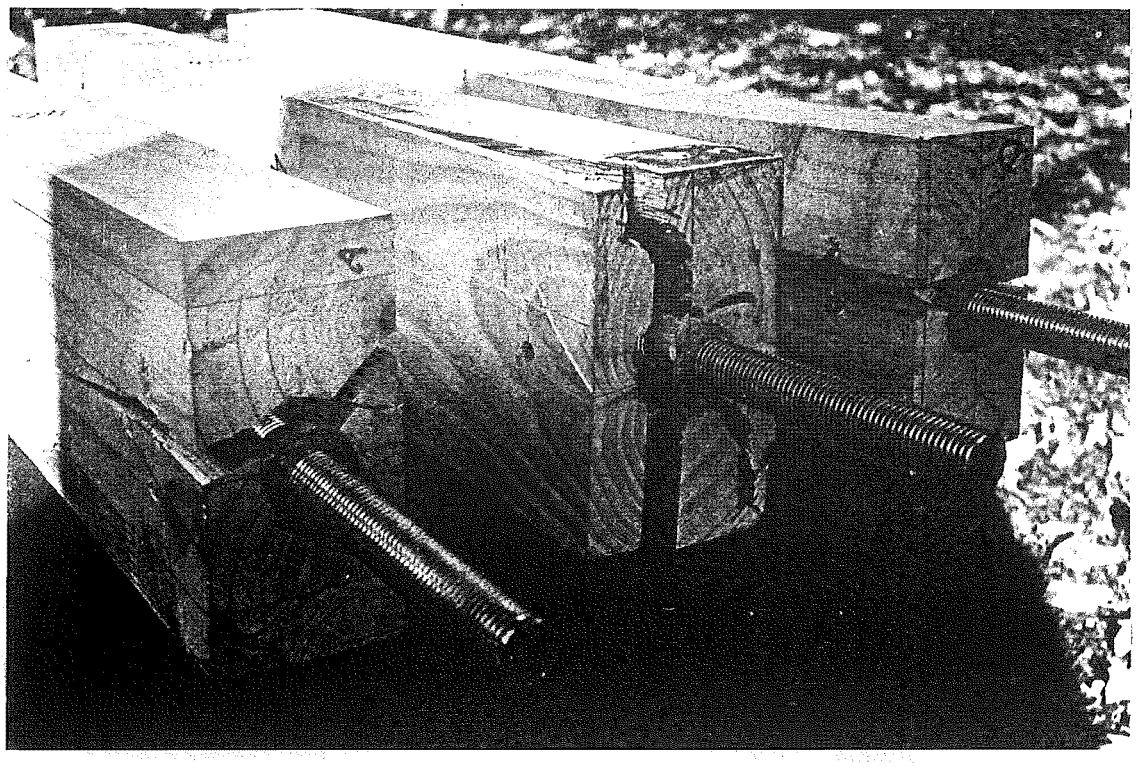

Figure 4.2 (c) Type 2 failure mode in a rectangular specimen. The middle specimen has transverse reinforcement to prevent splitting in the short direction.

Type 3 failure mode: The glulam timber fractures at the end of the steel rod across the cross-section and the connection remains intact (Figure 4.3).

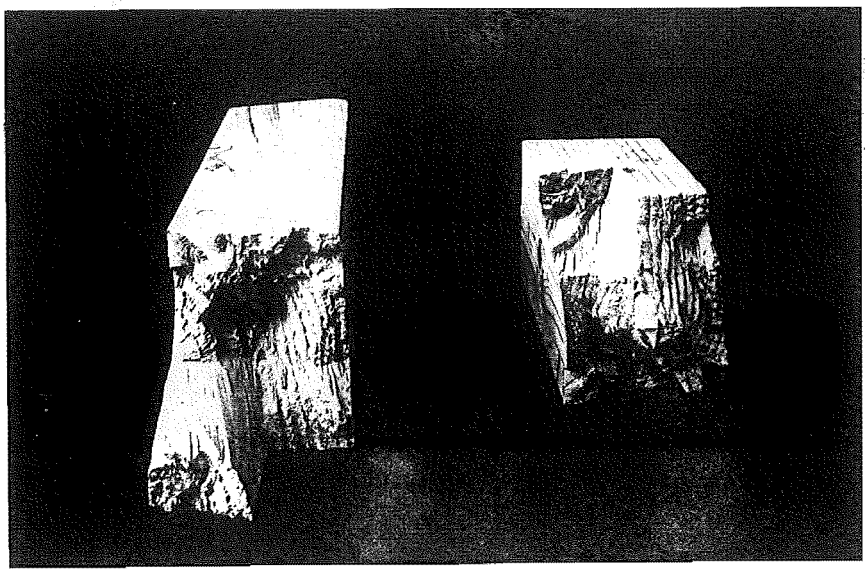

Figure 4.3 Type 3 failure mode

Type 4 failure mode: This category is a combination of pull-out, splitting and wood fracture. It indicates that both Type 2 and Type 3 failure modes occur simultaneously during the test. In this failure mode there is a split along the wood grain and a fracture across the cross-section at the inner end of steel bar (Figure 4.4).

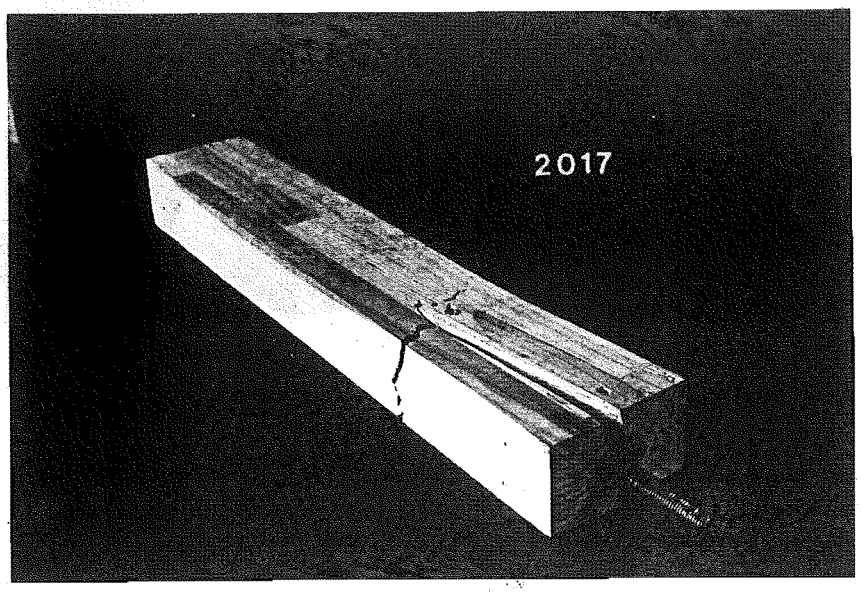

Figure 4.4 Type 4 failure mode

Type 5 failure mode: The glulam timber fractures across the cross-section in the middle portion of the specimen remote from the steel rod (Figure 4.5).

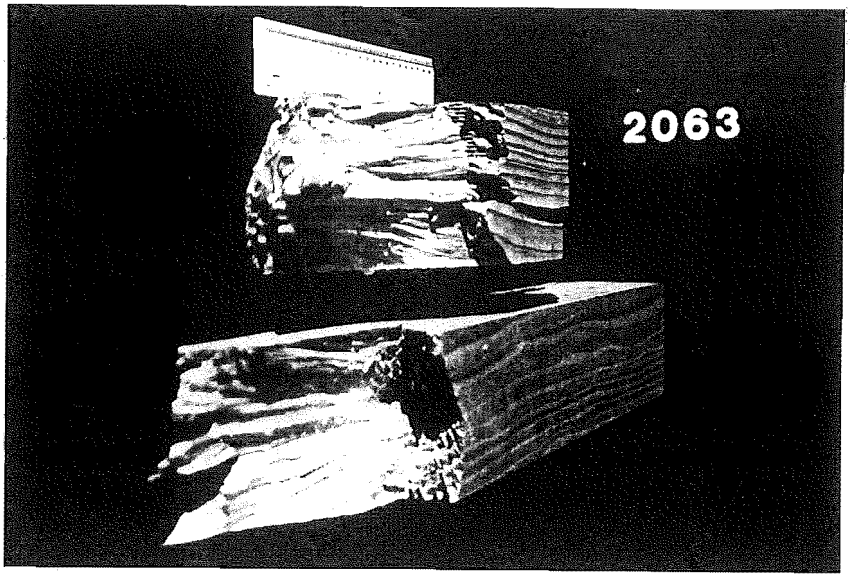

Figure 4.5 Type 5 failure mode

4.1.2 Distribution of Failure Modes in the Experiments

Tables 4.1 (a), (b) and (c) show the failure mode distribution in Experiments One and Two. For Experiment Four, only Type 2 failure mode occurred.

Table 4.1 (a) Distribution of failure modes in Experiment One

Type of Failure Mode	Number of Specimens					
	Dry specimens			Wet specimens		
	Threaded rod	Deformed bar	Total in dry	Threaded rod	Deformed bar	Total in wet
1	0 (-)	0 (-)	0 (-)	5 (8%)	8 (12%)	13 (20%)
2	27 (42%)	32 (50%)	59 (92%)	20 (31%)	17 (26%)	37 (57%)
3	4 (6%)	0 (-)	4 (6%)	6 (9%)	5 (8%)	11 (17%)
4	1 (2%)	0 (-)	1 (2%)	0 (-)	1 (2%)	1 (2%)
5	0 (-)	0 (-)	0 (-)	1 (2%)	1 (2%)	2 (4%)
Total	32 (50%)	32 (50%)	64 (100%)	32 (50%)	32 (50%)	64 (100%)

Note: The values in brackets are the ratios of number of failures in the specific failure mode to total number of the dry or wet specimens, presented in percentage.

Table 4.1 (b) Distribution of failure modes in Experiment Two in terms of different epoxies and embedment lengths

Failure Modes	Number of Specimens									Total
	Epoxy type									
	K-80			West System			Araldite 2005			
	Embedment length (mm)									
	80	160	240	80	160	240	80	160	240	
1	0	0	0	0	0	0	3	0	0	3 (3.7%)
2	9	9	6	9	8	7	6	5	6	65 (80.2%)
3	0	0	0	0	1	1	0	2	1	5 (6.2%)
4	0	0	1	0	0	0	0	1	1	3 (3.7%)
5	0	0	2	0	0	1	0	1	1	5 (6.2%)
Total	9	9	9	9	9	9	9	9	9	81 (100%)

Table 4.1 (c) Distribution of failure modes in Experiment Two in terms of different epoxies and edge distances

Failure Mode	Number of Specimens									Total
	Epoxy type									
	K-80			West System			Araldite 2005			
	Edge distance (mm)									
	d/2 +20	d/2 +30	d/2 +40	d/2 +20	d/2 +30	d/2 +40	d/2 +20	d/2 +30	d/2 +40	
1	0	0	0	0	0	0	1	1	1	3 (3.7%)
2	7	8	9	8	8	8	6	4	7	65 (80.2%)
3	0	0	0	1	1	0	2	1	0	5 (6.2%)
4	0	1	0	0	0	0	0	2	0	3(3.7%)
5	2	0	0	0	0	1	0	1	1	5(6.2%)
Total	9	9	9	9	9	9	9	9	9	81 (100%)

4.1.3 Analysis of Failure Modes

1. Type 1 failure mode

For Experiment One, Type 1 failure mode occurred only in the wet test specimens. However, in Experiment Two some specimens using Araldite 2005 epoxy also failed with Type 1 failure mode. In Experiment One, the failure occurred at the interface between wood and epoxy. This implies that the wood is much more sensitive to the wet environment than the epoxy or the steel. The failure was caused mainly by the shear failure in the wood (Figure 4.1 (a)). In Experiment Two, the failure mode differed slightly; resulting in a shear failure in the wood and larger plug of wood extracted together with the steel rod and the epoxy (Figure 4.1 (b)). No obvious shear failure occurred in the epoxy-wood interface.

The wet specimens in Experiment One had been exposed to a dry-wet cycling environment for 150 days (Table 3.8) before testing. The moisture content in the wood changed with the change of the environmental conditions, causing shrinkage and swelling in the wood; the dimensions of the wood around the connection changed. The dimensions of the epoxy and steel rod did not change. This resulted in stress concentration at the interface of the wood and the epoxy. This stress concentration could produce adhesive fracture and interface de-bonding. The shear strength in the wood also decreased when the moisture content of the wood increased. The New Zealand Timber Structure Standard (NZS 3603:1993) shows a significant difference in shear strength between the wet and dry wood. Obviously, if the shear strength between epoxy and wood or the shear strength in wood were less than the overall strength of the bond between epoxy and steel, Type 1 failure mode would occur.

A similar explanation could be applied for Type 1 failure mode in the specimens with Araldite 2005 epoxy in Experiment Two. It can be seen from Table 4.1 (b) that only 3 specimens with the shortest embedment length (80 mm) failed in this mode. This implies that the shear stress in wood around the connection could be higher than the shear strength of the wood due to short embedment length, but lower than the strength of epoxy bonding. Therefore, the wood shear failure around the bar occurred. In general, Type 1

failure mode was mainly caused by the stress concentration in the connection and the reduction of shear strength in the wood.

2. Type 2 failure mode

Type 2 failure mode was the most common failure in the short duration experiments and occurred mostly in the regions near the outer end of the specimen. Wood splitting occurred when the specimen was subjected to a tensile load and the load reached a certain level. With increasing the tensile load, the wood splitting developed both along the wood grain and over the cross-section, enlarging the embedment hole and causing the failure with the steel bar pulling out. With this failure mode the bond between the epoxy and the wood remained intact, but the bond between the epoxy and the steel was destroyed (Figure 4.2).

In Experiment One, Type 2 failure mode occurred more often in the connection with deformed reinforcing bar than with threaded rod connection. The greater number of Type 2 failure mode in deformed bar connections can be attributed to their different geometry as shown in Figure 4.6. The difference between bar types is explained further in section 4.2.2.

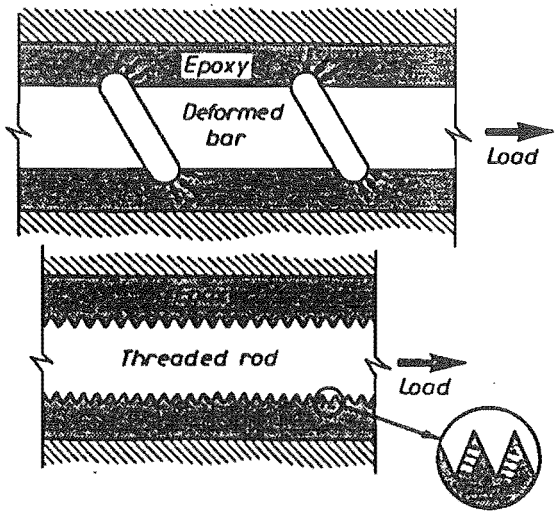

Figure 4.6 The geometrical characteristics of the threaded rod and the deformed bar (Townsend, 1990)

In Experiment Four, all specimens failed with Type 2 failure mode; the experiment was designed to obtain the Type 2 failure mode so that the effect of the steel reinforcement on the connection could be investigated. Although all specimens failed with Type 2 failure mode, none failed with wood splitting in the reinforced direction. Specimens with reinforcement failed either in the support end (specimens 4002, 4004, 4006) or fractured in the long direction of the cross-section (Figure 4.2 (c)). This indicates that the strength of the connection could be increased by preventing the wood from splitting. Type 2 failure mode could be caused by the stress concentrations and high transverse tensile stress at the outer end of the embedment region.

3. Type 3 failure mode

Type 3 failure mode occurred at the inner end of the embedment. The wood fractured over the cross-section but the epoxied steel connection remained undamaged. This failure was the tensile failure of the wood caused by high magnitude of the tensile stress and the stress concentration due to the presence of the embedment hole. It is of significance that a total of 15 Type 3 failures occurred but only 2 Type 5 failures in Table 4.1 (a). Further finite element analysis shows that both tensile stress in the longitudinal direction and shear stress in the interfaces are highest at the end of the embedment, confirming that Type 3 failure mode was caused by the stress concentration and the reduced cross-section at the inner end of the embedment.

4. Type 4 failure mode

Type 4 failure mode is a combination of Type 2 and Type 3 failure modes. The failure generally occurred along the wood grain through the embedment and over the cross-section at the inner bar end. It appears that Type 2 and Type 3 failures can develop simultaneously.

5. Type 5 failure mode

Type 5 failure mode was rare and when occurring, being located at the middle section of the specimen; it is a tensile failure in the wood without any damage in the

connections. Only 2 specimens failed with this mode in Experiment One and 5 specimens in Experiment Two.

6. Summary

In general, Type 2 failure mode was the most common one in the short duration experiments. Comparing wet and dry specimens in Experiment One, Type 1 failure mode often occurred in the wet specimens but not in the dry specimens. The failure modes varied among the different epoxies used in Experiment Two, revealing varying properties of epoxies in the connections.

4.2 INFLUENCE FACTORS

4.2.1 Environmental Effects

A comparison of the test results between the dry and wet specimens from Experiment One is given in Table 4.2. It shows that the strength decreased after the connection was exposed to a severe wet and dry cycling environment for a period of 150 days. The average tensile strength of the wet specimens was 23.8% less than the strength of the dry specimens.

Experiment One displays that the moisture content has a great influence on the tensile strength of the connection; it is important to consider any possible moisture content influence during design of timber structures. Further study and experiments might be needed to identify whether the high moisture content itself or the moisture content fluctuation has a major effect on the tensile strength.

Table 4.2 Ultimate tensile load of dry and wet specimens in Experiment One

Moisture Condition	Average Ultimate Tensile Load (kN)
Dry	80.7 kN
Wet	61.5 kN
Average	71.1 kN
Difference (%)	23.8%

Note: Difference (%) = (dry - wet) / dry x 100%

4.2.2 Effect of Steel Rod Surface Geometry

The effect of the steel rod surface was investigated in Experiment One. Table 4.3 shows that the average ultimate tensile load is 78.7 kN for the specimen with the threaded rod connection, and 63.4 kN for the deformed bar connection. This gives that the average pull-out strength of the specimens using the deformed bars was 19.4% less than that for the threaded rod connections and is similar for wet and dry specimens. Reasons for the difference can be explained as follows:

1. The ribs on the deformed bar can transfer the tensile load into a force perpendicular to the surface of the hole to enlarge the embedment hole. This could trigger the splitting of the wood during tensile loading.

2. The interface between the steel and the epoxy is stronger in the threaded rod connection than in the deformed bar connection due to the bolt-nut-like connection in the threaded rod connection.

3. There is more contact surface between the steel and the epoxy in the threaded rod connection than in the deformed bar connection.

Table 4.3 Ultimate tensile load in the connection using different type of bar

Bar Type	Average Ultimate Tensile Load (kN)		
	Moisture condition		Average
	Dry	Wet	
Threaded rod	90.0	67.5	78.7
Deformed bar	71.3	55.4	63.4
Average	80.7	61.5	71.1
Difference (%)	20.8%	17.9%	19.4%

Note: Difference (%) = (threaded - deformed) / threaded x 100%

4.2.3. Effects from Using Different Epoxies

It can be seen from Table 4.4 (a), for the dry specimens in Experiment One, the average ultimate tensile load for the connections using West System was 15.4% less than for K-80 epoxy. For the wet specimens, the tensile strength of the connection with West System epoxy was only 5.4% less than for K-80 epoxy. For Experiment Two, three epoxies were used. It can be seen from Table 4.4 (b), the average ultimate tensile load of the connection using West System was 13.1% less than for K-80. This is similar to the Experiment One result. For Araldite 2005, the average ultimate tensile load was 17.1% higher than for K-80 epoxy.

In general, the Araldite 2005 epoxy has the highest pullout strength among these epoxies and K-80 epoxy has a higher pullout strength than West System epoxy. K-80 epoxy is more sensitive to water than West System epoxy, therefore the change in the pullout strength of K-80 between dry and wet specimens was greater than for the West System. The West System epoxy may have better water resistance properties than K-80 epoxy.

Table 4.4 (a) Ultimate tensile load between different type of epoxy in Experiment One

Epoxy Type	Average Ultimate Tensile Load (kN)		
	Moisture condition		Average
	Dry	Wet	
West System	73.9	59.8	66.9
K-80	87.4	63.2	75.3
Average	80.7	61.5	71.1
Difference (%)	15.4%	5.4%	11.1%

Note: Difference (%) = (K80 - West System) / K80 x 100%

Table 4.4 (b) Ultimate tensile load using different types of epoxy in Experiment Two

Epoxy Type	Average Ultimate Tensile Load (kN)									
	Embedment length (mm)			Bar diameter (mm)			Edge distance (mm)			Aver-age
	80	160	240	16	20	24	d/2+ 20	d/2+ 30	d/2+ 40	
K-80	53	101.1	140.3	84.8	98.4	111.1	85.9	100.8	107.7	98.1
West	45.0	89.3	121.6	74.7	85.8	95.4	72.5	80.8	102.6	85.3
2005	61.5	127.4	155.7	96.8	118.9	129.0	103.8	108.7	132.2	114.9
Average	53.2	106.0	139.2	85.5	101.0	111.8	87.4	96.7	114.2	99.5
Ratio[1] (%)	15.1	11.7	13.3	11.9	12.8	14.1	15.6	19.8	4.7	13.1
Ratio[2] (%)	-16.0	-26.0	-10.1	-14.2	-20.8	-16.1	-20.8	-7.8	-22.7	-17.1

Note: K-80 = Araldite K-80 epoxy.

West = West System epoxy.

2005 = Araldite 2005 epoxy.

Ratio[1] (%) = (K80 - West System) / K80 x 100%

Ratio[2] (%) = (K80 -2005) / K80 x 100%

4.2.4 Effect of Different Embedment Length

Table 4.5 (a) shows that the ratio of the average ultimate tensile load for embedment lengths of 10d to 5d was 1.80 in Experiment One; similar trends were obtained between the wet and dry specimens and between the threaded rod and the deformed reinforcing bar connection. Table 4.5 (b) shows the results from Experiment Two, the ratio of the average ultimate tensile load for embedment length of 160 mm to 80 mm was 1.99. However the ratio was 2.62 when the embedment length increased from 80 mm to 240 mm. The results from Experiment Four are presented in Table 4.5 (c).

Table 4.5 (a) Ultimate tensile load for different embedment lengths in Experiment One

Embedment Length (mm)	Average Ultimate Tensile Load (kN)				
	Moisture condition		Bar type		Average
	Dry	Wet	Threaded	Deformed	
5d	58.3	43.0	57.6	43.8	50.7
10d	103.0	79.9	99.9	83.0	91.4
Average	80.7	61.5	78.7	63.4	71.1
Ratio (10d/5d)	1.77	1.86	1.73	1.89	1.80

In order to compare the results among the different short duration experiments, Table 4.5 (d) was constructed based on the same ratio of the embedment length to the bar diameter since the different ratios were used in the different experiments. In Table 4.5 (d), all different embedment lengths used in the experiments are converted in terms of the ratios of 5d, 10d and 15d. No conversion was made for Experiment One since the designed embedment lengths were 5d and 10d. For Experiment Two, the average ultimate

tensile load (UTL) values for bar diameter of 20 mm and 24 mm were converted from Table 4.5 (b) using interpolation. The original data for Experiment Four is also listed in Table 4.5 (d).

Table 4.5 (b) Ultimate tensile load for different embedment lengths in Experiment Two

Embed-ment Length (mm)	Average Ultimate Tensile Load (kN)						
	Epoxy type			Bar diameter (mm)			Average
	K-80	West System	Araldite 2005	16	20	24	
80	53.0	45.0	61.5	47.2	56.5	55.8	53.2
l/d ratio	4	4	4	5	4	3.3	
160	101.1	89.3	127.4	90.5	106.8	120.6	106.0
l/d ratio	8	8	8	10	8	6.7	
240	140.3	121.6	155.7	118.7	139.8	159.2	139.2
l/d ratio	12	12	12	15	12	10	
ratio[1]	1.91	1.98	2.07	1.92	1.89	2.16	1.99
ratio[2]	2.65	2.70	2.53	2.51	2.47	2.85	2.62

Note: ratio[1] = embedment 160 / embedment 80.

ratio[2] = embedment 240 / embedment 80.

l/d ratios in column 2,3,4 are the values calculated from the average bar diameter.

Table 4.5 (c) Ultimate tensile load for different embedment lengths in Experiment Four

Embedment (mm)	Ratio l/d	UTL (kN)	Remarks
200	10	114.6	average of all control specimens.
200	10	155.9	specimen 4008, failed in the reinforced end.
350	17.5	124.7	average of specimen 4002, 4004 and 4006.
ratio 17.5d/10d	1.09		

Note: The specimen failed in the end with transverse reinforcement (specimen 4008) is not considered in the ratio calculation.

In general, the results from all of the short duration experiments have similar trends. The results suggest that:

1. The ultimate tensile load is not directly proportional to the embedment length especially for the larger embedment length as shown in Table 4.5 (b). Therefore, the traditional method using the equation

$$\tau = \frac{F}{\pi dl} \qquad (4.1)$$

to calculate the shear stress of the bond can only be considered as a approximation,

where, F = tensile load applied in the steel rod (N)
d = nominal diameter of the steel bar (mm)
l = embedment length (mm)
τ = shear stress (MPa)

2. A threshold of the embedment length might exist beyond which further increasing the embedment length would not significantly increase the tensile strength of the connection.

The threshold of the embedment length depends on the overall strength of the connection, stress concentration and probability of the wood splitting around the connection. Further finite element analysis in Chapter Seven shows that increasing the embedment length will decrease the magnitude of the shear stress and transverse tensile stress but hardly improve the shear and tensile stress concentrations, which cause fracture or splitting of the wood.

To develop an empirical formula following analysis of the experiment results, the relationship between UTL and the embedment length can be proposed in the form of

$$F = Cx\,l^{\theta_1} \qquad (4.2)$$

where F = ultimate tensile load

C = a value which includes all factors involved except the embedment length.

l = embedment length

θ_1 = exponent to the embedment length

The θ_1 value can be calculated from the experiment results. For example, in Experiment One, for 16 mm bar diameter, if the embedment length increases from 5d to 10d, the θ_1 value can be calculated from $(\frac{10d}{5d})^{\theta_1} = 1.76$, hence θ_1 = 0.816. The exponent θ_1 corresponding to each individual embedment length ratio is calculated and listed in Table 4.5 (d). The θ_1 value for Experiment Four is much less than the others, indicating that the increased embedment length is likely beyond the threshold. Therefore, the range of the embedment length must be specified for application of the empirical formula. It should be noted, however that the small number of the test specimens make the data from Experiment Four somewhat less significant. 0.86 as the average value of θ_1 from Experiment One and Two could be used to develop the empirical formula.

Table 4.5 (d) Comparison of the average UTL with different embedment length in the short duration experiment

Embedment Length	Average Ultimate Tensile Load (kN)					
	Experiment One		Experiment Two			Experiment Four
	Bar diameter (d)		Bar diameter (d)			Bar diameter (d)
	16	24	16	20	24	20
5d	32.7	68.7	47.2	*69.1*[1]	*88.2*	-
10d	57.5	125.4	90.5	*123.3*	159.2	114.6[2]
15d	-	-	118.7	-	-	-
17.5d	-		-	-	-	124.7
10d/5d	1.76	1.83	1.92	1.78	1.80	-
θ_1	0.816	0.872	0.941	0.832	0.848	-
15d/5d	-	-	2.51	-	-	-
θ_1	-	-	0.838	-	-	-
17.5d/10d	-	-	-	-	-	1.09
θ_1	-	-	-	-	-	0.15

Note: 1. All figures in Italic are the converted values by interpolation.

2. The value was the average value from all control specimens (Specimen 4001, 4003,4005 and 4007).

4.2.5 Effect of Different Bar Diameters

Tables 4.6 show the difference of the average ultimate tensile load in terms of different steel bar diameters. In Table 4.6 (a), the values without brackets are the test results obtained directly from Experiment One. For bar diameter 24 mm, the values in brackets are the corrected values, which correspond to the same embedment lengths as used for the 16 mm bar diameter. These are two thirds of the value from the experiment results as the average embedment length for the 16 mm diameter bar is two thirds of that for the 24 mm bar. Based on the corrected values, in terms of the same embedment

length, the ratio of the average tensile load of 24 mm diameter to 16 mm diameter is 1.43. The results from Experiment Two are listed in Table 4.6 (b). The ratio of the average UTL for bar diameter 20 to bar diameter 16 is 1.18 and for bar diameter 24 to 16, the ratio is 1.31. This indicates that the ratio increase in strength is slightly less than that in bar diameter.

Table 4.6 (a) Ultimate tensile load for different steel bar diameters in Experiment One

Bar Diameter (mm)	Average Ultimate Tensile Load (kN)				
	Moisture condition		Bar type		Average
	Dry	Wet	Threaded	Deformed	
16	52.6	37.6	52.6	37.6	45.1
24	108.7 (72.5)	85.4 (56.9)	104.9 (69.9)	89.2 (59.5)	97.1 (64.7)
Ratio	1.38	1.51	1.33	1.58	1.43

Note: 1. Ratio = (the corrected value for bar diameter 24) / (the test value for bar diameter 16).

2. Values without bracket are the original test values.

3. Values in brackets are the corrected values (2/3 times test values).

Table 4.6 (c) is constructed based on the experiment results (Table 4.6 (a) and (b)) to analyse the relationship between the UTL and the steel bar diameter; the corrected UTL values are used for Experiment One. It can be seen from Table 4.6 (c) that the increase of the ultimate tensile strength is not directly proportional to the increase of the steel bar diameter. If the bar diameter increases from 16 mm to 24 mm in Experiment One, this gives an increase of the tensile strength expressed by the ratio of steel bar diameters $(\frac{24}{16})^{\theta_2} = 1.43$, hence, the exponent θ_2 = 0.882. The exponent θ_2 corresponding the different steel bar diameter ratio was calculated and listed in Table 4.6 (c). All θ_2 values are less than 1 as the ratio increase in strength is less than that in bar diameter. The average value of θ_2 will be used in the empirical equation.

Table 4.6 (b) Ultimate tensile load for different steel bar diameters in Experiment Two

Bar Diameter (mm)	Average Ultimate Tensile Load (kN)									
	Epoxy type			Embedment length (mm)			Edge distance (mm)			Aver-age
	K-80	West	2005	80	160	240	20+d/2	30+d/2	40+d/2	
16	84.8	74.7	96.8	47.2	90.5	118.7	72.7	86.7	97.0	85.5
20	98.4	85.5	118.9	56.5	106.8	139.8	91.3	95.2	116.6	101.0
24	111	95.4	129.0	55.8	120.6	159.2	98.2	108.4	128.9	111.8
ratio[1]	1.16	1.14	1.23	1.20	1.18	1.18	1.26	1.09	1.20	1.18
ratio[2]	1.31	1.28	1.33	1.18	1.33	1.34	1.35	1.25	1.33	1.31

Note: Ratio[1] = Bar diameter 20 / Bar diameter 16

Ratio[2] = Bar diameter 24 / Bar diameter 16

Table 4.6 (c) Comparison of the ratio of UTL for different bar diameter

Bar Diameter (mm)	Average Ultimate Tensile Load (kN)		
	Experiment One	Experiment Two	Average
16	45.1	85.5	
20	-	101.0	
24	64.7	111.8	
Ratio = 20/16 = 1.25	-	1.18	1.18
θ_2	-	0.747	0.747
Ratio = 24/16 = 1.5	1.43	1.31	1.37
θ_2	0.882	0.661	0.776
Average	-		0.76

4.2.6 Effect of Edge Distance

It can been seen in Table 4.7 (a) that the ratio of the average ultimate tensile load for edge distance of 1.5d to 2.25d is 1.21; the ratio for dry and wet specimens is same.

Townsend (1990) found that the tensile strength was proportional to $(r_e)^{0.5}$, where the r_e is the ratio of the edge distance to the bar diameter. In Experiment One, if the edge distance changes from 2.25d to 1.5d, this would predict a ratio of the ultimate tensile load for the two levels of edge distance as follows:

$$\left(\frac{2.25d}{1.5d}\right)^{0.5} = 1.22$$

This is essentially the same as the observed ratio of 1.21, supporting Townsend's findings. Similarly, the results for Experiment Two are shown in Table 4.7 (b), where the top rows of ratio^1 and ratio^2 are the ratios obtained from the experiment, the bottom rows of ratio^1 and ratio^2 in brackets are the ratios calculated from Equation 3.1. For column 2 to column 4, the average bar diameter was used for the calculation. For example, using the average bar diameter of 20 mm, the ratio^2 of the edge distance is given as:

$$\left(\frac{d/2+40}{d/2+20}\right)^{0.5} = \left(\frac{50}{30}\right)^{0.5} = 1.29$$

This is close to the observed values from Experiment Two. In summary, the results from both Experiment One and Two affirm Townsend's findings on the ratio of edge distance.

Table 4.7 (a) Ultimate tensile load for different edge distances in Experiment One

Edge Distance	Average Ultimate Tensile Load (kN)		
	Moisture condition		Average
	Dry	Wet	
1.5d	73.0	55.6	64.3
2.25d	88.3	67.3	77.8
Average	80.7	61.5	71.1
Ratio	1.21	1.21	1.21

Note: Ratio = 2.25d / 1.5d

Table 4.7 (b) Ultimate tensile load for different edge distances in Experiment Two

Edge Distance (mm)	Average Ultimate Tensile Load (kN)						
	Epoxy			Bar diameter (mm)			Average
	K-80	West	2005	16	20	24	
d/2+20	85.9	72.5	103.8	72.7	91.3	98.2	87.4
d/2+30	100.8	80.8	108.7	86.7	95.2	108.4	96.8
d/2+40	107.7	102.6	132.2	97.0	116.6	128.9	114.2
ratio[1]	1.17 (1.15)	1.11 (1.15)	1.05 (1.15)	1.19 (1.16)	1.04 (1.15)	1.10 (1.15)	1.11 (1.15)
ratio[2]	1.25 (1.29)	1.42 (1.29)	1.27 (1.29)	1.33 (1.31)	1.28 (1.29)	1.31 (1.27)	1.31 (1.29)

Note:
1. ratio[1] = (d/2 + 30)/ (d/2 + 20)
2. ratio[2] = (d/2 + 40)/ (d/2 + 20)
3. Values in the brackets are the calculated values from Equation 3.1.

4.2.7 Effect of Different Hole Diameters

Table 4.8 shows that the average ultimate tensile load was 67.0 kN for the specimens with a hole diameter of 1.15d and 75.2 kN for the specimens with a hole diameter of 1.4d. Therefore the average pull-out strength for the hole diameter of 1.15d was 10.9% less than that for the hole diameter of 1.4d. Furthermore, the average pull-out strength for the hole diameter of 1.15d was 14.6% less than that for the hole diameter of 1.4d in the dry specimens, while there was only a 5.7% difference in wet specimens.

Table 4.8 Ultimate tensile load for different hole diameters in Experiment One

Hole Diameter	Average Ultimate Tensile Load (kN)		
	Moisture condition		Average
	Dry	Wet	
1.15d	74.3	59.7	67.0
1.4d	87.0	63.3	75.2
Average	80.7	61.5	71.1
Difference (%)	14.6	5.7	10.9

Note: Difference (%) = (1.4d - 1.15d) / 1.4d x 100%

Townsend (1990) found that the hole diameter was a major influence on tensile strength. In his findings, the tensile strength was proportional to $(r_h)^2$, where r_h is the ratio of the hole diameter to the bar diameter. For a change of the hole diameter from 1.4d to 1.15d, this would predict a reduction of the tensile strength in the ratio

$$(\frac{1.15}{1.4})^2 = 0.675$$

giving a difference of (1-0.675) x 100=32.5%. In Experiment One, the average difference was 10.9%, much less than that predicted by Townsend. The difference of 10.9% is a reduction ratio of 0.891, which would be predicted by an exponent of 0.585, i.e.

$$\left(\frac{1.15}{1.4}\right)^{0.585} = 0.891$$

4.2.8 Effect of Connection Reinforcement

The effect of transverse reinforcement was investigated in Experiment Four. During the test all of the control specimens failed with Type 2 failure mode at the test end of the steel connection. For specimens with reinforcement, only one (4008) failed at the test end with wood splitting across the longer edge, viz. the direction lacking reinforcement (Figure 4.2 (c)). The other three failed at the support end while the connection at the test end remain intact. Table 4.9 shows the difference and the ratio in the ultimate tensile load between the reinforced connection and the connection without reinforcement.

Table 4.9 Analysis of the effect of connection reinforcement in Experiment Four

Code	Connection Type	UTL (test) (kN)	UTL (cal.) (kN)	MC (%)	Density (kg/m^3)	MOE (GPa)	Diff. (kN)	Ratio (%)	Failure Mode
4001	control	113.0	108.4	12.1	501	5.54			S-P/T
4002	reinforced	120.4	189.8	12.3	496	5.74	7.4	6.5	S-P/Spt.
4003	control	102.0	108.4	11.9	481	6.11			S-P/T
4004	reinforced	116.5	189.8	12.0	505	6.32	14.5	14.2	S-P/Spt.
4005	control	106.6	108.4	12.4	496	4.73			S-P/T
4006	reinforced	137.3	189.8	12.2	509	6.50	30.7	28.8	S-P/Spt.
4007	control	136.8	108.4	11.8	484	7.15			S-P/T
4008	reinforced	155.9	153.4	12.0	485	7.54	19.1	14.0	S-P/T/Lo
Avg.	control	114.6	108.4	12.1	491	5.88			-
Avg.	reinforced	132.5	180.7	12.2	499	6.52	17.9	15.6	-

Note: 1. UTL (test) = the ultimate tensile load from the experiment.

2. UTL (cal.) = the calculated ultimate tensile load using Equation 4.7 with the corresponding geometry parameters and factors ($k_b = k_m = 1$, $k_e = 0.86$).

3. Diff. = Difference of test values of UTL between the reinforced and the corresponded control specimens.
4. Ratio = (UTL in reinforced - UTL in control) / UTL in control x 100%

It can be seen from Table 4.9 that the strength of the connection with transverse reinforcement is stronger than the corresponding control specimen. For some specimens (4002, 4004, 4006), although failures did not occur in the reinforced connection, the ultimate tensile loads for these connections should be greater than the values shown in the table because the failures occurred at the support end before the reinforced connection had reached its ultimate tensile strength. Although the size of the cross-section used in the experiment would not normally be used in the real structures, it displays an important effect that the steel reinforcement can effectively improve the strength of the connection by preventing the wood splitting around the connection.

Experiment Four shows that either increasing the edge distance or using steel rod reinforcement can prevent wood splitting failure around the connection. If the edge distance is limited by the geometry of the wood cross-section used in a structure, a steel rod reinforcement would be the best simple solution. The experimental results also indicate that if wood splitting dominates the failure, the tensile strength of the connection would not increase significantly by simply increasing the embedment length without consideration of how to prevent the wood splitting.

4.3 AN EMPIRICAL MODEL

A model can be developed using several different approaches, to quantify the strength of the single epoxy bonded steel connection under tensile load and to explain the failure phenomena. The fracture mechanics approach has been successful to analyse the fracture process where dominant features, such as a pre-existing crack, can be identified. Unfortunately, when considering the epoxy bonded connection, the fracture process involves different materials with different characteristics and the interactions of many mechanisms operating at different rates. The knowledge required for developing physical models is not yet sufficiently comprehensive, and furthermore the fracture

mechanics study of the connection is beyond the scope of this thesis. Likewise, the finite element analysis technique may not adequately cope with different failure modes and allow the development of a calculation formula to design connections. An empirical model was developed and all of five different failure modes were covered in the model.

Based on the results of the short duration experiments and previous concepts from Townsend (1990), Gerold (1992) and Crews (1993), the following formula can be formed:

$$F = 85.4 k_b k_e k_m l^{0.86} d^{0.76} (\frac{h}{d})^{0.5} (\frac{e}{d})^{0.5} \qquad (4.3)$$

where,

F = ultimate tensile load of the connection (N)

d = steel bar diameter in mm ($16 \leq d \leq 24$)

l = embedment length in mm ($5d \leq l \leq 15d$)

h = hole diameter in mm ($1.15d \leq h \leq 1.4d$)

e = edge distance from centre of steel bar in mm ($1.5d \leq e \leq 3d$)

k_b = bar type factor

k_e = epoxy factor

k_m = moisture content factor

The values of k_b, k_e and k_m are shown in Tables 4.10 and are based on the results from the short duration experiments using the dry specimens with K-80 epoxy and the threaded rod as references. The bar type factor k_b is calculated from the ratio of the average values of UTL between the threaded rod and the deformed reinforcing bar in Experiment One.

The epoxy factor k_e is based on both Experiments One and Two with K-80 as the reference epoxy. The ratio of average values for UTL between West System epoxy and K-80 epoxy is 0.846 in Experiment One and 0.869 in Experiment Two. The average

value of 0.86 is employed as the epoxy factor k_e for West System epoxy. The k_e value for Araldite 2005 epoxy is 1.17 calculated from the ratio of average values of UTL between Araldite 2005 and K-80 in Experiment Two.

Table 4.10 (a) Bar type factor k_b

Bar Type	Bar Type Factor k_b
Threaded rod	1
Deformed bar	0.79

Table 4.10 (b) Epoxy type factor k_e

Epoxy Type	Epoxy Type Factor k_e
K-80	1
West System	0.86
Araldite 2005	1.17

The moisture content factor k_m is the ratio of average values for UTL between the wet and dry specimens, a value of 0.75 is used as k_m for the specimens with moisture content over 25%. The factor k_m is based on Experiment One and no value was given for the moisture content range between 18% - 25%. The conservative value 0.75 may be used if the connection would be used in the moisture content range between 18% - 25%. Further study could investigate the moisture content influence to the epoxied steel connection under the long duration load.

Table 4.10 (c) Moisture content factor k_m

Moisture Content (%)	Moisture Content Factor k_m
< 18%	1
> 25%	0.75

All of the exponents in Equation 4.3 are derived from the results of Experiment One and Two and described in Section 4.2. The constant 85.4 is the best fit value from the results of the experiments. The Equation 4.3 can be further modified into a non-dimensionalized form. The form can be deduced from:

$$F = 85.4 k_b k_e k_m (\frac{l}{d})^{0.86} d^{0.86} (\frac{d}{20})^{0.76} 20^{0.76} (\frac{h}{d})^{0.5} (\frac{e}{d})^{0.5} \qquad (4.4)$$

to

$$F = 85.4 k_b k_e k_m 20^{0.76} (\frac{l}{d})^{0.86} (\frac{d^{0.86} d^{0.76}}{20^{0.86} 20^{0.76}}) 20^{0.86} (\frac{h}{d})^{0.5} (\frac{e}{d})^{0.5} \qquad (4.5)$$

Furthermore

$$F = (85.4 * 20^{0.76} * 20^{0.86}) * \frac{1}{1000} k_b k_e k_m (\frac{l}{d})^{0.86} (\frac{d}{20})^{1.62} (\frac{h}{d})^{0.5} (\frac{e}{d})^{0.5} \qquad (4.6)$$

Finally, the following equation is proposed to predict the strength of the connection subjected to tensile load:

$$F = 10.94 k_b k_e k_m (\frac{l}{d})^{0.86} (\frac{d}{20})^{1.62} (\frac{h}{d})^{0.5} (\frac{e}{d})^{0.5} \qquad (4.7)$$

where, F = ultimate tensile load of the connection (kN)

4.4 ESTIMATION OF THE EMPIRICAL MODEL

4.4.1 Comparison of the Short Duration Experiment Result and the Model Prediction

Using Equation 4.7, the predicted values of ultimate tensile load corresponding to each individual specimens were calculated and compared with the experiment results. A linear correlation was calculated using the measured UTL values from the experiments as X values and the predicted one as Y. The coefficient of simple determination r^2 (Neter, J., et. al., 1988) was calculated for Experiments One and Two separately. In Experiment One (Table 4.11 (a)), each particular combination of bar type, epoxy type and moisture content was classified and represented in a subgroup corresponding to the different k_b, k_e and k_m values. Eight subgroups were obtained. Similarly, Table 4.11 (b) was obtained for Experiment Two. The high values of r^2 in Tables 4.11 indicate that the empirical model agrees with the results from the short duration experiments. In addition, the results from Experiments One and Two are plotted in Figure 4.7 to Figure 4.9 with UTL values from the experiments as X values and predicted values from the model as Y. Similarly, it can be seen from the figures that the experiment values agree with the model's predicted values as judged by closeness of the data points to 45° line.

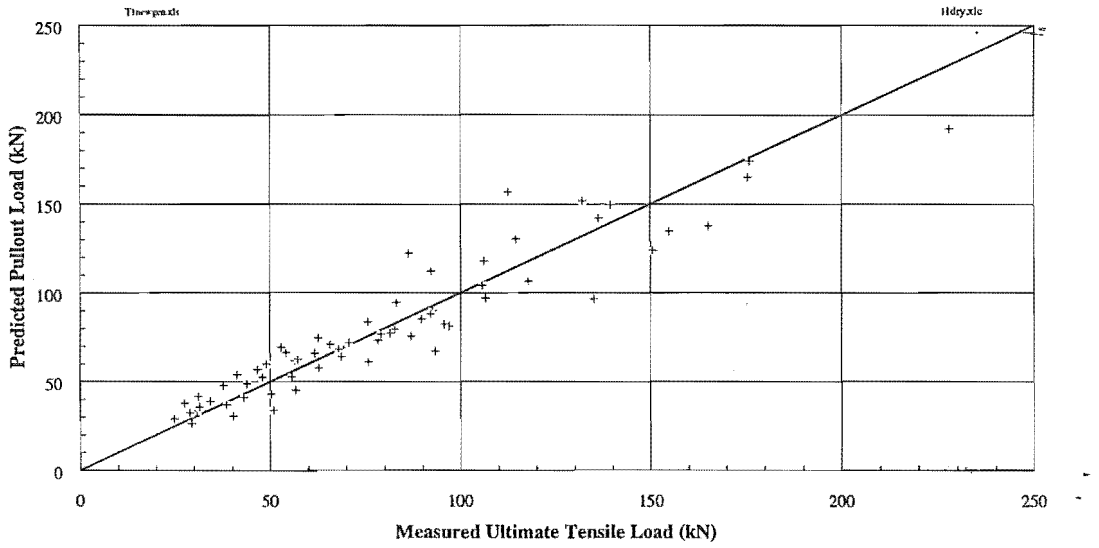

Figure 4.7 Estimation of the predicted values of UTL for dry specimens in Experiment One

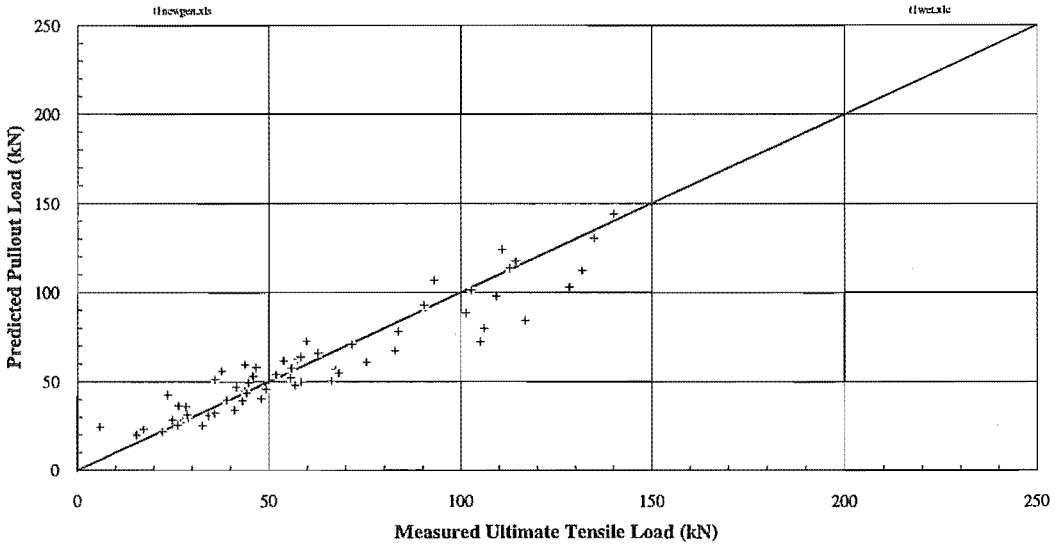

Figure 4.8 Estimation of the predicted values of UTL for wet specimens in Experiment One

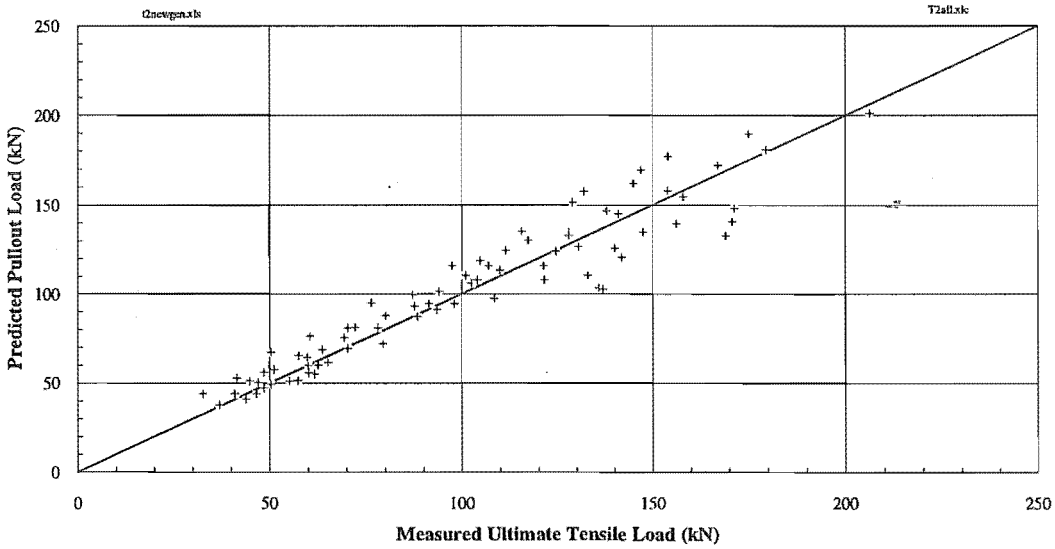

Figure 4.9 Estimation of the predicted values of UTL in Experiment Two

Table 4.11 (a) Estimation of the empirical model with Experiment One results

Subgroups	Contents	No. of Specimens	k_b	k_e	k_m	r^2
1	threaded/dry/WS	16	1	0.86	1	0.90
2	threaded/dry/K-80	16	1	1	1	0.90
3	deformed/dry/WS	16	0.79	0.86	1	0..87
4	deformed/dry/K-80	16	0.79	1	1	0.83
5	threaded/wet/WS	16	1	0.86	0.75	0.90
6	threaded/wet/K-80	16	1	1	0.75	0.97
7	deformed/wet/WS	16	0.79	0.86	0.75	0.92
8	deformed/wet/K-80	16	0.79	1	0.75	0.88
9	all of dry specimens	64	--	--	1	0.89
10	all of wet specimens	64	--	--	0.75	0.89
11	all specimens	128	--	--	--	0.89

Note:
1. threaded = the threaded steel rod connection.
2. deformed = deformed reinforcing bar connection.
3. WS = West System epoxy.
4. dry = the dry specimens.
5. wet = the wet specimens.

Table 4.11 (b) Estimation of the linear relationship between the experiment results and the model output in Experiment Two

Subgroups	Contents	No. of specimens	k_e	r^2
1	K-80	27	1	0.94
2	West System	27	0.86	0.91
3	Araldite 2005	27	1.17	0.87
4	All	81	--	0.91

Note: $k_b = k_m = 1$ for all subgroups.

4.4.2 Application to Multiple Bar Connections

In the short duration tensile load experiments, all specimens were constructed and tested as single epoxied steel rod connection. No tests were carried out with multiple bar connection. The beam splice testing results from Townsend (1990) were used to compare with the predicted values from both the Equation 4.7 and Townsend's equation (Townsend, 1990) shown as follows:

$$F = 9.2d\, l_g (r_h)^2 (r_e)^{0.5} \qquad (4.8)$$

where F = ultimate tensile load (N)

d = steel rod diameter (mm)

l_g = embedment length (mm)

r_h = ratio of hole diameter to bar diameter

r_e = ratio of edge distance to bar diameter

Townsend's formula was based on the connection using the deformed reinforcing bar and Araldite K-2005 epoxy. According to Townsend's finding, the

tensile strength in the connection with threaded steel rod appears to have almost twice of the strength than similar connection using deformed reinforcing bars. Therefore, the ultimate tensile load from Equation 4.8 was doubled when used for the threaded rod connection. Similarly, according to Townsend, a 15% increase of the value calculated from Equation 4.8 should be used for the connection using Araldite K-80 epoxy. The average values of the bond stress are listed in Table 4.12.

Table 4.12 Comparison of output from the empirical formula and beam splice test results

Speci-men	Code	Bar Type	Epoxy Type	e (mm)	l (mm)	Fail Mode	Bond Stress -tested (MPa)	Bond Stress -Deng (MPa)	Bond Stress -Town. (MPa)	Ratio[1]	Ratio[2]
1	BM1 -1(1)	T	K2005	35	300	5	5.7	8.1	10.1	0.71	0.57
2	BM1 -1(2)	D	K2005	35	275	no fail	7.6	6.5	5.0	1.18	1.51
3	BM1 -2(1)	D	K2005	35	275	5	7.2	6.5	5.0	1.11	1.43
4	BM2 -1(1)	D	K-80	35	250	5	5.6	5.6	5.8	1.00	0.97
5	BM2 -1(2)	D	K-80	35	250	5	6.3	5.6	5.8	1.12	1.09
6	BM3 -1(1)	D	K-80	45	250	2	6.4	6.4	6.6	1.01	0.98
7	BM3 -1(2)	D	K-80	45	250	5	7.0	6.4	6.6	1.10	1.07
8	BM4 -1(1)	D	K2005	45	250	5	5.0	7.4	5.7	0.67	0.88
									Mean	0.99	1.06
									COV	0.195	0.281

Note: 1. Bar type: T = threaded steel rod.
D = deformed reinforcing bar.

2. geometry: e = edge distance (mm).
l = embedment length (mm).

3. Failure mode: 2 = Type 2 failure mode: the connection pulls out with wood split around the connection.
   5 = Type 5 failure mode, wood failure, including wood tension and wood shear, mostly caused by finger joint crack in the test.
4. bond stress $_{test}$ = (Pullout force from test)/(3.14 x hole diameter x embedment)
5. bond stress $_{Deng}$ = (Pullout force from Equation 4.7)/(3.14 x hole diameter x embedment length)
6. bond stress $_{Town}$ = (Pullout force from Equation 4.8)/(3.14 x hole diameter x embedment length)
7. Ratio^1 = (bond stress $_{test}$)/ (bond stress $_{Deng}$)
8. Ratio^2 = (bond stress $_{test}$)/ (bond stress $_{Town}$)

The predicted values from both formulae closely approximate the test result. This suggests that the equations developed from single steel rod connection can be used for the multiple bar connection with different loading arrangement. It can be seen from the table that 6 specimens failed as a result of wood tension or wood shear, only one (Specimen 6) failed with wood splitting and steel bar pulling out. For specimen 6 with Type 2 failure mode, the ultimate tensile load from the test is the same as the predicted value from Equation 4.7.

4.4.3 Comparison of the Empirical Model with the European Formula

The comparison is made between the empirical formula developed by the author (Equation 4.7) and the European formula developed by Riberholt (1988b). Riberholt's formula is shown as follows:

$$F_{axest} = 0.627\rho d\sqrt{l_g} \qquad (4.9)$$

where, $F_{ax,\,est}$ = estimated pullout force of the connection (N)

d = the bolt diameter (mm)

l_g = the embedment length of the bolt (mm)

ρ = the density of the wood (kg/m^3)

The above equation is based on regression analysis of the Riberholt's test results with bolt diameters of 12 and 20 mm and a ratio of embedment length to bolt diameter of 15, and is considered suitable for two-component epoxy, phenol-resorcinol and other brittle glues. For shorter embedment length, Riberholt found that the equation tends to overestimate the axial bolt strength.

The comparison was conducted using the results from Experiment One, dry specimens with the threaded rod connection only being used. The results of the comparison are listed in Table 4.13. The ultimate tensile load values from Experiment One are compared with the predicted values from Equation 4.7 and European formula. A regression analysis was conducted and the R squared values were obtained for both predictions. It can be seen from the table that the Equation 4.7 has a better prediction for the experiment results as the R squared value is higher for Equation 4.7 than for the European formula. Similarly, the COV of the Ratio-1 is less than that for the Ratio-2. The European formula seems conservative for the experiment results as in average the experiment output is 11% above the predicted value from the European formula.

Table 4.13 Comparison of the European formula and the empirical formula developed from the short duration experiments

CODE	EPOXY	d (mm)	l (mm)	e (mm)	density (kg/m3)	UTL-t (kN)	UTL (Deng) (kN)	UTL (Europe) (kN)	Ratio-1	Ratio-2
1001	West	16	80	24	572	30.8	34.4	51.3	0.90	0.60
1002	West	16	80	36	461	43.1	42.1	41.4	1.02	1.04
1003	West	16	160	24	473	56.4	62.4	60.0	0.90	0.94
1004	West	16	160	36	537	87.0	76.4	68.1	1.14	1.28
1005	West	16	80	24	499	38.5	37.9	44.8	1.02	0.86
1006	West	16	80	36	527	56.8	46.4	47.3	1.22	1.20
1007	West	16	160	24	551	68.0	68.8	69.9	0.99	0.97
1008	West	16	160	36	471	75.5	84.3	59.8	0.90	1.26
1009	West	24	120	36	516	54.2	66.3	85.1	0.82	0.64
1010	West	24	120	54	506	97.0	81.2	83.4	1.19	1.16
1011	West	24	240	36	438	86.4	120.3	102.1	0.72	0.85
1012	West	24	240	54	523	139.5	147.3	121.9	0.95	1.14
1013	West	24	120	36	495	78.3	73.1	81.6	1.07	0.96
1014	West	24	120	54	505	92.6	89.6	83.2	1.03	1.11
1015	West	24	240	36	516	154.9	132.7	120.3	1.17	1.29
1016	West	24	240	54	521	175.6	162.6	121.5	1.08	1.45
1017	K-80	16	80	24	471	34.3	40.0	42.3	0.86	0.81
1018	K-80	16	80	36	513	37.7	48.9	46.0	0.77	0.82
1019	K-80	16	160	24	602	70.7	72.5	76.4	0.97	0.93
1020	K-80	16	160	36	443	92.1	88.8	56.2	1.04	1.64
1021	K-80	16	80	24	490	50.4	44.1	44.0	1.14	1.15
1022	K-80	16	80	36	573	55.6	54.0	51.4	1.03	1.08
1023	K-80	16	160	24	545	82.7	80.0	69.2	1.03	1.20
1024	K-80	16	160	36	549	106.7	98.0	69.7	1.09	1.53
1025	K-80	24	120	36	521	81.4	77.1	85.9	1.06	0.95
1026	K-80	24	120	54	505	83.2	94.4	83.2	0.88	1.00
1027	K-80	24	240	36	490	136.3	139.9	114.2	0.97	1.19
1028	K-80	24	240	54	559	176.0	171.3	130.3	1.03	1.35
1029	K-80	24	120	36	521	89.7	85.0	85.9	1.05	1.04
1030	K-80	24	120	54	528	105.8	104.2	87.0	1.02	1.22
1031	K-80	24	240	36	477	112.5	154.4	111.2	0.73	1.01
1032	K-80	24	240	54	508	228.0	189.0	118.4	1.21	1.93
Average					512.7				1.00	1.11
COV									0.13	0.25
R Square							0.90	0.76		

Note: West = West System epoxy

K-80 = Araldite K-80 epoxy

d = steel rod diameter (mm)

l = embedment length (mm)

e = edge distance (mm)

UTL-t = ultimate tensile load of the experiment (kN)

$UTL_{(Deng)}$ = ultimate tensile load calculated from Equation 4.7 (kN)

$UTL_{(Europe)}$ = ultimate tensile load calculated from Equation 4.9 (kN)

Ratio-1 = $(UTL\text{-}t)/(UTL_{(Deng)})$

Ratio-2 = $(UTL\text{-}t)/(UTL_{(Europe)})$

4.5 DISCUSSION AND CONCLUSIONS

Three short duration experiments were conducted, 5 failure modes being classified in these experiments. Most specimens failed as Type 1 and Type 2 failure modes.

These short duration experiments show a common phenomenon that for each specimen failure always started at the point where either the magnitude of the stress and the stress concentration are highest or where defects in the materials exist. It indicates the importance of identifying the locations of stress concentrations and any defects. Pith, sloping grain, knots and finger joint around the connection can be critical factors influencing the strength of the connection. Clearly there is potential to improve the strength and performance of the connection by optimising design in terms of selections of material and geometry. Further study using a finite element method analyses the stress distribution in the connection and identifies the locations where the failures are most likely to occur.

It can be seen from the experiment results that using a simple unified failure criterion to identify the failure and predict the strength would be unrealistic because of the complicated mechanisms of failure in the connection and variety of failure modes. A statistically based empirical model was developed to predict the strength of the

connection, and based on the short duration experiment results, the following conclusions can be drawn:

1. The ultimate tensile strength of the connection is correlated to all seven factors investigated in the short duration experiments. The moisture content in glulam timber, the bar diameter, and the embedment length are closely related to the strength and appear to have more influence on the strength than other factors.

2. An empirical equation based on the short duration experiments was developed to predict the axial capacity of the connection in tension or compression. Seven influencing factors investigated in the experiments were considered in the equation. The equation gives a good agreement with the experiments results.

3. The ultimate tensile strength of the connection with the deformed reinforcing bar is about 20% less than that of the connection with the threaded rod.

4. In terms of ultimate tensile strength, among different epoxies, Araldite 2005 is 17% greater than K-80 and the West System is about 14% less than K-80.

5. The ultimate tensile strength of the connection decreased about 24% in wet specimens compared with dry specimen, which indicates that the moisture content plays an important role in the strength of the connection.

6. Transverse steel reinforcement of the connection is recommended where wood splitting failure around the connection is likely occur.

7. The statistical analysis of Experiment One and Two (Appendix E) concludes that the average values of the ultimate tensile strength differ among all of the levels of each factor with at least 90% significance. In addition, there is no statistical evidence to suggest that interactions exist between any two factors.

CHAPTER FIVE

STRESS DISTRIBUTION IN THE CONNECTION: THEORETICAL MODEL

5.1 BACKGROUND

There are many methods which can be used to model an adhesive bonded connection and a number of analytical solutions for the state of stress or strain used in previous studies; they can be classified into two categories. One category is the closed form algebraic solution, in which a series of differential equations are set up to describe the state of stress or strain in an adhesive bonded connection, and to deduce the solutions using these algebraic functions. The other category is the finite element method, a powerful and efficient method used to analyse the stress or strain distribution which may help predict the strength and failure mode of the adhesive bonded joints.

Although the closed form solutions give a qualitative assessment of the effects of various parameters, they are unable to accurately describe the stress distribution and predict the strength (Adams and Harris, 1987). The reason is that a complete analysis of the various components of the stress is required, including variations through the thickness of both the adherents and the adhesive, and the joint strength could be significantly influenced by the local geometry in the critical regions of the joint. Any of these can make the closed form analytical solutions unattractive and impractical.

The finite element method offers an ideal and powerful numerical method. Essentially, the continuum is broken down into discrete elements, each of which can be assessed and each of which interacts with its neighbours in a rational fashion. Regions of high stress gradient can be accommodated by using a finer mesh of elements. In addition, material non-linearity and anisotropy can be include in the description of any element. Compared with the closed form algebraic solutions, the finite element method

can be used readily with different failure criteria, fracture mechanics and other material theory. The development of modern computers and available software has made the finite element method increasingly popular. For the above-mentioned reasons, the finite element method was chosen to model the epoxy adhesive bonded steel connection; a model using the finite element computation program ABAQUS (ABAQUS, 1993a) is programmed and computed on DEC station 2100.

5.2 OBJECTIVES AND SCOPE

The objectives of modelling the connection using the finite element method are to understand the mechanisms of the load transformation and the distributions of various stresses in the connection. The analysis of the stress distributions aims to explain the different failure modes observed in the short duration experiments and to study the effects of various geometrical and material properties of the connection so that the performance and capacity of the connection can be improved.

The model would focus on the numerical description of various stresses under the material linear elastic range of the connection. There is no intention to integrate the fracture mechanics theory or any failure criterion into the finite element model. Therefore, crack propagation and failure of the connection beyond the elastic range of the materials are not considered in the model.

The geometry of the model is simplified. Only a quarter of the specimen cross-section is used for modelling. The original square cross-section of the specimen is replaced with a circular cross-section with similar ratio of wood to steel in the model. A smooth steel rod is modelled to represent the threaded rod. The connection with deformed steel rod is not considered in this model. A general explanation of the different failure modes is made after the analysis of the stress distribution in the connection.

5.3 FINITE ELEMENT MODEL

5.3.1 Parameters of the Model

The model geometry is based on the short duration experiments; a sketch of the geometry of the specimen modelled is shown in Figure 5.1 and the geometry parameters of the model are given in Table 5.1. These parameters will be used as standard input for the model. The model with standard input will be used as the reference model for further parametric study.

Table 5.1 Input parameters used in the finite element model

Parameters	Magnitude
Specimen length (L)	900 mm
Model length (L/2)	450 mm
Steel rod embedment length (l)	300 mm
Steel rod diameter (d)	20 mm
Epoxy thickness (t_e)	3 mm
Embedment hole diameter (h)	26 mm
Edge distance (e)	45 mm
Cross-section dimension (a x b)	90 x 90 mm
Wood to steel ratio of the cross-section (W_S)	25.8
Equivalent radius of the cross-section (R)[1]	50 mm

Note: 1. The equivalent radius of cross-section is the radius of an equivalent circle giving the same wood to steel ratio at the cross-section.

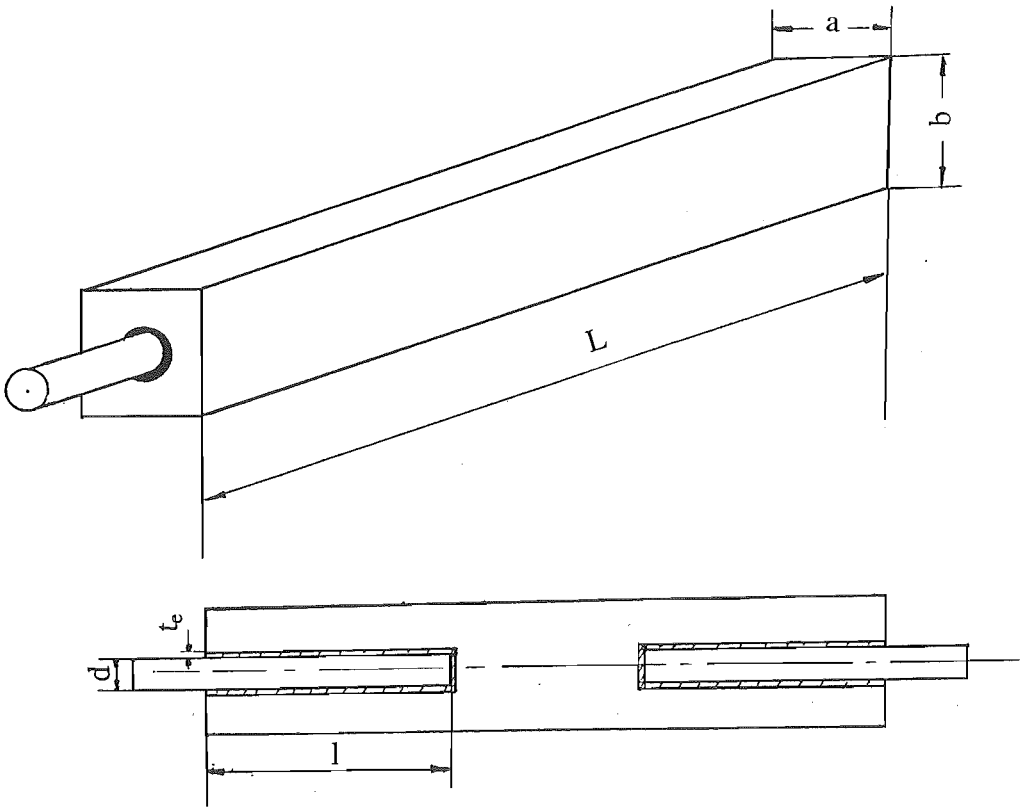

Figure 5.1 Sketch of the geometry of the specimen modelled

5.3.2 Basic Assumptions and Material Properties

The connection is modelled in 3 dimensional space such that full details of the stress distributions and variations in the connection can be determined. The following assumptions were made to obtain a practical and relatively simple model, and to achieve tractable results.

1. The epoxies used in the connections are isotropic and linear elastic materials.

2. The glulam timber is an orthotropic linear elastic material.

3. The mechanical properties of the glulam timber along the radial and tangential direction are the same.

4. The steel rod is an isotropic, linear elastic material with a smooth surface.

5. The applied tension stress is uniformly distributed over the cross-section of the steel rod at the outer end of the embedment.

The mechanical properties of the material used in the finite element model are defined and given in Table 5.2.

Table 5.2 (a) The mechanical properties of steel and epoxy used in the finite element model

Material	Modulus of Elasticity (GPa)	Poisson's Ratio
Epoxy	4	0.3
Steel	200	0.3

Table 5.2 (b) Mechanical properties of glulam timber in the finite element model

Modulus of Elasticity (GPa)		Shear Modulus (GPa)		Poisson's Ratio	
E_L	9	G_{LR}	0.6	ν_{LR}	0.37
				ν_{LT}	0.42
E_R	0.72	G_{LT}	0.564	ν_{RT}	0.47
				ν_{TR}	0.35
E_T	0.45	G_{RT}	0.06	ν_{RL}	0.041
				ν_{TL}	0.033

Note: 1. The subscripts L, R, T present the longitudinal, radial and tangential direction of wood respectively.

2. The notation for the material directions and corresponding axes in Cartesian coordinates of the 3 dimensional space are shown in Figure 5.2.

The source of the mechanical properties of glulam timber are described in Table 5.3.

Table 5.3 The calculation and selection of mechanical properties of glulam timber

Mechanical Properties	Source Value or Calculation Formula	Reference
E_L	9000 MPa	NZTIF (1989)
E_R	$E_R = (1.6/20) \times E_L$	Bodig and Jayne (1982) pp. 115
E_T	$E_T = (1/20) \times E_L$	
G_{LR}	$G_{LR} = (1/15) \times E_L$	NZTIF (1989) pp. C-1-2
G_{LT}	$G_{LT} = (9.4/10) \times G_{LR}$	Bodig and Jayne (1982) pp. 115
G_{RT}	$G_{RT} = (1/10) \times G_{LR}$	
ν_{LR}	0.37	Bodig and Jayne (1982) pp. 117
ν_{LT}	0.42	
ν_{RT}	0.47	
ν_{TR}	0.35	
ν_{RL}	0.041	
ν_{TL}	0.033	

It is difficult to characterise the mechanical properties of glulam timber accurately in the absence of information and experimental data on New Zealand grown *Pinus Radiata.* As input data for the finite element model, the empirical formulae were adopted to obtain the mechanical properties values. As can be seen from Table 5.3, all of the modulus calculation are based on the modulus of elasticity E_L for New Zealand *Pinus Radiata.* For Poisson's ratios, the data was directly adopted from Douglas fir experiment data (Bodig and Jayne, 1982). Although the empirical formulae and Poisson's ratio were developed from Douglas fir experiment data, it had been used for some other species. Since New Zealand *Pinus Radiata* has similar properties to American Douglas fir, it seems rational to use them to provide model input; such values could be changed easily to test the model sensitivity for the input.

Based on assumption 3, the average value of the modulus of elasticity in the radial and the tangential directions from Table 5.2 (b) was calculated for both transverse directions. The same principle was applied to the shear modulus and Poisson's ratio. The calculated data was converted into the ABAQUS program input format and shown in Table 5.4.

Table 5.4 ABAQUS input data for glulam timber properties

Modulus of Elasticity (MPa)			Poisson's Ratio			Modulus of Rigidity (MPa)		
585	585	9000	0.41	0.037	0.037	60	582	582

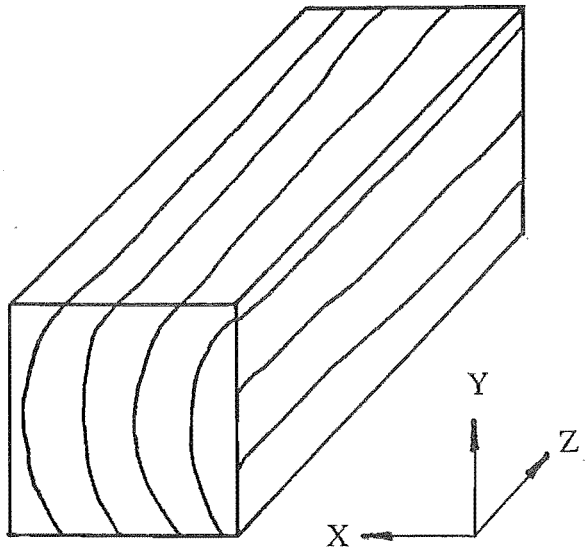

Notation in text	Notation in ABAQUS	Wood grain
x	1	radial (R)
y	2	tangential (T)
z	3	longitudinal (L)

Figure 5.2 The defined grain direction of the glulam timber in Cartesian coordinates

5.3.3 The Finite Element Model

1. ABAQUS program

ABAQUS is a powerful and general finite element program developed by Hibbitt, Karlsson & Sorensen, Inc.(ABAQUS, 1993a and 1993b) for universal use and

has been widely used for many research and industrial projects. There are many advantages and features in this program; it has a very large element library and powerful 3-dimensional finite element analysis functions.

2. Mesh and element generation

The geometry of the test specimen has been given in Figure 5.1. One half of the length of the specimen and one-quarter of the cross-section is analysed because of symmetry. Cartesian coordinates are used in this model. In this way, a relative simple and universal model can be developed to meet requirements for further study, such as the parametric study, the composite material characteristics and failure criteria. The finite element mesh of the connection is generated to give a good approximation to the stress distribution. From previous researches (Adams, 1990 and Gerold, 1992), the critical sections of the connection are expected to be at or near both ends of the steel rod embedment where the magnitudes of the stresses and their gradients are higher. In contrast, in the middle section of the embedment the stress distributions are expected to be approximately uniform. Furthermore, in terms of the cross-section of the specimen, critical regions are expected at the steel-epoxy and epoxy-wood interfaces, but away from the interface towards to the surface of wood, no stress concentration and very small magnitude of the stresses are anticipated. In order to get more accurate numerical results, the mesh is generated for different element sizes: small elements are used in the supposed higher stress gradient regions; large elements are used in the regions where the stresses are expected to be uniform. In addition, through the thickness of the epoxy, a very fine mesh of six elements is defined to show the variation of the stresses through the thickness of the epoxy and to investigate the stress distributions along both interfaces. The mesh is formed for a circular specimen rather than a rectangular specimen as this could simplify the model. Previous research (ABAQUS, 1993a) and pilot finite element analysis for the connection show that no significant influence occurs by changing the shape if the wood to steel ratio remains similar.

The mesh of the finite element model of the connection is shown in Figures 5.3 (a) and (b). Figure 5.3 (a) shows the mesh in the x-y plane at the origin ($z = 0$) of model which represents the cross-section of the specimen at the outer end. Figure 5.3 (b) shows the mesh in a 3-dimensional space with the x and y axes parallel to the radial and

tangential directions of the glulam timber respectively, while the z axis is parallel to the longitudinal direction of the specimen and along the centre line of steel rod.

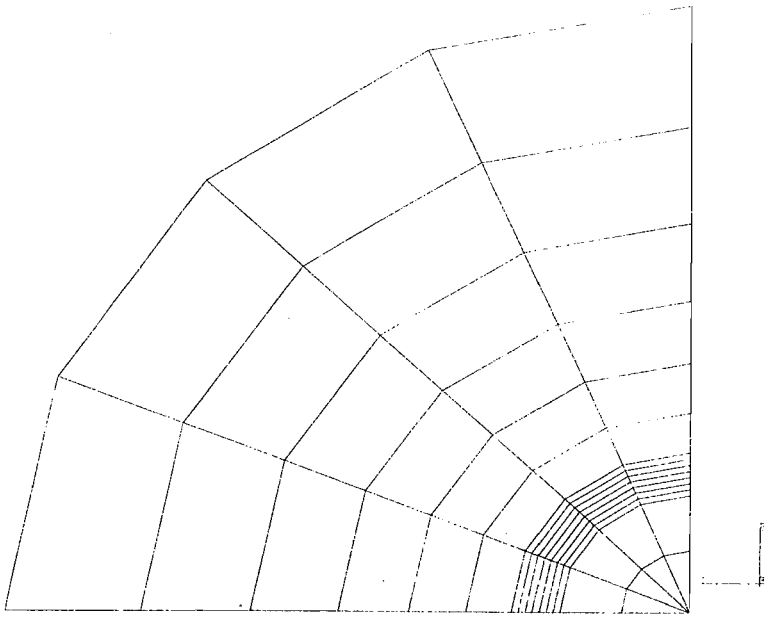

Figure 5.3 (a) The finite element mesh in the x-y plane at the origin (z = 0) of the model

Two kinds of element are chosen to meet geometry requirement. One is a 6-node linear triangular prism (C3D6) used in the central zone of the steel rod along the embedment length; the other is an 8-node linear brick (C3D8) used in the rest of the model. These two elements are easy to generate and have sufficient accuracy for this model. The model has 2640 elements and 3555 nodal points.

3. Gap at the end of steel rod

The gap at the end of the steel rod has been considered during the mesh, element generation and material properties assignation. Based on the results and failure modes from the short duration experiments (Experiment One and Experiment Two), it is believed that poor adhesion between the end of the rod and the epoxy is equivalent to a gap between the end of the steel rod and the epoxy. Although the gap was filled by the epoxy sometimes, it is unlikely to form a proper bond between the end of the rod and wood. Therefore, in the finite element model, this region was treated as a gap. The gap was produced in the model by generating small elements at the end of the steel rod without assigning any material properties on them.

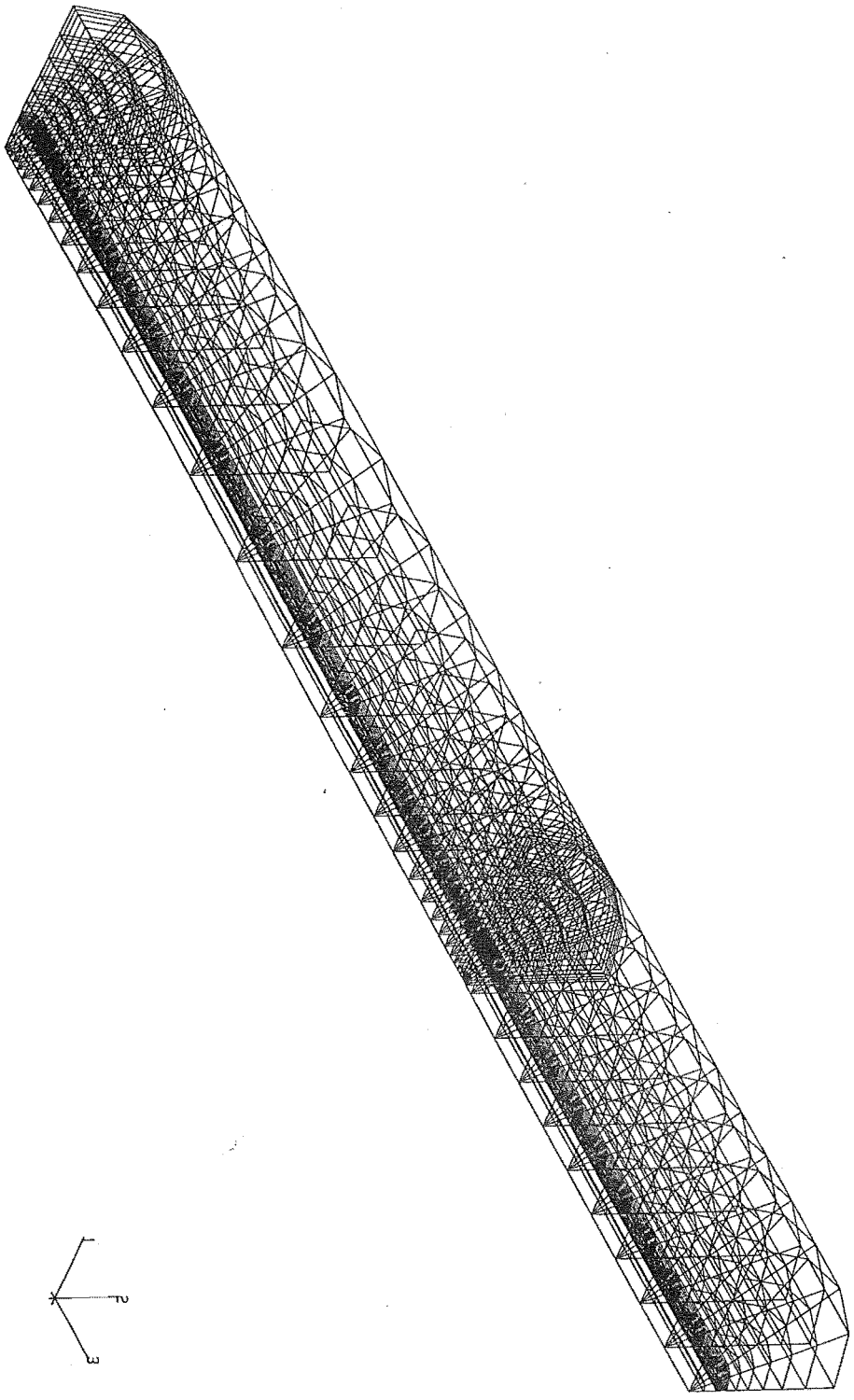

Figure 5.3 (b) The finite element mesh of the model in 3-dimensional space

4. Boundary conditions

The boundary conditions are defined as follows: the vertical surface (in y-z plane) is restrained in the x direction; The horizontal surface (in x-z plane) is restrained in the y direction; the mid-face (plane z = 450) is restrained in the z direction. Therefore, the centre line is considered to be restrained in both the x and the y directions.

5. Loading

A concentrated tensile load at the outer end of the steel rod is transformed into a uniformly distributed tensile stress on the one-quarter steel rod cross-section at the outer end of the embedment (in x-y plane, z = 0 of Figure 5.3 (b)), the direction being along the negative z axis. The magnitudes of the load used in the analysis are based on the short duration experiments results. Only low load levels are used to model the connection in which linear elastic conditions are expected. It is possible, in theory, to extend the model into the non-linear range and to explore various failure criteria, but that is beyond the scope of this study. Two load levels are used in the model. One is 50 kN, which is used for a general study of the stress distribution in the connection and for further parametric study. The other is 15 kN, which is used for comparing the model output with the results from the experimental stress distribution analysis. No failure is expected to occur with such low magnitudes of tensile load. The programme of the model is listed in Appendix F.

In the following chapter the output of the model will be presented. An experimental stress distribution analysis will be described and the comparison between the model output and the experimental result of the stress distribution will be given.

CHAPTER SIX

STRESS DISTRIBUTION IN THE CONNECTION: EXPERIMENTAL VERIFICATION AND MODEL PREDICTION

6.1 OBJECTIVES AND SCOPE

An experimental study of the stress distribution was undertaken to investigate the stress distributions at the interface between the steel rod and the epoxy along the embedment. The experiment results were analysed and compared with the output of the finite element model, with the intention of testing the validity of the model and to study the effects of different steel bar surface and end geometry. The experiment also attempted to measure the transverse stress.

Although the epoxied steel connection consists of 3 materials and two material interfaces, the experiment concentrated on the interface between the steel rod and the epoxy along the embedment. This is not only of primary interest to the project, but the interface is a key region to expose the stress distribution of the connection. Furthermore, the direct influence from any defects or inhomogeneity in the glulam timber can be avoided.

6.2 DESIGN OF THE EXPERIMENT

This experiment was defined as Experiment Five and included four specimens. They were coded as 5000, 5001, 5002 and 5003. Specimen 5000, a preliminary specimen, was prepared and tested before the other specimens were designed. Specimen 5000 was to provide a primary investigation of the stress distribution and to confirm the methodology of the experiment. After specimen 5000 had been

successfully tested, the other specimens were designed. To simplify the description and discussion of the experiment, the design, experimental procedure and discussion will cover all of the specimens regardless of the time sequence. The experiment plan is shown in Table 6.1.

Table 6.1 Parameters of Experiment Five

Code	5000	5001	5002	5003
Epoxy Type	K-80	West System	West System	West System
Steel Bar Type	Threaded	Threaded	Smooth	Threaded
Specimen Width (mm)	90	90	90	90
Specimen Height (mm)	90	90	90	90
Specimen Length (mm)	800	750	750	750
Embedment l_t (mm)	300	400	400	400
Embedment l_s (mm)	300	200	200	200
Number of Gauges on Surface of Steel	6	13	13	8
Number of Gauges on End of Wood	-	6	-	-

Note: l_t = embedment length at the test end.

l_s = embedment length at the support end.

Figures 6.1 to 6.4 show the geometry of steel rods and locations of the strain gauges for specimens 5000, 5001, 5002 and 5003 respectively. In specimen 5000, 6 strain gauges were used and they were glued on six small individual grooves respectively. The grooves were machined on the surface of the threaded rod to provide a flat smooth surface for the strain gauges. Similarly, a threaded steel rod was used in specimen 5001 as shown in Figure 6.2, but a groove was machined along the entire embedment length on the surface of the threaded rod for gluing the strain gauges. A smooth surface steel rod was used in the test end of specimen 5002 (Figure 6.3) instead of the threaded rod. Compared with specimen 5001, specimen 5002 has similar layout of the strain gauges, same embedment length and same nominal bar diameter. This is to compare stress distribution between the threaded rod and the smooth surface bar.

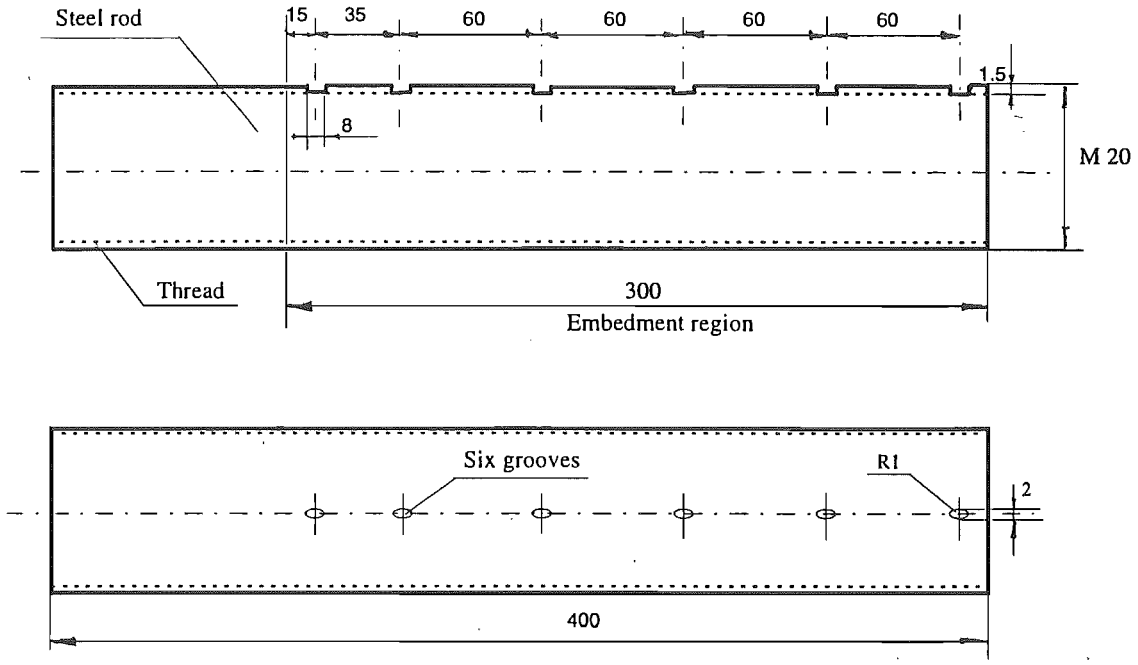

Figure 6.1 Geometry of steel rod and location of strain gauges for specimen 5000 (not to scale)

A hole was drilled in the inner end of the threaded rod in the specimen 5003 as shown in Figure 6.4. As can be observed, most strain gauges were located near the end of the steel rod and corresponding with specimen 5001, permitting the comparison of stress distribution with the specimen 5001 and to investigate any change of stress distribution if geometry of connection was changed.

A design outline of the specimens is shown in Figure 6.5. Specimen 5001 has 6 strain gauges on the outer end surface of the wood to measure the stress distribution on the cross-section. A 1.5 mm diameter hole was located above each individual strain gauge, the strain gauge lead wires being fed through these holes to the surface of the specimen.

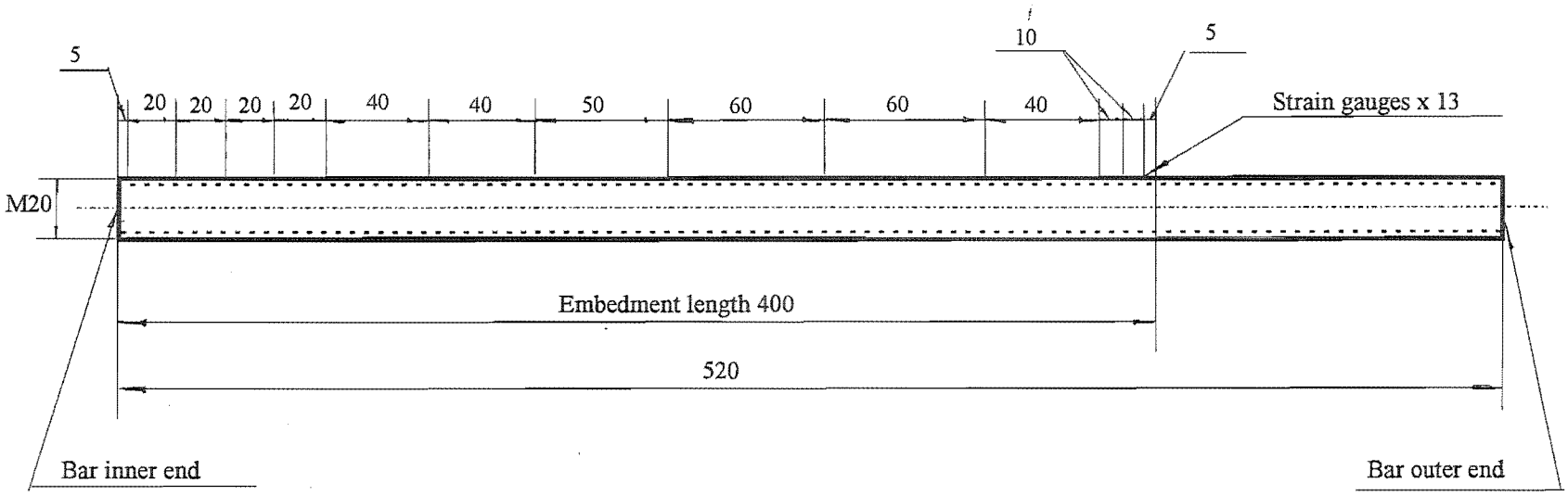

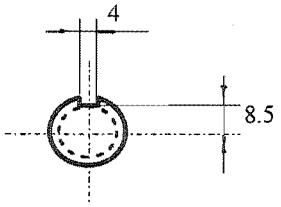

Unit: mm
Material: Threaded steel rod

Figure 6.2 Geometry of steel rod and location of strain gauges in specimen 5001 (not to scale)

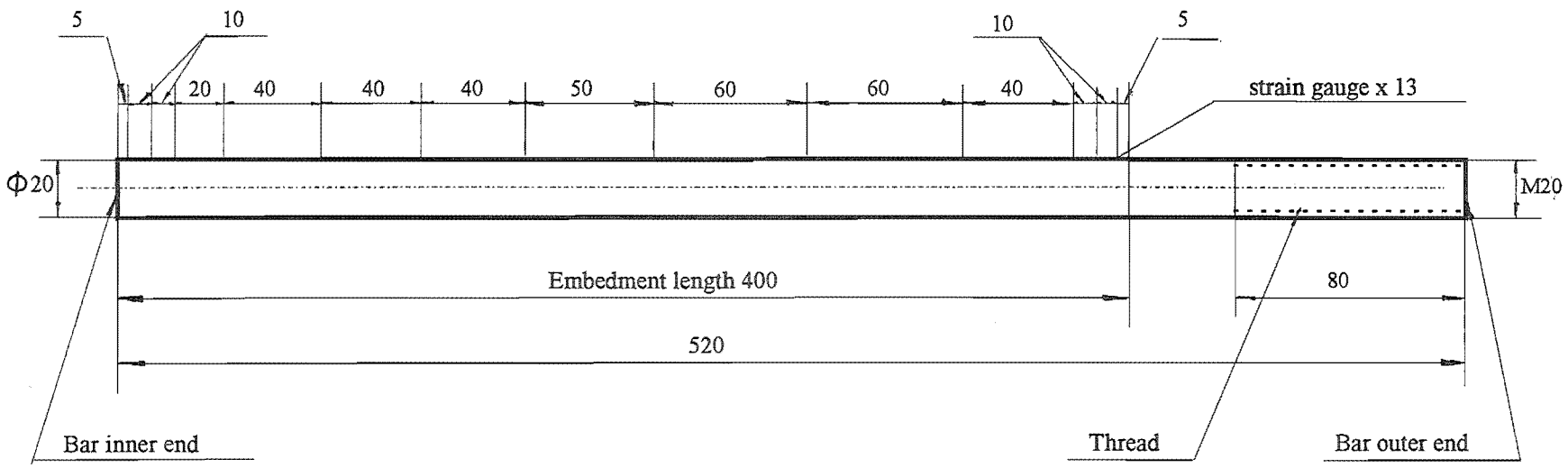

Unit: mm
Material: Smooth surface steel rod

Figure 6.3 Geometry of steel rod and location of strain gauges in specimen 5002 (Not to scale)

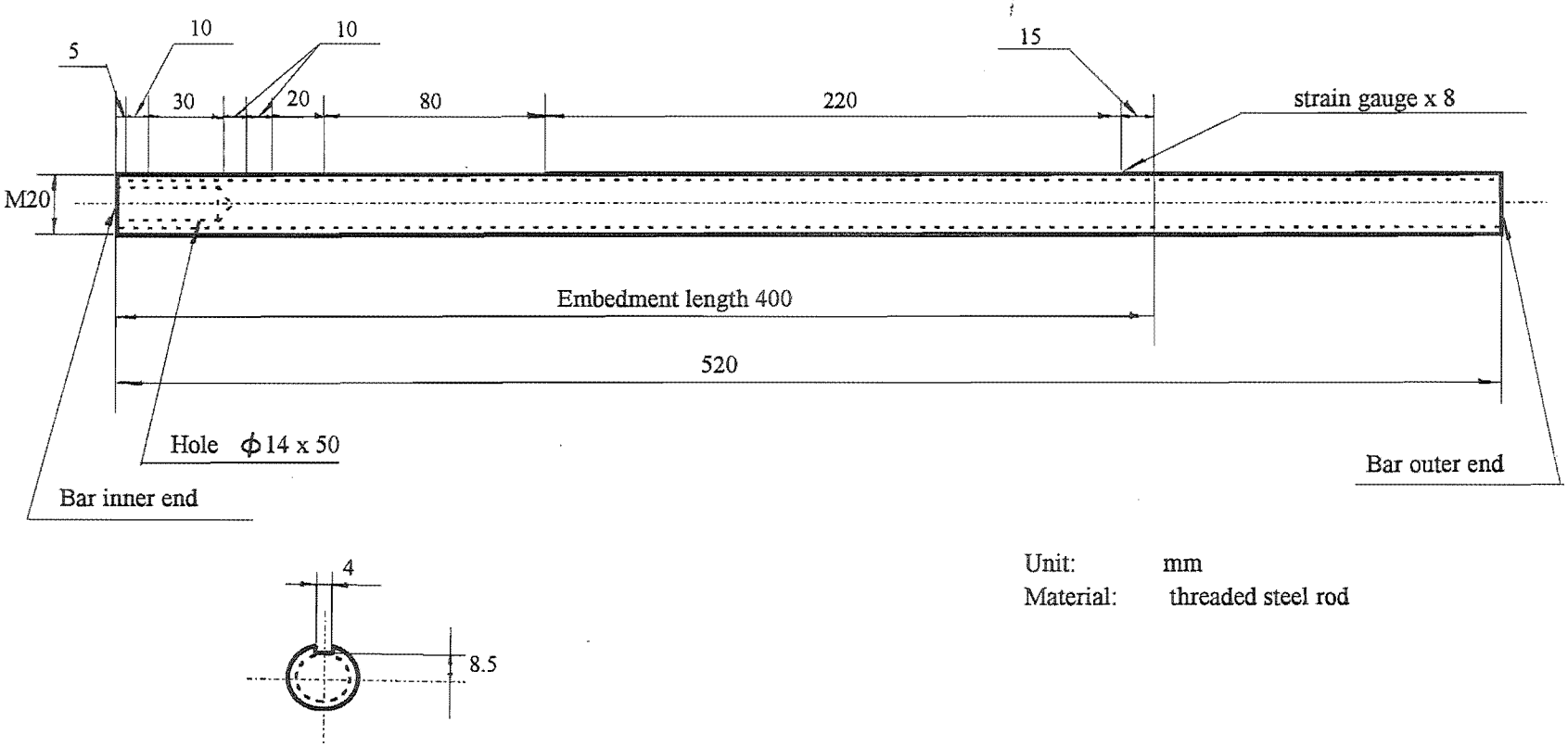

Figure 6.4 Geometry of steel rod and location of strain gauges in specimen 5003 (Not to scale)

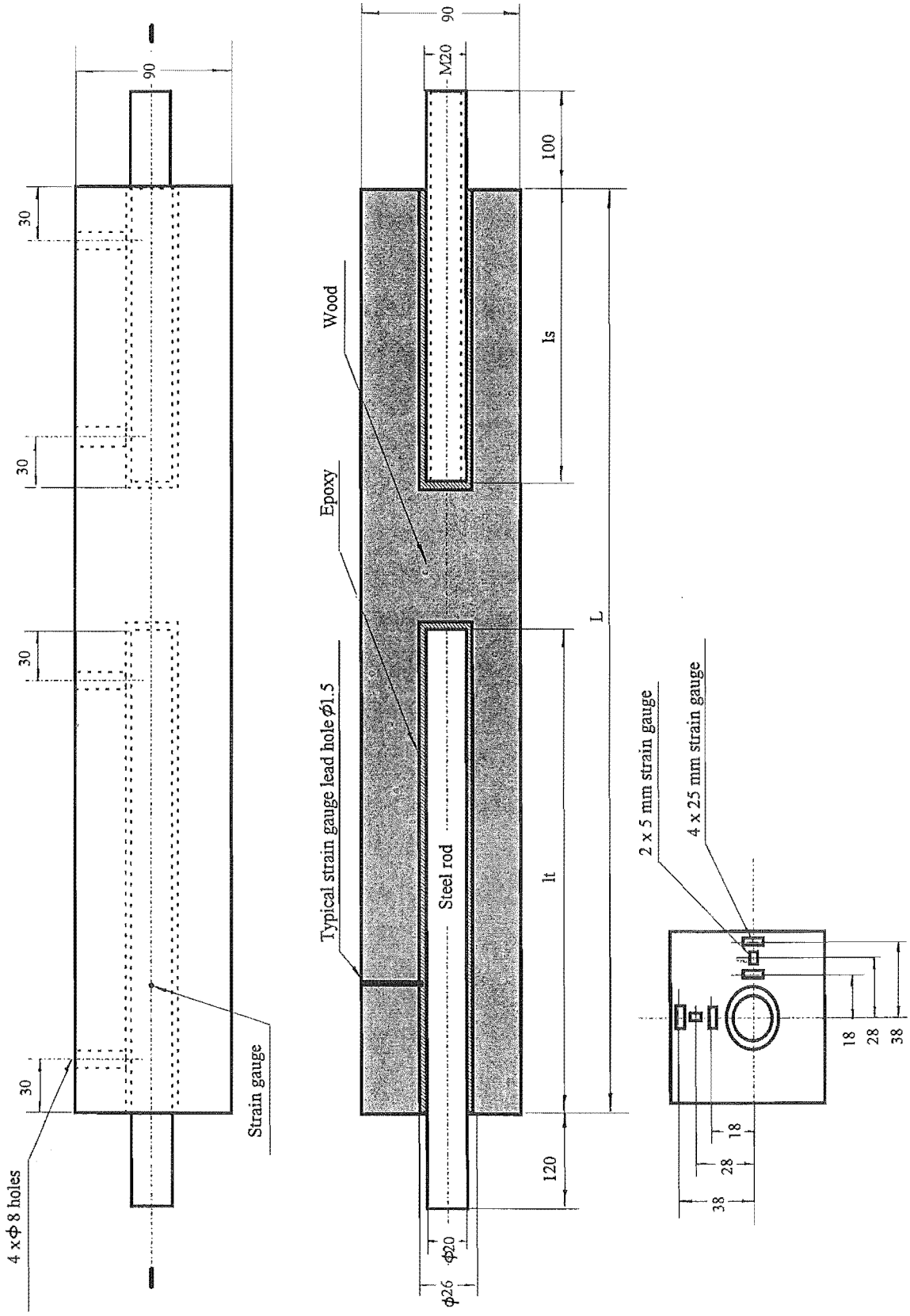

Figure 6.5 Design outline of the specimens (not to scale)

6.3 MATERIALS

The glulam timber was chosen from the same batch as used in the short duration experiments; the material properties have been described in Chapter Three. Two kinds of steel rod were used in the experiment. One was a high strength threaded steel rod having the same mechanical properties as the one used in Experiment One. The mechanical properties have been described in Chapter Three. The other was a smooth surface steel rod with tensile strength 400 MPa and yield 240 MPa. Two kinds of epoxy were used. K-80 epoxy used in specimen 5000. West System epoxy used for the other specimens. Both epoxies had been used in the short duration experiments. The characteristics of the epoxies and their formulation procedures have been described in detail in Chapter Three.

Three kinds of electric resistance type strain gauge were used in the experiment. Namely, they are 1 mm, 5 mm and 25 mm strain gauges respectively. The strain gauge (Type: FLK-1-3LJB-11) is designed to use on metal surfaces to obtain accurate strain reading in the applied area. The gauge length is 1 mm and gauge factor is 2.11. The nominal electric resistance for the batch of strain gauges is 120 ± 0.5Ω. This type of strain gauge was used on the surface of the steel to measure the strain. The other two kinds of strain gauge were used on wood: 25 mm strain gauges (Type KF-25-C8-11) and 5 mm strain gauges (Type KFC-5-C1-11). All are commonly used general purpose strain gauges and can be used on metal, plastic, composite material and wood. Four strain gauges with a gauge length of 25 mm were used. The gauge factor is 2.11 and the resistance is 119.9± 0.3Ω in the batch. Two 5 mm length strain gauges were used. The gauge factor is 2.11 and the resistance is 120.1 ± 0.3Ω.

6.4 SPECIMEN PREPARATION

Four pieces of glulam timber were selected from glulam timber members with cross-section of 90 x 90 mm. For specimens 5001, 5002 and 5003, great effort was made to obtain similar specimens in terms of wood grain, modulus of elasticity and density. The selection procedure was as follows:

1. Nine glulam timber members were selected to obtain a similar wood grain pattern and glue line position, and to eliminate any defects in the embedment region at the test end, such as knot, slope grain, pith and finger joint.

2. For each selected glulam timber member, a temporary code was marked and the density was obtained by measuring the weight and dimension.

3. The modulus of elasticity of each of these timber members was measured using 3-point bending test on the 100 kN AVERY universal testing machine. This is to pre-select the glulam timber used for the specimens to reduce the variation among the specimens.

4. 3 pieces of glulam timber were selected from the 9 selected members to obtain closely similar properties in terms of modulus of elasticity and density.

The final selected timber members were coded and machined to the required dimensions, and modulus of elasticity, density and moisture content were recorded. The embedment holes were drilled according to the experiment plan (Table 6.1). Injection holes, air holes and gauge lead wire holes were drilled as shown in Figure 6.5. The location of each lead wire hole is not shown in Figure 6.5 but it can be obtained from Figures 6.1 to 6.4 respectively since the hole corresponds to the location of each strain gauge.

The steel rods were cut to the required length. For threaded rods used in the test end, grooves were machined along the embedment to provide suitable surfaces for the strain gauges. For specimen 5000, 6 small identical grooves were machined; the location and dimension of the grooves are shown in Figure 6.1. For specimens 5001 and 5003, the grooves were machined along the entire embedment length as shown in Figure 6.2 and Figure 6.4; for specimen 5002 no machining was required. The surface was slightly scored with emery paper before gluing strain gauges. Threaded rods were used at the support end of all specimens.

The strain gauges were glued to the surface of the steel rod using superglue 401 after the surface had been carefully cleaned with MEK (methyl-ethyl-ketone), the manufacturer's instruction and standard procedure being strictly followed. The surface of the strain gauge and the adjacent area were protected from water and rust by applying several coatings of SN4. Each strain gauge was checked before the specimen was assembled.

The steel rod was fitted into the glulam timber and the leads for each strain gauge led through the adjacent hole above the strain gauge. After assembly, the epoxy injection procedure was carried out; K-80 epoxy was used in specimen 5000 and West System was used for the other specimens. The procedure of the specimen assembling and epoxy injection is similar to the procedure used for the short duration experiments. The detail of this procedure has been described in Chapter Three.

For specimen 5001, six strain gauges were glued on the end surface as shown in Figure 6.5. Two 5 mm gauges were glued in radial direction and four 25 mm strain gauges applied in tangential direction. Similar procedure for gluing the strain gauges on steel was used to glue the strain gauges on the surface of the wood.

6.5 EXPERIMENTAL PROCEDURE

The specimens were tested on the Instron Universal Testing Machine (Model 1116) with a 50 kN load cell, the tensile load being applied in the longitudinal direction. The load was adjusted manually from 0 to 30 kN, with readings in 5 kN increments. For each loading level, two readings were recorded, one obtained while the tension was increased in each step and the other obtained while the load was decreased in each step. The results were very similar. this procedure was repeated 4 times and readings were recorded. The readings from each loading level were repeatable at each strain gauge without any significant variation. At any defined load level, for example 15 kN, an average value for 8 readings from four repeated tests was calculated for each strain gauge.

6.6 RESULTS OF THE EXPERIMENT

The experimental results are listed in Table 6.2. Since the reading from each strain gauge was linear with different load levels, only the data corresponding to the 15 kN tensile load level was used to compare with the finite element model output. The values in the table are the average values.

Based on these data, with linear interpolation, the strain can be defined along the embedment length. Therefore, the tensile stresses can be calculated from the tensile strain as:

$$\sigma = E\varepsilon \qquad (6.1)$$

where, σ = tensile stress (MPa)

E = modulus of elasticity of steel, $E=2 \times 10^5$ MPa

ε = tensile strain (mm/mm)

Table 6.2 Test results of Experiment Five

5000			5001			5002			5003		
Gauge No.	Gauge Location (mm)	Micro-strain	Gauge No.	Gauge Location (mm)	Micro-strain	Gauge No.	Gauge Location (mm)	Micro-strain	Gauge No.	Gauge Location (mm)	Micro-strain
			1	5	290	1	5	224			
1	15	285	2	15	258	2	15	207	1	15	259
			3	25	243	3	25	198			
2	50	246	4	65	211	4	65	165			
			5	125	148	5	125	149			
3	110	189	6	185	129	6	185	135			
			7	235	114	7	235	128	2	235	103
4	170	148	8	275	107	8	275	125			
			9	315	98	9	315	112	3	315	71
5	230	119	10	335	85				4	335	61
									5	345	91
6	290	66	11	355	74	10	355	82	6	355	191
			12	375	55	11	375	50			
						12	385	32	7	385	114
			13	395	37	13	395	18	8	395	85

Note: Gauge location was measured from the outer end of the embedment in the longitudinal direction.

Assuming that tensile stress is uniformly distributed over the cross-section of the steel rod, the corresponding tensile force can be calculated as follows:

$$P = \sigma A \tag{6.2}$$

where, P = tensile force (N)

A = stress area of the steel rod (mm^2)

The average shear stress between any two adjacent strain gauges on the steel-epoxy interface can be expressed rationally as:

$$\tau = \frac{\Delta P}{\pi d_s \Delta z} \tag{6.3}$$

where, τ = average shear stress over Δz length (MPa)

ΔP = the difference in tensile force over Δz length (N)

Δz = distance between two adjacent strain gauges (mm)

d_S = diameter of the steel rod where the strain gauges are located (mm)

In this experimental stress distribution analysis, the average shear stress between any two adjacent strain gauges can be calculated using equations 6.1 to 6.3. For the regions close to either inner or outer embedment end, the average shear stress can be obtained using the data from the closest strain gauge to the end and the boundary condition at the end of the embedment. That is, the tensile force is 15 kN at the outer end of the embedment while it should equal zero at the inner end of the steel rod.

Taking specimen 5000 as an example, Figure 6.6 shows the analytical procedure for the stress distribution experiment. The same principle and procedure were used for other specimens. As can be seen from Figure 6.6, the first data point from left in the strain-distance plot, was calculated based on the assumption that the 15 kN tensile force

was applied on the steel rod at the outer end of the embedment. Therefore, the corresponding stress on the steel rod can be calculated as:

$$\sigma = \frac{P}{A} \tag{6.4}$$

and the corresponding strain on the steel rod surface at the outer end of the embedment is given by:

$$\varepsilon = \frac{\sigma}{E} \tag{6.5}$$

Data points for shear are located mid-way between two corresponding adjacent data points for tensile force.

Step one:

Plot the strain values obtained from the experiment

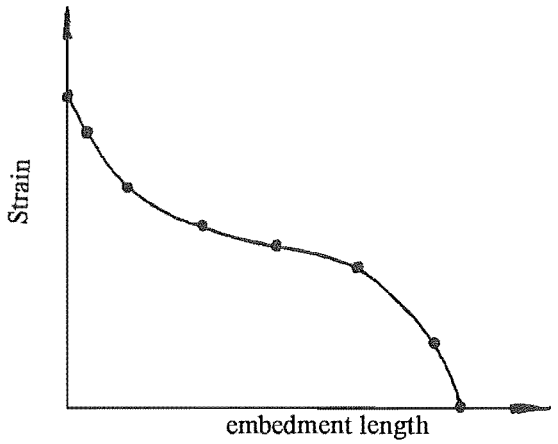

Step two:

Calculate tensile stress.

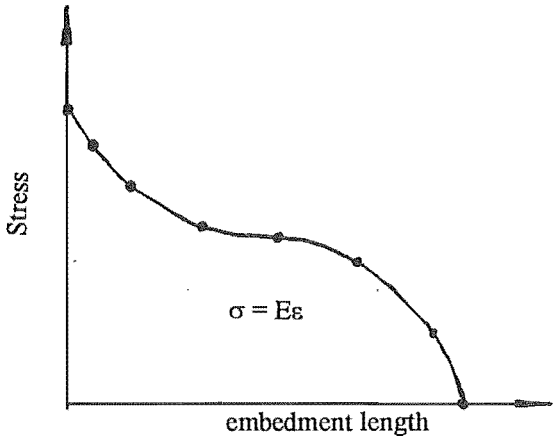

Step three:

Calculate tensile force.

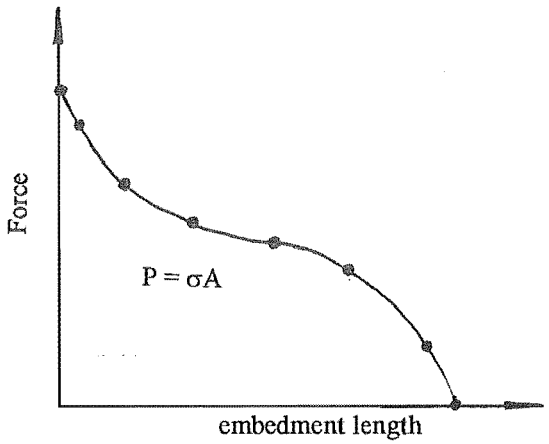

Step four:

Calculate shear stress.

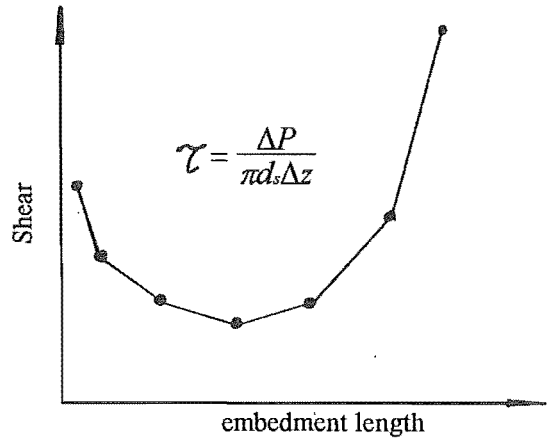

Figure 6.6 Diagram of analysis method for the stress distribution

6.7 CORRELATION OF EXPERIMENTAL AND THEORETICAL RESULTS

The theoretical analysis of the epoxied steel connection was carried out with the finite element method using the ABAQUS computer program; the experimental method relied on the strain measurement technique. The correlation between the experimental results and the finite element model output verifies the validity and accuracy of the finite element model.

In order to make the comparison, the finite element model was re-computed with the parameters corresponding to each individual experimental specimen. The model parameters are listed in Table 6.3. The results for each specimen were compared with the corresponding model output and shown graphically in Figure 6.7 to Figure 6.11 respectively.

Table 6.3 Parameters used in the finite element model for the corresponding experimental specimens

ABAQUS Programme Code	Corresponding Specimen	Parameters					
		Epoxy MOE (GPa)	Steel MOE (GPa)	Bar Diameter (mm)	Embedment (mm)	End Hole Depth (mm)	End Hole Diameter (mm)
T4-B	5000	4	200	17	300	-	-
exp5-2	5001	4	200	17	400	-	-
exp5-1	5002	4	200	20	400	-	-
exp5-7	5003	4	200	17	400	50	14

Note: The mechanical properties of the glulam timber remain unchanged for all corresponding test specimen and can be referred from Table 5.2 (b) in Chapter Five.

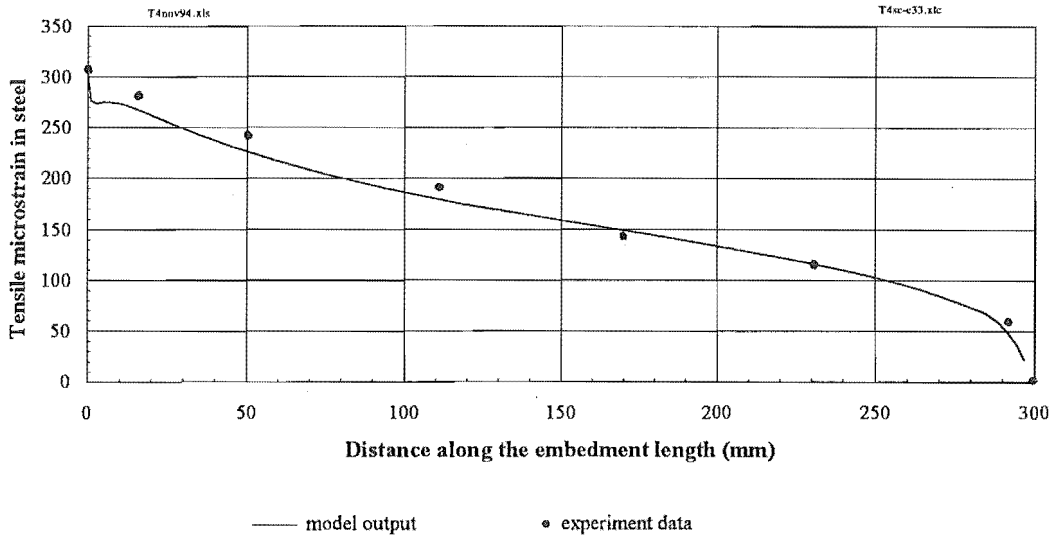

(a) Tensile strain distribution along the embedment at the steel-epoxy interface

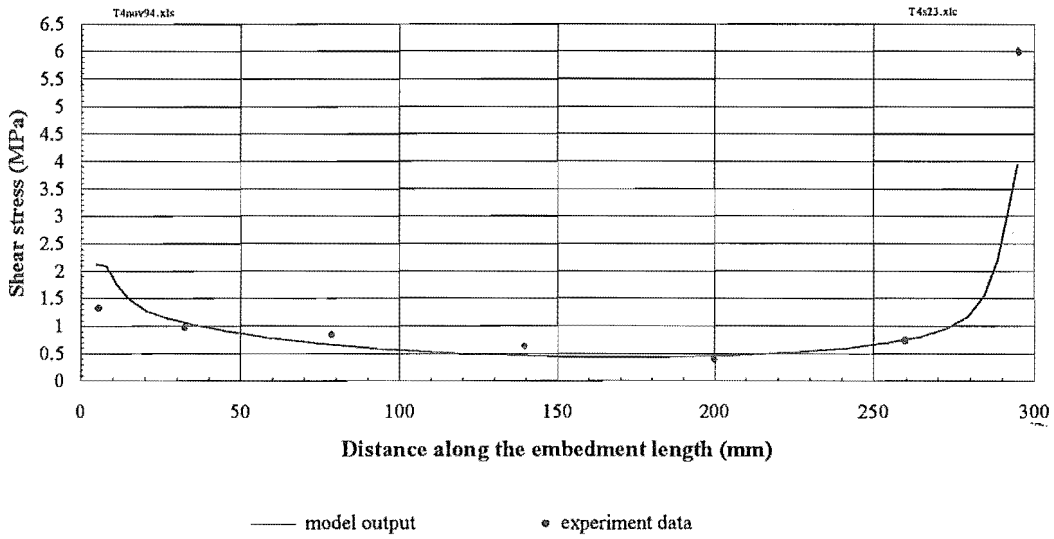

(b) Shear stress at the interface along the embedment

Figure 6.7 Comparison of the experimental results for specimen 5000 with the corresponding finite element model output

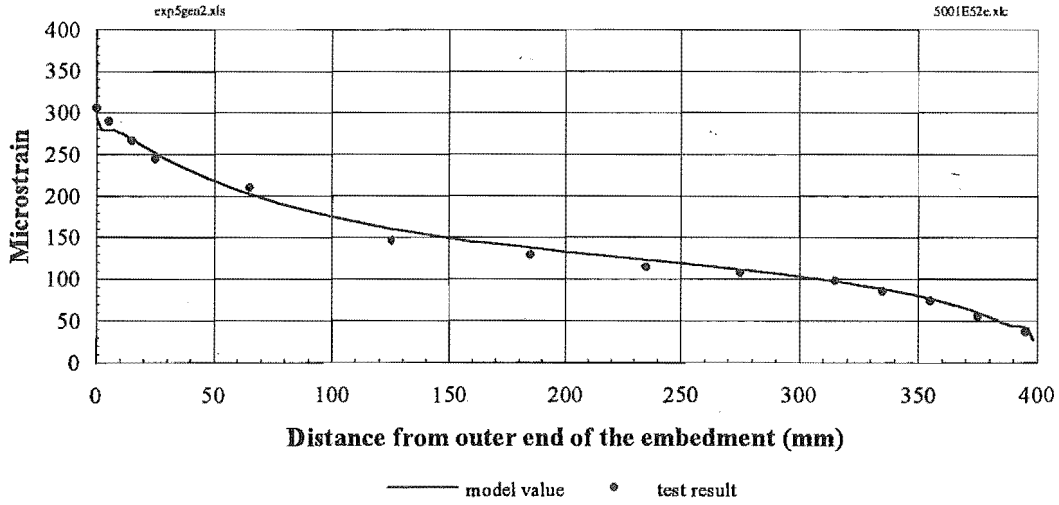

(a) Tensile strain distribution along the embedment at the steel-epoxy interface

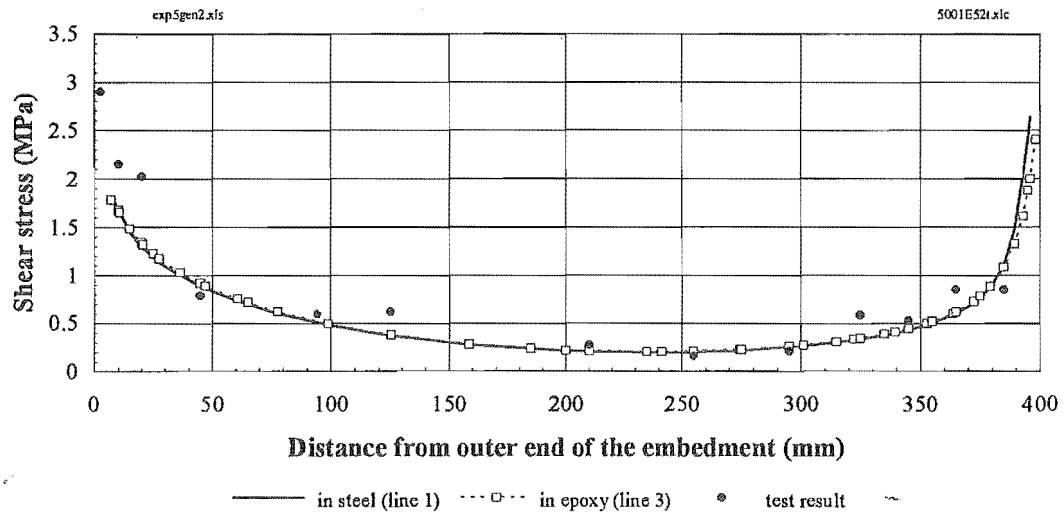

(b) Shear stress at the interface along the embedment

Figure 6.8 Comparison of the experimental results for specimen 5001 with the corresponding finite element model output

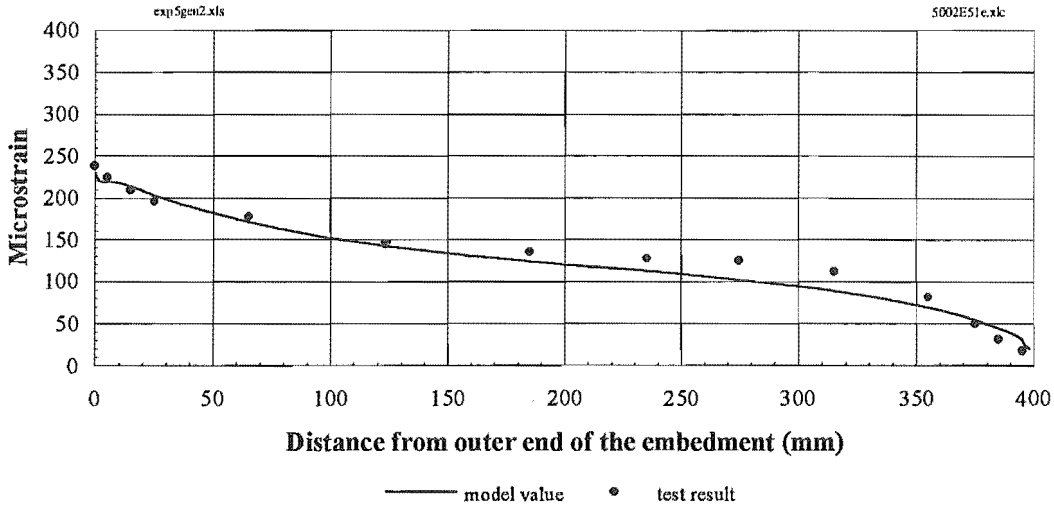

(a) Tensile strain distribution along the embedment at the steel-epoxy interface

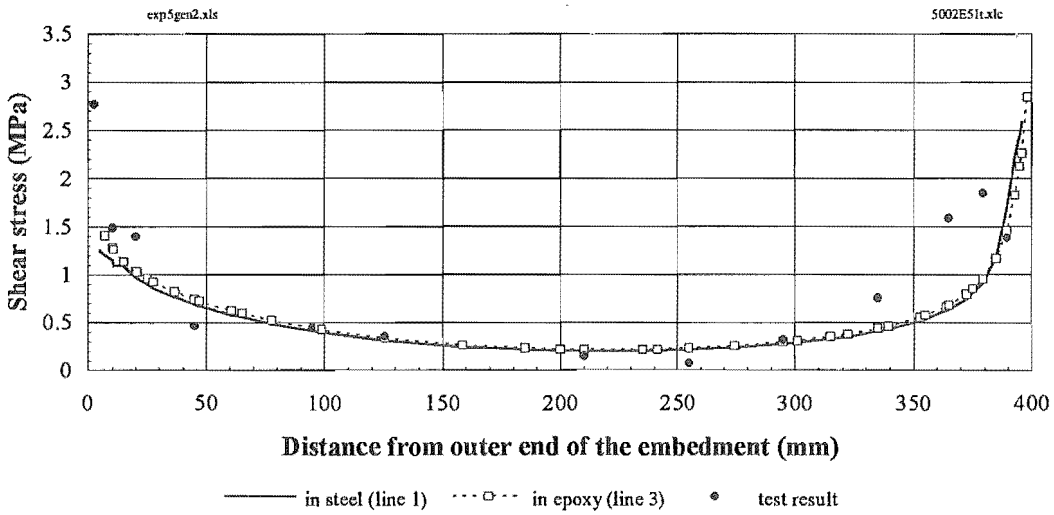

(b) Shear stress at the interface along the embedment

Figure 6.9 Comparison of the experimental results of specimen 5002 with the corresponding finite element model output

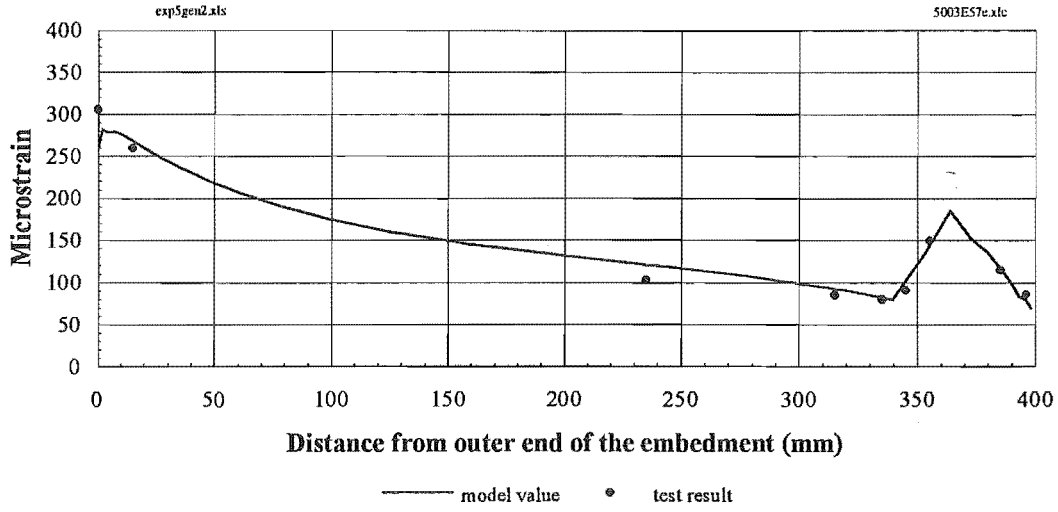

(a) Tensile strain distribution along the embedment at the steel-epoxy interface

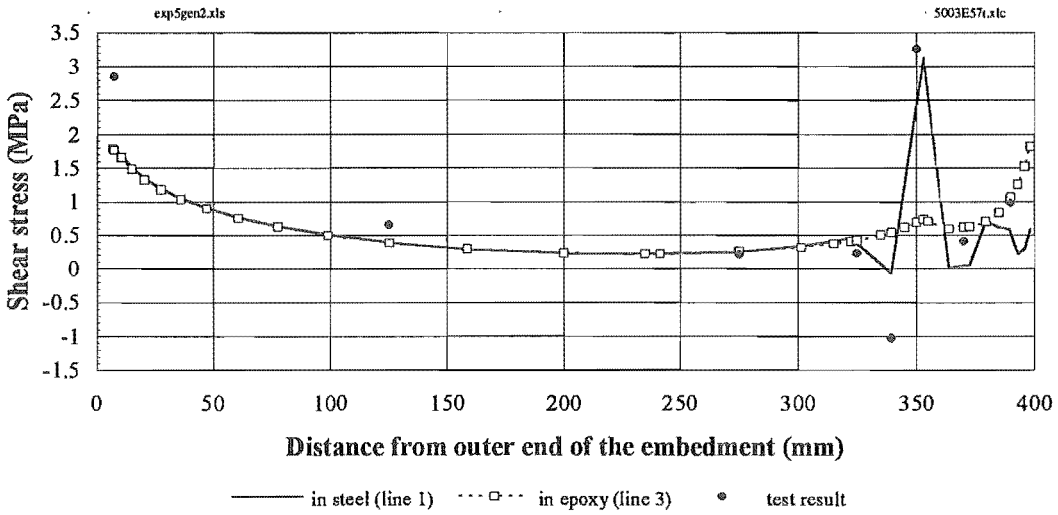

(b) Shear stress at the interface along the embedment

Figure 6.10 Comparison of the experimental results of specimen 5003 with the corresponding finite element model output

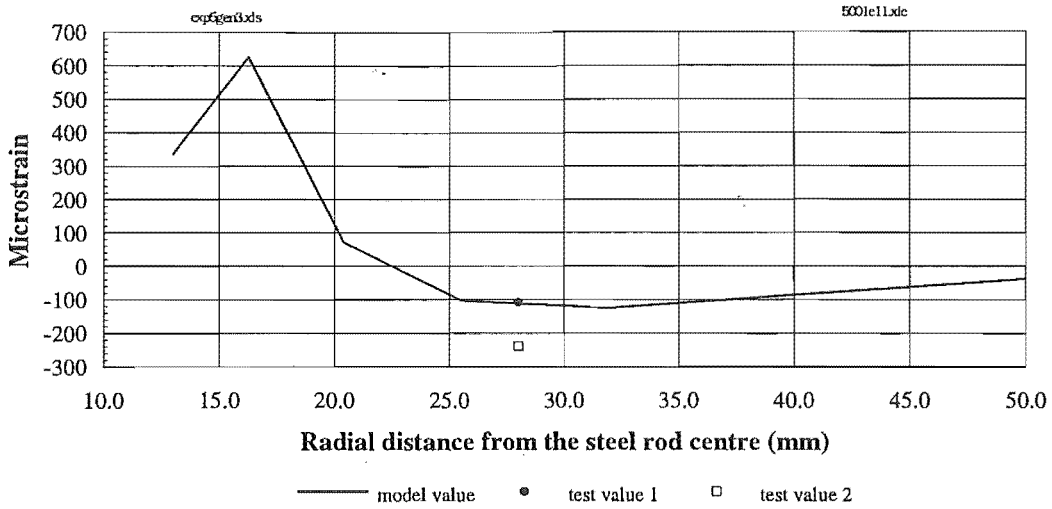

(a) Strain in radial direction

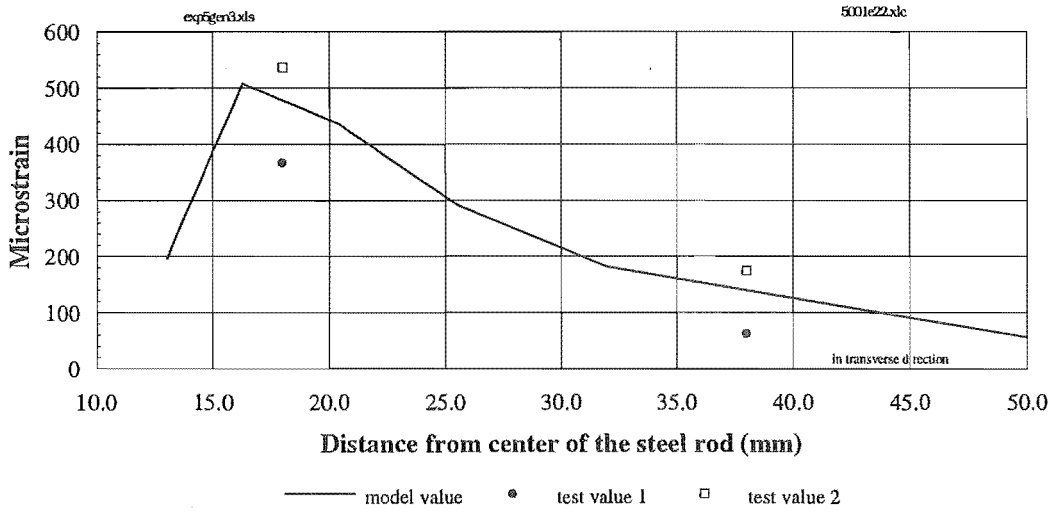

(b) Strain in transverse direction

Figure 6.11 Comparison of the strain gauge data at the end cross-section of specimen 5001 with the model prediction

As can be seen from Figures 6.7 to 6.11, the stress distribution patterns in the experimental specimens are very similar among the smooth and threaded steel rod connections. The experimental and finite element results are in reasonably good agreement. This suggests that the model can be used with confidence for further study to analyse the stress distribution in the connection with threaded rod. A parametric study using the finite element model will show the potential application of the model (Chapter 7).

6.8 STRESS DISTRIBUTION PREDICTED IN THE MODEL

An analysis of the stress distribution was carried out using the finite element model once the model had been verified by the experimental method. The analysis seeks to understand the stress distributions and to identify the regions of stress concentration. The standard input parameters of the model were used as shown in Table 5.1. The tensile load on the steel rod was 50 kN.

6.8.1 Some Considerations Concerning the Stress Distribution Analysis

After the model was computed with ABAQUS finite element programme, the following outputs could be produced for each individual node point:

1. The principal normal stress: σ_x, σ_y, σ_z[1]
2. Shear stress: τ_{xy}, τ_{xz}, τ_{yz}[2]
3. Displacement: u_x, u_y, u_z[3]

Although the output of the model could cover all of stress components and displacements, only some of stress components were considered and the displacements of the model were not considered in the study of stress distribution. This study was based on the analysis of the failure modes from short duration experiments, the model assumption and primary data analysis of the model output. For example, from primary data analysis, it was noted that the magnitude of shear stress τ_{xy} in the cross-section of the model was very small, which corresponds to experimental results that the failure modes were not caused by the shear stress τ_{xy}. Therefore, four stress components were selected to analyse the stress distribution as listed in Table 6.4.

---

1 A component of normal stress is parallel to the axis of the subscript.

2 The first subscript of a shear stress component is the coordinate normal to the element face. The shear stress component parallel to the axis of the second subscript.

3 A component of displacement is parallel to the axis of the subscript.

Table 6.4 Stress component used in stress distribution analysis

Stress Component		
Expression in text	Symbol used in text	Symbol used in ABAQUS
Shear stress along the embedment	τ_{yz}	S_{23}
Tensile stress along the embedment	σ_z	S_{33}
Tangential stress	σ_x	S_{11}
Radial stress	σ_y	S_{22}

6.8.2 Simplifying Presentation

Although a great number of output data were obtained after the finite element model was computed, only part was required for the study of stress distribution. In this study, the major regions of interest were the regions around the steel-epoxy interface, the epoxy-wood interface and both ends of the embedment.

The original format of the output was in the sequence of node numbers regardless the physical position in the connection; it is difficult and tedious to present the results in such a data format. Therefore, this format must be modified so that the output data can be easily and clearly presented in terms of the geometric location. A simplification of the model output was considered. Further data processing was carried out using ABAQUS POST program (ABAQUS 1993b) and Excel in order to abstract the required data.

The output data was abstracted from the y-z plane of the model. It is believed that the 3-dimensional model space can be well presented using the 2-dimensional y-z plane because of symmetry (Figure 5.3 (b)). This is why the shear stress in the embedment direction can be represented by one shear stress component τ_{yz} in the y-z plane (Table 6.4). The y-z plane of the model is sketched in Figure 6.12 to show the location of the data abstracted. A similar simplification procedure for the data presentation was also used in the further parametric study.

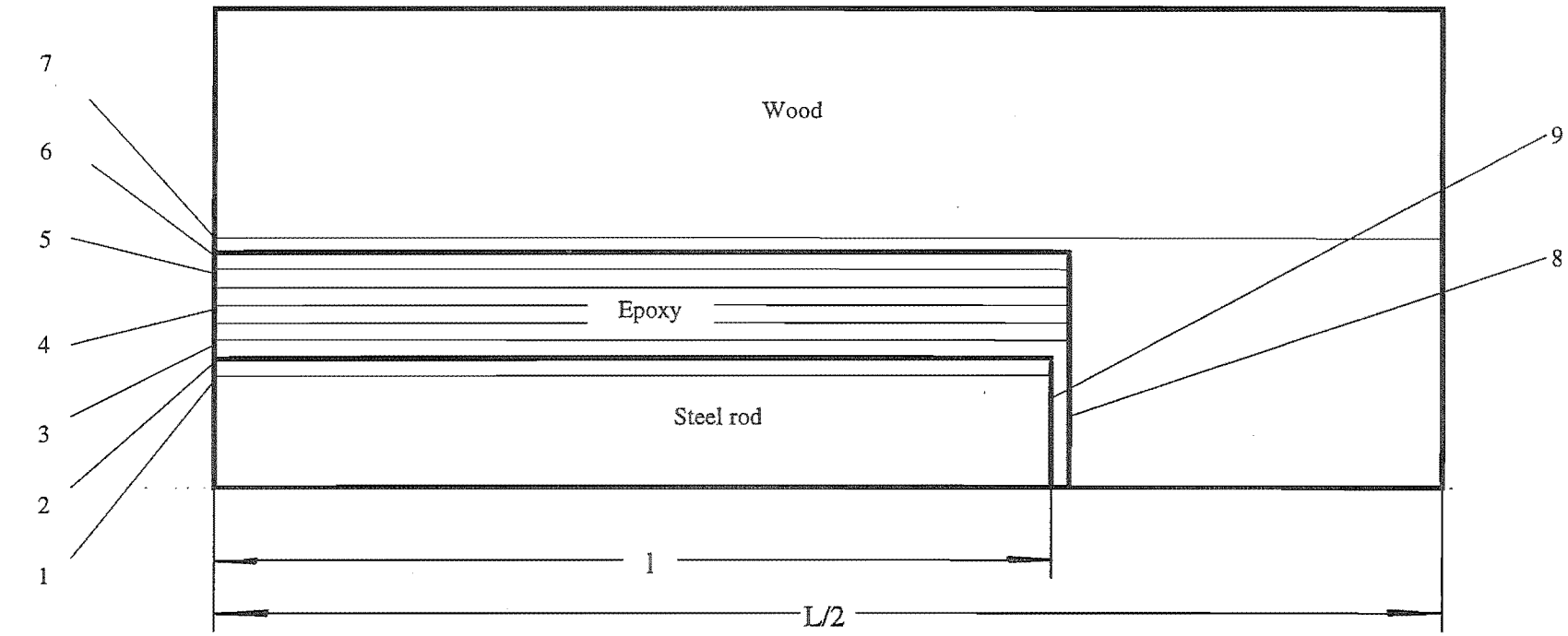

1 = 0.5mm away from the steel-epoxy interface, inside steel. 2 = The steel-epoxy interface.

3 = 0.5mm away from the steel-epoxy interface, inside epoxy. 4 = The centre of epoxy.

5 = 0.5mm away from the wood-epoxy interface, inside epoxy. 6 = The wood-epoxy interface.

7 = 0.5mm away from the wood-epoxy interface, inside wood. 8 = The end of embedment hole.

9 = The end of steel rod.

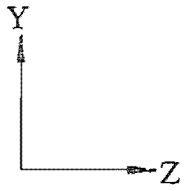

Figure 6.12 Sketch of Y-Z plane of the model (Not to scale)

6.8.3 Shear Stress Distribution

Figure 6.13 shows the shear stress distribution within the epoxy layer along the embedment length. The top solid line represents the shear stress at the steel-epoxy interface. The bottom dotted line represents the shear stress along the epoxy-wood interface. Both lines are actually located inside the epoxy close to the interfaces (line 3 and line 5 respectively in Figure 6.12); the central dashed line is the shear stress at the centre of epoxy. As expected, the highest shear stress concentration regions are at both embedment ends. The stress concentration is higher at the inner embedment end than at the outer end.

The average shear stress in the steel-epoxy interface is 2.65 MPa. The value is calculated using Equation 4.1. A line parallel to the x-axis drawn in Figure 6.13 to represent the average shear stress, indicates that the shear stress is below the average in the central region of the embedment, whereas it is much higher than the average in both embedment end regions. The shear stress close to the steel-epoxy interface is about four times more than the average shear stress at the inner end of the embedment.

A stress gradient exists across the thickness of the epoxy, especially at both embedment end regions. The highest shear stress is at the steel-epoxy interface and the lowest shear stress is at the epoxy-wood interface. The shear stress and the shear stress concentrations decrease across the epoxy thickness from the steel-epoxy interface to the epoxy-wood interface.

6.8.4 Tensile Stress Distribution

Figure 6.14 shows the tensile stress distribution along the entire embedment length; the top solid line being the tensile stress distribution in the wood at the region very close to the epoxy while the bottom dotted line represents the tensile stress distribution at the centre of the epoxy. The average tensile stress is also shown on the figure, this assumes that the tensile stress is uniformly distributed over the cross-section, so that the stress can be calculated using Equation 6.4 with the whole cross-section of the model as the stress area. It can be observed that the highest tensile stress

concentration regions for both epoxy and wood are at the inner embedment end and the epoxy has a higher tensile stress concentration value than in the wood. In this region the tensile stresses are higher than the average tensile stress.

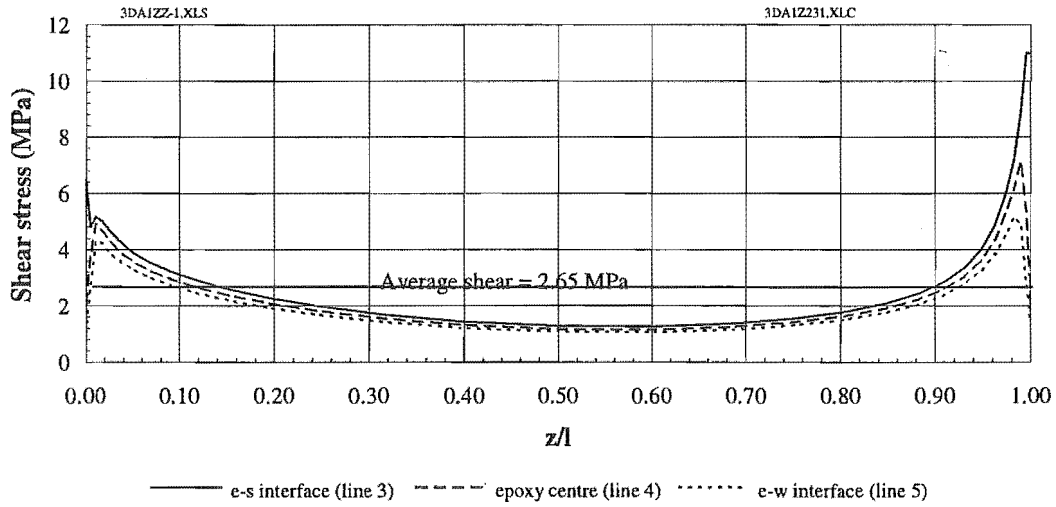

Figure 6.13 Shear stress distribution along the embedment

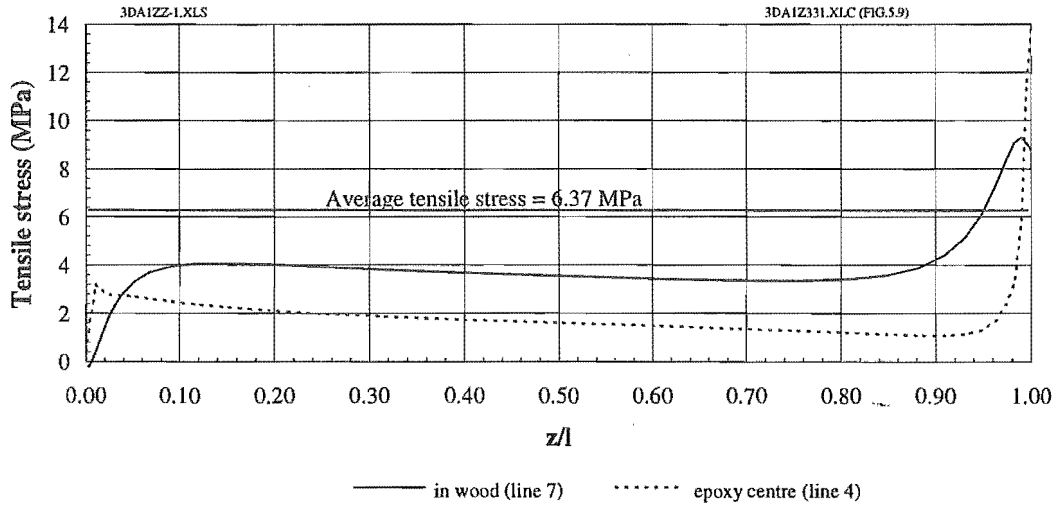

Figure 6.14 Tensile stress distribution along the embedment

6.8.5 Tangential Stress Distribution

The tangential stress is in terms of the mesh of the finite element model, the tangential direction is the direction tangential to the arc of the mesh outline in the model and shown in Figure 6.15. Figure 6.16 shows the tangential stress distribution along the embedment. It only shows the first 30 mm of the embedment length from the outer end

of the embedment, as the magnitudes of the stress are close to zero elsewhere. As can be observed from the figure, the stress has a higher value at the steel-epoxy interface than at the epoxy-wood interface. All of the tangential stresses are below the average tensile stress along the longitudinal direction (6.37 MPa), which is shown on the figure for comparison. It is noticed that Figure 6.16 does not represent the stress distribution in the connection with deformed rod as the deformations could not be easily modelled and are not considered in the model. Likewise for the radial stress distribution.

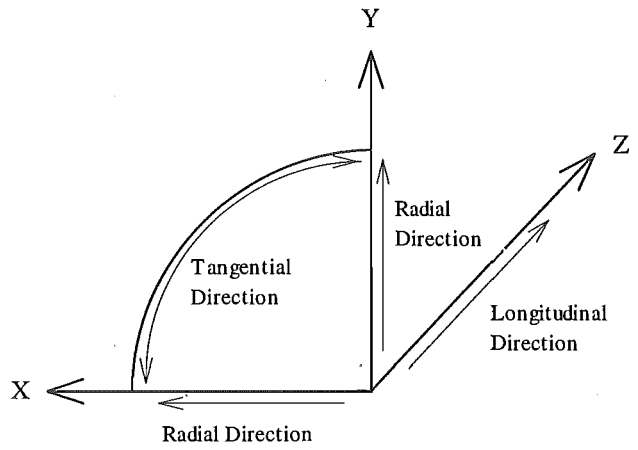

Figure 6.15 Longitudinal, tangential and radial direction of the model in stress analysis

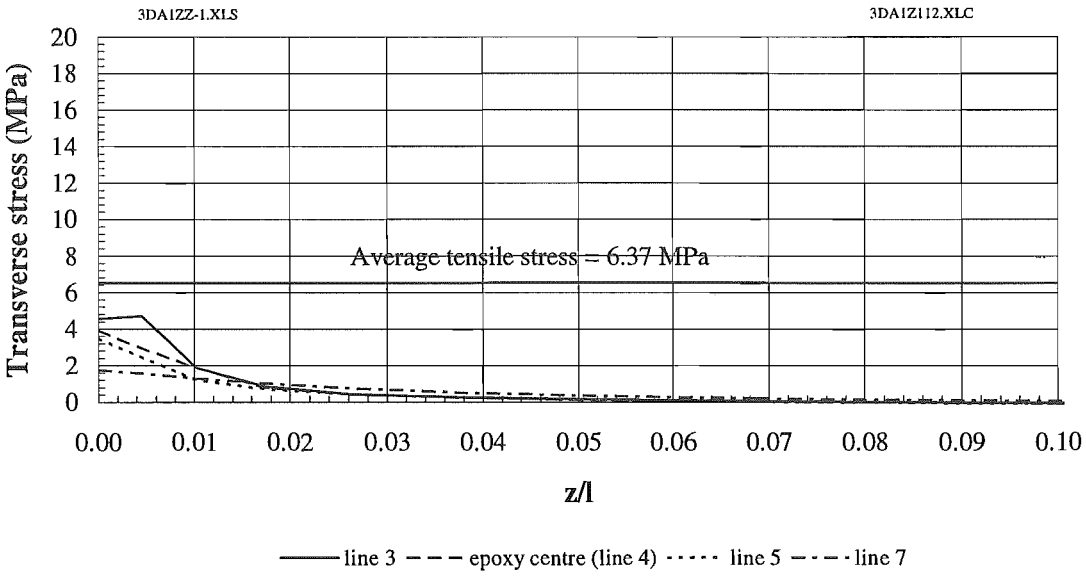

Figure 6.16 Tangential stress distribution along the embedment

6.8.6 The Radial Stress Distribution

Figure 6.17 displays the radial stress distribution along the embedment length. The radial direction is in terms of the arch of the mesh outline in the finite element model, the direction of the stress being parallel to the y-axis and does not correspond to the radial direction of the wood grain. Significant magnitudes of the stress only can be observed at the outer end of the embedment region. Within this region, the highest stresses are at the outer end. Comparing the two interfaces, the radial stress is much higher in the steel-epoxy interface than in the epoxy-wood interface. At the region very close to the embedment end, the stresses in both interfaces and in the epoxy centre are greater than the average longitudinal tensile stress (6.37 MPa), whereas the radial stress is below the average longitudinal tensile stress in the wood.

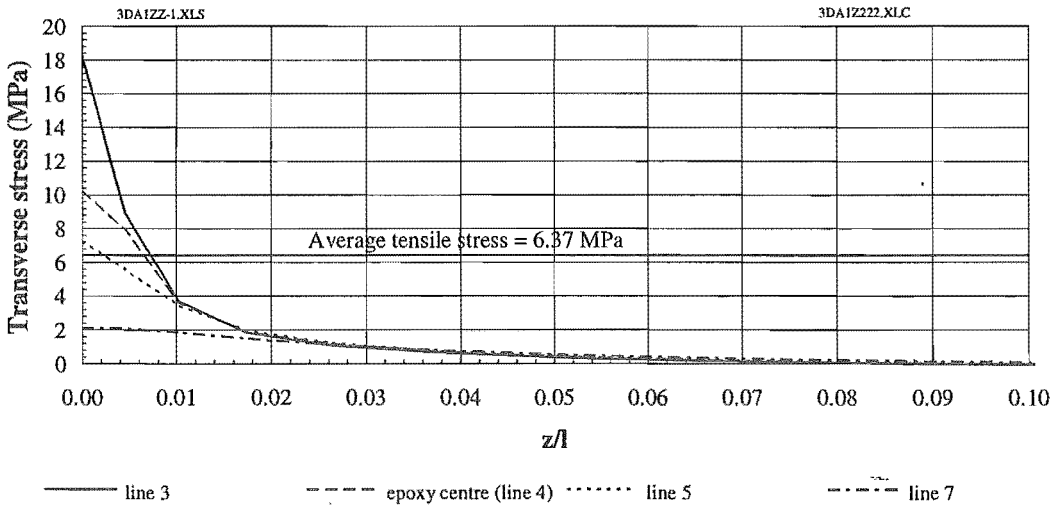

Figure 6.17 The radial stress distribution along the embedment

6.9 DISCUSSION

6.9.1 Experimental Results and the Finite Element Model

Although tensile strains were measured only on the surface of the steel rod along the embedment length for experimental study on the stress distribution of the

connection, the results can represent the characteristics of the steel-epoxy interface. With simple calculations, the experiment results can be converted into the shear stress of the steel-epoxy interface and force in the wood in longitudinal direction as described graphically in Figure 6.6.

A comparison of experimental data points in specimen 5001 with the corresponding model output in Figure 6.8, indicate that the model programmed using the smooth surface steel rod can provide a sufficiently accurate representation of the connection with the threaded rod. Furthermore, a comparison of specimen 5001 (Figure 6.8) with specimen 5002 (Figure 6.9), suggests that no significant difference exists in terms of the stress distribution between the threaded rod connection and the connection with the smooth surface steel bar, since both specimens fit the model output and with similar patterns.

The experiment has used a practical and reliable method to investigate the stress distribution in the connection. The experimental results and the corresponding model output are in accord.

6.9.2 Stress Concentrations and Failure Modes

A better understanding of the stress distribution and the mechanism of the connection can be obtained by the finite element model since failure in the connection seems mostly to occur at a region with high stress concentration. There is a strong correlation between the failure mode and stress concentration.

In terms of tangential and radial stresses, both have a high stress concentration at the outer end of the embedment, accompanied by higher shear stress in the same region. It seems likely that the combination of these stresses causes Type 2 failure mode; the glulam timber around the connection splits at the outer embedment end region and the steel bar pulls out from the epoxy confinement. This failure mode is one of the major failure modes in the short duration experiments.

The stress gradient over the cross-section at the outer end of the embedment may also contribute to this failure mode. It can be seen from Figure 6.13, Figure 6.16 and Figure 6.17 that the shear stress and both transverse stresses are much higher in the steel-epoxy interface than in the epoxy-wood interface, possibly one reason why most Type 2 failures occur in the steel-epoxy interface.

In terms of the tensile stress, the highest stress concentration is at the inner end of the embedment, probably causing the tensile failure at the inner end of the embedment. This kind of failure has been observed in the short duration experiments and has been defined as Type 3 Failure Mode. Shear stress is highest in the same region.

6.9.3 Effect of Geometry Change to Stress Distribution

Comparing Figure 6.10 with Figure 6.8, the shear stress distribution changes with the geometry of the connection. This phenomenon suggests that it is possible to improve the capacity and performance of the epoxy bonded steel connection by modifying the geometry to reduce the stress concentrations and this possibility is investigated in a parametric study using the finite element model in Chapter 7.

6.10 CONCLUSIONS

The following conclusions can be drawn from the theoretical model and experimental verification:

1. The output from the finite element model are in accord with the experimental results. The model programmed using a smooth surface steel rod can accurately represent the connection with the threaded rod. The model used to analyse the epoxied steel connection is therefore valid.

2. Along the embedment, the highest shear stress concentration occurs at the both ends of the embedment, with the stress concentration at the inner end higher than the outer end of the embedment.

3. High shear stress gradient occurs across the thickness of the epoxy at the regions close to either the inner or the outer embedment end, whereas only a marginal stress gradient occurs elsewhere. The highest shear stress gradient exists at the inner embedment end region.

4. The highest tensile stress concentration occurs at the inner end of the embedment.

5. At the outer end of the embedment both the tangential and the radial stresses have their highest values, and it appears that the values at the steel-epoxy interface are higher than those at the epoxy-wood interface. All of the transverse stresses analysed in this study are tensile stresses.

6. There is a strong correlation between the failure mode and the stress concentration.

CHAPTER SEVEN

STRESS DISTRIBUTION IN THE CONNECTION: A PARAMETRIC STUDY

7.1 OBJECTIVE

A theoretical model of the epoxied steel connection has been established using the finite element method with a computational program ABAQUS. A parametric study has been undertaken using this theoretical model.

The parametric study is to analyse and determine quantitatively the effects of the material properties and various geometries of the connection. This parametric study should result in a more comprehensive understanding of the connection and gives the potential for development of a better design philosophy to produce more reliable and efficient connections.

7.2 DESIGN OF THE PARAMETRIC STUDY

7.2.1 The Reference Model and Parameters

The parametric study is based on the theoretical model described in Chapter Five. This model is modified and used as the reference model. The study has been carried out by varying one parameter at a time from the reference model. The rest of the parameters remain unchanged. Four geometric parameters are considered: edge distance (e), embedment length (l), thickness of epoxy (t_e) and steel rod end geometry. Only one parameter related to material property is subjected to change, this is the modulus of elasticity (MOE) of the epoxy. The parameters varied in the study are shown in Table 7.1.

By changing the MOE of the epoxy, the following combinations of material properties can be obtained:

$$E_S > E_W > E_a$$

or $$E_S > E_W = E_a$$

or $$E_S > E_a > E_W$$

where, E_S = modulus of elasticity of the steel

E_W = modulus of elasticity of the wood

E_a = modulus of elasticity of the epoxy

7.2.2 Non-dimensionalized Stress

All of the stresses presented in this study are non-dimensionalized with respect to one of the following nominal stresses in the reference model.

(1) The nominal tensile stress σ_{nz} of the reference model, being the average tensile stress over the cross section of the model:

$$\sigma_{nz} = \frac{P}{A} \qquad (7.1)$$

where, σ_{nz} = nominal tensile stress of the reference model (MPa)

P = applied tensile load in the connection (N), in this study P = 50,000 N

A = stress area of the reference model (mm^2), $A = \pi R^2$

R = radius of the cross-section of the reference model (mm)

(2) The nominal shear stress τ_{nyz} of the reference model on y-z plane, being the average shear stress over the surface of the steel rod:

$$\tau_{nyz} = \frac{P}{\pi dl} \qquad (7.2)$$

where, τ_{nyz} = nominal shear stress of the reference model (MPa)

d = steel rod diameter in the reference model (mm)

l = embedment length of the reference model (mm)

The nominal tensile and shear stress values are listed in Table 7.1. During the parametric study and analysis of stress distribution, three non-dimensionalized stresses were used. They are defined as follows:

Tensile stress ratio: σ_z / σ_{nz}

Shear stress ratio: τ_{yz} / τ_{nyz}

Transverse stress ratio: σ_x / σ_{nz}

where, σ_z = the principal stress component in z direction of the model coordinate

σ_x = the principal stress component in x direction of the model coordinate

τ_{yz} = shear stress in y-z plane of the model space

7.2.3 Non-dimensionalized Coordinates

The location of the stress is defined by non-dimensionalized coordinates, that is, z/l in the longitudinal direction and r/R in radial direction. In the parametric study with Cartesian coordinates (Figure 5.3 (a)), r is presented by y within the y-z plane and R is the relevant radius of the cross-section in the modelled specimen.

The design of the parametric study and values of the parameters are shown in Table 7.1 and divided into 5 subgroups. The data analysis and comparisons are made within the subgroups. Efforts have been made to cover most aspects of the connection while simplifying the data analysis and presentation.

Table 7.1 The design of parametric study and the values for the parameters

Groups	Parameter	Unit	Absolute magnitude	Non-dimensional		σ_{nz} (MPa)	τ_{nyz} (MPa)	R (mm)	Program code
				Parameter	Values				
Reference model	d	mm	20	-		6.37	2.65	50	3DA-1
	e	mm	45	e/d	2.25				
	l	mm	300	l/d	15				
	t_c	mm	3	t_c/d	0.15				
	E_s	GPa	200	E_s/E_w	25				
	E_w	GPa	8	-	-				
	E_a	GPa	4	E_a/E_w	0.5				
	L	mm	450	L/l	1.5				
Subgroup one	e	mm	30	e/d	1.5	6.37	2.65	34	3DA-2-1
			45		2.25			50	*3DA-2-2*
			60		3			68	3DA-2-3
			75		3.75			85	3DA-2-4
			90		4.5			102	3DA-2-5
Subgroup two	l	mm	200	l/d	10	6.37	2.65	50	3DA-3-1
			250		12.5				3DA-3-2
			300		15				*3DA-3-3*
			350		17.5				3DA-3-4
			400		20				3DA-3-5
Subgroup three	t_c	mm	2	t_c / d	0.1	6.37	2.65	50	3DA-4-1
			3		0.15				*3DA-4-2*
			4		0.2				3DA-4-3
			6		0.3				3DA-4-4
Subgroup four	E_a	GPa	4	E_a / E_w	0.5				*3DA-5-1*
			8		1.0				3DA-5-2
			12		1.5				3DA-5-3
Subgroup five	l_h	mm	20	l_h/d	1.0	6.37	2.65	50	3DA-6-3
			45		2.25				3DA-6-4
			-		-				*3DA-6-5*

Note: 1. The code numbers in Italic style represent the models corresponding to the reference model.

2. For subgroup five, the holes in the steel rod end are 18 mm in diameter.

7.3 PRESENTATION OF THE RESULTS

7.3.1 Scope of Presentation

The data obtained from y-z plane (2-3 plane in ABAQUS notation) of the model space in Figure 5.3 can represent the 3 dimensional characteristics of the model because of symmetry, although the data is obtained from a 2 dimensional plane. In this way, the analysis is simplified.

The y-z plane of the model space and the locations of the data used in the parametric study are sketched in Figure 7.1. The line a-a is located in the epoxy close to the steel-epoxy interface and can be used to analyse the stress distribution around the steel-epoxy interface. The line c-c is in the centre of the epoxy and is used to analyse the stress distribution in the epoxy. Similarly, the line f-f can be used to analyse the stress in the wood near the epoxy-wood interface.

Based on the preliminary study of the stress distribution using the finite element model in Chapter Six and the analysis of the failure modes in the short duration experiments (Chapter Four), the parametric study concentrated on the regions where the magnitudes of the stresses and their gradients are likely to be highest. The regions where the failures occurred mostly in the short duration experiments also were considered. These regions are listed as follows:

1. Shear stress distribution along the embedment at the centre of the epoxy (line c-c in Figure 7.1).

2. Shear stress distribution along the embedment in a region close to the steel-epoxy interface (line a-a in Figure 7.1) and the epoxy-wood interface (line f-f in Figure 7.1).

3. Tensile stress distribution in the wood along the embedment in a region close to the interface (line f-f).

4. Tensile stress distribution over the cross-section at the inner end of the steel rod (represented by line L-L).

5. Transverse stress in the wood along the embedment in a region close to the epoxy-wood interface (line f-f).

6. Transverse stress over the cross-section near the outer end region of the specimen (represented by line P-P).

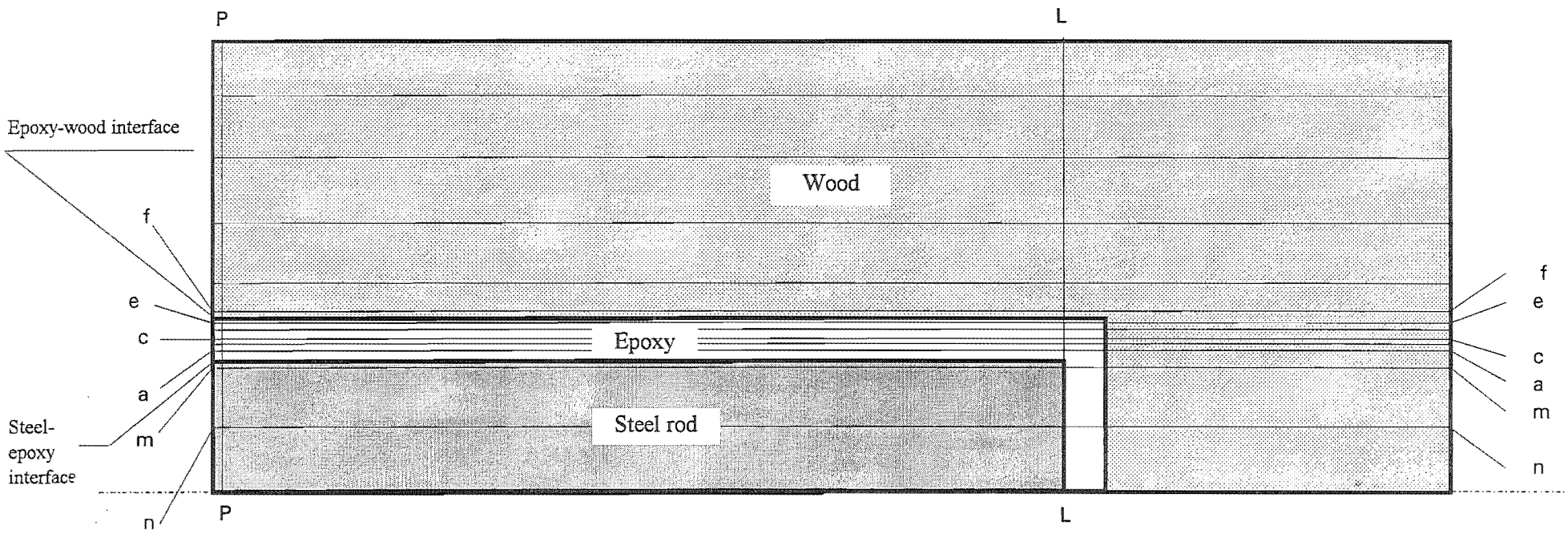

Figure 7.1 The y-z plane of the model and the abstracted data locations (Not to scale)

7.3.2 Shear Stress

1. Effect of edge distance

Figure 7.2 shows the distribution of the shear stress ratio along the longitudinal direction at the centre line of the epoxy, obtained from the different models corresponding to the different edge distance. In Figure 7.2, the straight line at 1.0 parallel to the x-axis corresponds to a uniform shear stress along the embedment, in which, the magnitude equals to the nominal shear stress (the average shear stress) of the reference model. The highest shear stress concentration region is in the section close to the inner end of the embedment. At this region, the shear stress increases as the edge distance decreases. For an edge distance of e=30 mm, the shear stress is almost 4.5 times the nominal shear stress. The shear stress concentration is less at the outer embedment end region than at the inner end. Furthermore, for small edge distances, the shear stress concentrations are higher at the inner embedment end than at the outer end. For larger edge distance, the shear stress concentrations are lower at the inner embedment end than the outer end. It seems that an edge distance of 60 mm gives the best overall shear stress distribution in the epoxy, with similar stress concentrations at the inner and outer ends of the bar.

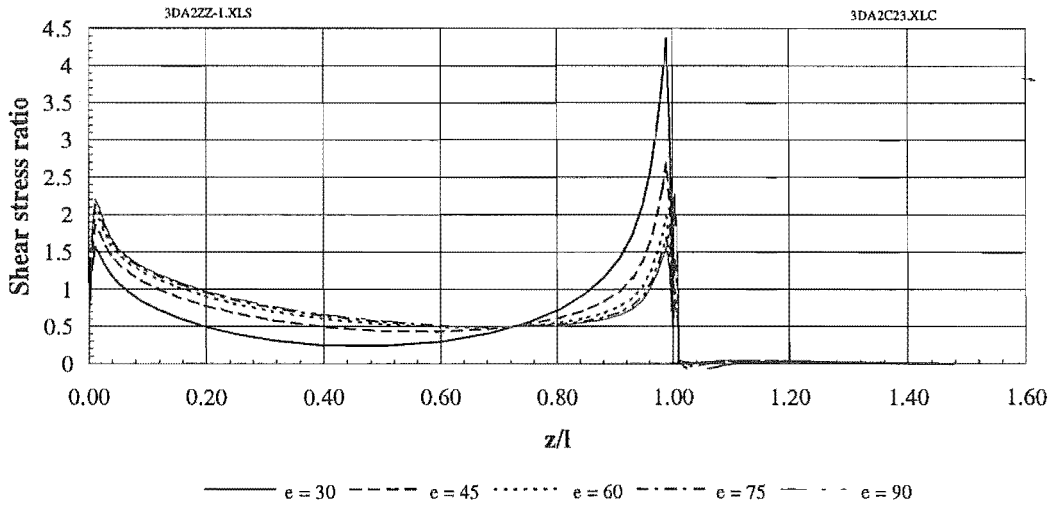

Figure 7.2 Effect of the edge distance on the shear stress distribution (line c-c)

2. Effect of embedment length

Figure 7.3 shows the distribution of the shear stress ratio along the embedment at the centre of the epoxy. From the figure, it can be seen that the overall magnitude of the shear stress decreases as the embedment length increases; that is the average shear stress in the epoxy of the connection can be decreased by increasing the embedment length. However it seems that there is no significant modification of the stress concentration due to increasing the embedment length. Both embedment end regions have a higher shear stress with the highest shear stress concentration region being close to the inner embedment end.

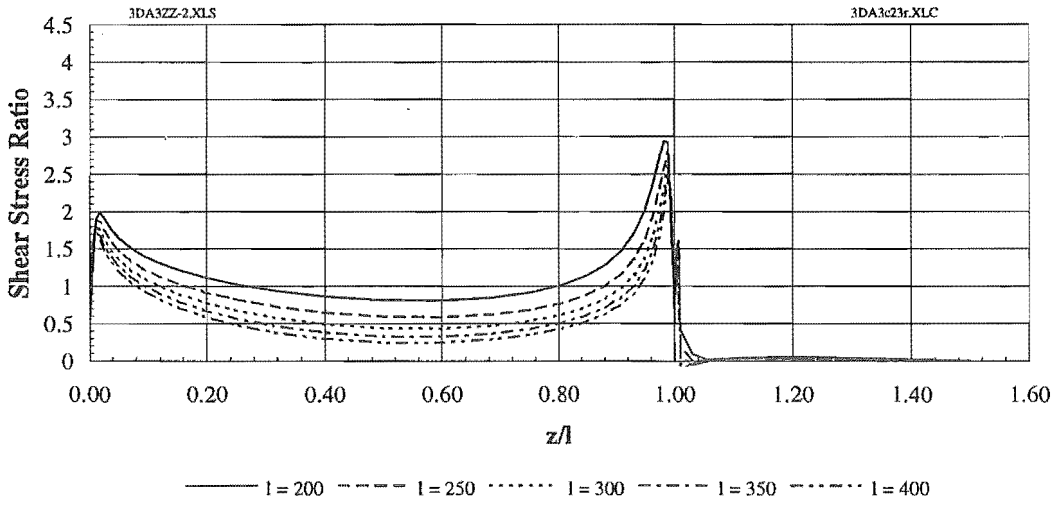

Figure 7.3Effect of the embedment length on the shear stress distribution (line c-c)

3. Effect of epoxy thickness

Figure 7.4 shows the shear stress distributions at the centre of the epoxy along the embedment in terms of different epoxy thickness. it can be seen that the epoxy thickness has a great influence on the shear stress concentration at the both embedment ends, especially at the inner end of the embedment. At this end, the peak value of the shear stress is double when the thickness of the epoxy decreases from 6 mm to 2 mm. However, no significant modification occurs at the centre region of the embedment when the thickness of the epoxy changes.

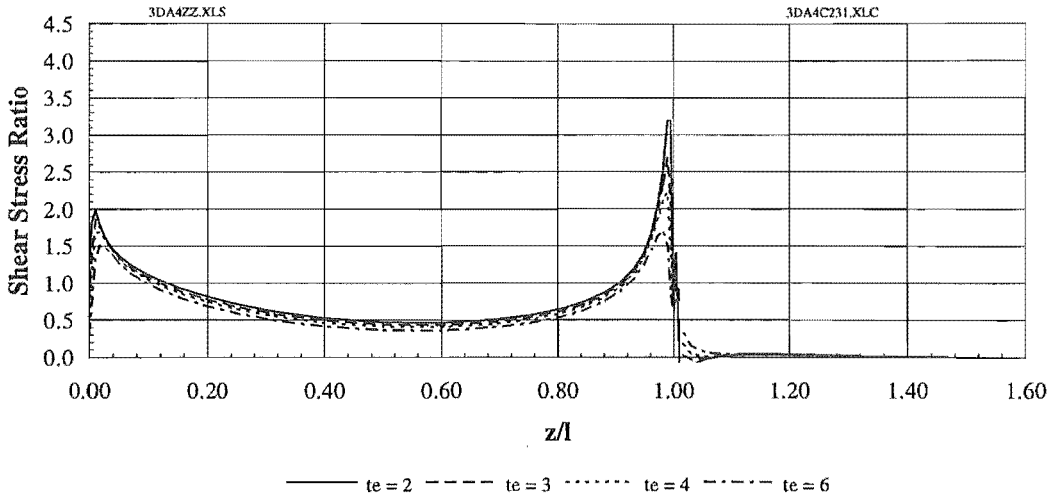

Figure 7.4 Effect of the epoxy thickness on the shear stress distribution (line c-c)

4. Effect of modulus of elasticity of the epoxy

Figure 7.5 shows the shear stress distribution at the centre of the epoxy along the embedment direction. It indicates that the MOE of the epoxy has little influence on the shear stress, especially at middle section of the embedment length. A modest effect can be observed only at the both ends of the embedment, when the shear stress increases as the epoxy MOE increases.

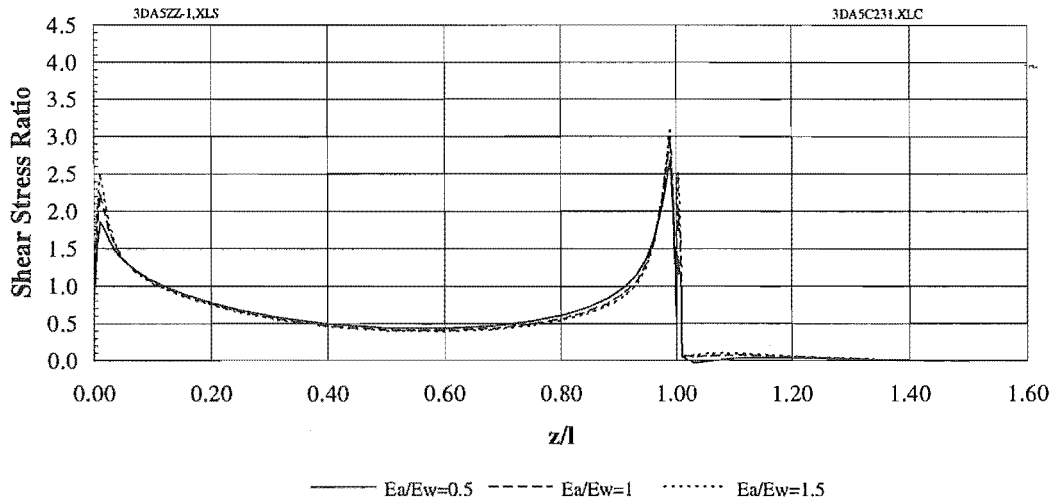

Figure 7.5 Effect of epoxy properties on shear stress distribution (line c-c)

5. Effect of the geometry of the steel rod

Figure 7.6 shows the distribution of the shear stress ratio with different end geometries of the steel rod. It can be seen from the figure, at the inner end embedment region the shear stresses vary with different steel rod end geometry, but in other regions the shear stresses are similar. At the inner embedment end region, comparing the peak value of shear stress in the reference model, the peak value in the epoxy falls almost 50% in the connection with a hole in the end of the steel rod. This indicates that the shear stress concentration in the epoxy can be improved by changing the geometry at the end of the steel rod. There is not much difference in the peak stress level for holes of 20 mm and 45 mm depth.

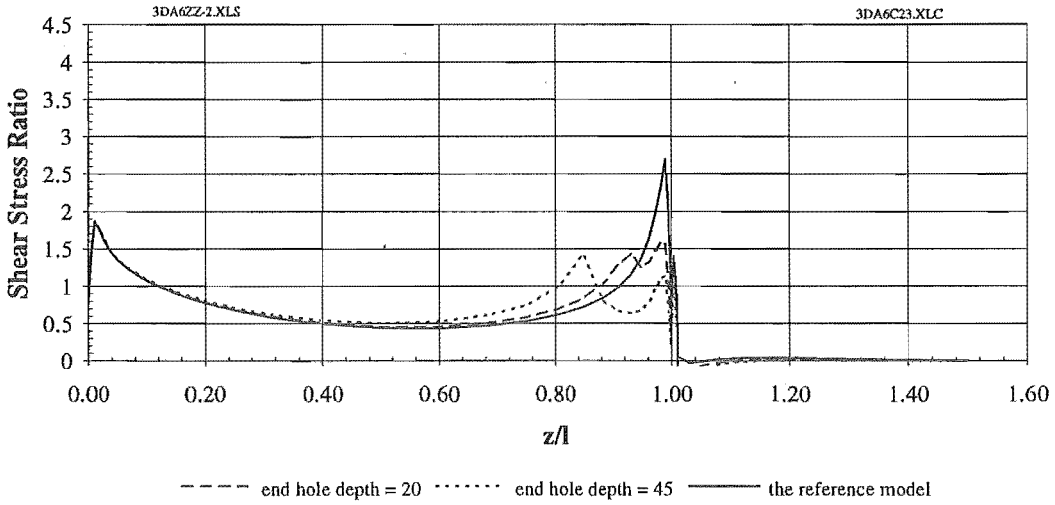

Figure 7.6 Effect of the geometry of the steel rod on shear stress distribution (line c-c)

7.3.3 Tensile Stress

1. Effect of the edge distance

Figure 7.7 shows the distribution of the tensile stress ratio in wood along the embedment in the region close to the epoxy-wood interface (line f-f). The magnitude of the tensile stress changes significantly as the edge distance changes. The lines from top to bottom represent different edge distances, from small to large respectively and indicate that the average tensile stress increases as the edge distance decreases.

However in terms of the tensile stress concentration, no improvement can be made by increasing edge distance. For example, compared with the edge distance of e=45 mm of the reference model, for the edge distance e=30 mm, the peak value of the tensile stress at the embedment end region is approximately 2.25 times larger than that for the reference model. This is expected as the average tensile stress for the edge distance e=30 mm is 2.25 times greater than that for the reference model due to reducing the stress area. Furthermore, Figure 7.7 also shows that the highest tensile stress region is at the inner end of the embedment. A detailed study was made around this region and the results are presented in Figures 7.8.

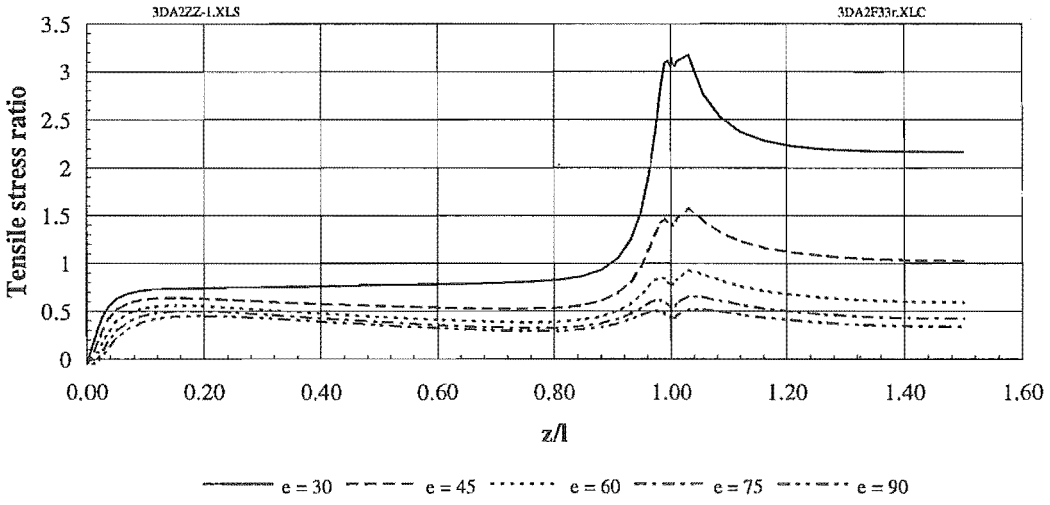

Figure 7.7 Effect of edge distance change on tensile stress (line f-f)

Figures 7.8 describe the tensile stress distribution over the cross-section at the inner end of the embedment (line L-L in Figure 7.1). There is no tensile stress at the end of the steel rod because the model is defined with no bond between the steel and the epoxy at this region. Figure 7.8(a) displays the tensile stress within the epoxy layer from the steel-epoxy interface to the epoxy-wood interface and it can be seen from the figure that the tensile stress increases as the edge distance decreases. The gradient of the tensile stress is very high over the thickness of the epoxy, especially in the region close to the steel-epoxy interface; the highest tensile stress is at the steel-epoxy interface.

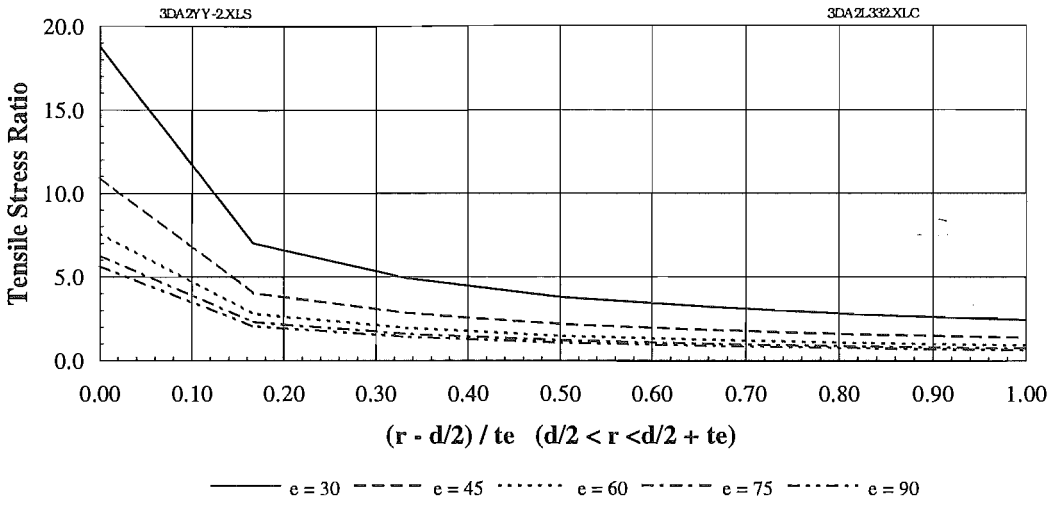

Figure 7.8 (a) Tensile stress distribution over the cross-section - within the epoxy (line L-L)

At the same cross-section, similar stress distributions can be observed within the wood in Figure 7.8(b). The highest tensile stress occurs in the epoxy-wood interface. In practice this stress concentration in the wood may result in cracking at the inner end of the embedment over the cross-section of the specimen. This is the major cause of Type 3 failure mode.

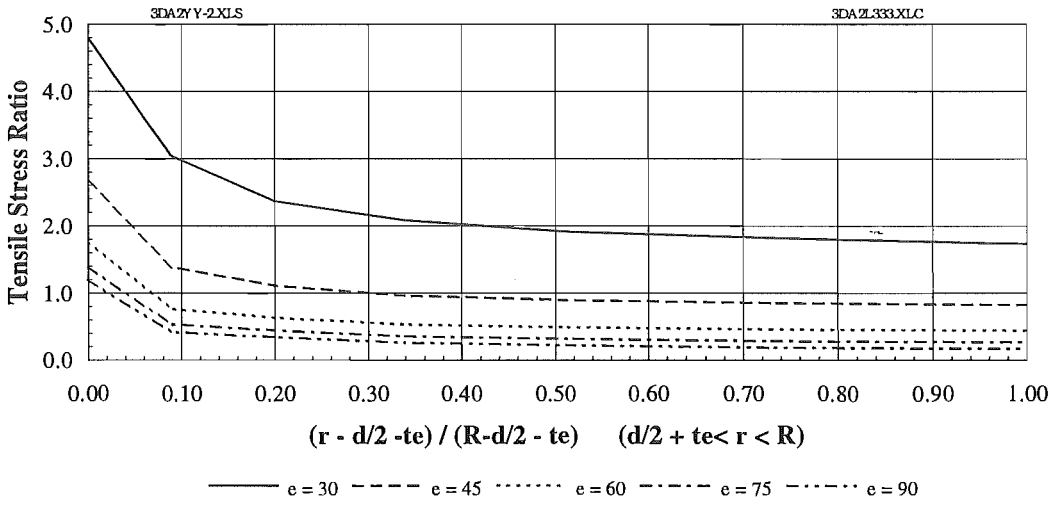

Figure 7.8 (b) Tensile stress distribution over the cross-section - within the wood (line L-L)

2. Effect of embedment length

Figure 7.9 shows the tensile stress distribution in wood along the embedment (line f-f). It can be seen that no significant modifications occurs in terms of the stress concentration and magnitude of the tensile stress.

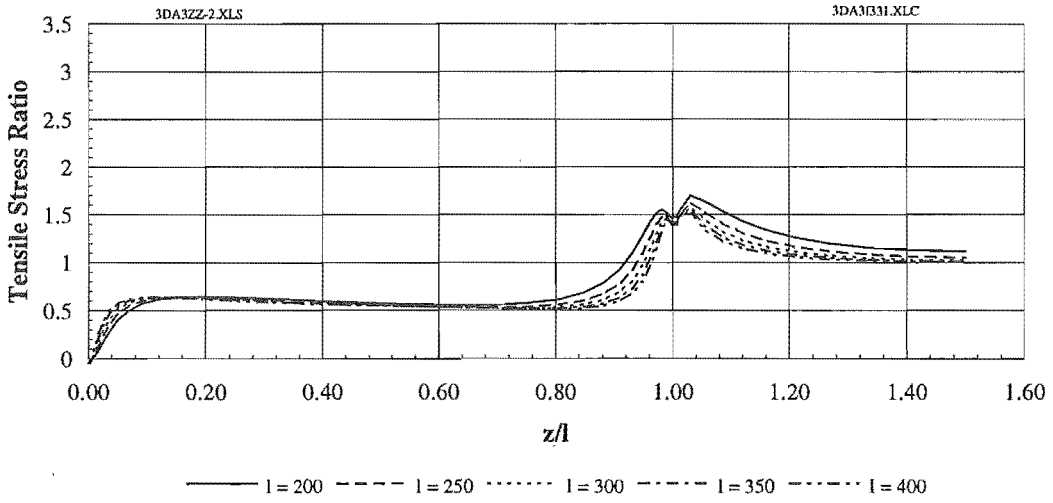

Figure 7.9 Tensile stress distribution with effect of embedment length change (line f-f)

Figure 7.10 shows the distribution of the tensile stress ratio within the wood over the cross-section at the inner embedment end (line L-L). It indicates that the modification of the stress only can be observed at the epoxy-wood interface. In general, no significant modifications of the tensile stress distribution occur when the embedment length changes.

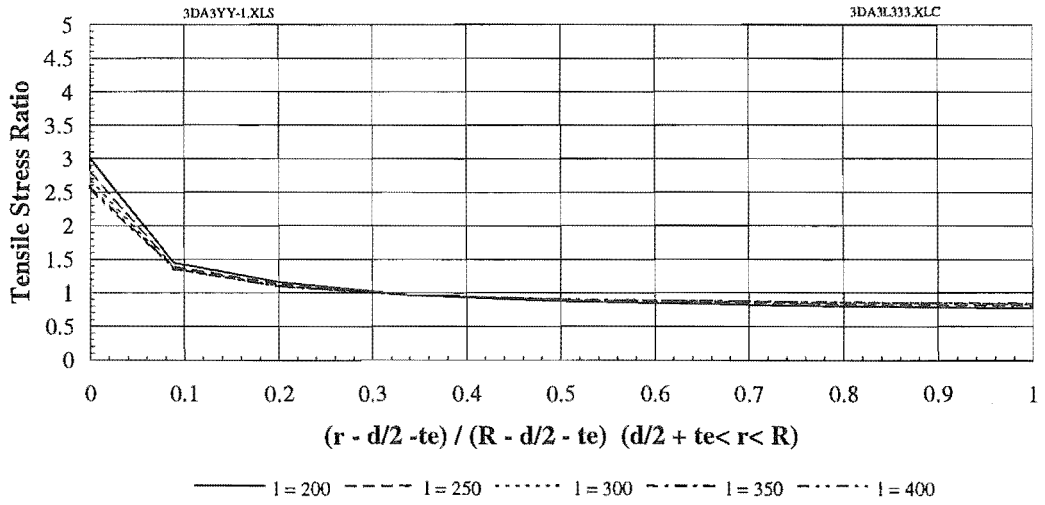

Figure 7.10 Tensile stress distribution in wood over the cross-section (line L-L)

3. Effect of epoxy thickness

Figure 7.11 displays the tensile stress distribution inside the wood along the embedment length at the region close to the epoxy-wood interface. The effect due to the change in the thickness of the epoxy only occurs at both ends of the embedment, but no obvious effect occurs along the central region of the embedment.

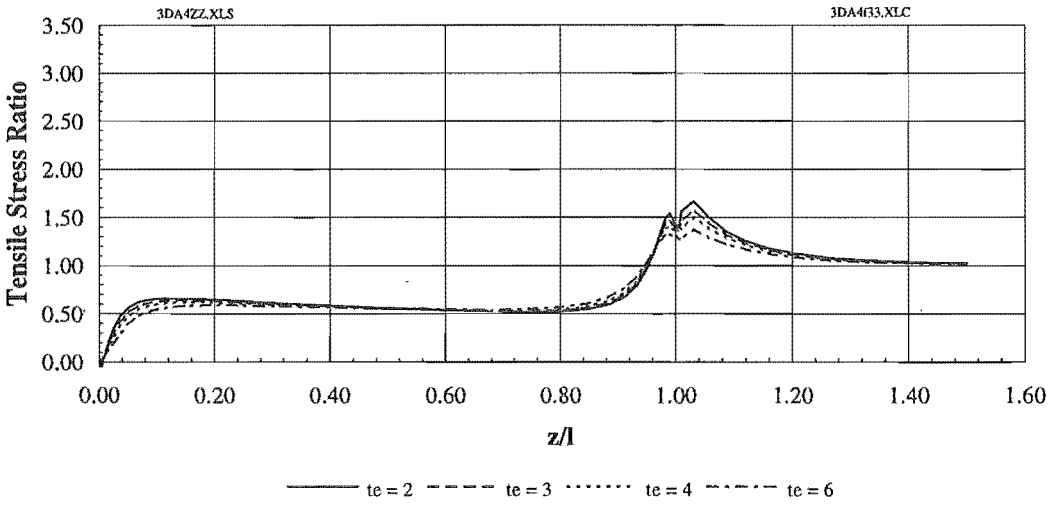

Figure 7.11 Effect of the epoxy thickness on tensile stress distribution (line f-f)

Figures 7.12 (a) and (b) show the tensile stress distribution over the cross-section at the inner end of the embedment where the tensile stresses are highest (line L-L). Figure 7.12 (a) plots the tensile stress distribution within the epoxy. The x-axis represents the thickness of the epoxy and shows that there are obvious effects due to the epoxy thickness change. The tensile stress increases as the thickness of the epoxy decreases. Figure 7.12 (b) shows the stress distribution within the wood at the same cross-section. The effect due to the epoxy thickness change only can be observed around the epoxy-wood interface area and there are no obvious effects in the other area.

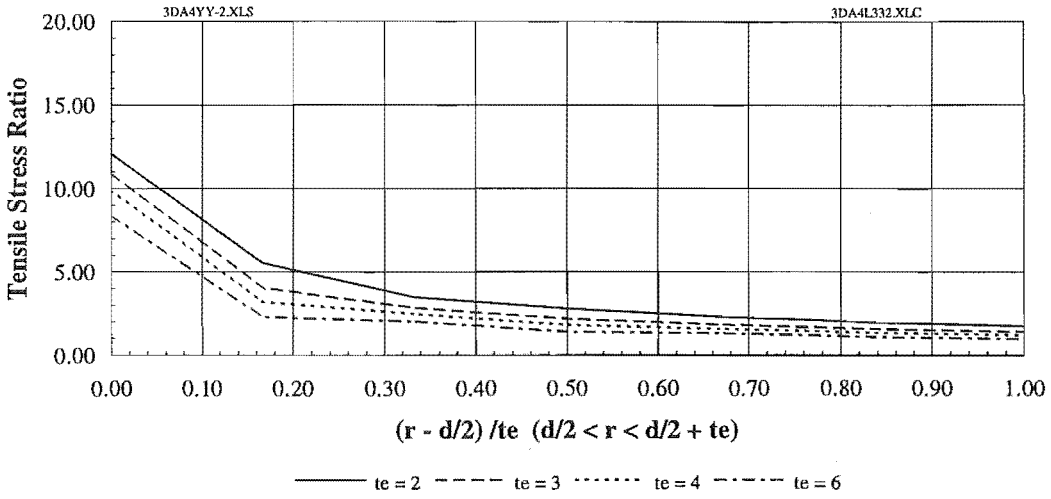

(a) within the epoxy

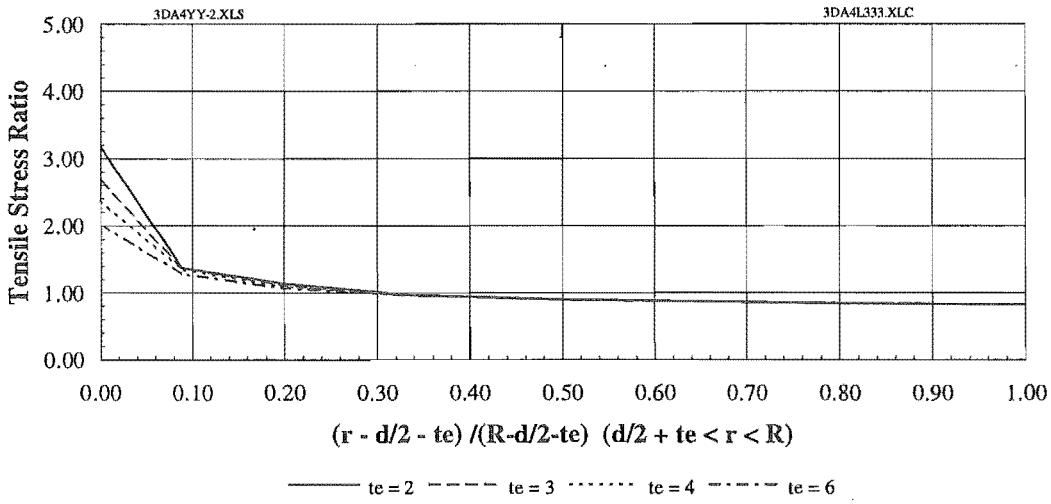

(b) within the wood

Figures 7.12 Tensile stress distribution over the cross-section at the inner end of the embedment (line L-L)

4. Effect of modulus of elasticity of epoxy

Figure 7.13 shows the tensile stress distributions in the wood along the embedment in terms of different modulus of elasticity in the epoxy. Only minor modification of the tensile stress occurs at the inner embedment end and at this region the tensile stress increases slightly with decreasing MOE value of the epoxy. No significant effect can be observed over the rest of the embedment.

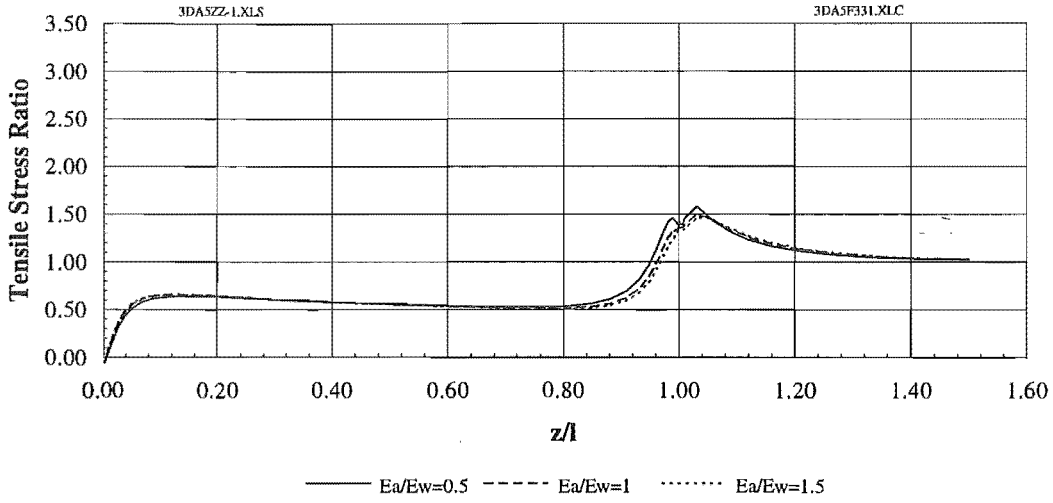

Figure 7.13 Effect of the MOE of the epoxy on the tensile stress distribution along the embedment (line f-f)

Figure 7.14 shows the tensile stress distribution within the wood over the cross-section at the inner embedment region in terms of the different modulus of elasticity for the epoxy. Only minor effect can be observed, occurring in the region around the epoxy-wood interface.

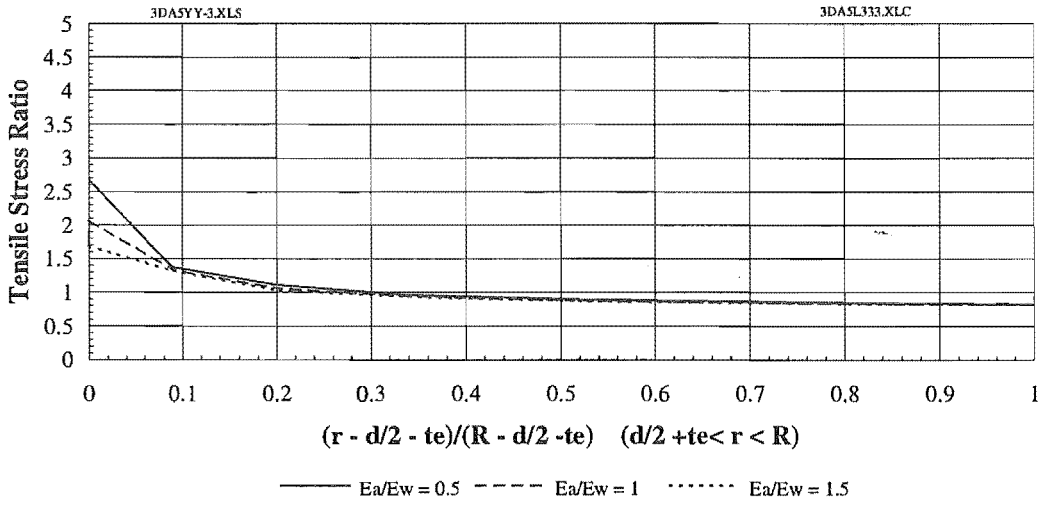

Figure 7.14 Effect of the MOE of the epoxy on the tensile stress distribution over the cross-section (line L-L)

Figure 7.15 plots the tensile stress distribution in the wood along the embedment. Each line represents different geometries at the steel rod end, the solid line representing the reference model. The dashed line represents the rod with a hole of a diameter of 18 mm and depth of 20 mm at the end. The dotted line corresponds the rod with a hole diameter of 18 mm and depth of 45 mm. The finite element analysis results show that no significant changes occur in tensile stress concentration due to changes in the steel rod end geometry. As can be seen although the magnitude of the tensile stress does not change significantly, the gradient of the tensile stress distribution does change, resulting in a change in the shear stress distribution shown in Figure 7.6.

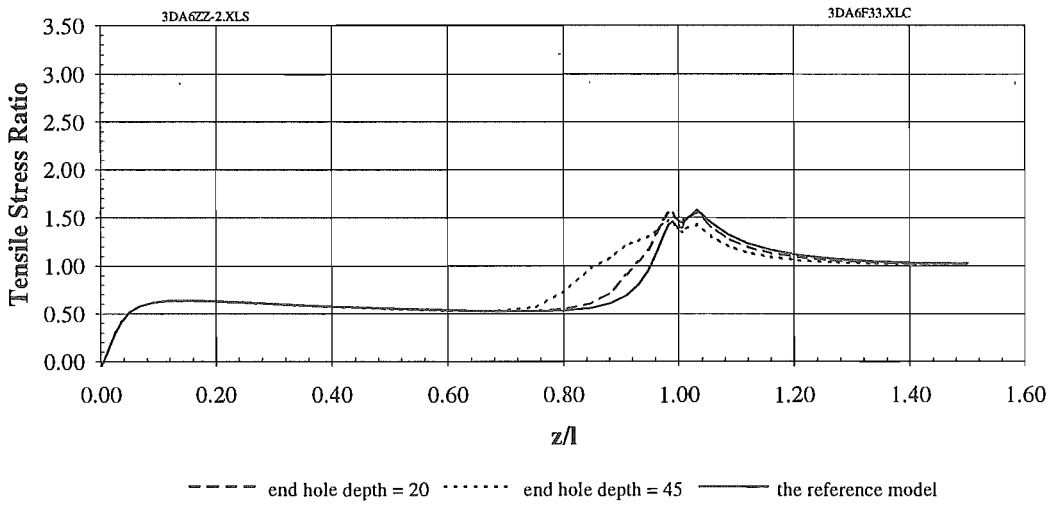

Figure 7.15 Effect of the geometry of steel rod on tensile stress (line f-f)

7.3.4 Transverse Stress

In the short duration tensile loading experiments, Type 2 failure mode was the most common failure, viz. the steel rod pullout failure with the splitting of the wood at the outer end of the embedment. Based on this observation and the analysis results from the reference model, the data analysis in this section concentrated on the transverse stress in wood at the region close to the epoxy-wood interface along the embedment (line f-f in Figure 7.1) and over the cross-section close to the outer end of the

embedment (line P-P in Figure 7.1), where the Type 2 failure mode and the highest transverse stresses occur.

1. Effect of edge distance

Figure 7.16 shows the transverse stress distribution in the wood along the longitudinal direction, recording the highest magnitudes of stresses at the outer end of the embedment. Although some modifications can be observed with the change of the edge distance, no significant changes occur in terms of the magnitude of the stress and the stress concentration.

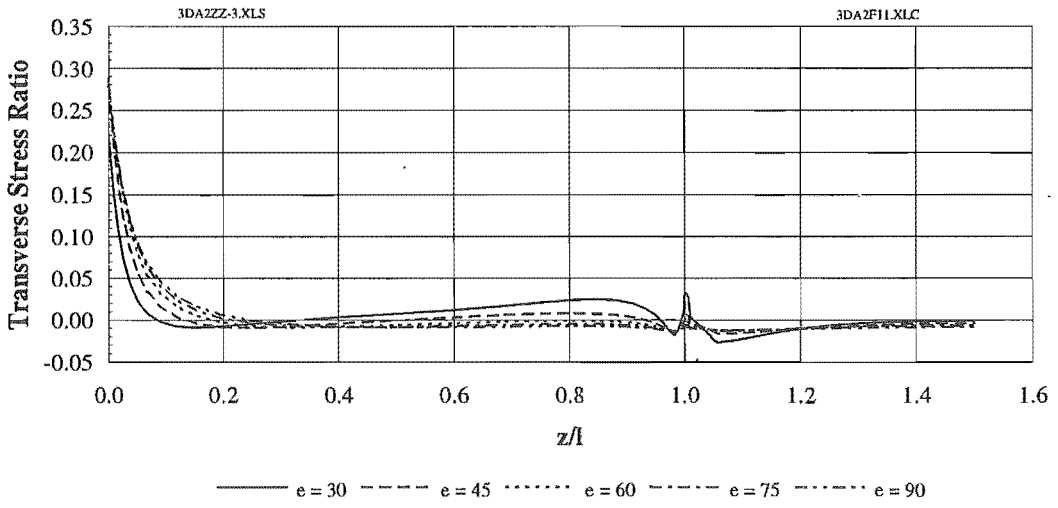

Figure 7.16 Effect of the edge distance on the transverse stress distribution along the embedment (line f-f)

2. Effect of embedment length

The influence of the embedment length on the transverse stress is presented in Figure 7.17 and Figure 7.18. Figure 7.17 shows the transverse stress along the embedment. The difference in the stress due to the different embedment lengths can be observed in the region near the outer end of the embedment; the stress increases coincide with decreasing the embedment length. No significant changes are observed in the other regions away from the outer embedment end. Figure 7.18 (a) displays the transverse stress across the thickness of the epoxy over the cross-section near the outer end of the embedment, indicating that stress increases as the embedment length

decreases. It also shows that the stress gradient along the thickness of the epoxy: at the steel-epoxy interface (r = d/2) the stress reaches the highest value, while at the epoxy-wood interface (r = d/2 + t_e) the stress has its lowest value; the transverse stress distribution within the wood at the same cross-section is shown in Figure 7.18 (b). At the epoxy-wood interface the stress increases more than 55 % as the embedment length decreases from 400 mm to 200 mm. Away from the interface towards the wood surface both the magnitudes of the transverse stresses for all of embedment lengths and their differences become smaller.

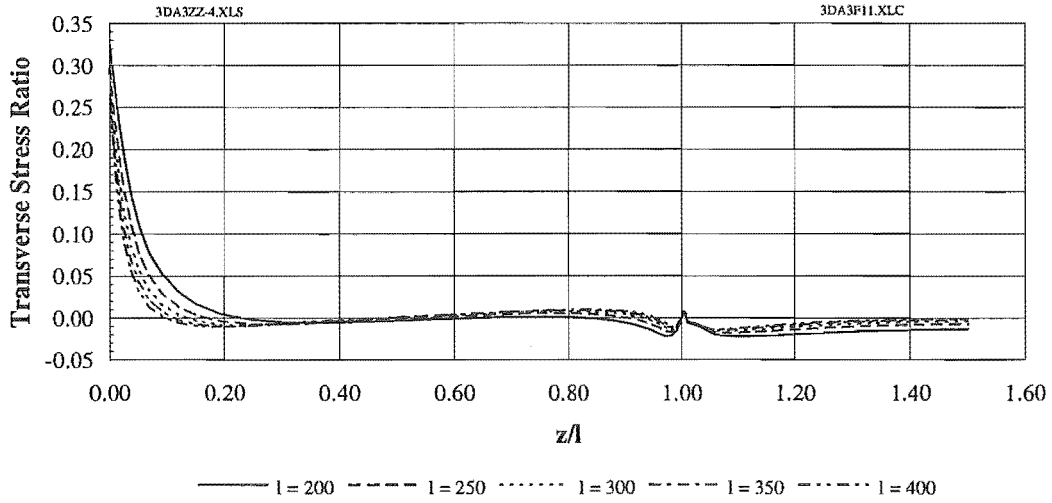

Figure 7.17 Effect of the embedment length on the transverse stress distribution in longitudinal direction (line f-f)

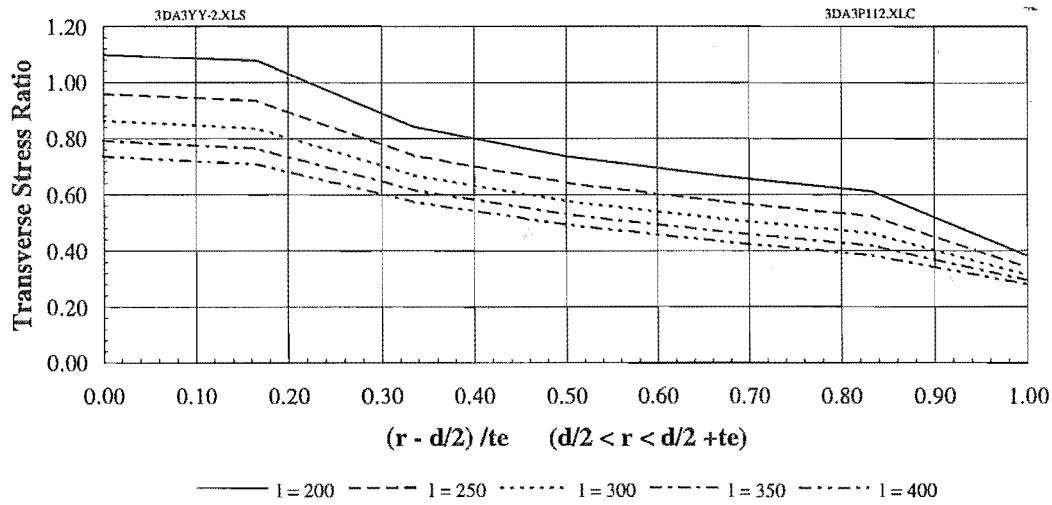

Figure 7.18 (a) Effect of the embedment length on the transverse stress distribution across the thickness of the epoxy (Line P-P)

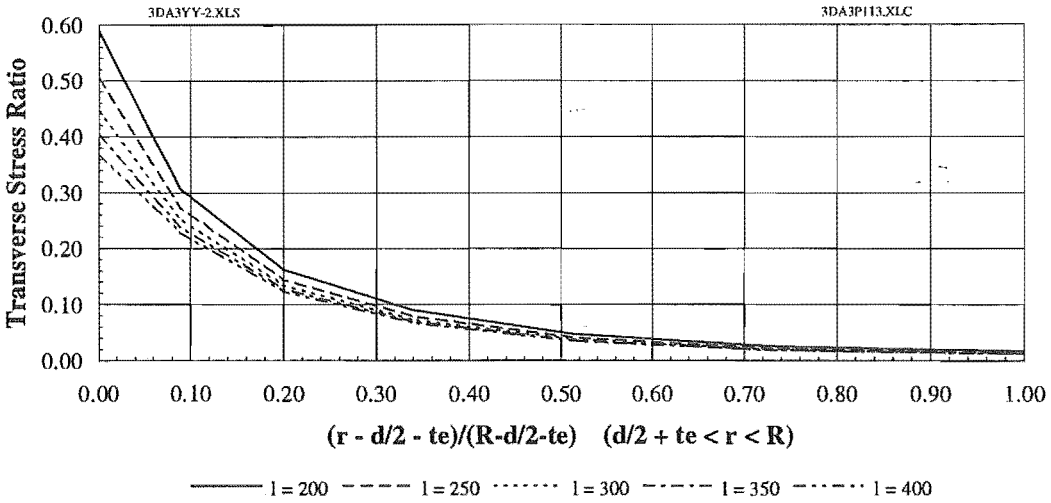

Figure 7.18 (b) Effect of the embedment length on the transverse stress distribution within the wood over the cross-section (Line P-P)

3. Effect of thickness of epoxy

Figure 7.19 shows the transverse stress distribution in the wood along the embedment at the region close to the epoxy-wood interface. Change in the stress due to the change of the epoxy thickness only occurs in a small region close to the outer end of the embedment. No significant change can be observed for the rest of the embedment length. Figure 7.20 shows the transverse stress distribution within the wood over the cross-section at the outer end of the embedment. The highest stress is at the epoxy-wood interface and the greatest difference in the stress among the different epoxy thickness is in the region close to the interface. Both the magnitudes and the differences of the stress become smaller away from the interface towards the wood surface.

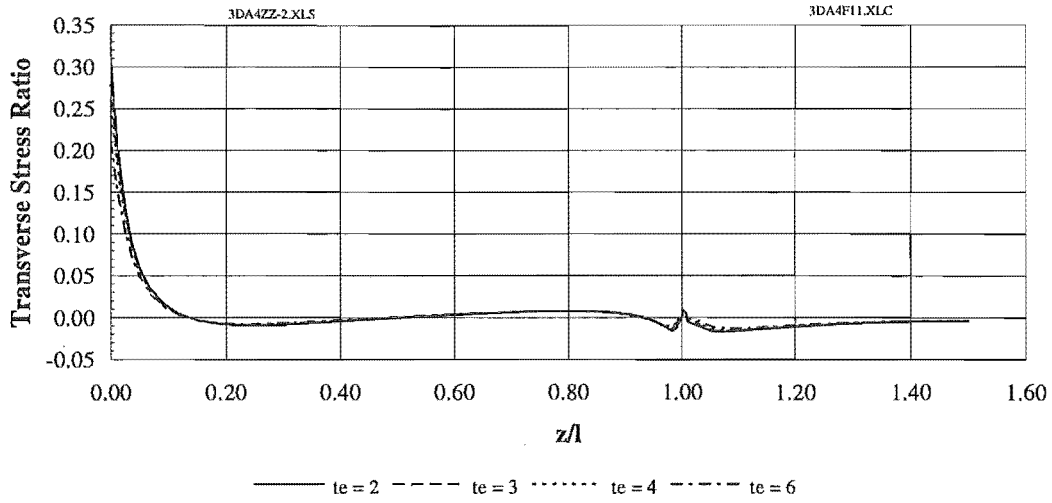

(a) The stress distribution in the longitudinal direction along the entire model

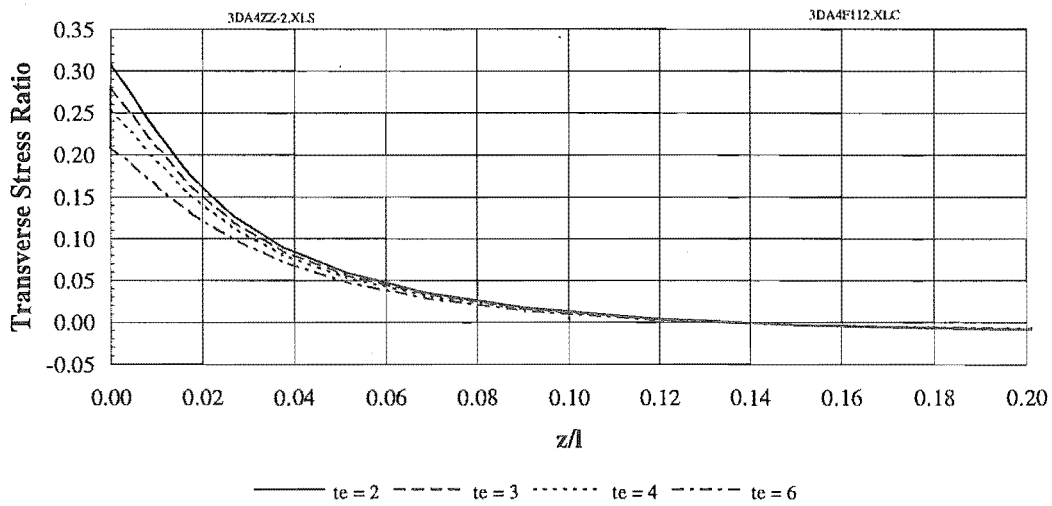

(b) The stress distribution at the region close to the outer embedment end

Figure 7.19 Effect of the epoxy thickness on the transverse stress (line f-f)

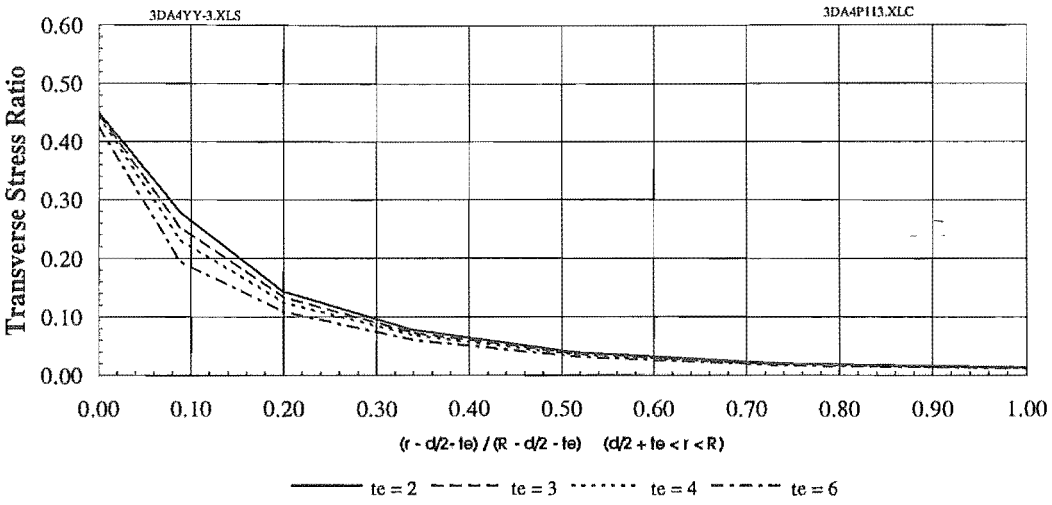

Figure 7.20 Transverse stress distribution within the wood over the cross-section at the outer end of the embedment (line P-P)

4. Effect of modulus of elasticity of the epoxy

Figures 7.21 display the effect of the modulus of elasticity of the epoxy on the transverse stress distribution. Figure 7.21 (a) shows the stress distribution in the wood over the cross-section near to the outer end. Figure 7.21 (b) displays the stress distribution in wood along the embedment. Although minor difference in the stress can be observed at the epoxy-wood interface in the cross-section close to the embedment end (Figure 7.21 (a)), in general, no significant modification occurs in the wood due to the change of the MOE in the epoxy (Figure 7.21 (b)).

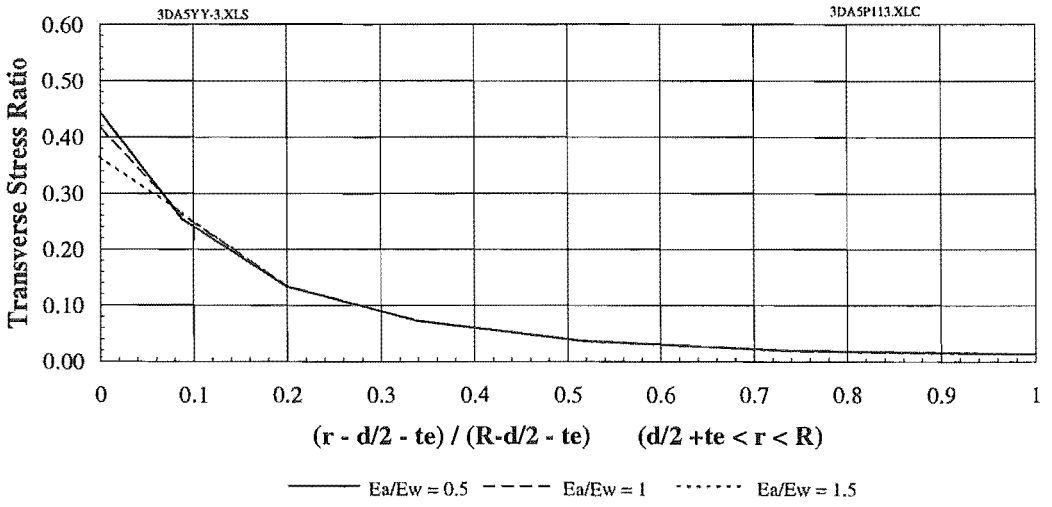

(a) In wood at the cross-section near the outer embedment end (line P-P)

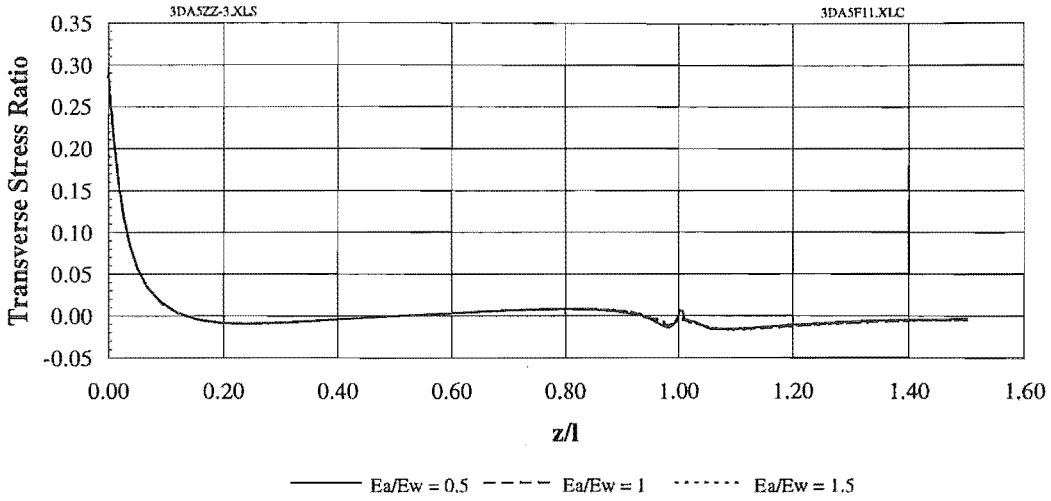

(b) In wood along the longitudinal direction (line f-f)

Figure 2.21 Effect of the modulus of elasticity of the epoxy on the transverse stress

5. Effect of the geometry at the steel rod end

There are no effects on the transverse stress at the outer end of the embedment region because the geometry was changed at the inner end of steel rod only. This does not affect the regions away from the inner end of the steel rod. In the region close to the inner end of the steel rod, although the hole at the end of the steel rod would result in a different stress distribution, the differences are not significant since the magnitudes of the stress are almost zero in that region (Figure 7.22).

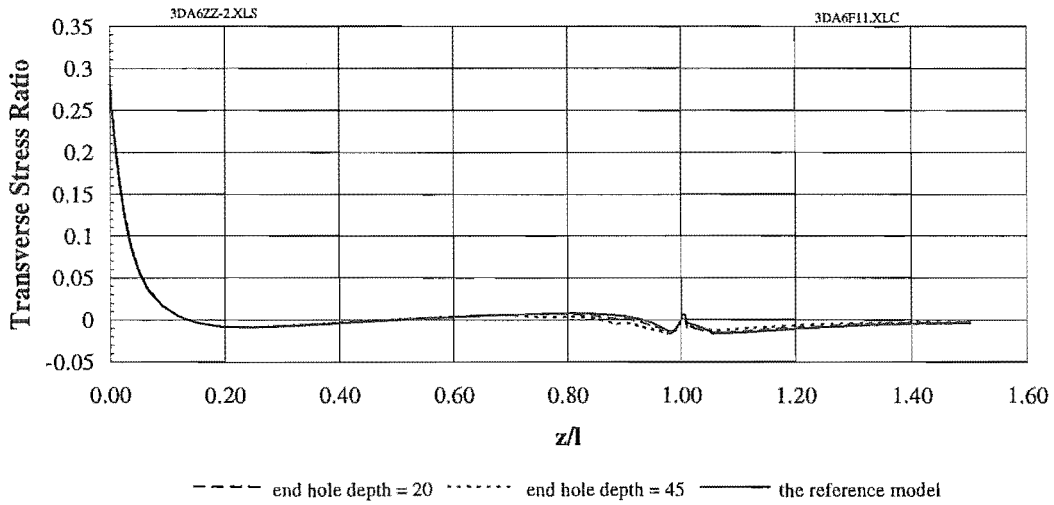

Figure 7.22 Effect of geometry change at the steel rod end on the transverse stress (line f-f)

7.4 DISCUSSION AND CONCLUSION

This study concentrated on the analysis of the longitudinal tensile stress in wood, shear stresses in the epoxy and interfaces, and transverse stress around the outer end of the connection. Other stresses are not only of much smaller magnitude compared with the stresses analysed in the parametric study, but also have little effect on the performance and capacity of the connection. Therefore, these stresses were not considered in this study.

The stresses presented in the parametric study play an important and dominant role in the various failure modes of the epoxied steel connection, and can be used to describe the mechanism of failure and behaviour of the connection. Furthermore, an improvement in these stress distributions could make a major contribution to an optimised connection with high load capacity and best performance.

7.4.1 Discussion on the Shear Stress

Comparing the influences of the different parameters in terms of shear stress distribution in the epoxy, the stress concentration can be improved significantly by changing the edge distance and by drilling a hole at the end of the steel rod. Changes in the epoxy thickness also have major effects on the shear stress distribution. The modification of the modulus of elasticity in the epoxy and the embedment length have minor effects on the shear stress distribution. In terms of the average shear stress, a significant change only can be made by changing the embedment length. As expected, the average shear stress doubles if the embedment length were reduced from 400 mm to 200 mm. However in terms of the stress concentration, the peak value for the shear stress does not change significantly if the same reduction applies.

7.4.2 Discussion on the Tensile Stress

The major tensile stress concentration occurs in the region around the inner embedment end. At this region the tensile stress along the embedment in the wood is the highest. Most parameters analysed in the parametric study have no significant effect to improve the tensile stress concentration. The thickness and the MOE of the epoxy only have minor influence on the tensile stress distribution. It noted that the edge distance must be considered since the average tensile stress can be modified significantly by changing the edge distance.

7.4.3 Discussion on the Transverse Stress

Transverse stress concentration occurs in the outer embedment end region, the highest stress, which may cause the connection failure, occurs in the steel-epoxy interface at the outer end of the embedment. Only the embedment length and the epoxy thickness have significant effects to modify the transverse stress distribution. The other parameters have no significant effects in modifying the stress concentration.

7.4.4 General Discussions

After the parametric study and the analysis of the stress distribution, the explanation why tensile strength is not directly proportional to the embedment length could be as follows:

1. The shear stress distribution along the embedment length was not uniform (Figure 7.3), therefore the relationship between the embedment length and shear stress may not be linear.

2. There are shear stress concentrations in the regions close to both ends of the embedment (Figure 7.3). This stress concentration is not reduced significantly by increasing the embedment length. Therefore, further increasing the embedment length would not increase the connection loading capacity linearly.

3. Tensile stress concentration in the region close to the inner end of the embedment (Figure 7.9) is the major cause of Type 3 and Type 4 Failure Modes; the stress concentration does not reduce significantly by increasing the embedment length. Therefore, further increasing the embedment length would have not any significant effect in increasing the loading capacity of the connection if it was likely fail with Type 3 and Type 4 Failure Modes.

7.4.5 Concluding Remarks

Based on the results of the comprehensive parametric study, the following conclusions can be drawn:

1. The threshold of edge distance exists; this study suggests that the edge distance should be no more than 3 bar diameters. Further increasing edge distance does not yield any significant benefit in terms of the stress distributions.

2. A thick epoxy layer results in a better stress distribution than does a thin one.

3. The shear stress concentrations around the connection can be reduced by using an epoxy with a lower modulus of elasticity.

4. A better shear stress distribution at the inner end of the connection can be achieved by drilling a hole at the inner end of the steel rod.

5. The transverse stress concentration and the average shear stress can be reduced by increasing the embedment length.

CHAPTER EIGHT

LONG DURATION LOAD AND ENVIRONMENT EFFECTS

8.1 INTRODUCTION

Time-dependent behaviour is one of the most important characteristics of the epoxy-bonded steel glulam connection. Timber is different from other major structural materials (steel, concrete) in that its strength tends to reduce under long duration loads (Bodig and Jayne, 1982; Madsen, 1992). The connection as a composite of wood-steel-epoxy, may manifest creep rupture or static fatigue - a phenomenon of fracture under sustained load at a level less than that required to cause fracture under a short duration load. This study takes into account load duration and environmental conditions since design capacity may vary with duration of load and environmental factors (such as moisture content in the structure). If the duration of load is short, the failure load would be greater than if continuously applied. A safe and rational design of the connection must be based on adequate information of the connection characteristics and performance under long duration load. A experimental study on the effects of long duration load and environmental condition was undertaken.

8.2 OBJECTIVES AND SCOPE

The objectives of the study are to understand the time-dependent behaviour and characteristics of the connection subjected to the sustained long duration load under different environmental conditions. The strength of the connection is investigated under long duration load and compared with the strength of the connection subjected to short duration load to obtain adequate information of the connection performance under long duration load. The study also investigates the influence of environmental conditions

and seeks to understand the behaviour of the glulam timber structure - moisture content fluctuation and shrinkage - under relative high humidity service conditions.

Two projects were undertaken to realise the above objectives, viz. a long duration tensile loading experiment as Experiment Three and a project monitoring the moisture content and shrinkage of the glulam timber in a swimming pool (the swimming pool project). Experiment Three formed the major part of the study. The swimming pool project was to generally investigate moisture content fluctuation and shrinkage of glulam timber in a relative high humidity environment.

The experiment was initiated and the specimens would be continually subjected to the sustained tensile load until the failure would occur. Moisture content was considered as a major environmental factor in both projects. A comprehensive study of the detailed mechanism of time dependent behaviour is beyond the scope of this study.

8.3 TEST PROGRAMME OF EXPERIMENT THREE

8.3.1 Design of the Experiment

The design of Experiment Three was based on the results of Experiment One. Load level and five other factors directly adopted from Experiment One were selected as the main factors in the experiment - embedment length, bar diameter, moisture contents, bar type, epoxy type and load level. Hole diameter and edge distance appeared less significant in the short duration experiments and were not considered as main factors in this experiment. The levels for each factor are listed in Table 8.1.

Table 8.1 Design of long duration experiment

Levels	Embedment l (mm)	Bar Diameter d (mm)	Moisture	Bar Type	Epoxy Type	Load Level
1	7.5d	16	dry/control	threaded	West System	40%
2	10d	20	wet/cycle	deformed	K-80	60%
3	15d	-	-	-	-	-

The experiment was designed on the same principle as Experiment One, that the likely failure would occur in the connection rather than in the glulam timber or in the steel rod. Two load levels would be used in the experiment. The load levels were defined as 40% and 60% of axial tensile capacity of the connection under the short duration load. The values for each specimen was calculated using Equation 2.6. Since the Equation 2.6 was developed from deformed reinforcing bar, for the connection using threaded steel rod, a 26.3% increase is considered based on the results from Experiment One (Table 4.3). The edge distance used in the experiment is 2.25d, same as the high level of edge distance in Experiment One. The hole diameter is 1.275d, which is the average of the two hole diameters used in Experiment One.

Two different environmental conditions were applied in the experiment: A dry environmental condition and a wet-dry cycle environmental condition. The dry environmental condition corresponded to normal indoor conditions with a little heating in winter, but no cooling in the summer. The average temperature was about 20°C with range of 8°C to 26°C and the average relative humidity about 55%. The wet-dry cyclical environmental condition simulated natural outdoor weather conditions which were provided by a water irrigation system and natural air circulation. 24 control specimens were maintained in the dry environmental condition and the other 24 as outdoor specimens subjected to a series of wet-dry cycles.

The wet-dry cyclical environmental conditions were separated into two stages as shown in Table 8.2. Stage One included the first wet and dry cycle. Stage Two consisted of several subsequent wet and dry cycles. The moisture content during wet cycle of Stage One was designed to reach fibre saturation point, while in Stage Two, the maximum target moisture content was 23% in wet cycles. This is lower than that in Stage One.

Stage Two programme continued after Stage One terminated. At the beginning of Stage Two, all of the specimens were reloaded to the target load and the specimens which had failed in the Stage One were replaced.

Table 8.2 Proposed moisture content in the outdoor specimens

Stage	Environment	Moisture Content Range (%)
Stage One	wet	25 - 29
	dry	12 - 16
Stage Two	wet	19 - 23
	dry	12 - 16

8.3.2 Materials

The same materials were used in Experiment Three as used in the short duration experiments and have been described in detail in Chapter Three. The glulam timber was selected from the same batch as in Experiments One and Two. K-80 and West System epoxy were used. Two type of steel rod were selected. One was high strength threaded rod with diameters of 16 mm and 20 mm (AISI4140); the other was high strength deformed reinforcing bars (HD430) with a nominal diameter of 20 mm.

8.3.3 Construction of Loading Frames

Several loading methods were investigated as described in some previous reports. In Riberholt's test (Figure 8.1), concrete blocks were used as weights to load

the specimens as a beam. A simple layout of beams using a reaction rig to get the required loading was proposed by Crews' study (Figure 8.2).

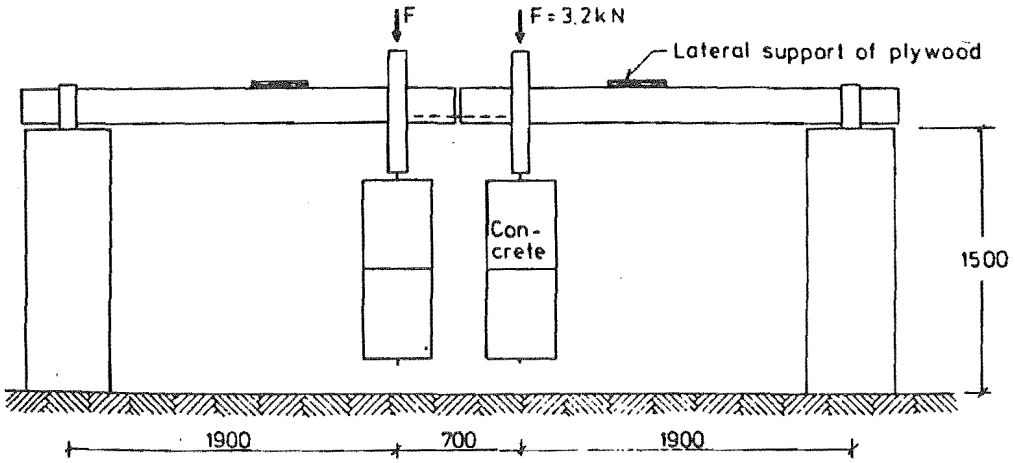

Figure 8.1 Load Configuration of Long Duration Experiment (Riberholt, 1986)

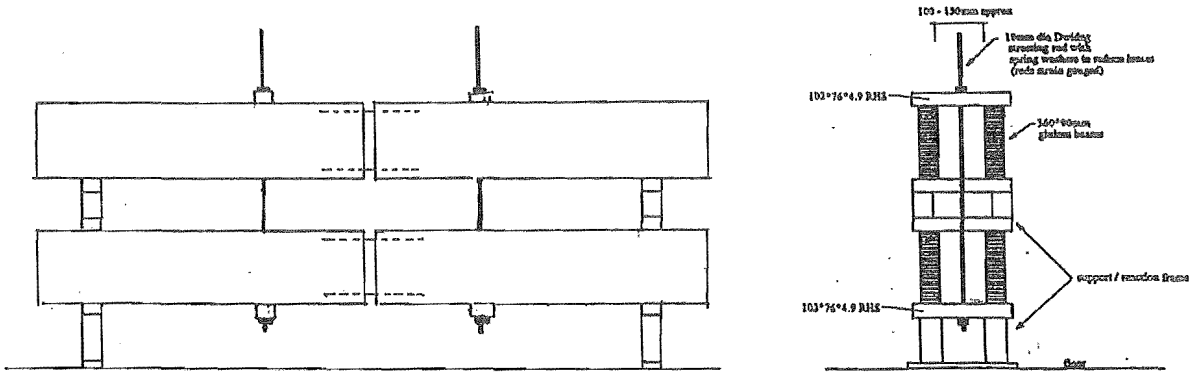

Figure 8.2 Sketch of the Set-up for Long Duration Test (Crews, 1993)

A large quantity of glulam timber is required in both cases described above because the specimens are loaded in bending. In addition, a big test area is essential because of the span of the glulam beams. Therefore an alternative loading method has to be obtained during the experiment design to eliminate the limitation of available material resource and space. A loading method using direct tension was designed to get

more test specimens and to use less test space. Spring was used for each loading frame with intention to keep the constant tensile load on the specimen while relaxation of the specimen occurred.

48 loading frames were constructed as shown in Figure 8.3. Each consisted of two steel channels (100x50 mm), two steel end plates and four steel strips. A steel plate was welded to the end of the two steel channels. Both channels were parallel and exactly the same length. Four steel strips were welded on the channels to reinforce the frame against buckling. The configuration of a loading frame with a test specimen subjected tensile load is shown in Figure 8.4.

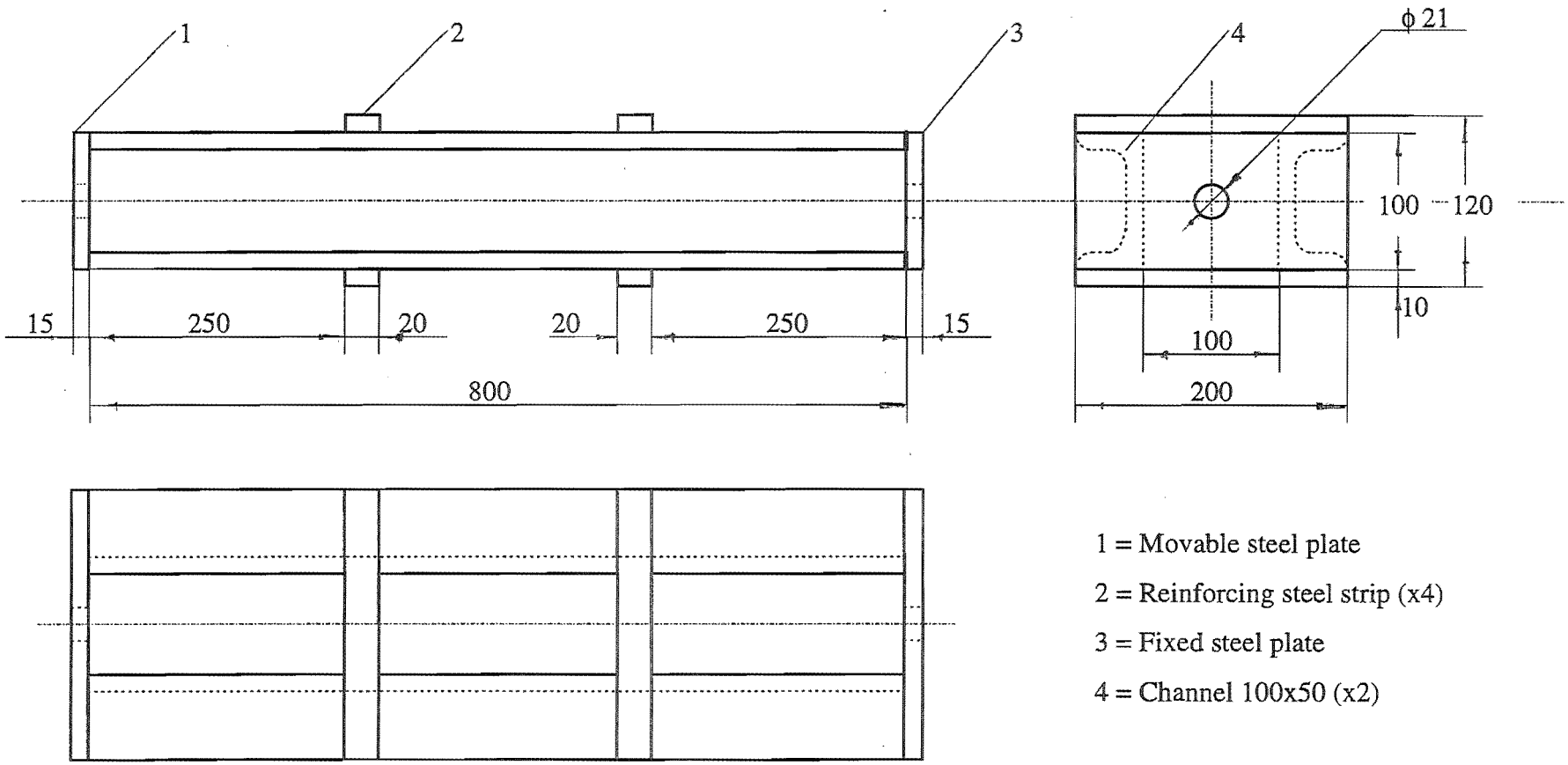

Figure 8.3 Sketch of loading frame for long duration experiment (Not to scales)

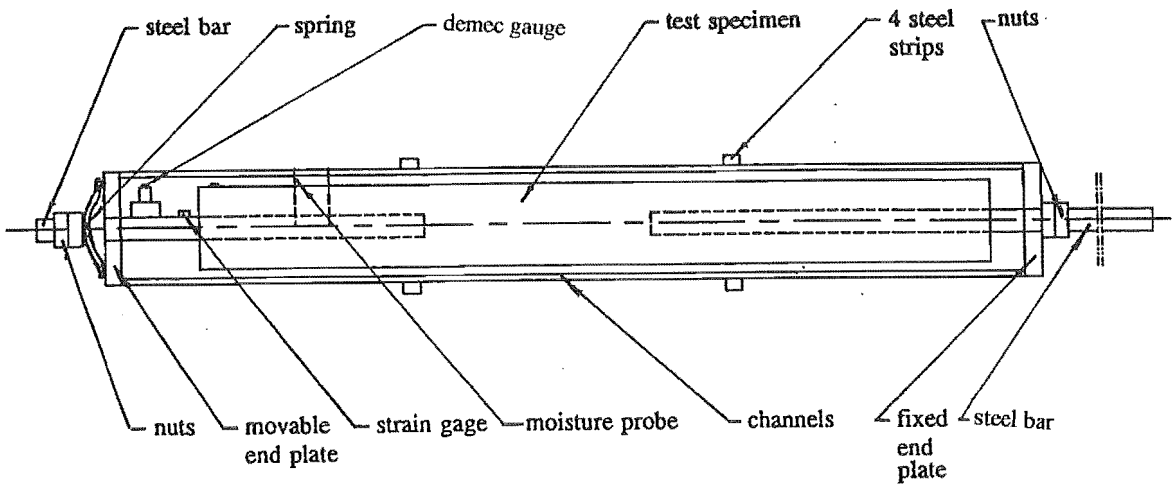

Figure 8.4 Configuration of a specimen under the test

8.3.4 Testing Sites and Irrigation System

Two test sites were arranged for the indoor and outdoor specimens. The control specimens were located in a laboratory area as shown in Figure 8.5 with a normal indoor environment in the Department of Civil Engineering, University of Canterbury (Christchurch, New Zealand). For the outdoor specimens, a timber shed was constructed to locate these specimens and to provide the environment condition sought for the experiment. Figures 8.6 (a) and (b) show a overview of the testing site and the outdoor specimens.

The shed and irrigation system were built to simulate the outdoor climate environment while the specimens were not directly exposed to the sun. Easy adjustment of air circulation and humidity were also considered. The shed was built with 50 x 100 mm timber stud as frame and rigid translucent sheeting for the roof. The wall was made from galvanised chicken mesh covered by garden shade cloth. The cloth was movable to adjust the air circulation. A irrigation system with a adjustable electronic water timer control unit (Rainmatic 2500) was built to obtain the required moisture in the specimens. The system consisted of 3 sprinklers and 24 fine nozzles. The sprinklers were attached underneath the roof and could be adjusted individually to obtain the required moisture content in the specimens. The fine nozzles were located nearby the

specimens and produced a fine mist of water during the wet parts of the cycles. The irrigation system could be controlled automatically by the electronic water timer control unit or manually.

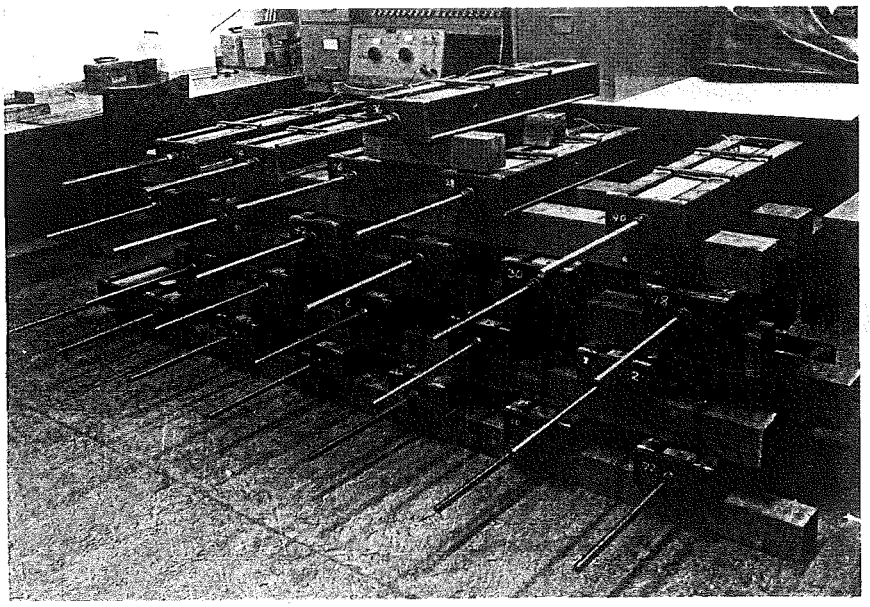

Figure 8.5 Overview of the long duration experiment: the control specimens

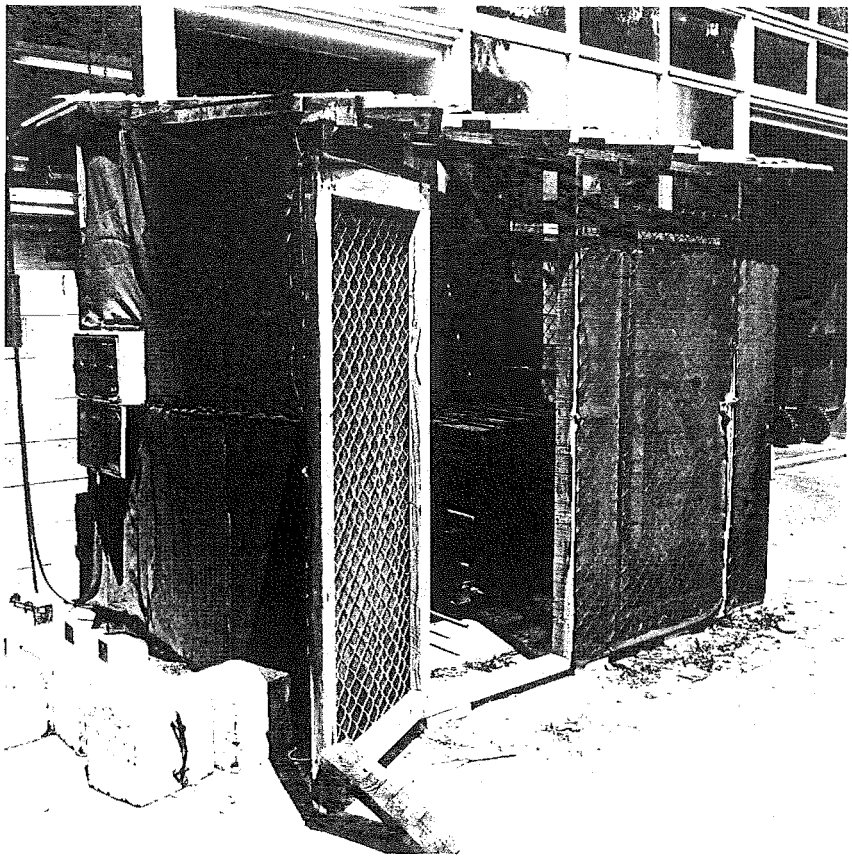

Figure 8.6 (a) Overview of the long duration experiment: the outdoor test site

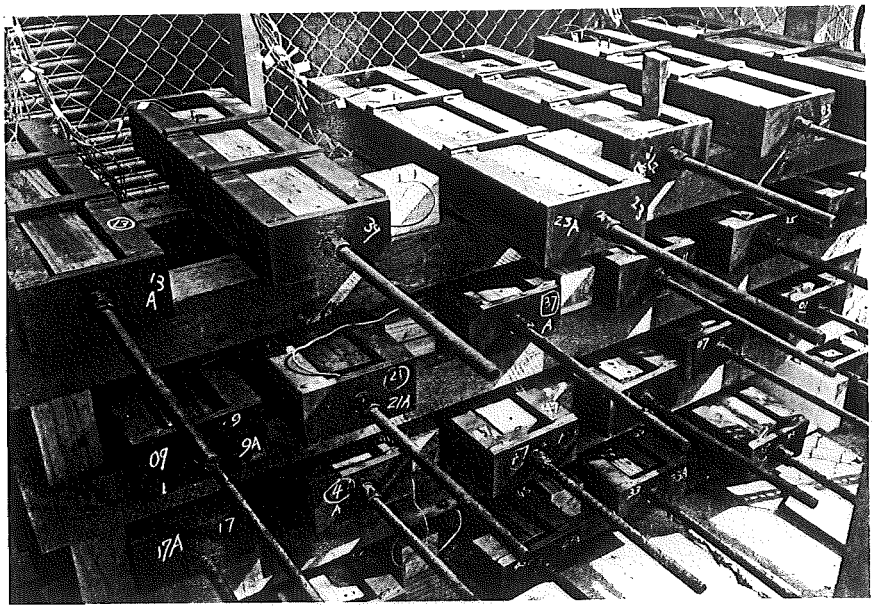

Figure 8.6 (b) Overview of the long duration experiment: the outdoor specimens

8.3.5 Instrumentation

1. Moisture content measurement

Moisture content in each specimen was measured by a electric resistance type moisture meter (Timbermaster Model D184T, Protimeter Ltd.), the meter being connected to a pair of metal probes in each specimen via electric leads and a multi-channel switch box. Permanent probes were made from 2.5 x 60 mm galvanised steel nails to prevent rusting and to obtain a good contact with the wood and were sealed tightly with 2 mm diameter PVC collar to insulate them from the wood. Only the tip of each probe was exposed to provide the contact surface with the wood. In this manner, the moisture content can be measured at the same required depth. A pair of probes was embedded into each specimen and located at the centre region of the connection (Figure 8.4); the distance between two probes was 29 mm. Electric leads were soldered onto the top of the probes and connected with the switch box. Insulation of the probes at the surface of the specimens was achieved with several coatings of SN4. The reading from the electric moisture meter was calibrated by the oven dry method. Two glulam timber blocks were used and the moisture contents were recorded using the moisture meter via

a pair of embedded probes and by oven dry method. The calibration results are listed in Table 8.3.

Table 8.3 Calibration for the electric moisture meter using the probes

Code	Original weight (g)	Oven dry weight (g)	Moisture content (%)[1]	Moisture content (%)[2]
MC-1	138.2	123.5	12.7	11.9
MC-2	122.2	109.7	11.2	11.4

Note: 1. Moisture content readings measured from the moisture meter.

2. Moisture content readings obtained using the oven dry method.

2. Measurement of sustained tensile load

A 5 mm length strain gauge (KFC-5-C1-11 electric resistance type foil strain gauge from Showa Measuring Instruments Co. Ltd.) was glued to the surface of the steel rod close to the embedment end. The gauge factor was 2.11 and the resistance was 120.1 ± 0.3Ω; the location of the strain gauges is shown in Figure 8.4. The strain gauges were calibrated by the AVERY General Purpose Universal Testing Machine (Type 7104 DCJ, 1000 kN). Readings were directly measured from a P-3500 Digital Strain Indicator. A quarter bridge circuit was used. This calibration was reproduced to set the target tensile load for each specimen while the loading procedure was carried out.

3. Measurement of displacement

The displacement of the connections was monitored by a DEMEC (demountable mechanical) gauge, the displacement being read between two DEMEC steel targets (DEMEC gauge measuring points). One was installed on the steel rod and the other glued to the surface of the wood specimen 50 mm from the end. For the threaded steel rod, the DEMEC target was glued on a small steel rod which was welded on a steel nut as shown in Figure 8.7 (a). The nut with the DEMEC target was mounted and fixed

after the specimen was prepared. For the deformed reinforcing bar, the target was welded directly to the bar as shown in Figure 8.7 (b). The displacement was monitored on 12 specimens representing different bar type, epoxy, bar diameter, load level, embedment and environment (Table 8.6). It is assumed that no tensile elongation of the steel rod occurs under the sustained tensile load and the shrinkage or swelling of the wood on the surface near to the end of the specimen are negligible, so that the measurement from the DEMEC gauge would sufficiently represents the displacement of the connection. Therefore, the rheological behaviour of the connection under the sustained tensile load may be described by this displacement.

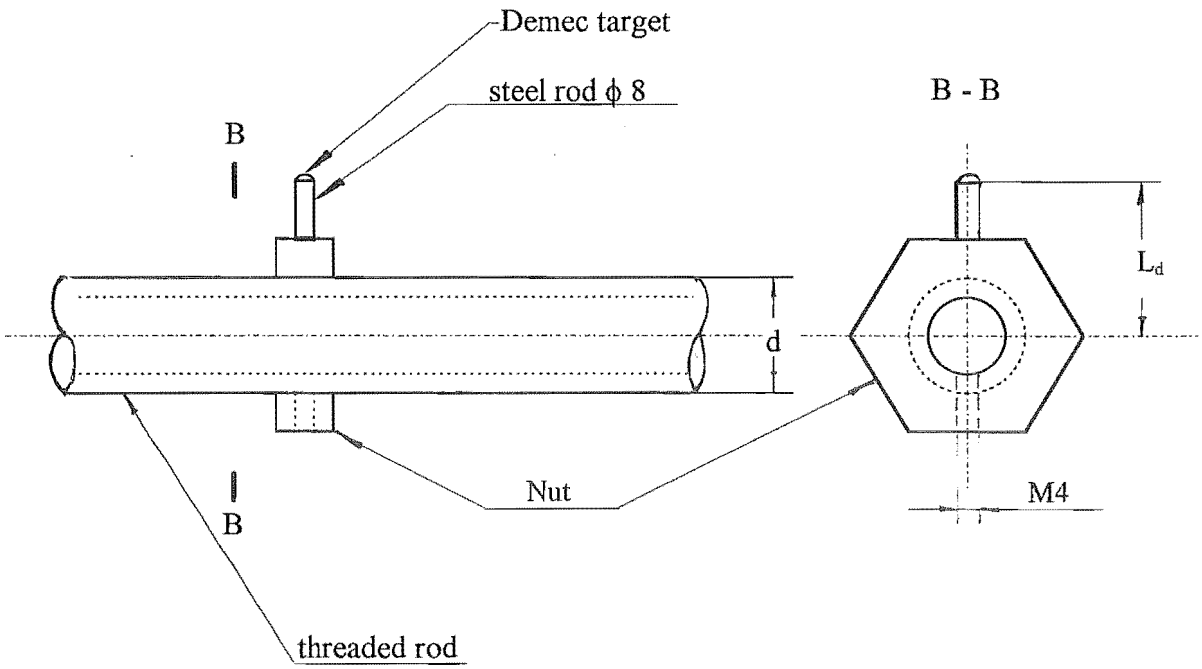

Number	d (mm)	L_d (mm)
2	16	36
8	20	42

Figure 8.7 (a) Layout of DEMEC gauge target installation on a threaded rod (Not to scale)

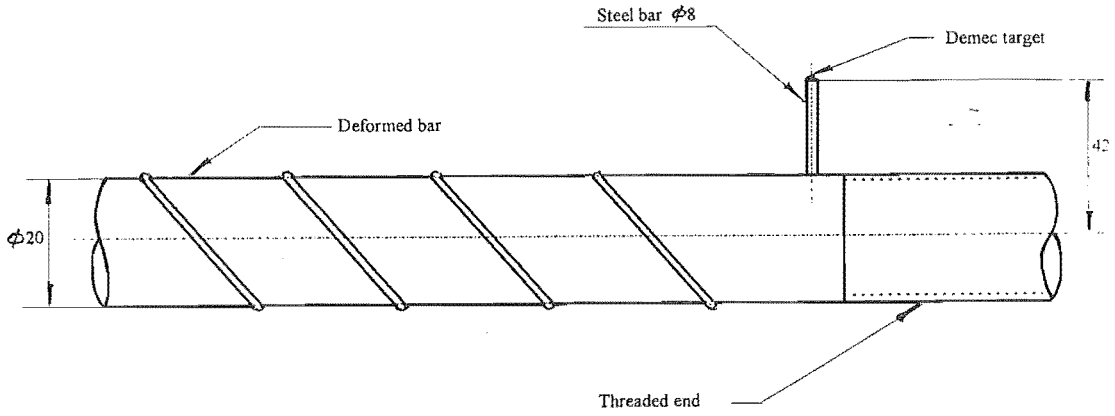

Figure 8.7 (b) Layout of DEMEC gauge target installation on a deformed bar (Not to scale)

8.3.6 Specimen Preparation

The glulam timber was cut to the required dimensions followed Table 8.4 and each glulam specimen was coded; the weight and dimensions were then recorded for calculating average density. Embedment holes, injection holes and moisture probes holes were drilled.

Steel rods were cut into the required length according to Table 8.4. The long threaded steel rod at the support end is to facilitate the hydraulic jack in loading the specimens. The procedures of the specimen assembling, epoxy preparation and injection being the same as procedures used in the short duration experiments described in Chapter Three.

Table 8.4 The dimensions of the specimens in Experiment Three

Code	Dimension of the Glulam Timber (mm)						Dimension of the Steel Rod (mm)					
							Threaded rod			Deformed bar		
	L	l_t	l_s	l_m	a	h	d	l_{st}	l_{ss}	d	l_{st}	l_{ss}
3001	600	120	180	300	72	20	16	270	630	-	-	-
3002	600	120	180	300	72	20	16	270	630	-	-	-
3003	600	120	180	300	72	20	16	270	630	-	-	-
3004	600	120	180	300	72	20	16	270	630	-	-	-
3005	600	160	240	200	72	20	16	310	690	-	-	-
3006	600	160	240	200	72	20	16	310	690	-	-	-
3007	600	160	240	200	72	20	16	310	690	-	-	-
3008	600	160	240	200	72	20	16	310	690	-	-	-
3009	600	240	240	120	72	20	16	390	690	-	-	-
3010	600	240	240	120	72	20	16	390	690	-	-	-
3011	600	240	240	120	72	20	16	390	690	-	-	-
3012	600	240	240	120	72	20	16	390	690	-	-	-
3013	600	150	250	200	90	26	20	300	700	-	-	-
3014	600	150	250	200	90	26	20	300	700	-	-	-
3015	600	150	250	200	90	26	20	300	700	-	-	-
3016	600	150	250	200	90	26	20	300	700	-	-	-
3017	700	200	300	200	90	26	20	350	750	-	-	-
3018	700	200	300	200	90	26	20	350	750	-	-	-
3019	700	200	300	200	90	26	20	350	750	-	-	-
3020	700	200	300	200	90	26	20	350	750	-	-	-
3021	700	300	300	100	90	26	20	450	750	-	-	-
3022	700	300	300	100	90	26	20	450	750	-	-	-
3023	700	300	300	100	90	26	20	450	750	-	-	-
3024	700	300	300	100	90	26	20	450	750	-	-	-
3025	600	150	250	200	90	26	20	300	700	-	-	-
3026	600	150	250	200	90	26	20	300	700	-	-	-
3027	600	150	250	200	90	26	20	300	700	-	-	-
3028	600	150	250	200	90	26	20	300	700	-	-	-
3029	700	200	300	200	90	26	20	350	750	-	-	-
3030	700	200	300	200	90	26	20	350	750	-	-	-
3031	700	200	300	200	90	26	20	350	750	-	-	-
3032	700	200	300	200	90	26	20	350	750	-	-	-
3033	700	300	300	100	90	26	20	450	750	-	-	-
3034	700	300	300	100	90	26	20	450	750	-	-	-
3035	700	300	300	100	90	26	20	450	750	-	-	-
3036	700	300	300	100	90	26	20	450	750	-	-	-
3037	600	150	250	200	90	26	20	-	700	20	300	-
3038	600	150	250	200	90	26	20	-	700	20	300	-
3039	600	150	250	200	90	26	20	-	700	20	300	-
3040	600	150	250	200	90	26	20	-	700	20	300	-
3041	700	200	300	200	90	26	20	-	750	20	350	-
3042	700	200	300	200	90	26	20	-	750	20	350	-
3043	700	200	300	200	90	26	20	-	750	20	350	-
3044	700	200	300	200	90	26	20	-	750	20	350	-
3045	700	300	300	100	90	26	20	-	750	20	450	-
3046	700	300	300	100	90	26	20	-	750	20	450	-
3047	700	300	300	100	90	26	20	-	750	20	450	-
3048	700	300	300	100	90	26	20	-	750	20	450	-

Note:

L = overall length of the glulam timber specimen

l_t = length of the embedment hole in the test end

l_t = length of the embedment hole in the test end

l_s = length of the embedment hole in the support end

l_m = distance between the two inner ends of the embedment holes

a = cross-section dimension, a = b = 2 x e (edge distance)

h = the diameter of the embedment hole

d = the steel bar diameter

l_{st} = length of the steel bar used in the test end

l_{ss} = length of the steel bar used in the support end

8.3.7 Experiment Set-up

The specimens were put into the loading frames and fixed by the end plates and nuts. Each specimen was aligned and pre-loaded by adjusting the nuts on both ends of the specimen. For each specimen, the target tensile load shown in Table 8.6 was applied by a hydraulic jack with a bracket and the load level was maintained by the nuts on both end of the specimen and the reaction frame. All loading was monitored by the P-3500 Digital Strain Indicator. The initial load for each specimen was slightly higher than the target load as the load would drop slightly after the hydraulic jack was released. After 150 days, the same loading procedure was repeated to restore the target load level as the target load was sustained with minor reduction due to the relaxation of the specimen. The wires of the strain gauges and the moisture probes were connected to the switch box after the specimens were loaded. The outdoor specimens were loaded in the dry condition with moisture content below 15%.

8.3.8 Experimental Procedure

The data for both wet and dry specimens were recorded every week in a period of 570 days then every month. For each specimen, the tensile load and moisture content was measured. The displacements of the connection in the selected specimens were measured by the DEMEC gauge.

Table 8.5 Scheme of the wet-dry cycles for the outdoor specimens

Cycles		Environment	Period of Time (days)	Irrigation	Moisture Content[1] (%)
Stage One	1	wet	90	irrigation on[2]	25-29
		dry	60	irrigation off[3]	12-16
Stage Two	2	wet	90	irrigation on	19-23
		dry	60	irrigation off	12-16
	3	wet	90	irrigation on	19-23
		dry	90	irrigation off	12-16
	4[4]	wet	90	irrigation on	19-23
		dry	90	irrigation off	12-16

Note: 1. This is the expected range of the average moisture content.

2. The irrigation system was controlled automatically by the electronic water timer control unit (Rainmatic 2500). Water would spry regularly several times every day during the entire wet part of the cycle. The timer can be adjusted to obtain the target moisture content.

3. The irrigation system was switched off permanently so there was no water spray.

4. The wet-dry cycle would be continued until 85% outdoor specimens fail.

The schedule of the wet-dry cycles for the outdoor specimens is listed in Table 8.5. At the beginning of Stage Two, any specimen which failed in the Stage One was replaced by another specimen with exactly same parameters and all of the specimens were reloaded to the target load.

8.4 RESULTS OF EXPERIMENT THREE

8.4.1 Moisture Content Fluctuations

Figure 8.8 shows the average moisture content both in the outdoor and indoor specimens. The indoor (control) specimens remained approximately constant in the test period; the average moisture content of the indoor specimens was about 10% within a very small range of fluctuation. Conversely, the average moisture content in the outdoor specimens changed with time and simulated natural environmental conditions.

It also can be seen from the figure that the average moisture content between Stage One and Stage Two was different. The average moisture content during the wet part of the cycle in Stage One was about 28%, almost the fibre saturation point of *Pinus Radiata* (29%). By way of contrast, the average moisture content at the wet cycles of Stage Two only reached about 21%.

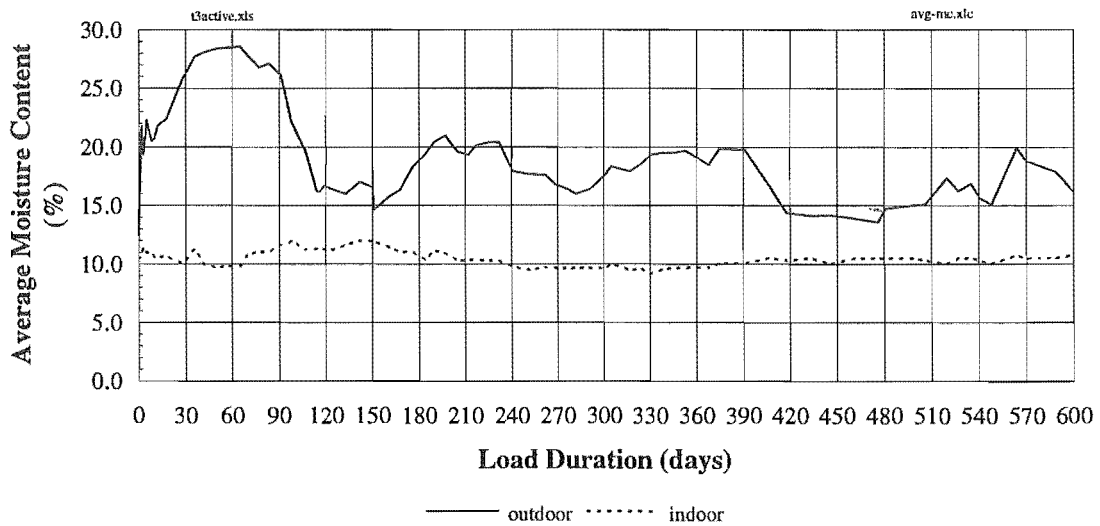

Figure 8.8 Average moisture content during the long duration experiment

8.4.2 Sustained Tensile Load in the Specimens

Figures 8.9 show the overall tensile load fluctuation due to the fluctuating environmental condition and the rheological behaviour of the wood and the connection. Figures 8.9 display the tensile load ratio of each specimen. The ratio is defined as tensile load at a certain time divided by the target tensile load for each specimen. Figure 8.9 (a) shows the tensile load ratio for all outdoor specimens. Figure 8.9 (b) displays the tensile load ratio for the indoor specimens. As can be seen from Figure 8.9 (a), most failures of the connections occurred at Stage One, in which the specimens were subjected to a harsh environment. Only 3 specimens failed under Stage Two's relative mild moisture environment.

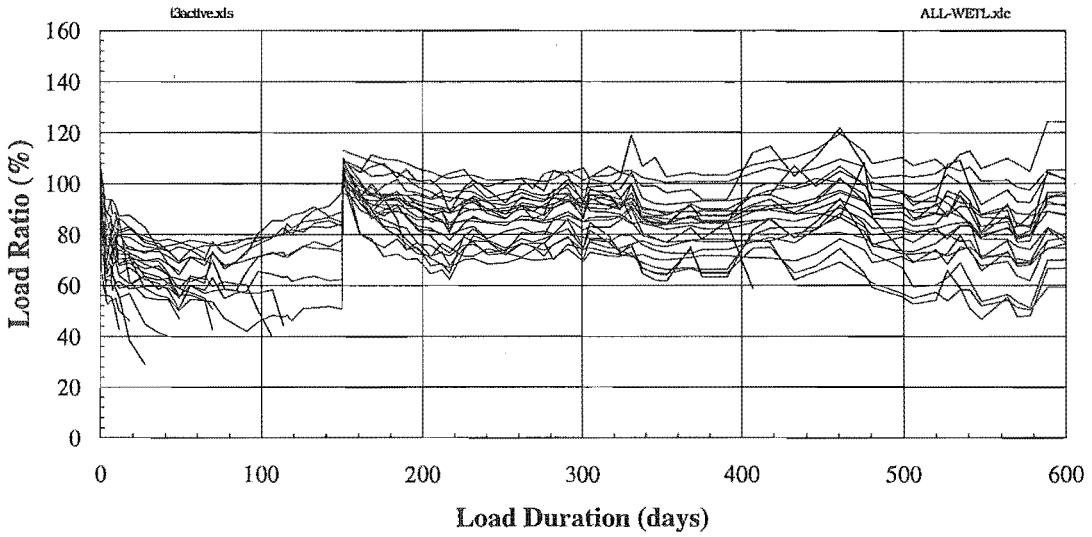

Figure 8.9 (a) Overall tensile load fluctuation in outdoor specimens

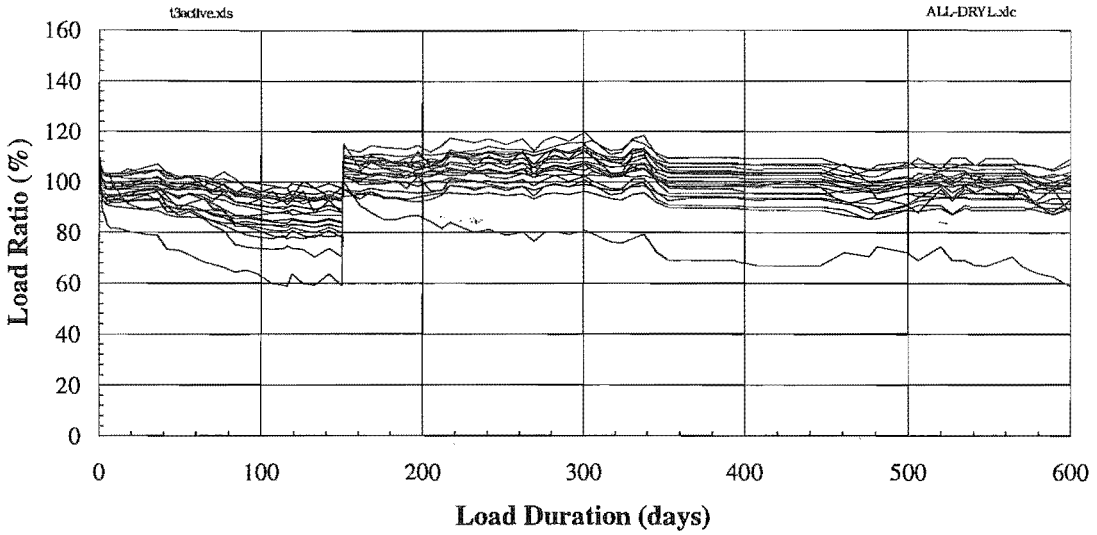

Figure 8.9 (b) Overall tensile load fluctuation in indoor specimens

8.4.3 Failed Specimens and Failure Mode

During the 600 days of testing, most indoor specimens still sustained the tensile load. Only two specimens failed both with Type 3 failure mode. Of the outdoor specimens, 15 specimens failed with Type 2 failure mode at Stage One while only 3 specimens failed in Stage Two. The results are shown in Table 8.6.

Table 8.6 (a) Results of Experiment Three - Stage One

Code	Bar Type	Epoxy Type	d (mm)	h (mm)	l (mm)	e (mm)	MC	Load Level	DEMEC	Target Load (kN)	Duration (days)	Failure Mode
3001	T	K-80	16	20	120	36	cycle	low		24.1		
3002	T	K-80	16	20	120	36	control	low		24.1		
3003	T	K-80	16	20	120	36	cycle	high	•	36.1		
3004	T	K-80	16	20	120	36	control	high	•	36.1		
3005	T	K-80	16	20	160	36	cycle	low		32.1	114	s/p
3006	T	K-80	16	20	160	36	control	low		32.1		
3007	T	K-80	16	20	160	36	cycle	high		48.2		
3008	T	K-80	16	20	160	36	control	high		48.2		
3009	T	K-80	16	20	240	36	cycle	low		48.2	49	s/p
3010	T	K-80	16	20	240	36	control	low		48.2		
3011	T	K-80	16	20	240	36	cycle	high		72.3		
3012	T	K-80	16	20	240	36	control	high		72.3		
3013	T	K-80	20	26	150	45	cycle	low	•	40.7	107	s/p
3014	T	K-80	20	26	150	45	control	low	•	40.7		
3015	T	K-80	20	26	150	45	cycle	high	•	61.1	36	s/p
3016	T	K-80	20	26	150	45	control	high	•	61.1		
3017	T	K-80	20	26	200	45	cycle	low		54.3	12	s/p
3018	T	K-80	20	26	200	45	control	low		54.3		
3019	T	K-80	20	26	200	45	cycle	high		81.4	49	s/p
3020	T	K-80	20	26	200	45	control	high		81.4		
3021	T	K-80	20	26	300	45	cycle	low		81.4	42	s/p
3022	T	K-80	20	26	300	45	control	low		81.4		
3023	T	K-80	20	26	300	45	cycle	high	•	122.1	65	s/p
3024	T	K-80	20	26	300	45	control	high	•	122.1		
3025	T	WS	20	26	150	45	cycle	low		40.7		
3026	T	WS	20	26	150	45	control	low		40.7		
3027	T	WS	20	26	150	45	cycle	high	•	61.1	42	s/p
3028	T	WS	20	26	150	45	control	high	•	61.1		
3029	T	WS	20	26	200	45	cycle	low		54.3		
3030	T	WS	20	26	200	45	control	low		54.3		
3031	T	WS	20	26	200	45	cycle	high		81.4		
3032	T	WS	20	26	200	45	control	high		81.4		
3033	T	WS	20	26	300	45	cycle	low		81.4	18	s/p
3034	T	WS	20	26	300	45	control	low		81.4		
3035	T	WS	20	26	300	45	cycle	high		122.1	70	s/p
3036	T	WS	20	26	300	45	control	high		122.1		
3037	D	K-80	20	26	150	45	cycle	low		32.2	28	s/p
3038	D	K-80	20	26	150	45	control	low		32.2		
3039	D	K-80	20	26	150	45	cycle	high	•	48.4		
3040	D	K-80	20	26	150	45	control	high	•	48.4		
3041	D	K-80	20	26	200	45	cycle	low		43	49	s/p
3042	D	K-80	20	26	200	45	control	low		43		
3043	D	K-80	20	26	200	45	cycle	high		64.5		
3044	D	K-80	20	26	200	45	control	high		64.5		
3045	D	K-80	20	26	300	45	cycle	low		64.5	70	s/p
3046	D	K-80	20	26	300	45	control	low		64.5		
3047	D	K-80	20	26	300	45	cycle	high		96.7	70	s/p
3048	D	K-80	20	26	300	45	control	high		96.7		

Table 8.6 (b) Results of Experiment Three - Stage Two

Code	Bar Type	Epoxy Type	d (m	h (m	l (mm	e (m	MC	Load Level	DEMEC	Target Load (kN)	Duration (days)	Failure Mode
3001	T	K-80	16	20	120	36	cycle	low		24.1		
3002	T	K-80	16	20	120	36	control	low		24.1		
3003	T	K-80	16	20	120	36	cycle	high	•	36.1		
3004	T	K-80	16	20	120	36	control	high	•	36.1		
3005A	T	K-80	16	20	160	36	cycle	low		32.1		
3006	T	K-80	16	20	160	36	control	low		32.1		
3007	T	K-80	16	20	160	36	cycle	high		48.2		
3008	T	K-80	16	20	160	36	control	high		48.2		
3009A	T	K-80	16	20	240	36	cycle	low		48.2		
3010	T	K-80	16	20	240	36	control	low		48.2		
3011	T	K-80	16	20	240	36	cycle	high		72.3		
3012	T	K-80	16	20	240	36	control	high		72.3		
3013A	T	K-80	20	26	150	45	cycle	low	•	40.7	181	s/p
3014	T	K-80	20	26	150	45	control	low	•	40.7		
3015A	T	K-80	20	26	150	45	cycle	high	•	61.1		
3016	T	K-80	20	26	150	45	control	high	•	61.1		
3017A	T	K-80	20	26	200	45	cycle	low		54.3		
3018	T	K-80	20	26	200	45	control	low		54.3		
3019A	T	K-80	20	26	200	45	cycle	high		81.4		
3020	T	K-80	20	26	200	45	control	high		81.4		
3021A	T	K-80	20	26	300	45	cycle	low		81.4		
3022	T	K-80	20	26	300	45	control	low		81.4		
3023A	T	K-80	20	26	300	45	cycle	high	•	122.1		
3024	T	K-80	20	26	300	45	control	high	•	122.1	176	w/f
3025	T	WS	20	26	150	45	cycle	low		40.7		
3026	T	WS	20	26	150	45	control	low		40.7		
3027A	T	WS	20	26	150	45	cycle	high	•	61.1		
3028	T	WS	20	26	150	45	control	high	•	61.1		
3029	T	WS	20	26	200	45	cycle	low		54.3		
3030	T	WS	20	26	200	45	control	low		54.3		
3031	T	WS	20	26	200	45	cycle	high		81.4		
3032	T	WS	20	26	200	45	control	high		81.4		
3033A	T	WS	20	26	300	45	cycle	low		81.4		
3034	T	WS	20	26	300	45	control	low		81.4		
3035A	T	WS	20	26	300	45	cycle	high		122.1		
3036	T	WS	20	26	300	45	control	high		122.1		
3037A	D	K-80	20	26	150	45	cycle	low		32.2		
3038	D	K-80	20	26	150	45	control	low		32.2		
3039	D	K-80	20	26	150	45	cycle	high	•	48.4	407	s/p
3040	D	K-80	20	26	150	45	control	high	•	48.4		
3041A	D	K-80	20	26	200	45	cycle	low		43		
3042	D	K-80	20	26	200	45	control	low		43		
3043	D	K-80	20	26	200	45	cycle	high		64.5		
3044	D	K-80	20	26	200	45	control	high		64.5		
3045A	D	K-80	20	26	300	45	cycle	low		64.5	241	s/p
3046	D	K-80	20	26	300	45	control	low		64.5		
3047A	D	K-80	20	26	300	45	cycle	high		96.7.		
3048	D	K-80	20	26	300	45	control	high		96.7	262	w/f

Note: T = threaded steel rod.

D = deformed reinforcing bar.

WS = West System epoxy.

d = steel bar diameter.

h = embedment hole diameter.

l = embedment length.

e = edge distance.

MC = moisture condition.

s/p = the connection pullout with wood split - Type 2 failure mode.

w/f = wood failure across the cross-section at the end of the connection - Type 3 failure mode.

• = the specimen with DEMEC measuring point.

8.4.4 Typical Results Among Different Environmental Conditions

Two pairs of specimens have been selected to demonstrate typical results from the experiment. Figure 8.10 (a) shows moisture content fluctuation with time. Both specimens (3003, 3004) have exactly the same geometry with 16 mm diameter threaded steel rod and 120 mm embedment length. The same load level was used for both specimens. Specimen 3003 was exposed in outdoor environment with wet-dry cycles. The moisture content of the specimen in the wet part of the cycle of Stage One was obviously higher than that in the other wet parts of the cycles in Stage Two. The moisture content remained about 10% with very small fluctuations in the corresponding indoor control specimen (3004).

Figure 8.10 (b) shows the displacement of the connection in these two specimens. The increase of displacement in both specimens at the beginning of Stage Two (day 150) is due to the reloading of the specimens. Apart from this, no obvious further displacement was observed in the control specimen. At the second dry cycle of Stage Two, the displacement in specimen 3003 appeared to increase, showing the rheological behaviour of the connection.

Figure 8.10 (c) shows the load fluctuation against time. For specimen 3003, the major fluctuation of load occurred in Stage One. At the beginning of Stage One, the tensile load appeared to decrease significantly. In Stage Two, after reloading, the load level seems quite stable with minor fluctuations. For specimen 3004, no major decrease of tensile load occurred, although minor fluctuation existed. A similar result can be observed in the specimens with the deformed reinforcing bar connection as shown in Figures 8.11. Two specimens are shown in the figures: one is an outdoor specimen (3039) subjected to the wet-dry cycle environment. The other is the corresponding control specimen in the indoor environment (3040). Both have exactly the same parameters in the connection. The figures are similar to Figure 8.10, except the wet specimen failed at 407 days.

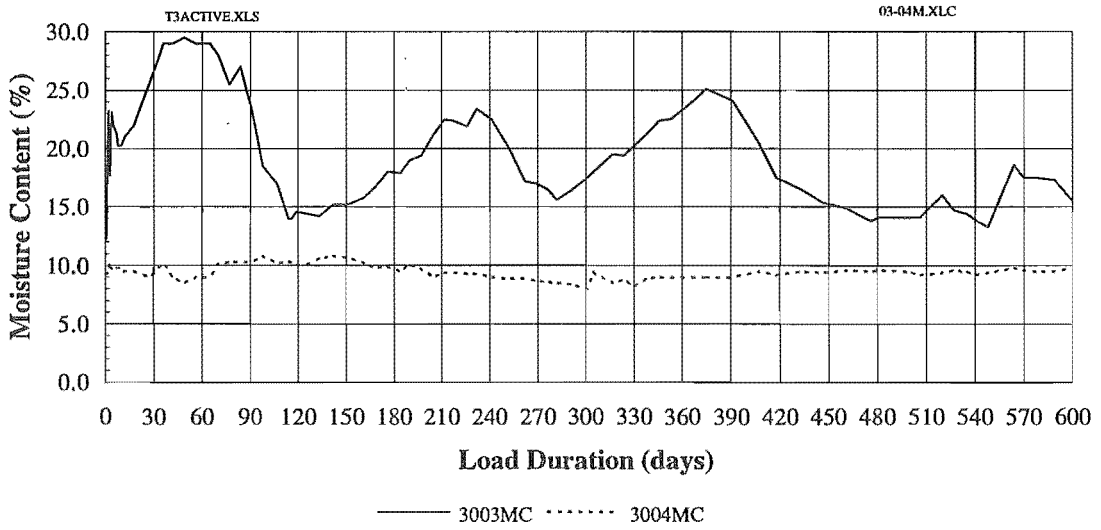

Figure 8.10 (a) Moisture content fluctuation at the long duration experiment

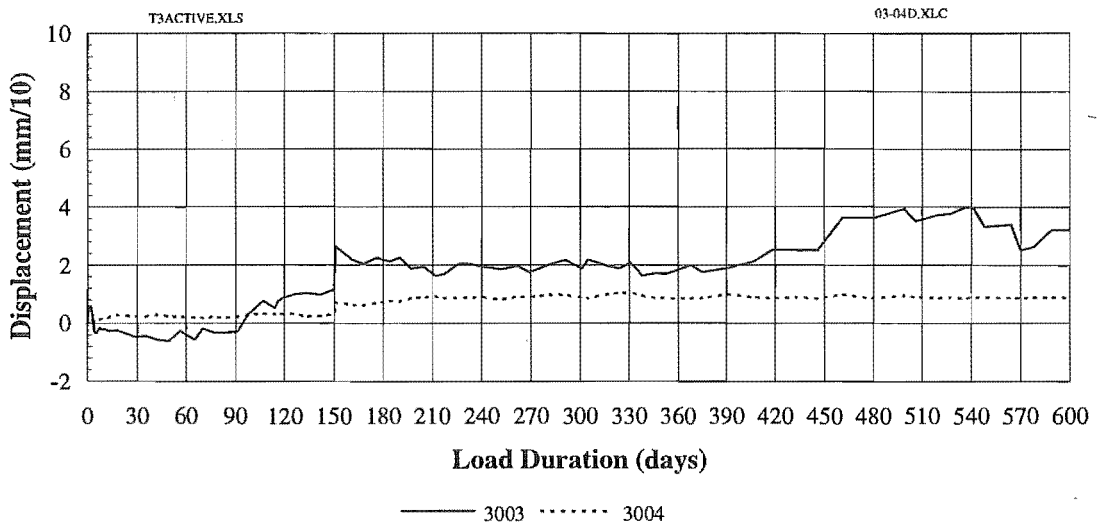

Figure 8.10 (b) Displacement of the connection at the long duration experiment

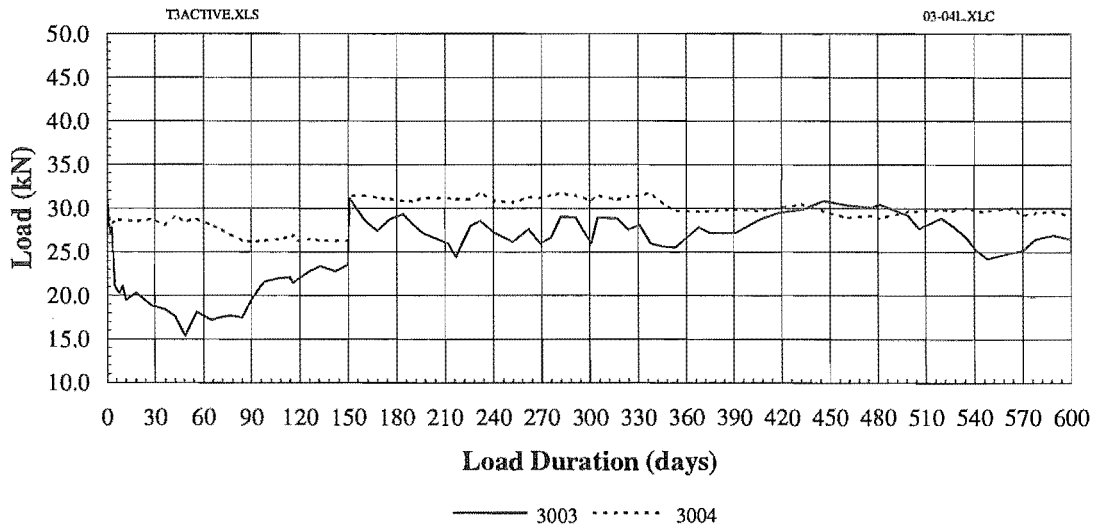

Figure 8.10 (c) Tensile load variation at the long duration experiment

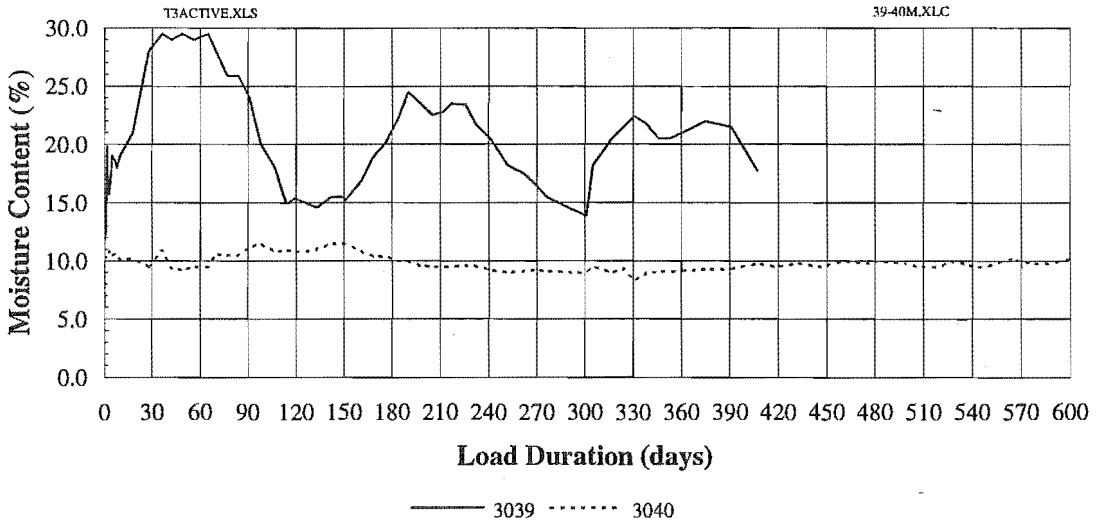

Figure 8.11 (a) Moisture content fluctuation at the long duration experiment

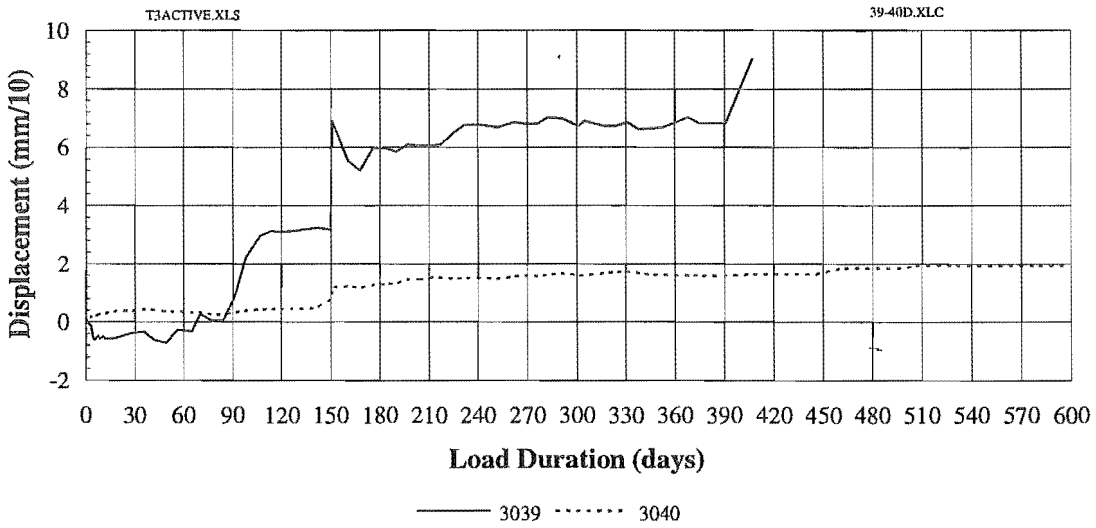

Figure 8.11 (b) Displacement of the connection at the long duration experiment

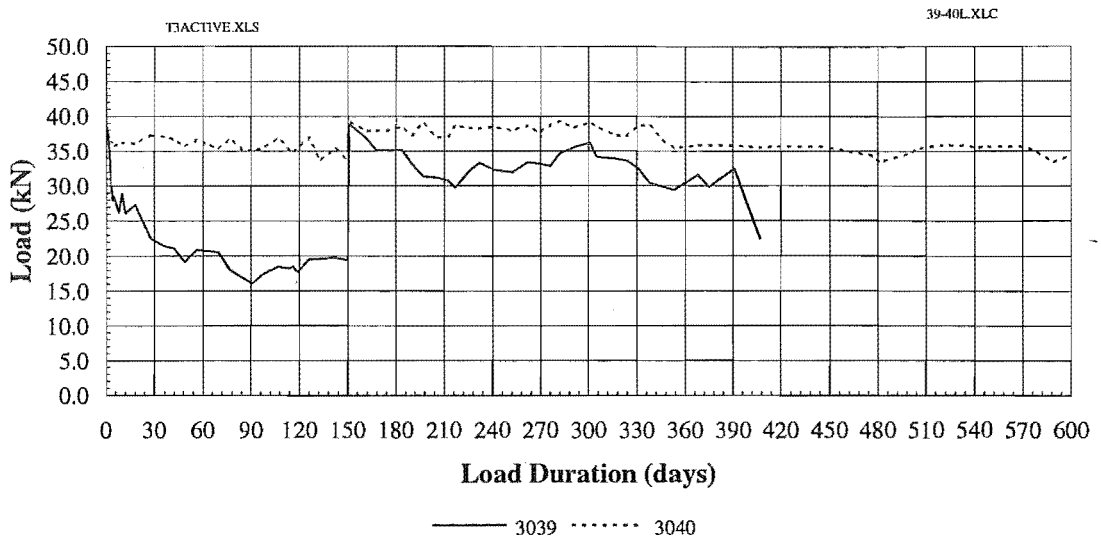

Figure 8.11 (c) Tensile load variation at the long duration experiment

8.4.5 Typical Results Under Two Different Load Levels

Figures 8.12 show the displacement of the connections under two different load levels. In Figure 8.12 (a), specimens were subjected to outdoor environment with same geometry, but loaded in two different load levels. The specimens 3013 and 3013A were sustained lower tensile load while specimens 3015 and 3015A were subjected to higher tensile load during the experiment. Similarly, Figure 8.12 (b) compares the displacement in the corresponding control specimens under two load levels.

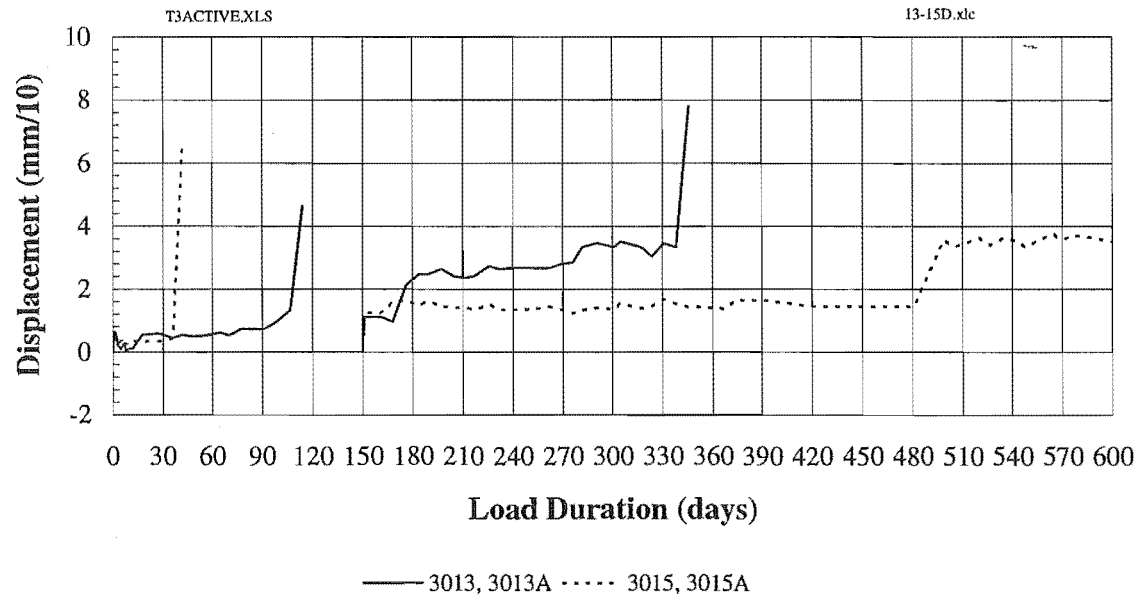

Figure 8.12 (a) Displacement of the outdoor specimens under different load levels

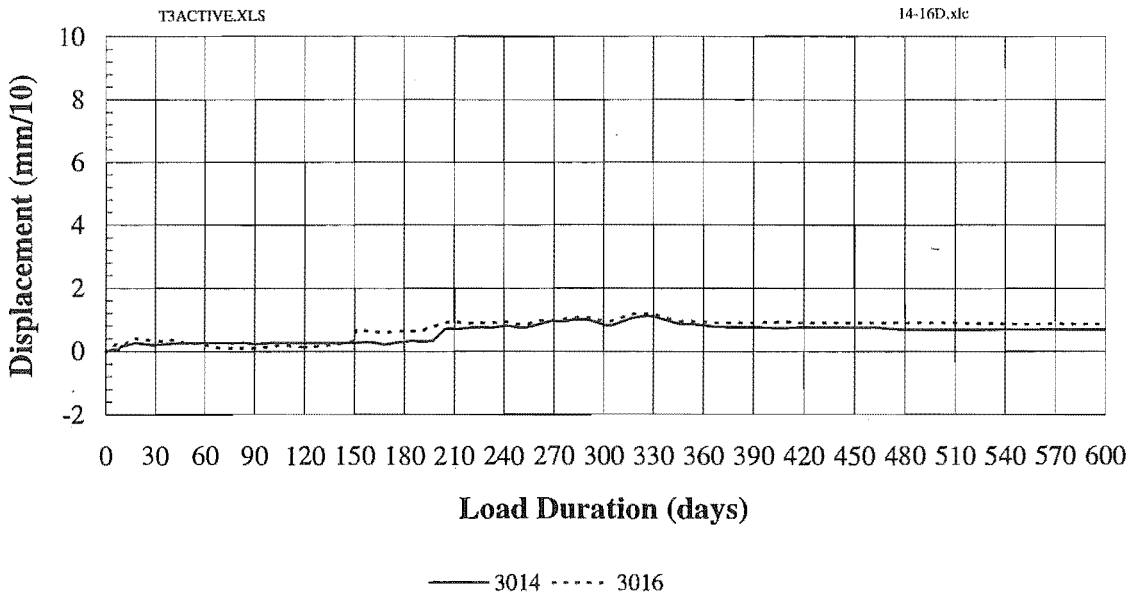

Figure 8.12 (b) Displacement of the indoor specimens under different load levels

8.5 MEASUREMENT OF MOISTURE CONTENT AND SHRINKAGE *IN SITU*

8.5.1 Test Programme

A project was carried out to investigate the moisture content and shrinkage of glulam timber structures under high humidity service conditions. The transverse dimension change only caused by moisture content fluctuations were of interest. This is defined as: the transverse dimension change from initial measurement divided by initial dimension, expressed as a percentage; shrinkage occurs if the value is negative. Conversely, swelling occurs if the value is positive. The term "transverse dimension change" is used to include either shrinkage or swelling perpendicular to the wood grain along the width of the measured glulam timber column.

Glulam timber structures at a swimming pool complex (Jellie Park Sports Centre, Christchurch, New Zealand) were selected for the project. Four columns in main entry hall with outdoor environment and four columns inside the swimming pool

main entry hall with outdoor environment and four columns inside the swimming pool building were selected to measure the moisture content and the shrinkage. The locations are shown in Figure 8.13 (a) and Figure 8.13 (b) respectively. The main entry hall of the swimming pool complex is shown in Figure 8.14.

In the following text, a measuring point is defined as a group of DEMEC gauge targets with a pair of associated moisture probes. The readings from a measuring point would include a transverse dimension change and a moisture content value representing a specific part of the glulam timber structure.

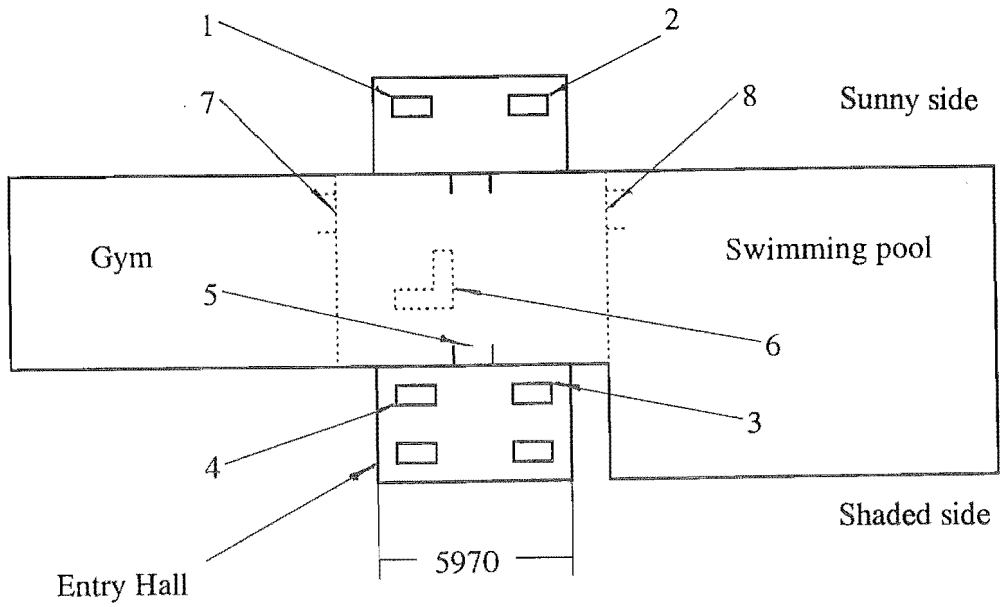

1 = glulam timber column / test point: 01AT and 01AB

2 = glulam timber column / test point: 01BT and 01BB

3 = glulam timber column / test point: 02AT and 02AB

4 = glulam timber column / test point: 02BT and 02BB

5 = main entry

6 = reception

7 = gym entry

8 = indoor swimming pool entry

Figure 8.13 (a) Sketch of location of outdoor columns

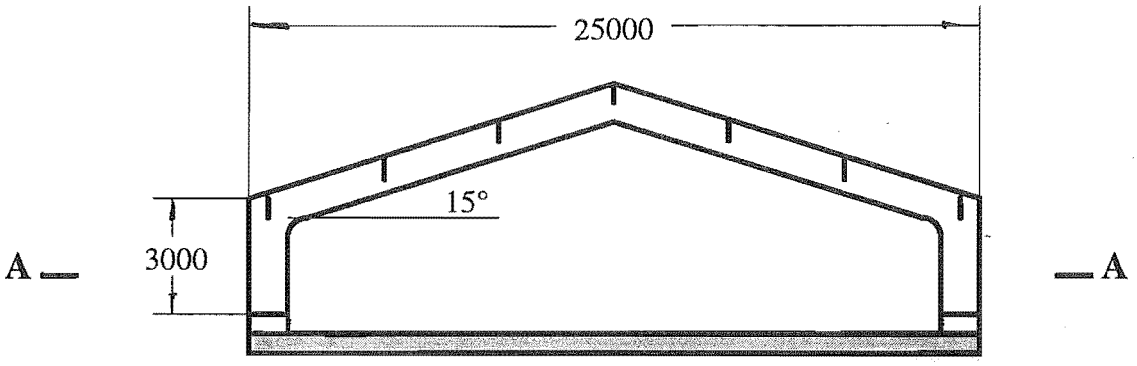

560 x 115 glulam

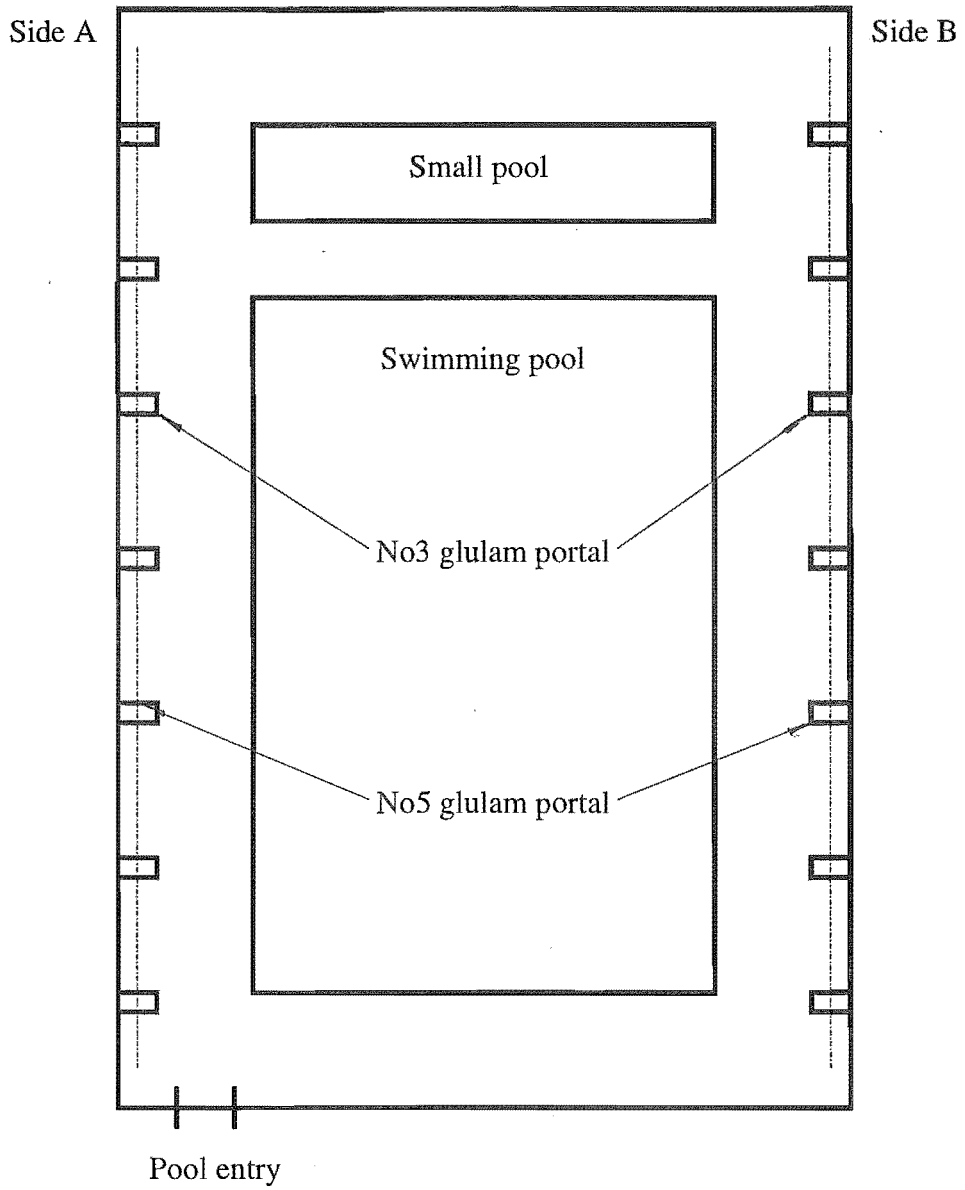

Figure 8.13 (b) Sketch of the locations of the indoor columns measured

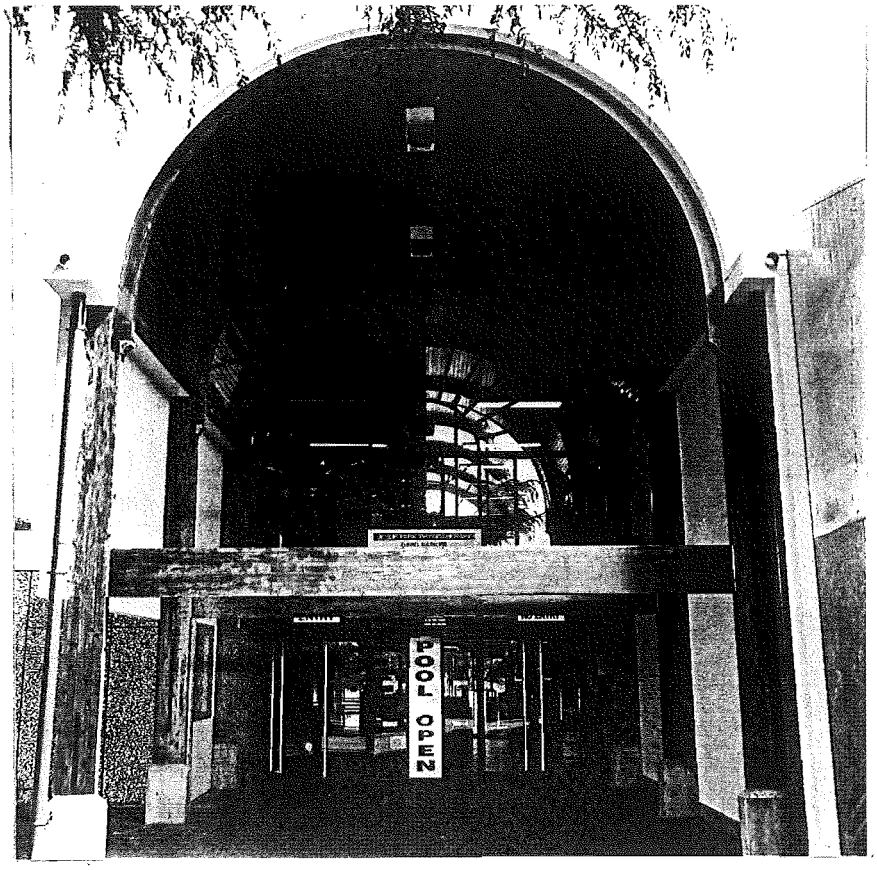

Figure 8.14 The main entry hall of the swimming pool complex

Figures 8.15 show details of the measuring points for the indoor columns. The moisture content in the columns was measured by a electric resistance type moisture meter (Timbermaster Model D184T, Protimeter Ltd) via a pair of probes embedded in the column. The principle and method of moisture content measurement have been described in the previous section. The shrinkage was measured by a 203 mm (8") DEMEC gauge, the location of the DEMEC reading points is shown in Figure 8.15.

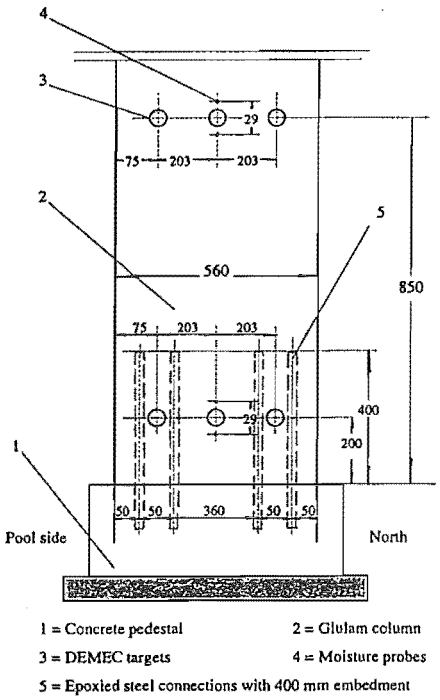

Figure 8.15 (a) Measurement point details at the indoor portals - Side A (I3AT, I3AB, I5AT, I5AB, Not to scale)

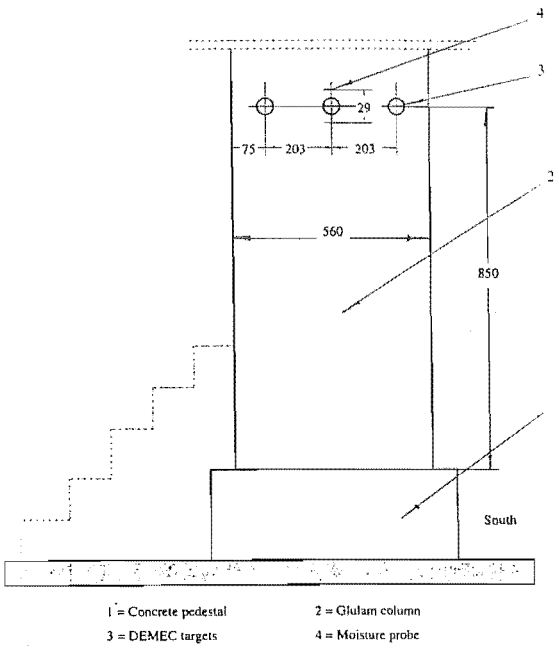

Figure 8.15 (b) Measurement point details at the indoor portals - side B (I3BT, I5BT, Not to scale)

The moisture content and the transverse dimension change in the outdoor columns were measured using the same method. The location of measurement points is shown in Figure 8.16. All of measurement points were coded and are described in Table 8.7.

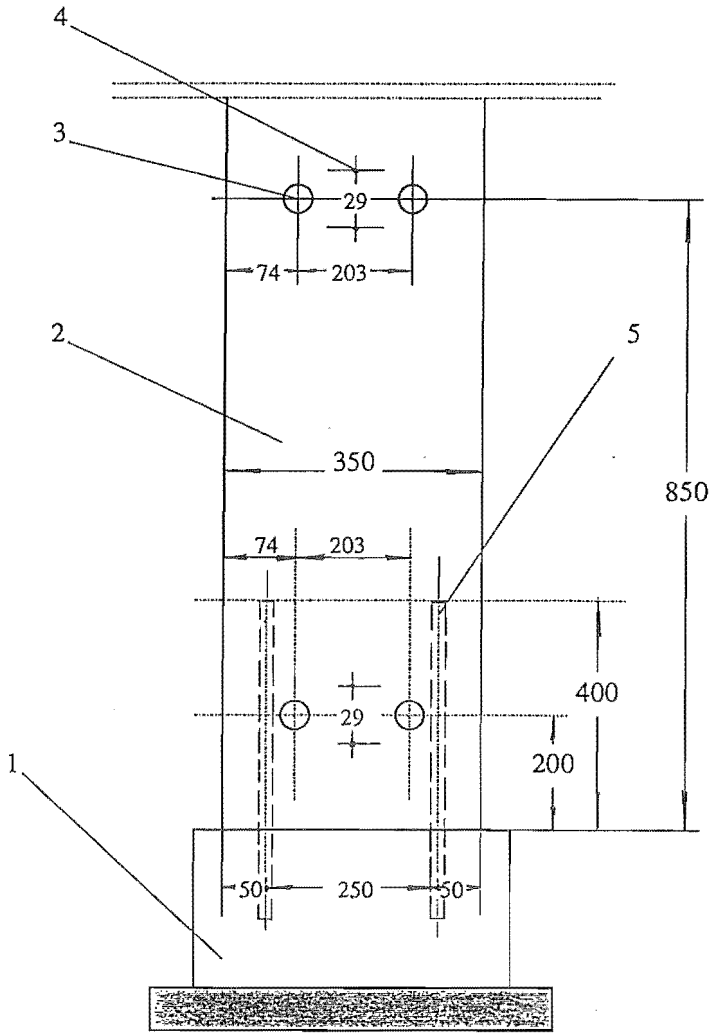

1 = Concrete pedestal
2 = Glulam column
3 = DEMEC targets
4 = Moisture probe
5 = Epoxied steel connections with 400 mm embedment

Figure 8.16 Location of moisture probes and DEMEC targets in a outdoor column (Not to scales)

Table 8.7 Locations of the measurement point

Code	Location of Measurement Point	Environment Condition
I3AT	indoor, No.3 portal, Side A, top point	indoor, exposed to the sun, close to outdoor condition during the summer[1]
I3AB	indoor, No.3 portal, Side A, bottom point	
I3BT	indoor, No.3 portal, B side, top point	indoor, not exposed to the sun
I5AT	indoor, No.5 portal, Side A, top point	indoor, exposed to the sun, close to outdoor condition during the summer
I5AB	indoor, No.5 portal, Side A, bottom point	
I5BT	indoor, No.5 portal, B side, top point	indoor, not exposed to the sun
O1AT	outdoor, sunny side arch, west side column, top point	outdoor environment, humidity changes with different season and climate, exposed to the sun
O1AB	outdoor, sunny side arch, west side column, bottom point	
O1BT	outdoor, sunny side arch, east side column, top point	
O1BB	outdoor, sunny side arch, east side column, bottom point	
O2AT	outdoor, shaded side arch, east side column, top point	outdoor environment, humidity changes with different season and climate, not exposed to the sun
O2AB	outdoor, shaded side arch, east side column, bottom point	
O2BT	outdoor, shaded side arch, west side column, top point	
O2BB	outdoor, shaded side arch, west side column, bottom point	

Note: 1. During the summer season the indoor environmental condition was close to the outdoor environmental condition because the doors are kept open in the day time.

2. Relative humidity in the indoor swimming area ranged from 60% to 75%.

8.5.2 Measurement Set-up and Procedure

The DEMEC gauge targets were glued on the surface of the columns as shown in Figures 8.15 and Figure 8.16 to measure the transverse dimension change. Moisture probes were embedded into the columns 50 mm depth. The same probes were used as for Experiment Three. The configuration of measuring point for the indoor columns was different between side A and side B (Figure 8.13 (b) and Figures 8.15 (a) and (b)), but was exactly same in outdoor columns (Figure 8.13 (a) and Figure 8.16).

The moisture content and transverse dimension change readings were recorded regularly at intervals of two weeks. The interval between readings was extended to one month one year after the project started. The measurements had been carried out for more than 640 days.

8.6 RESULTS OF MOISTURE CONTENT AND SHRINKAGE MEASUREMENT

Figure 8.17 (a) shows moisture content fluctuations measured from the No. 3 glulam timber portal (I3AT, I3AB and I3BT). The range of moisture change during the entire test period was less than 2.5% at all measuring points and the pattern of fluctuations at different points was similar. Figure 8.17 (b) shows the transverse dimension change at the corresponding measuring points. As previous defined, swelling occurs if the curves lie above zero. Shrinkage occurs if the curves are below zero. The values of shrinkage or swelling were very small.

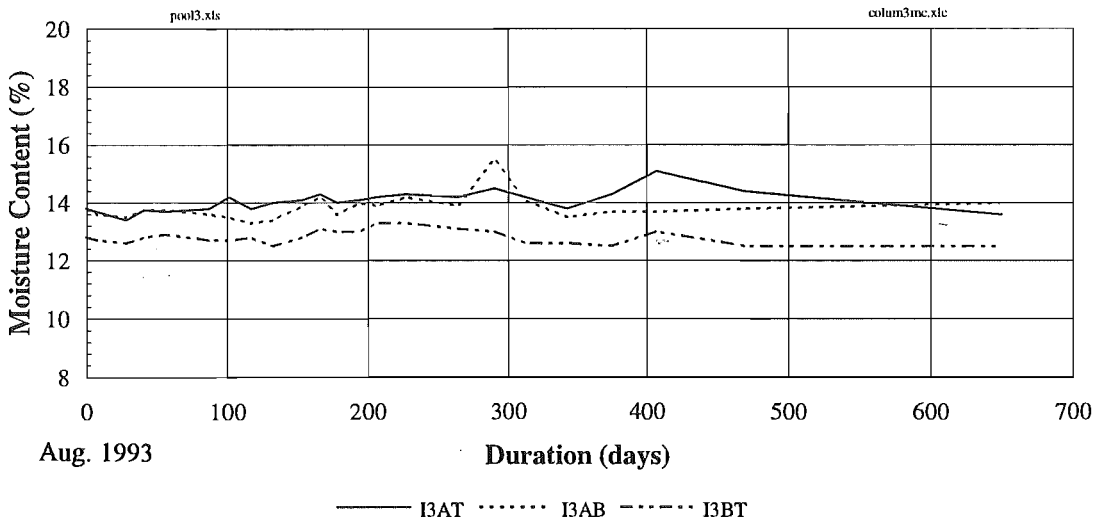

Figure 8.17 (a)Moisture content fluctuations at the specific measuring points of No. 3 glulam timber portal

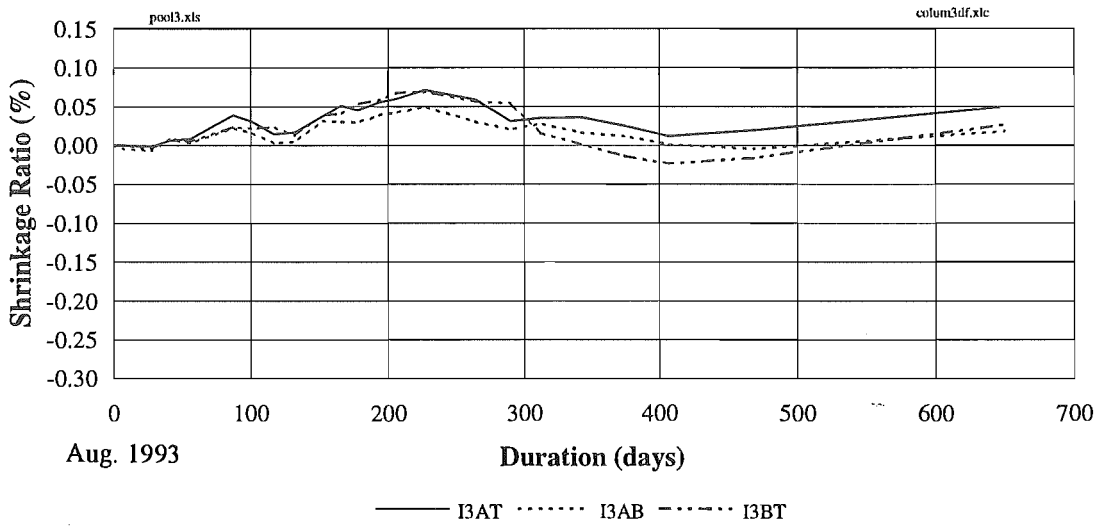

Figure 8.17 (b) Transverse dimension changes at the specific measuring points on the No.3 glulam timber portal

Figures 8.18 (a) and (b) display the fluctuations in moisture content and the transverse dimension change in No.5 glulam timber portal (I5AT, I5AB and I5BT) respectively. Similar results were obtained as in Figure 8.17.

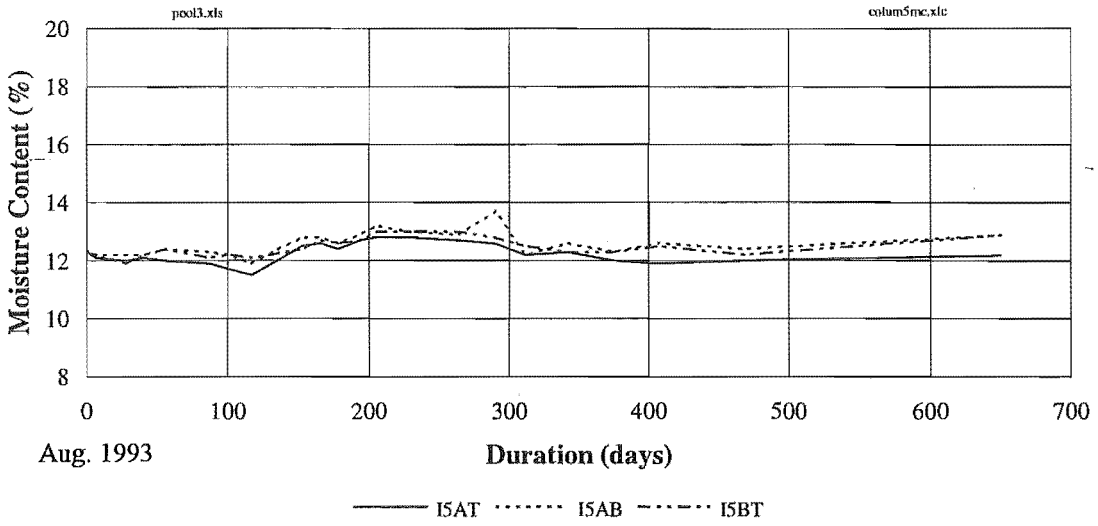

Figure 8.18 (a)Moisture content fluctuations at the specific measuring points on the No. 5 glulam timber portal

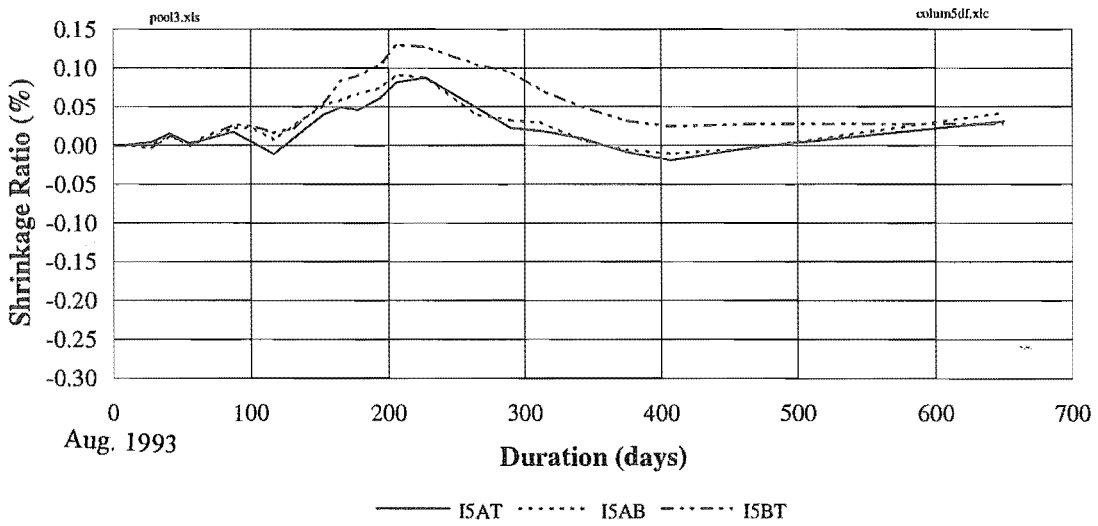

Figure 8.18 (b) Transverse dimension changes at the specific measuring points on the No.5 glulam timber portal

Figure 8.19 (a) shows the moisture content fluctuations in the outdoor columns (O1AT, O1AB, O1BT, O1BB). Figure 8.19 (b) displays the transverse dimension change at the corresponding measuring points.

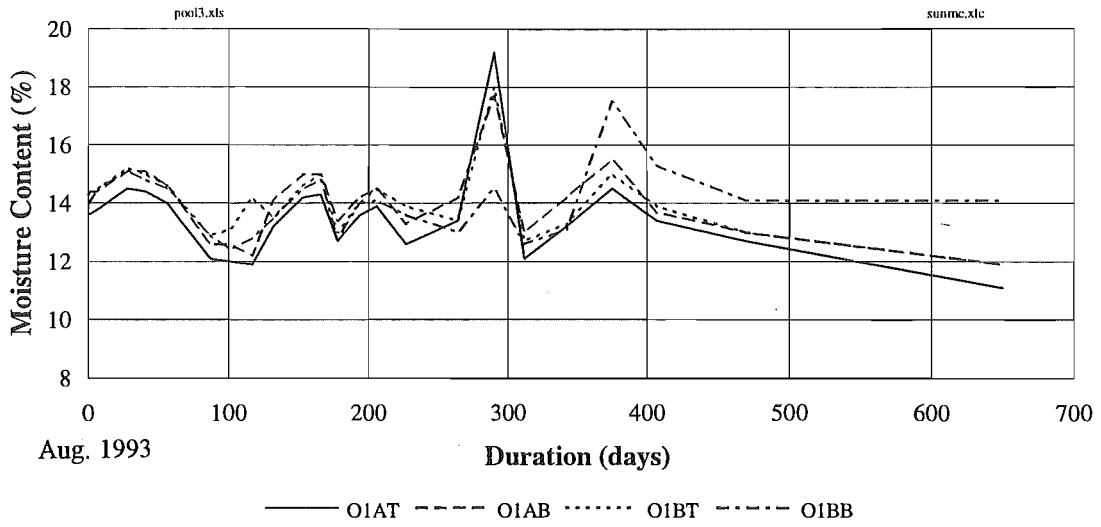

Figure 8.19 (a)Moisture content fluctuations at the specific measuring points on the outdoor columns (O1AT, O1AB, O1BT, O1BB)

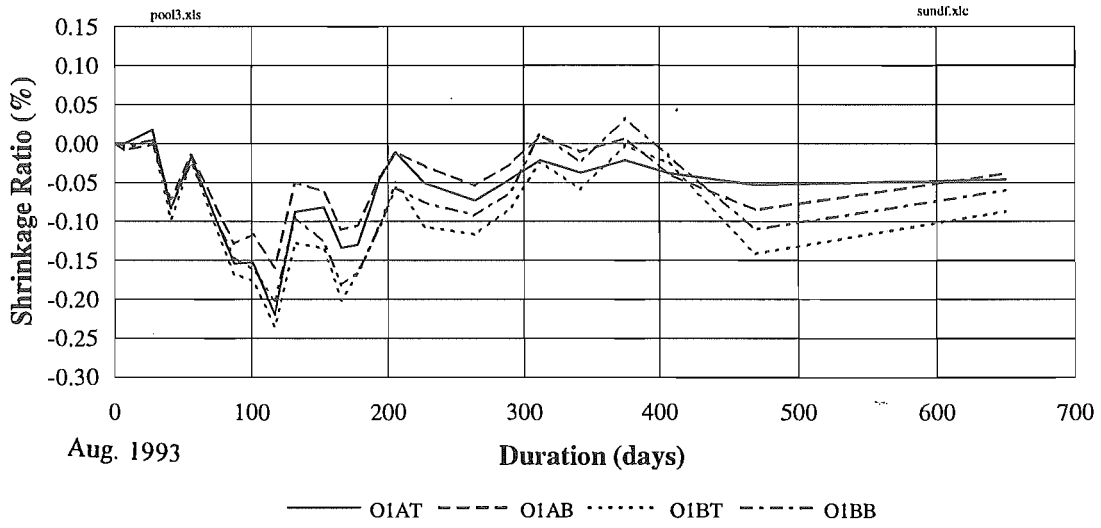

Figure 8.19 (b) Transverse dimension changes at the specific measuring points on the outdoor columns (O1AT, O1AB, O1BT, O1BB)

Figures 8.20 (a) and (b) show the fluctuations of moisture content and the transverse dimension change in outdoor column (O2AT, O2AB, O2BT, O2BB) respectively. It can be seen that the shrinkage reading for the measuring point O2BT

was terminated after about 460 days due to the DEMEC gauge target failure. Figure 8.19 and Figure 8.20 represent different environmental conditions although the data are all from outdoor columns.

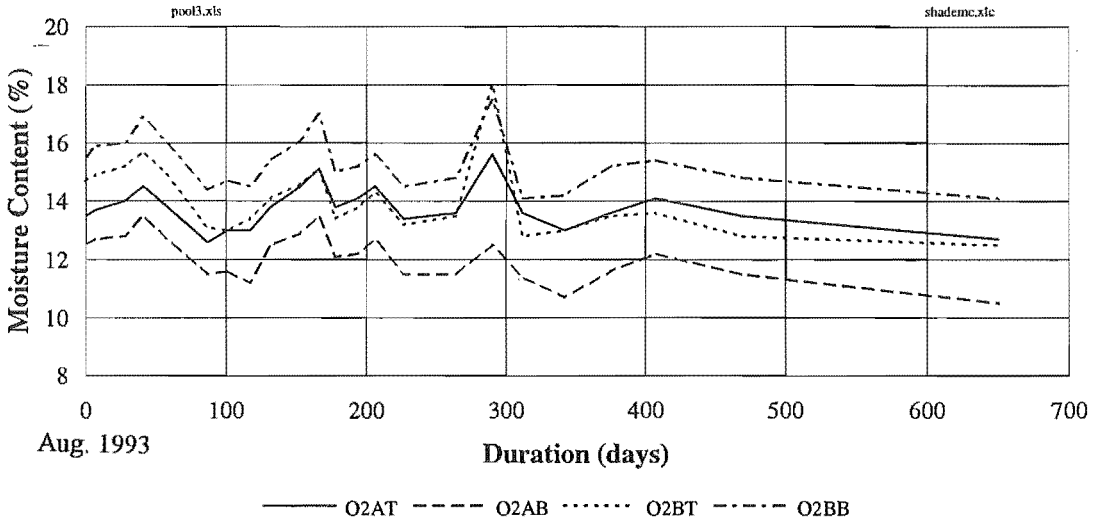

Figure 8.20 (a)Moisture content fluctuations at the specific measuring points in the outdoor columns (O2AT, O2AB, O2BT, O2BB)

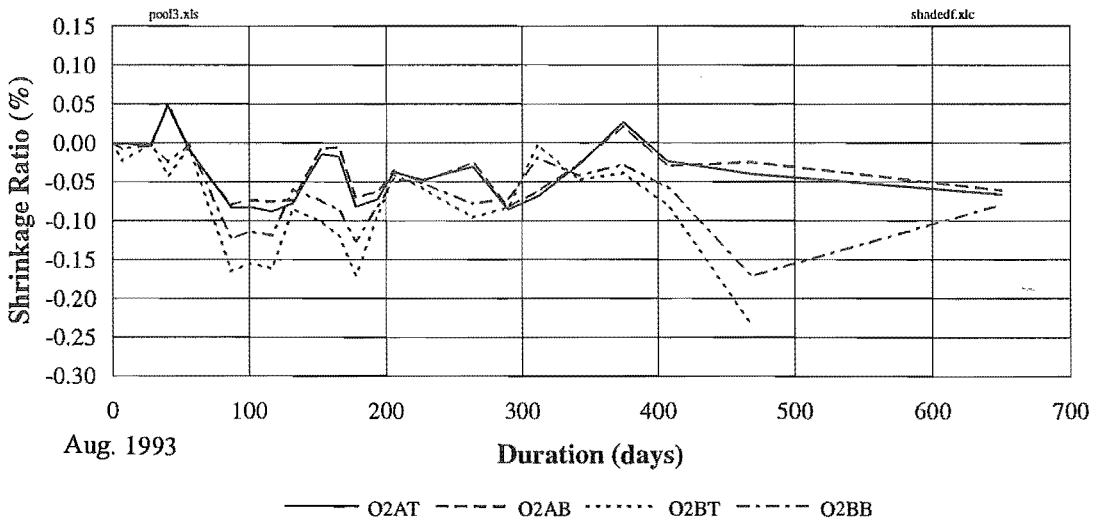

Figure 8.20 (b) Transverse dimension changes at the specific measuring points in the outdoor columns (O2AT, O2AB, O2BT, O2BB)

8.7 DISCUSSION

8.7.1 Discussion of Experiment Three

Although this long duration experiment was carried out on a small scale and the time span of sustained tensile load was less than the life time of structures, some useful information has been obtained.

1. Time-dependent behaviour

Time-dependent behaviour can be observed in Experiment Three. The overall relaxation of the specimens can be identified by the change of tensile load level in Figure 8.9. The typical rheological behaviour of the connection can be studied by analysing the change of load level and the displacement of the connection in Figure 8.10 and Figure 8.11.

Figure 8.9 revealed there was some relaxation of the specimens and this caused the tensile load level to decrease. Most relaxation in the specimens occurred in the initial period of loading both in Stage One and Stage Two, including both indoor and outdoor specimens. However, it should be emphasised that the relaxation can be identified by the change of load level, but the change of load level was a more complicated process and not only caused by the relaxation of the specimen. Other factors such as rheological behaviour of wood, swelling or shrinkage of wood caused by moisture movement and displacement of the connection could also cause some change of load level.

The moisture content fluctuations make a large contribution to the time-dependent behaviour of the connection. The experimental results indicate that mild environmental conditions (Stage Two) reduce the rate and magnitude of the relaxation compared to harsh environment conditions (Stage One). It was also established that the rate of the relaxation appeared higher in the wet part of the cycles than in the dry part of

the cycles, and this brought about change of load level, less relaxation occurred in the indoor specimens than in the outdoor specimens.

Figure 8.10 (b) and Figure 8.11 (b) show typical displacements of the connections which may respond elastically or viscoelastically. Although the fluctuation of the load level tended to mask the displacement of the connection, it still can be observed. As can been from Figure 8.11 (b), at the initial period of the dry cycle of Stage One (day 90), the displacement of the connection changed significantly while the load level remained with marginal fluctuation. At the start of dry part of the third cycle (day 390), the displacement increased while the load level decreased. This indicated that the connection started to fail.

The effect of different load levels to the displacement was investigated and presented in Figures 8.12. No obvious trend can be identified. The displacement of the connection measured is a complicated superposition of creep and swelling of wood on the specimen surface, the rheological behaviour and failure of the connection. For each specimen, the displacement of the connection behaved differently. However, based on the observation of this experiment, a general statement can be made as follows:

The displacement of the connection was caused by many contributing factors acting in different rates and in different magnitude at the same time. No obvious rheological behaviour can be observed in the connections. There seems to be no simple correlation can be made between the displacement and load level. However, if the displacement tended to decrease marginally while the load level decreased, it seems likely that the axial tensile load will be sustained and the connection remains intact; if displacement increased while the load level decreased, the connection was starting to fail. Some creep or fracture in microscopic scale occurred in the connection if the displacement tended to increase marginally while the load level remained roughly same or fluctuated with small magnitude. In this case, it seems likely that the connection will remain intact.

This study did not contemplate making a detailed quantitative description of the time-dependent behaviour. The rheological behaviour of the connection is complicated

and it is probably the combined function of time, moisture content, the magnitude of load and any other relevant factors.

2. Effect of environmental conditions

Environmental conditions appear to have a major effect on the decrease in strength of the connection as shown in Table 8.8. Comparing the indoor control specimens with the outdoor specimens, there were no connection failures in the indoor specimens while 18 outdoor specimens failed within the 600 day testing period. As can be seen from Figure 8.8, the average moisture content of the indoor specimens was about 10% while the average moisture content in the outdoor specimens ranged from 14% to 28%.

Within the outdoor specimens, the strength of the connection decreased significantly when the moisture content of the specimen was close to 28%. Only a minor reduction in strength occurred when the average moisture content fluctuated in the range from 14% to 22%. This can be deduced from the experiment since more than one half of the outdoor specimens failed in Stage One while only 3 specimens failed in Stage Two.

Table 8.8 Number of failed specimens in the different environment conditions

Moisture Condition	Number of Failed Specimens		
	Stage One	Stage Two	
		original	replaced
Wet-dry cycle	15	1	2
Dry	0	0	-
Total	15	1	2

3. Effect of different epoxy

Table 8.9 compares the number of failures for the outdoor specimens with different epoxies. The comparison is made only in the outdoor specimens because there were no connection failures in the dry specimens. Two corresponding groups of the specimens are shown in the table (specimen code 3013 to 3035). The West System epoxy appears to have better water resistant properties than K-80 epoxy. This trend is very similar to the Experiment One result.

Table 8.9 Number of failed outdoor specimens with the different epoxies

Epoxy Type	Number of Failures in the Connections		
	Stage One	Stage Two	
		original	replaced
K-80	6	0	1
West System	3	0	0

4. Effect of load level

Table 8.10 shows the number of failed specimens at two different load levels for the outdoor specimens. It is not clear why there were more failures in low load level than in high load level, but the results suggest that the strength of wood is very low once the moisture content of wood is close to 28% and that a threshold of load level exists (Barrett and Foschi, 1978a, 1978b). The threshold is minimum tensile load required to produce the failure; the load levels defined in the experiment would be less sensitive if the threshold is lower than both load levels.

Table 8.10 Number of failed outdoor specimens in different loading level

Load Level	Number of Failures in Connections of the Specimens		
	Stage One	Stage Two	Total
Low	9	2	11
High	6	1	7

5. Effect of geometry of the connection

Table 8.11 shows the number of failures for the two different bars. Table 8.12 lists the number of failures for the different embedment lengths. Table 8.13 shows the number of failures for the two different bar diameters. The comparisons in Table 8.11 to Table 8.13 were made using two corresponding groups of specimens, viz. to compare the two different bar diameters, two relevant groups of specimens with two different bar diameters are used; the other parameters are exactly same between the two groups. Only the wet specimens are discussed; no significant differences exist for the different bars and the different embedment lengths. For the different bar diameters more failures occurred with the 20 mm diameter bar than the 16 mm. This suggests that target loads for the experiment calculated using Equation 2.6 might be too sensitive when considering the diameter of the steel bars. The results suggest that the effect of geometry has less influence in the connection under long duration load with the wet-dry cycle environment than in the connection subjected short duration load.

Table 8.11 Number of the failed outdoor specimens with different steel bars

Bar Type	Number of Failed Outdoor Specimens		
	Stage One	Stage Two	
		original	replaced
Threaded rod	6	0	1
Deformed bar	4	1	1

Table 8.12 Number of failed outdoor specimens for different embedment lengths

Embedment Length (mm)	Number of Failed Outdoor Specimens		
	Stage One	Stage Two	
		original	replaced
7.5d	4	1	1
10d	4	0	0
15d	7	0	1

Note: d = steel rod diameter (mm).

Table 8.13 Number of failed outdoor specimens for different bar diameters

Steel Rod Diameter (mm)	Number of Failed Outdoor Specimens		
	Stage One	Stage Two	
		original	replaced
16	2	0	1
20	6	0	0

8.7.2 Discussion of Moisture and Shrinkage of Glulam Timber under Various Environments

1. Indoor measurement points

As can be seen from Figure 8.17 (a) and Figure 8.18 (a), the fluctuations in moisture content in the indoor glulam timber structures (No.3 and No.5 glulam portal) under a relative high humidity environment is less than 2.5%. The changes in moisture content at the different locations for the same structure appear quite similar, the curves in the figures following similar patterns. The moisture content fluctuation is quite uniform within the structure.

With very small fluctuations of moisture content in the indoor glulam timber structures, it can be expected that the transverse dimension change in the indoor columns would be negligible. This is confirmed by the results displayed in Figure 8.17 (b) and Figure 8.18(b). The transverse dimension changes for all indoor measuring points are less than 0.15%, including both shrinkage and swelling values. Figure 8.17 and Figure 8.18 confirm that the moisture content fluctuations are the major factor contributing to the shrinkage or swelling in the glulam timber.

2. Outdoor measurement points

The maximum moisture content fluctuation is about 8% in Figure 8.19 (a) and is 5.5% in Figure 8.20 (a). The moisture content fluctuations are similar among different locations in the same structure and as with the indoor columns, this indicates that the

moisture content fluctuations are quite uniform within the same outdoor glulam timber structure under similar environment conditions. The values are slightly different between Figure 8.19 (a) and Figure 8.20 (a) and is due to different environment conditions. The values in Figure 8.19 (a) were taken from those columns exposed to the sun, while the values in Figure 8.20 (a) were moisture contents for these columns not exposed to the sun.

Figure 8.19 (b) and Figure 8.20 (b) show that the maximum range of the transverse dimension change is about 0.25%. This is negligible.

3. Comparisons of different environmental conditions

Comparing the results of outdoor and indoor measurements, the fluctuation of moisture content is higher in outdoor glulam timber than in indoor. Consequently, the transverse dimension changes are likely to be higher in outdoor glulam timber columns than in indoor columns. However, the magnitude of the transverse shrinkage or swelling in the columns in both indoor and outdoor environments is negligible.

4. Comparisons of different locations in the same column

There are two measuring points in most investigated columns. One is within the epoxy bonded steel connection region and the other is located away from the connection as shown in Figure 8.15 (a) and Figure 8.16. This is to compare the difference in moisture content and change of transverse dimension between two different locations within a column. From Figure 8.17 to Figure 8.20, no obvious differences can be identified from the experiment. This suggests that the connection has no significant effect to change the transverse dimension and moisture content in glulam timber.

8.8 CONCLUSIONS

All failure specimens under the outdoor wet-dry cycle environment failed with Type 2 failure mode. Two specimens only under the indoor condition failed, both with Type 3 failure mode.

The moisture content of wood plays an important role in the strength of the connection. The connection performs well under normal indoor environmental conditions. However, the connection cannot be recommended for any situation when the moisture content could exceed 22%. The strength of the connection decreases significantly when the moisture content becomes close to 28%. A low threshold of the tensile strength exists at this moisture content level; it is below the two load levels used in the experiment.

Different types of epoxies also appear to affect the strength of the connection in terms of different water-resistant properties. The performance of West System epoxy was superior to K-80 in a wet environment. Major relaxation and creep occurred during the initial period of loading.

In general, the empirical equation developed from the short duration experiments can also be used in the long duration load situation with deduction considering of environmental conditions and duration of load.

The measurement of moisture content and transverse dimension change of the glulam timber columns *in situ* suggests that the glulam timber structures can be used safely in an indoor environment with a relatively high humidity, and in a normal outdoor environment. The structures show that moisture content fluctuation and transverse dimension change due to the moisture movement are negligible in such conditions provided the surface is well protected with proper water resistant coatings. Furthermore, the epoxy bonded steel connection can be used safely in glulam timber structures in similar environmental conditions. There is no obvious correction between the load level and the magnitude of displacement.

CHAPTER NINE

SUMMARY, CONCLUSIONS AND RECOMMENDATIONS

9.1 SUMMARY OF THE RESEARCH

Research was undertaken both experimentally and theoretically to study the epoxy bonded single steel rod connection in glue laminated timber.

The experimental programme consisted of two groups: short duration and long duration experiments. Short duration experiments comprised three different tests designated as Experiment One, Experiment Two and Experiment Four. Long duration experiments included Experiment Three and *in situ* measurement of moisture content and shrinkage. The experiments carried out in this study are summarised in Table 9.1.

Table 9.1 The summary of the experiments carried out in this study

Experiment	Load Duration	Brief Description	Number of Specimens
Experiment One	short	single replication of 2^7 factorial experiment	128
Experiment Two	short	single replication of 3^4 factorial experiment	81
Experiment Three	long	sustained tensile loading, wet and dry environmental condition	48
Experiment Four	short	four replication, with or without transverse reinforcement	8
in situ Measurement	long	measurement of moisture content and shrinkage in glulam columns	14

From Experiments One and Two, five failure modes were observed and analysed. The tensile strength of the connection was also analysed in detail in terms of different geometry, bar type, epoxy type and moisture content and an empirical formula was developed to predict the capacity of the connection. The effect of reinforcement of the connection was investigated in Experiment Four. Long duration experiments gave useful information on the load duration effect and the effect of environmental conditions.

A theoretical model was established using the finite element method and the characteristics of the connection were investigated using this model. The stress distributions in the connection were analysed; parametric studies were carried out using this model to investigate the effects of each individual parameters in the connection including the edge distance, the embedment length, the epoxy thickness, the steel bar end geometry and MOE of the epoxy.

This research resulted in a better understanding about the mechanical and physical properties of the connection and the effects of individual factor in the connection including different geometry, bar type, epoxy type and influence from different environmental conditions. Arising out of this research, a general design guideline has been proposed for the epoxied steel connection.

9.2 CONCLUSIONS

9.2.1 Strength and Failure Characteristics of the Connection Subjected to Short Duration Tensile Load

1. Five different failure modes were identified in the short duration experiments; different failure modes were caused by different stress concentrations and various defects in the connection. The failure occurs at the point where either stress concentrations are highest or where defects exist, or a combination of both.

2. The tensile strength is correlated to all seven factors investigated in the short duration experiments. The moisture content in glulam timber, the embedment length and the bar diameter are closely related to the strength and appear to influence the strength more than the other factors.

3. A statistically-based empirical equation has been developed to predict the axial capacity of the connection in tension or compression; it gives a good agreement with the experimental results. This equation could be used to predict the strength of the connection with other combination of materials, provided that calibration tests are carried out.

4. The moisture content in the connection plays an important role in affecting the strength. Tensile strength decreases significantly when the moisture content reaches 28%.

5. Tensile strength is higher in the connection using a threaded bar than when using a deformed reinforcing bar.

6. Of the three epoxies used in this study, Araldite 2005 achieved the highest tensile strength in the connection, next was K-80 and then the West System epoxy.

7. Transverse steel reinforcement can effectively improve the performance and tensile strength by preventing wood splitting around the connection.

9.2.2 Strength and Failure Characteristics of the Connection Subjected to Long Duration Tensile Load

1. Specimens under the outdoor wet-dry cycle environment failed with Type 2 failure mode - the wood splits and the connection pulls out. Two specimens only under the indoor conditions failed, both with Type 3 failure mode - tensile wood failure at the end of the connection.

2. The moisture content of wood plays an important role in the strength of the connection, although it performs well under normal indoor environmental conditions. The connection cannot be recommended for any situation when the moisture content could exceed 22%.

3. Major relaxation and creep occurred during the initial period of loading.

4. Different types of epoxies affect the strength of the connection; that is related different water-resistant properties observed in the epoxies used.

5. In general, the empirical equation developed from the short duration experiments can be used in the long duration load situation provided due consideration is given to environmental conditions and to the duration of load.

6. The measurement of moisture content and shrinkage *in situ* suggests that glulam timber structures and the epoxied steel connection can be used in an indoor environment where the relative humidity may be relatively high; also, in an outdoor environment provided the surface is protected with water resistant coatings.

9.2.3 The Theoretical Model

1. The output from the finite element model accords with the results from the experimental stress distribution tests. The model programmed using a smooth surface steel rod is sufficiently accurate to analyse the connection with a threaded rod.

2. The highest shear stress concentrations in the epoxy occur at the both ends of the embedment, the stress concentration at the inner end being higher than that at the outer end. The shear stress gradient is very high within the epoxy over the cross-section at the inner end of the embedment.

3. The highest tensile stress concentration occurs at the inner end of the embedment.

4. Both the tangential and the radial stresses have their highest values at the outer end of the embedment, and the values at the steel-epoxy interface are higher than at the epoxy-wood interface.

5. There is a strong correlation between the failure modes and the stress concentrations. The connections which failed with Type 1 failure mode (shear failure) are most likely due to the high magnitude of the shear stress along the embedment and highest shear stress concentration in the epoxy-wood interface at the both ends of the embedment. Type 2 failure mode (split and pullout failure) occurred at the highest tangential stress region accompanied by higher shear stress in the same area. The highest tensile stress concentration at the inner end of the embedment is a major cause of the connection failure with Type 3 failure mode (tensile failure of the wood at the steel bar end).

9.2.4 The Parametric Studies

Parametric studies using the finite element model show that the design of the connection can be optimised by developing a better geometry for the connection. The results of the comprehensive parametric study suggest the following conclusions:

1. A threshold of edge distance exists. Increasing edge distance above this does not yield any significant improvement in the stress distributions. The threshold to the edge distance is about three bar diameters.

2. A thick epoxy layer in the connection would result in a better stress distribution than a thin layer. The thickness of the epoxy used in the parametric study is up to 6 mm and it is likely to continue reducing the stress concentration by further increasing thickness of the epoxy. However, practically, the thickness of epoxy should not exceed 6 mm.

3. Shear stress concentrations around the connection can be reduced by using an epoxy with a lower modulus of elasticity.

4. A better shear stress distribution at the inner end of the connection can be achieved by drilling a hole at the end of the steel rod.

5. To some extent, the performance and capacity of the connection can be improved by increasing the embedment length as the average shear stress and transverse stress concentration are reduced.

9.3 RECOMMENDATIONS FOR FURTHER STUDY

9.3.1 Further Experimental Studies

1. Further experimental work could be conducted to expand the principle and analytical method for multiple steel rods connections. Connections need to be tested under different loading configurations, such as tension, compression and bending.

2. Methods to prevent wood splitting could be further studied, including the steel rod transverse reinforcement and placing the connection at an angle to the laminates in the longitudinal direction.

3. The strength and characteristics of the connection using other epoxy formulations and cement grout could be investigated to establish a range of bonding agents with acceptable performance in water resistance and fire resistance.

4. A study should be carried out to explore chemical pre-treatment of bonding surfaces both in wood and steel as a means of improving the durability, water resistance and fire resistance of the epoxy bonded connection.

9.3.2 Further Theoretical Studies

1. The finite element model developed in this research is based on the assumption that all of materials involved in the connection are linear elastic materials and the connection behaves elastically. A finite element model with non-linear visco-elastic properties for the materials in the connection needs to be developed and integrated with fracture mechanics theory to analyse the fracture propagation in the wood and the epoxy of the connection. Comprehensive failure criteria, considering the multi-axial stress states, the crack propagation and expected failure modes in wood and epoxy could be developed based on this finite element model to predict the failure.

2. More comprehensive parametric studies can be conducted using the finite element model to further investigate stress distribution, so that a better understanding can be obtained for different geometry of the connection. The surface effect of the steel bar (rib in the deformed reinforcing bar), a modification of the embedment hole in wood and the interactions among different parameters could be considered in the further parametric studies.

3. Time dependent behaviour of the connection can be further studied using damage accumulation theory. However, sufficient information on the time dependent behaviour of the connection is required before developing the theory.

REFERENCES

ABAQUS (1993a) ABAQUS User's Manual. Verson 5.3,.Hibbitt, Karlsson & Sorensen, Inc.

ABAQUS (1993b) ABAQUS / Post Manual. Verson 5.3,.Hibbitt, Karlsson & Sorensen, Inc.

Adams, R.D. (1986) The Mechanics of Bonded Joints. International Conference on Structural Adhesives in Engineering. IMechE Conference Publications 1986-6. C180/86:17-24. University of Bristol, London.

Adams, R.D. and Harris, J.A. (1987) Bonding of Composites to Metals. Adhesion 12, The 25th Conference on Adhesion and Adhesives, 193-204, The City University, London, UK Elsevier Applied Science, London.

Adams, R.D. (1990) Testing of Adhesives - Useful or Not. Adhesion 15, The 26th Conference on Adhesion and Adhesives, 1-18, The City University, London, UK Elsevier Applied Science, London.

Adhesive Technologies Ltd. (1992) Information sheet of West System - Resin and Hardener. Adhesive Technologies Ltd.

Barber, D.J. (1994) Fire Resistance of Epoxied Steel rods in Glulam Timber. Research Report 94/1, Department of Civil Engineering, University of Canterbury, Christchurch.

Barrett, J.D. (1982) Effect of Loading Time on Design. In: Structural Use of Wood in Adverse Environments. Edited by Meyer, R.W. and Kellogg, R.M., Van Nostrand Reinhold, New York.

Barrett, J.D. and Foschi, R.O. (1978a) Duration of Load and Probability of Failure in Wood. Part I. Modelling Creep Rupture. Canadian Journal of Civil Engineering 5(4): 505-514.

Barrett, J.D. and Foschi, R.O. (1978b) Duration of Load and Probability of Failure in Wood. Part II. Constant, Ramp, and Cyclic Loadings. Canadian Journal of Civil Engineering 5(4): 515-532.

Batchelar, M.L. and Hunt, R.D. (1991) Composite Plywood and Steel Gusset Plates for Moment-Resisting Joints in Timber Frames. Proceedings of the 1991 International Conference on Timber Engineering, London, United Kingdom, volume 3, pp. 104-110.

Bikerman, J.J. (1968) The Science of Adhesive Joints. 2nd edition, Academic Press, New York and London.

Bodig, J. and Goodman, J.R. (1973) Prediction of Elastic Parameters for Wood. Wood Science 5(4): 249-264.

Bodig, J. (1982) Moisture Effects on Structural Use of Wood. In: Structural Use of Wood in Adverse Environments. Edited by Meyer, R.W. and Kellogg, R.M., Van Nostrand Reinhold, New York.

Bodig, J. and Jayne, B.A. (1982) Mechanics of wood and wood composites. Van Nostrand Reinhold, New York. 712p.

Brewis, D.M. (1986) Factors Affecting Bonding of Metals. Materials Science and Technology 2(8): 761-767.

Buchanan, A.H. and Fairweather, R. (1992) Glulam Portal Frames with Steel Knee Joints: Design Guide for Hunter Laminates Ltd.

Buchanan, A.H. and Fairweather, R.H. (1993) Seismic Design of Glulam Structures. Bulletin of the New Zealand National Society for Earthquake Engineering, 24(4): 415-436.

Buchanan, A.H. and Fletcher, M.R. (1989) Glulam Portal Frame Swimming Pool Construction. Proceedings of the Second Pacific Timber Engineering Conference, Auckland, New Zealand, Volume 1 pp 245-249.

Bulleit, W.M. (1984) Reinforcement of Wood Materials: A Review. Wood and Fibre Science 16(3): 391-397.

Caster, D. (1980) Correlation between Exterior Exposure and Automatic Boil Test Results. Proceedings of 1980 Symposium of Wood Adhesives - Research, Application, and Needs, Pages 179-188. USDA Forest Service, Forest Products Laboratory, Madison, WL.

Ceccotti, A. and Vignoli, A. (1988) The Effects of Seismic Events on the Behaviour of Semi-Rigid Joint Timber Structures - A Simulation of the Influence of Structural Scheme and of Joint Characteristic. Proceedings of the 1988 International Timber Engineering Conference, Seattle, USA, Volume 1, p. 823-837.

CIBA-GEIGY (1989 (a)) Instructions for Araldite. Building and Construction Adhesives, CIBA-GEIGY.

CIBA-GEIGY (1989 (b)) Adhesive Lap Joints for Timber/Steel Composites. CIBA-GEIGY Araldite Epoxy Systems, CIBA-GEIGY.

Collett, B.M. (1972) A Review of Surface and Interfacial Adhesion in Wood Science and Related Fields. Wood Science and Technology 6: 1-42.

Cook, R.D. (1981) Concepts and Applications of Finite Element Analysis. 2nd edition, John Wiley & Sons, New York. 537p.

Crawford, R.J. (1987) Plastics Engineering. 2nd edition, Pergamon Press.

Crews, K.I. (1992) A Study Tour Investigating Research and Development Trends in Structural Applications of Timber for Expansion of the Non-Residential Market for Forest Products in Australia. Gottstein Report, July 1992.

Crews, K.I. (1993) An Overview of Design Considerations for Large Span Non-residential Timber Structures in Australia. M.E. Thesis, School of Civil Engineering, University of Technology, Sydney, Australia.

de Bruyne, N.A. (1956) The Extent of Contact between Glue and Adherent. Aero Research Technical Notes Bulletin No. 168, The Technical Service Department, Aero Research Limited, Duxford, Cambridge.

de Bruyne, N.A. (1956) The Adhesive Properties of Epoxy Resins: Journal of Applied Chemistry. 6, July, 1956, pp. 303-310.

Fairweather, R.H. (1992) Beam Column Connections for Multi-Storey Timber Buildings. Research Report 92-5, Department of Civil Engineering, University of Canterbury, Christchurch, New Zealand.

Foschi, R.O. and Barrett, J.D. (1982) Load-Duration Effects in Western Hemlock Lumber. ASCE 108(ST7): 1494-1510.

Fridley, K.J., Tang, R.C. and Soltis, L.A. (1991) Moisture Effects on Load-duration Behaviour of Lumber. Part I. Effect of Constant Relative Humidity. Wood and Fibre Science 23(1): 114-127.

Frost, K.D. (1990) Epoxy and Steel Dowel 'Bolt' Joints in Glulam Timber. Research Report, School of Architecture, Victoria University of Wellington, November 1990.

Gardner, G.P. (1989) A Reinforced Glued Laminated Timber System. Proceedings of the Second Pacific Timber Engineering Conference, Vol. 2, Auckland, New Zealand.

Gerhards, C.C. (1979)Time-Related Effects of Loading on Wood Strength: A Linear Cumulative Damage Theory. Wood Science 11(3): 139-144.

Gerhards, C.C. and Link, C.L. (1987) A Cumulative Damage Model to Predict Load Duration Characteristics of Lumber. Wood and Fibre Science 19(2): 147-164.

Gerold, M. (1992) Verbund von Holz und Gewindestangen aus Stahl. Bautechnik 69(4): 167-178.

Gopu, V.K.A. (1981) Repaired Pitch-Cambered Glulam Beams. Journal of the Structural Division, American Society of Civil Engineers 107 (7): 1251-1262.

Holzer, S.M. and others. (1989) A Review of Creep in Wood: Concepts Relevant to Develop Long-term Behaviour Predictions for Wood Structures. Wood and Fibre Science 21(4): 376-392.

Houwink, R. and Salomon, G. (1965) Adhesion and Adhesives. Volume 1 Adhesives. Elsevier Publishing Company, Amsterdam.

Hoyle, R.J. and others. (1986) Creep of Douglas Fir Beams Due to Cyclic Humidity Fluctuations. Wood and Fibre Science 18(3): 468-477.

Huang, C.L. and Kirmser, P.G. (1975) A Criterion of Strength for Orthotropic Materials. Fibre Science and Technology 8: 103-112.

Hult, J. (1966) Creep in Engineering Structures. Blaisdell Publishing Company.

Hwang, W. and Han, K.S. (1986) Cumulative Damage Models and Multi-stress Fatigue Life Prediction. Journal Composite Material 20(4): 125-153.

Johansson, C.J. (1995) Glued-in Bolts. In: STEP Lectures, Volume 1. Centrum Hout, Netherlands.

Johnson, W.S. (1987) Stress Analysis of the Cracked-Lap-Shear Specimen: An ASTM Round-Robin. Journal of Testing and Evaluation 15(6): 303-324.

Kinloch, A.J. (1983) Durability of Structural Adhesives. Applied Science Publishers, London.

Komatsu, K., Kawomoto, N., Kazumi, H. and Harada, M. (1991) Modified Glulam Moment-Resisting Joints. Proceedings of the 1991 International Conference of Timber Engineering, London, United Kingdom, Volume 3, pp 3.111-3.118.

Kupers, J. (1977) Long Duration Tests on Timber Joints. CIB-W18, Stockholm.

Law, P.W. and Yttrup, P.J. (1989) Epoxy Injected Bolts in Shear. Proceedings of the Second Pacific Timber Engineering Conference, Auckland, New Zealand, 1989, Volume 3, pp 85-91.

Lees, W.A. (1986) Adhesive Selection. International Conference on Structural Adhesives in Engineering. IMechE Conference Publications 1986-6. C160/86:207-214. University of Bristol, London.

Lees, W.A. (1987) Stress in Bonded Joints. Adhesion 12, The 26th Conference on Adhesion and Adhesives, The City University, London, UK.

Madsen, B. (1992) Structural Behaviour of Timber. Timber Engineering Ltd., Vancouver, British Colombia.

Marian, J.E. (1962) Surface Texture in Relation to Adhesive Bonding. Symposium of Properties of Surfaces, Special Technical Publication No. 340, Published by the American Society for Testing and Materials.

Marian, J.E. and Stumbo, D.A. (1962a) Adhesion in Wood Part I. Physical Factors. Holzforschung 16(5): 134-148.

Marian, J.E. and Stumbo, D.A. (1962b) Adhesion in Wood Part II. Physico-chemical Surface Phenomena and the Thermodynamic Approach to Adhesion. Holzforschung 16(6): 168-180.

Marian, J.E. and Stumbo, D.A. and Maxey, C.W. (1958) Surface Texture of Wood as Related to Glue Joint Strength. Forest Product Journal 8(12): 345-351.

Marra, A.A. (1992) Technology of Wood Bonding: Principles in Practice. Van Nostrand Reinhold, New York.

Mays, G.C. (1985) Structural Applications of Adhesives in Civil Engineering. Material Science and Technology 1(11): 937-943.

McIntosh, K.A. (1989) From Theory to Reality - 30 Years in Glulam Manufacture. Proceedings of the Second Pacific Timber Engineering Conference, University of Auckland, Auckland, New Zealand, pp. 229-234.

Mehlhorn, G. and Klein, D. (1980) Finite Element Analysis of Reinforced Concrete Slabs and Panels. Proceedings of the Europe-U.S. Workshop, Ruhr-Universitat Bochum, Germany.

Mehlhorn, G. and Keuser, M. (1985) Isoparametric Contact Elements for Analysis of Reinforced Concrete Structures: Finite Element Analysis of Reinforced Structures. Proceedings of the seminar sponsored by the Japan Society for the Promotion of Science and the U.S. National Science Foundation, Tokyo, Japan, pp 329-347.

Metriguard, Inc. (1990) Metriguard Model 239A Stress Wave Timer Manual. Metriguard, Inc., P.O. Box 399, Pullman, Washington, U.S.A.

Minitab, Inc. (1989) User's Manual. Minitab Data Analysis Software, Release 7.2, Standard Version, Minitab Inc., 1989.

Nestic, R. and Milner, H.R. (1991) Shrinkage Induced Stresses in Adhesive Joints of Glued Laminated Timber. Journal of the Institute of Wood Science 12(4): 225-231.

Neter, J. and others. (1988) Applied Statistics. 3rd edition, Allyn and Bacon, Inc., Boston. 608p.

New Zealand Journal of Timber Construction (1986) Prime Award - Glue Laminated Timber Space Frame Enclosing Rankine Brown Courtyard. 2(3): 3-4.

Nielsen, A. (1972) Rheology of Building Materials. D6:1972, National Swedish Building Research.

Nielsen, L.F and Kousholt, K (1980) Stress-Strength-Life Time Relationship for Wood. Wood Science 12(3): 163-164.

NZS 3402 (1989) Steel Bars for the Reinforcement of Concrete. Standards Association of New Zealand, Wellington, 15p.

NZS 3602 (1990) Code of Practice for Specifying Timber and Wood-based Products for Use in Buildings. Standards Association of New Zealand, Wellington, 24p.

NZS 3603 (1993) Timber Structure Standard. Standards Association of New Zealand, Wellington, 132p.

NZS 3606 (1987) Specification for the Manufacture of Glue Laminated Timber. Standards Association of New Zealand, Wellington, 20p.

NZS 3616 (1978) Specification for Finger-jointed Timber. Standards Association of New Zealand, Wellington, 21p.

NZS 3631 (1988) New Zealand National Timber Grading Rules. Standards Association of New Zealand, Wellington, 108p.

NZS 4203 (1993) Code of Practice for General Structural Design and Design Loadings for Buildings. Standards Association of New Zealand, Wellington.

Ohashi, Y. and Sakamoto, I (1989) Study on Laminated Timber Moment-Resisting Joint. Proceedings of the Second Pacific Timber Engineering Conference, Auckland, New Zealand, 1989, Volume 2, pp 38-42.

Olson, W.Z. and Blomquist, R.F. (1962) Epoxy-Resin Adhesives for Gluing Wood. Forest Products Journal 12(2): 74-80.

Pentoney, R.E. and Davidson, R.W. (1962) Rheology and the Study of Wood. Forest Products Journal. 12(5): 243-248.

Piechnik, S. and Pachla, H. (1980) The Continuous Field of Damage and its Influence on the Creep Process in Concrete under Tensile Loading. Proceedings of the Third International Union of Theoretical and Applied Mechanics, Leicester, UK.

Preiswerk, E.J. (1950) Ethoxylenes: what they are, where they are going. Modern Plastics. pp. 85-87.

Riberholt, H. (1986) Glued Bolts in Glulam. Serie R No 210. Department of Structural Engineering, Technical University of Denmark.

Riberholt, H. (1988a) Glued Bolts in Glulam - Part 2. Serie R No 228. Department of Structural Engineering, Technical University of Denmark.

Riberholt, H. (1988b) Glued Bolts in Glulam - Proposals for CIB Code International Council for Building Research Studies and Documentation Working Commission W18. Timber Structures Meeting Twenty-one, Vancouver, Canada.

Rodd, P.D. (1988) Timber Joints Made with Improved Circular Dowel Fasteners. Proceedings of the 1988 International Conference on Timber Engineering, Seattle, USA, 1988, Volume 1, pp 26-37.

Rodd, P.D. and others. (1989) Resin Injected Mechanically Fastened Timber Joints. Proceedings of the Second Pacific Timber Engineering Conference, Auckland, New Zealand, 1989, Volume 2, pp 131-136.

Rodd, P.D. and others. (1991) Prediction of Embedment Characteristics for Laterally Loaded Resin Injected Bolts in Timber. Proceedings of the 1991 International Timber Engineering Conference, London, United Kingdom, Volume 3, pp 3.50-3.57.

Schneberger, G.L. (1970) Chemical Aspects of Adhesive Bonding Part III Chemistry in the Bonding Shop. Adhesive Age 1970(4): 41-44.

Schniewind, A.P. 1967. Creep-Rupture Life of Douglas-Fir Under Cyclic Environmental Conditions. Wood Science and Technology 1(4): 278-288.

Schniewind, A.P. (1968) Recent Progress in the Study of the Rheology of Wood. Wood Science and Technology 2(3): 188-206.

Schniewind, A.P. and Lyon, D.E. (1973) Further Experiments on Creep-Rupture Life under Cyclic Environmental Conditions. Wood and Fibre 4(4): 334-341.

Schniewind, A.P. (1977) Fracture Toughness and Duration of Load Factor II. Duration Factor for Cracks Propagating Perpendicular-to Grain. Wood and Fibre 9(3): 216-226.

Simpson, W.T. and Loehnertz, S.P. (1994) Resistance Moisture Meter Correction Factor for Pacific Yew. Forest Products Journal 44(1): 63-64.

Smulski, S.J. (1989) Creep Functions for Wood Composite Materials. Wood and Fibre Science 21(1): 45-54.

Sugiyama, H. (1967) On the Effect of the Loading Time on the Strength Properties of Wood: A Review on Japanese Research. Wood Science and Technology 1(4): 289-303.

Syme, D.R. (1989) Timber Jointing Systems in Europe. Proceedings of the Second Pacific Timber Engineering Conference, Auckland, New Zealand, Volume 2, pp 138-142.

Tabor, L.J. Effective Use of Epoxy and Polyester Resins in Civil Engineering Structures. CIRIA Report 69, Construction Industry Research and Information Association, London.

Taylor, F.D. and West, D.J. (1990) Use of Stainless Steel Pins for In-situ Measurement of Moisture Contents in the Structural Members of A Glulam Framed Church. Journal of Institute of Wood Science 12(2): 71-76.

Townsend, P.K. (1990) Steel Dowels Epoxy Bonded in Glue Laminated Timber. Research Report 90-11, Department of Civil Engineering, University of Canterbury, Christchurch, New Zealand.

Tukovsky, S.B. (1991) Use of Glued-In Bars for Reinforcement of Wood Structures. Proceedings of the 1991 International Timber Engineering Conference, London, United Kingdom, Volume 3, pp 3.143-3.148.

U.S. Forest Products Laboratory (1989) Handbook of Wood and Wood-based Materials for Engineers Architects and Builders. USDA Handbook 72, New York: Hemisphere Pub. Co.

van Resburg, B.W.J. and others. (1984) Steel Reinforced Timber Structural Elements. Proceedings of the Pacific Timber Engineering Conference, Auckland, New Zealand, Volume 1, pp 97-108.

Vick, C.B., Richter, K., River, H.B. and Fried, A.R (1995) Hydroxymethylated Resorcinol Coupling Agent for Enhanced Durability of Bisphenol-A Epoxy Bonds to Sitka Spruce. Wood and Fiber Science 27(1): 2-12.

Wake, W.C. (1982) Adhesion and the Formulation of Adhesives. Second edition, Applied Science Publishers Ltd., London.

Wake, W.C. (1986) Structural Applications of Adhesives. International Conference on Structural Adhesives in Engineering. IMechE Conference Publications 1986-6. C151/86:161-168. University of Bristol, London.

Walford, C.B. (1989) Portal Frames. In Section B-2 of Timber Use Manual. New Zealand Timber Industry Federation, Wellington.

Walker, J.C.F. and others. (1993) Primary Wood Processing: Principles and Practice. Chapman & Hall, London.

Williamson, F.L. and Nearn, W.T. (1958) Wood to Wood Bonds with Epoxide Resins - Species Effect. Forest Products Journal 8(6): 182-188.

Wood, L. (1951) Relation of Strength of Wood to Duration of Load. U.S. Department of Agriculture, Report No. 1916, Forest Products Laboratory, Madison, Wis.

Zandbergs, J.G. and Smith, F.W. (1988) Finite Element Fracture Prediction for Wood with Knots and Cross Grain. Wood and Fibre Science 20(1): 97-106.

Zisman, W.A. (1963) Influence of Constitution on Adhesion. Industrial and Engineering Chemistry 55(10): 19-38.

APPENDIX A THE MOISTURE CONTENT AND DENSITY OF THE SPECIMENS IN EXPERIMENT ONE

CODE	MOISTURE (%)	DENSITY (kg/m^3)	CODE	MOISTURE (%)	DENSITY (kg/m^3)
1001	15.8	572	1033	10.1	482
1002	13.2	461	1034	15.7	500
1003	10.8	473	1035	12.1	461
1004	14.3	537	1036	10.7	534
1005	16.0	499	1037	11.2	513
1006	12.5	527	1038	13.2	556
1007	15.4	551	1039	12.8	529
1008	12.3	471	1040	14.6	515
1009	11.4	516	1041	10.3	498
1010	14.8	506	1042	12.7	465
1011	13.4	438	1043	13.8	509
1012	10.4	523	1044	11.3	455
1013	13.6	495	1045	14.9	455
1014	15.9	505	1046	14.1	455
1015	15.1	516	1047	12.7	514
1016	16.0	521	1048	10.5	479
1017	12.1	471	1049	13.7	493
1018	14.6	513	1050	11.8	518
1019	14.2	602	1051	14.9	470
1020	15.8	443	1052	12.8	498
1021	15.9	490	1053	11.4	551
1022	10.3	573	1054	14.2	492
1023	13.7	545	1055	12.7	497
1024	13.2	549	1056	13.8	520
1025	15.8	521	1057	12.1	583
1026	11.2	505	1058	14.2	461
1027	10.2	490	1059	12.7	526
1028	11.3	559	1060	9.9	484
1029	10.2	521	1061	15.9	493
1030	14.5	528	1062	10.8	495
1031	11.2	477	1063	13.9	532
1032	11.8	508	1064	10.2	455

Appendix A (continued)

CODE	MOISTURE (%)	DENSITY (kg/m^3)	CODE	MOISTURE (%)	DENSITY (kg/m^3)
1065	11.2	502	1097	10.5	436
1066	14.3	507	1098	15.4	517
1067	12.8	496	1099	12.8	627
1068	10.5	507	1100	10.3	521
1069	15.8	524	1101	12.4	479
1070	12.7	504	1102	10.9	524
1071	12.7	510	1103	10.2	609
1072	14.6	576	1104	14.6	542
1073	11.2	558	1105	15.2	518
1074	12.8	472	1106	10.5	492
1075	13.7	537	1107	15.4	509
1076	13.1	494	1108	10.2	516
1077	15.8	520	1109	15.8	536
1078	13.4	447	1110	10.9	510
1079	10.8	510	1111	10.5	504
1080	15.7	536	1112	11.7	524
1081	10.5	548	1113	15.4	441
1082	12.3	499	1114	12.8	474
1083	10.1	463	1115	10.5	591
1084	14.6	519	1116	12.8	429
1085	13.8	518	1117	15.4	490
1086	10.2	511	1118	12.9	419
1087	15.6	471	1119	11.2	492
1088	14.5	511	1120	12.8	503
1089	10.2	575	1121	11.5	519
1090	14.3	487	1122	14.2	519
1091	11.5	510	1123	15.6	526
1092	10.8	508	1124	10.5	490
1093	13.6	545	1125	13.5	519
1094	15.4	460	1126	12.1	487
1095	13.2	521	1127	15.2	432
1096	11.7	542	1128	11.3	495

The moisture content readings were recorded by the electric resistance type moisture meter (Timber Master Model D184T, Protimeter Ltd.) with the Hammer Electrode before the specimens were assembled with the steel bars. The density was calculated from the oven-dry weight and the air-dry volume of each specimen. The

mean value of moisture content of the specimens in Experiment One is 12.8% with standard deviation of 1.86%. The average density of the specimens is 508 kg/m^3 with standard deviation of 37.31 kg/m^3.

APPENDIX B MOISTURE CONTENT MEASUREMENT FOR THE WET SPECIMENS IN EXPERIMENT ONE

Code		MC1	MC2	MC3	MC4	MC5	MC6
Dimensions		600x48x48	600x48x48	600x72x72	600x72x72	600x108x108	600x108x108
Cycle		Moisture content (%)					
1	Dry	14.3	13.8	16.5	17.2	15.3	12.9
	Wet	19.2	20.4	21.5	21.0	20.5	20.4
2	Dry	17.5	17.8	18.5	19.0	16.4	12.8
	Wet	28.0	26.8	27.8	28.5	28.5	28.4
3	Dry	17.7	17.4	16.5	18.4	16.8	17.0
	Wet	28.5	28.0	28.0	27.4	27.6	28.5
4	Dry	16.0	16.8	15.6	15.8	17.8	17.0
	Wet	27.6	28.3	28.0	27.5	28.0	28.5
5	Dry	16.5	17.0	17.8	16.5	17.0	17.2
	Wet	28.0	28.2	28.5	27.4	28.0	28.0
6	Dry	17.5	17.5	17.0	16.5	19.0	18.0
	Wet	28.0	28.0	27.5	28.5	28.0	28.0

The moisture content was measured using the electric resistance type moisture meter (Timber Master Model D184T, Protimeter Ltd.) with the Hammer Electrode. The readings were taken at the location of 1/3 length of the samples along the centre line at the both ends with 30 mm depth of penetration. The readings shown in the table are the average values for each samples. The readings were calibrated by the oven dry specimens. The dimension of the samples for moisture content measurement corresponded to the dimension of the specimens in Experiment One.

APPENDIX C THE MOISTURE CONTENT AND DENSITY OF THE SPECIMENS IN EXPERIMENT TWO

CODE	MOISTURE (%)	DENSITY (kg/m^3)	CODE	MOISTURE (%)	DENSITY (kg/m^3)
2001	10.1	493	2042	15.8	523
2002	15.7	495	2043	13.2	461
2003	12.1	532	2044	10.8	473
2004	10.7	455	2045	14.3	537
2005	16.0	513	2046	11.2	499
2006	12.5	556	2047	13.2	527
2007	15.4	529	2048	12.8	551
2008	15.8	515	2049	14.6	471
2009	13.2	498	2050	10.3	516
2010	10.8	498	2051	12.7	506
2011	14.3	551	2052	13.8	438
2012	10.4	492	2053	11.3	523
2013	13.6	497	2054	14.9	495
2014	15.9	455	2055	14.1	505
2015	15.1	514	2056	12.7	516
2016	14.2	479	2057	10.5	521
2017	12.1	493	2058	13.7	471
2018	14.6	518	2059	11.8	513
2019	14.2	506	2060	14.9	502
2020	14.8	438	2061	12.8	443
2021	15.9	523	2062	11.4	490
2022	10.3	495	2063	14.2	573
2023	13.7	497	2064	12.7	545
2024	13.2	487	2065	10.2	549
2025	15.8	504	2066	14.5	529
2026	11.2	461	2067	11.2	515
2027	10.2	498	2068	11.8	498
2028	11.2	461	2069	13.2	520
2029	10.2	526	2070	15.8	583
2030	14.9	508	2071	15.9	523
2031	12.8	443	2072	10.3	495
2032	11.4	490	2073	10.8	473
2033	11.2	499	2074	14.3	537
2034	12.4	487	2075	11.2	499
2035	13.4	498	2076	12.4	485
2036	14.2	502	2077	11.3	556
2037	12.5	484	2078	9.9	465
2038	13.6	493	2079	10.3	461
2039	12.1	495	2080	12.7	534
2040	11.8	532	2081	13.8	513
2041	10.2	455			

The measurement of the moisture content and density of the specimens in Experiment Two were carried out with the same method as Experiment One. The maximum of moisture content was 16.0% while the minimum value was 9.9%. The average moisture content is 12.9% with standard deviation of 1.83%. The average density of the specimens for Experiment Two is 502.5 kg/m^3 with standard deviation of 30.5 5 kg/m^3.

APPENDIX D LOAD AND DISPLACEMENT OF THE SPECIMENS IN THE SHORT DURATION EXPERIMENT

This appendix presents the load and displacement information for the epoxy bonded steel connection subjected short term tensile loading. It covers most influence factors considered in the short duration experiments although only partial load-displacement data from Experiment One are included to avoid tedious presentation (refer Table 3.9). The load was measured by the 250 kN load cell and recorded by the computer. The displacement was the average reading of two high resolution potentiometers taken directly from the electric circuit (Burr-Brown amplifier). The load-displacement graphs can be classified as eight subgroups and shown in Table D-1.

Table D-1

Subgroups	Specimen Parameters	No. of Specimens	Specimen Code
1	threaded/dry/WS/d=16	8	1001 - 1008
2	threaded/dry/WS/d=24	8	1009 - 1016
3	threaded /dry/K-80/d=16	8	1017 - 1024
4	threaded/dry/K-80/d=24	8	1025 - 1032
5	threaded/wet/K-80/d=16	8	1049 - 1056
6	threaded/wet/K-80/d=24	8	1057 - 1064
7	deformed/dry/K-80/d=16	8	1081 - 1088
8	deformed/dry/K-80/d=24	8	1089 - 1096

Note: threaded = the threaded steel rod connection.

deformed = deformed reinforcing bar connection.

dry = the dry specimens.

Appendix D (continued)

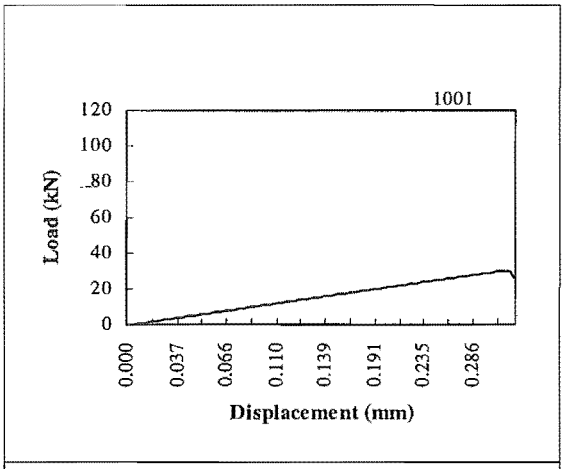

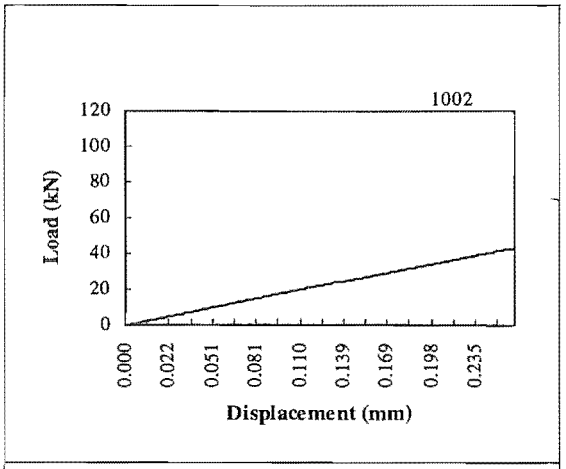

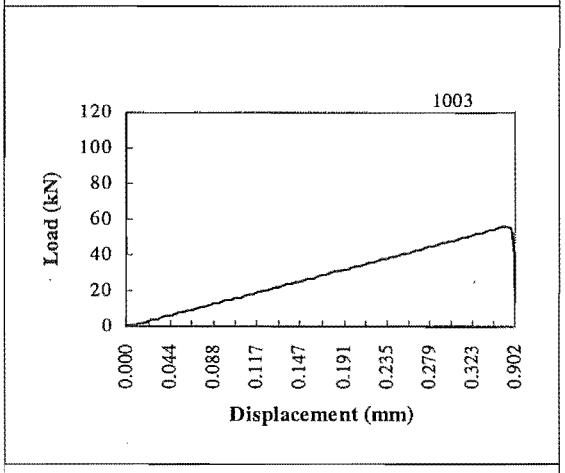

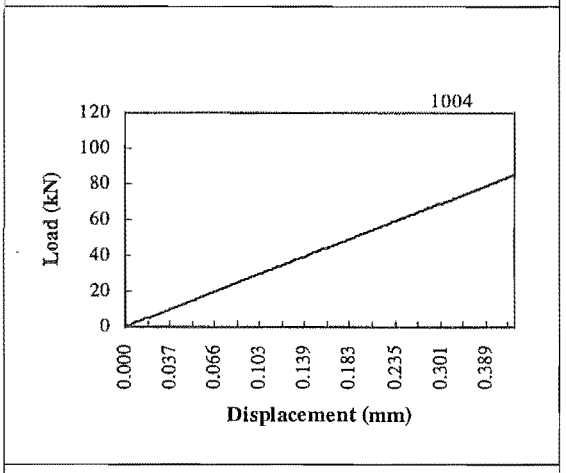

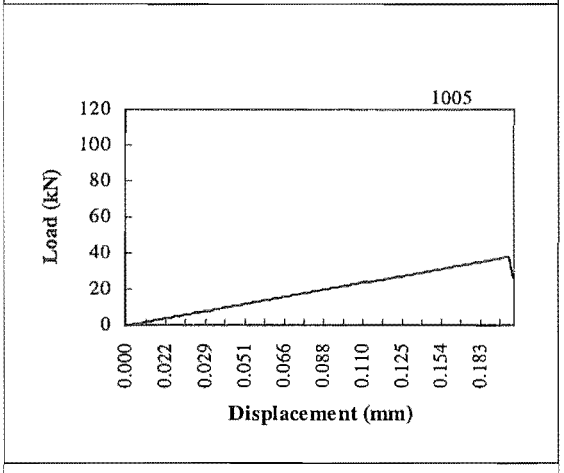

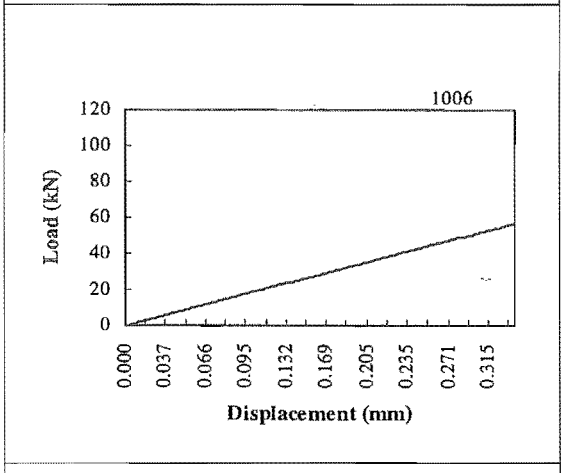

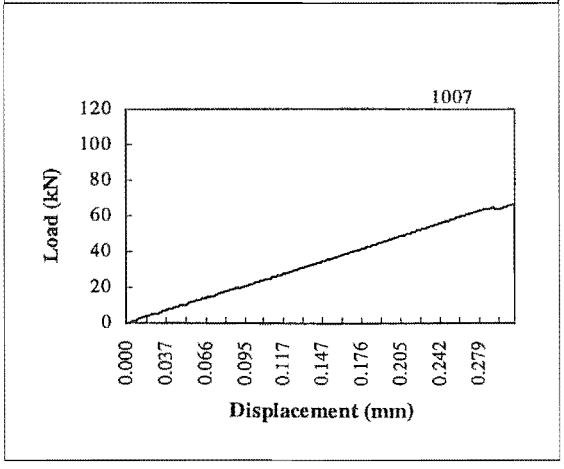

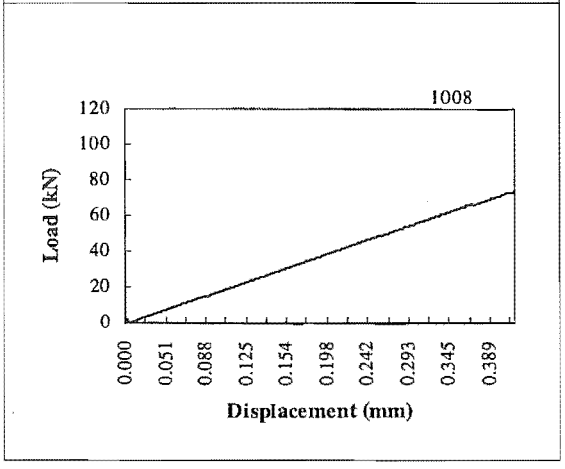

Appendix D (continued)

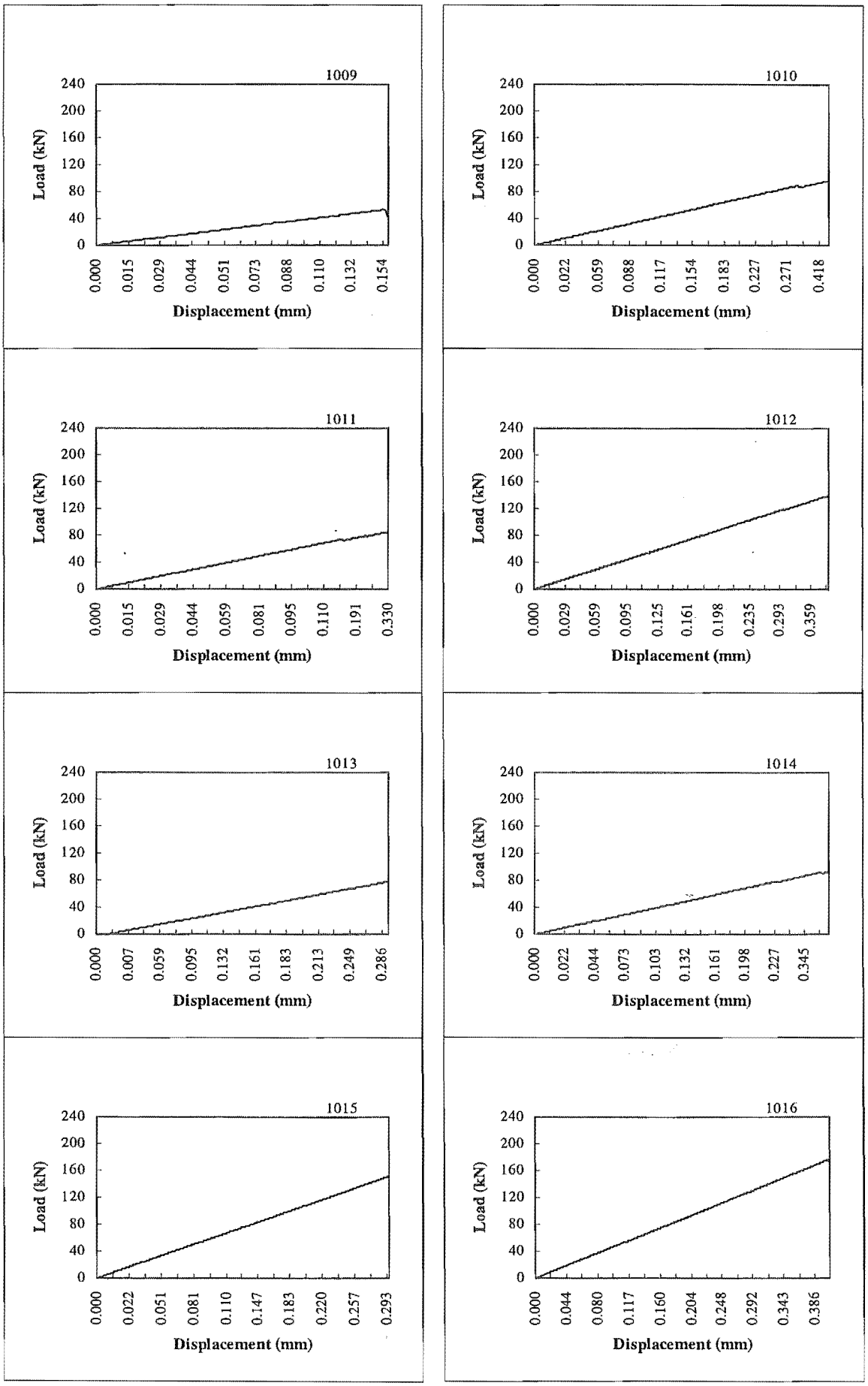

Appendix D (continued)

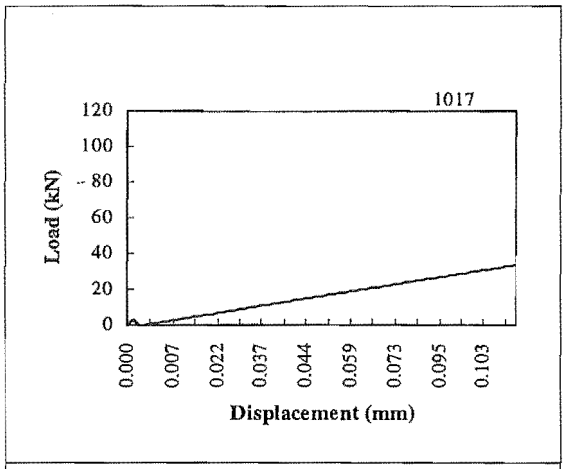

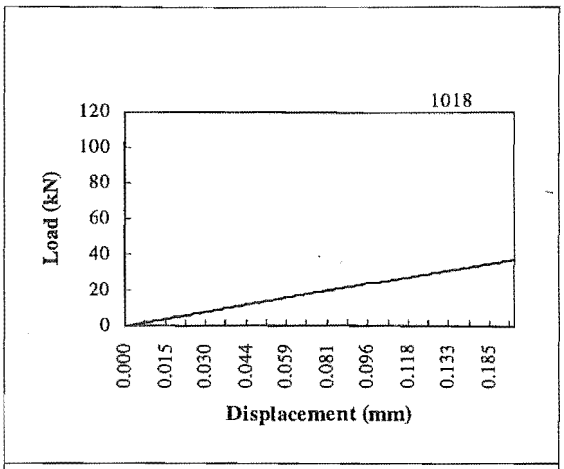

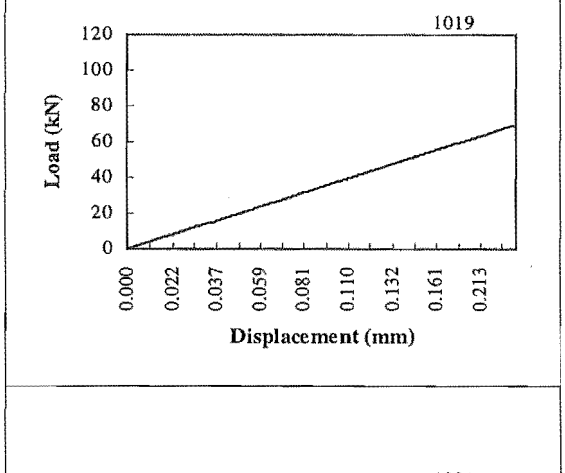

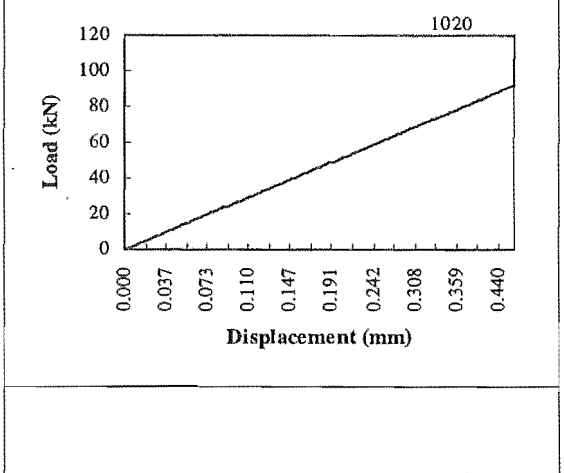

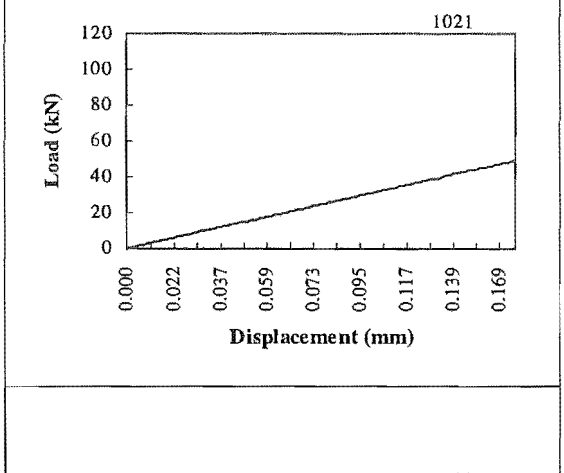

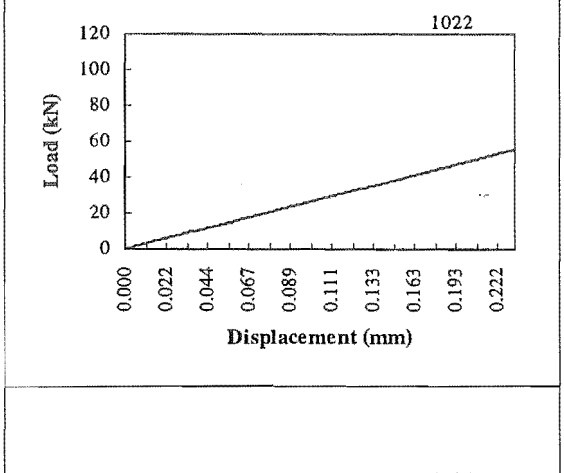

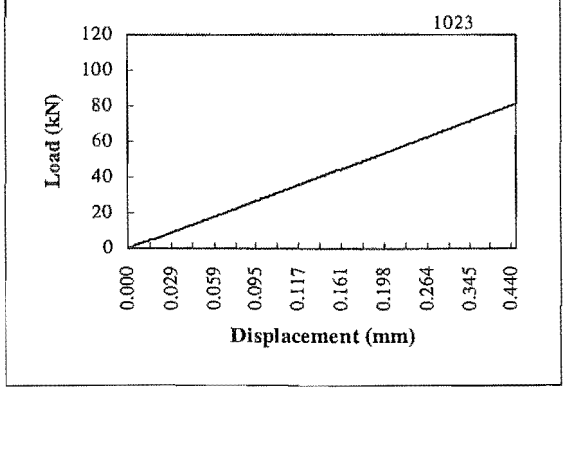

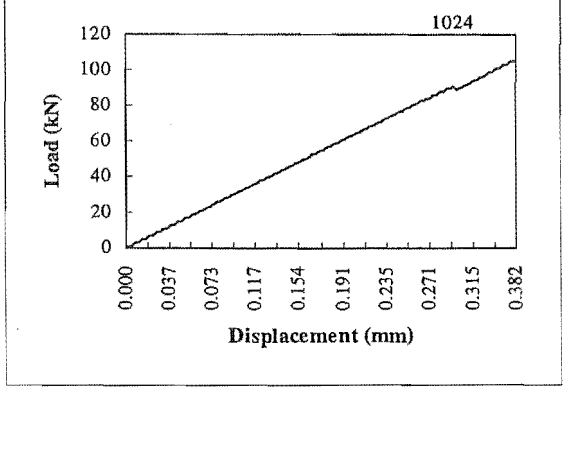

Appendix D (continued)

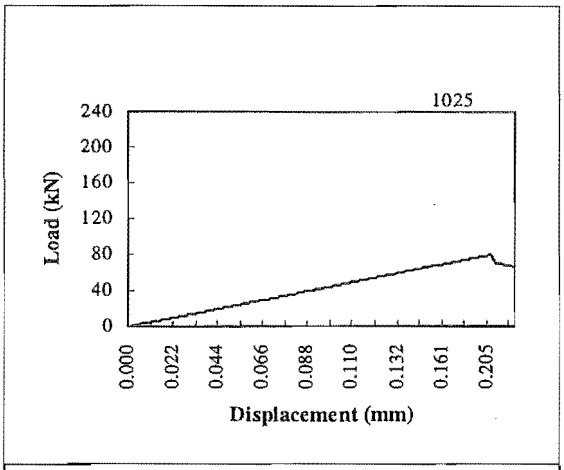

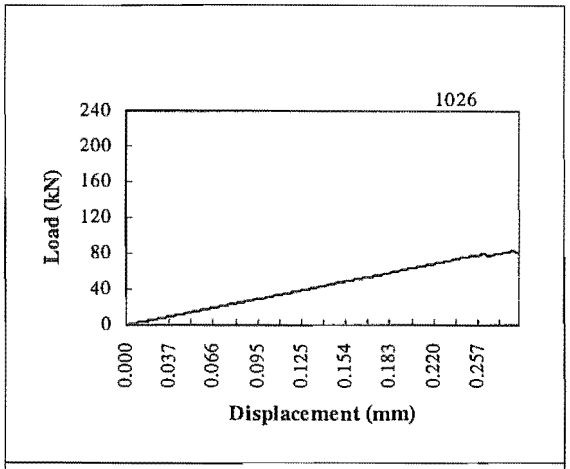

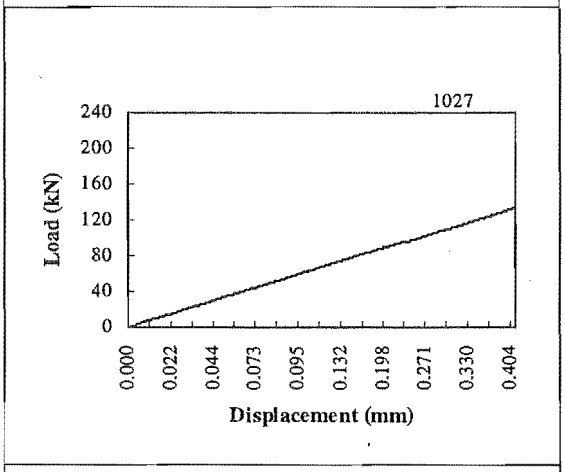

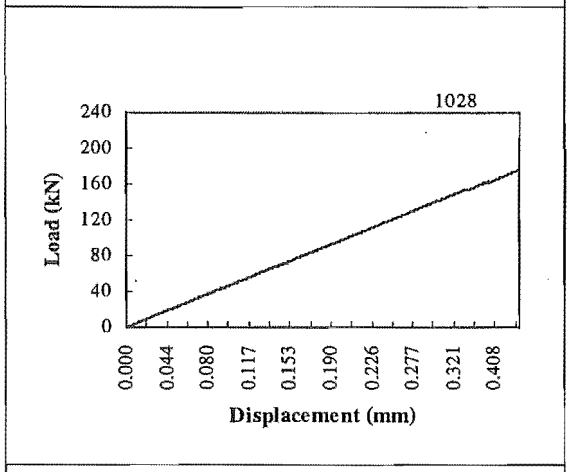

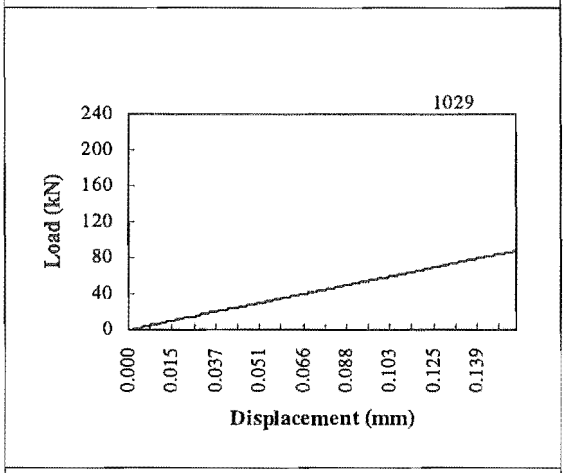

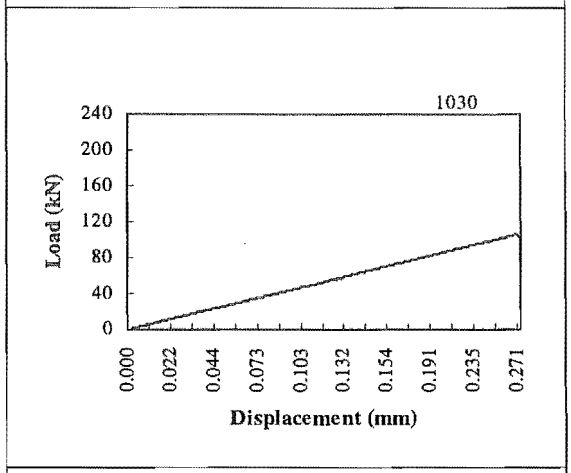

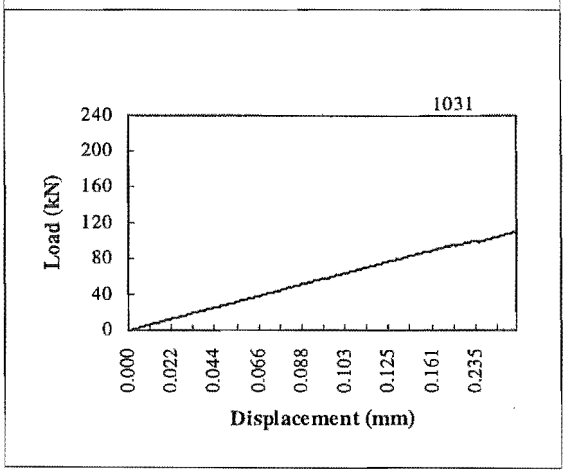

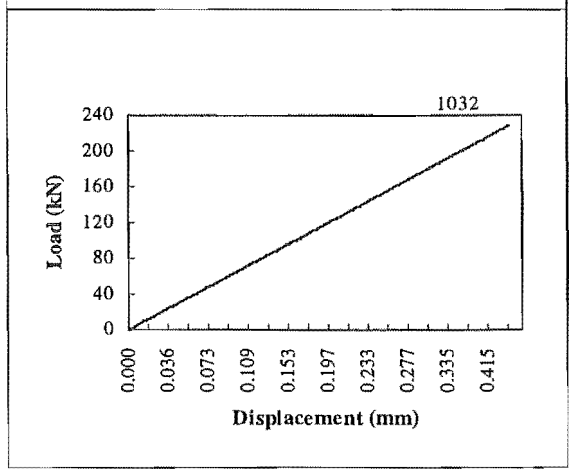

Appendix D (continued)

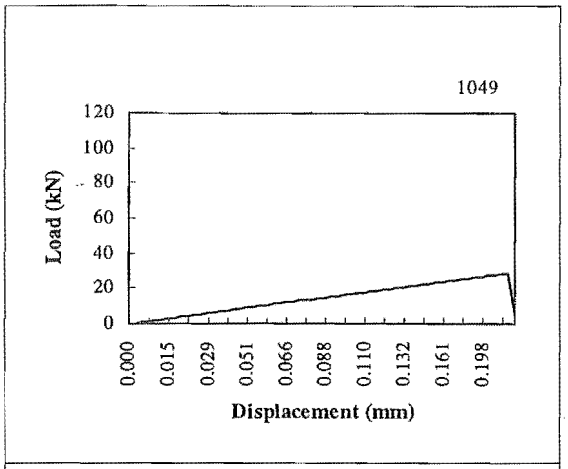

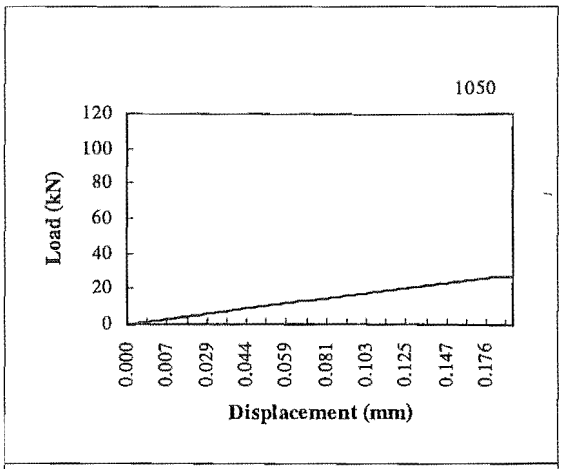

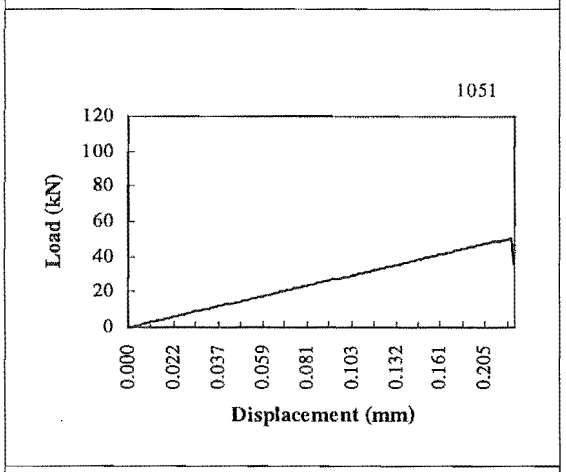

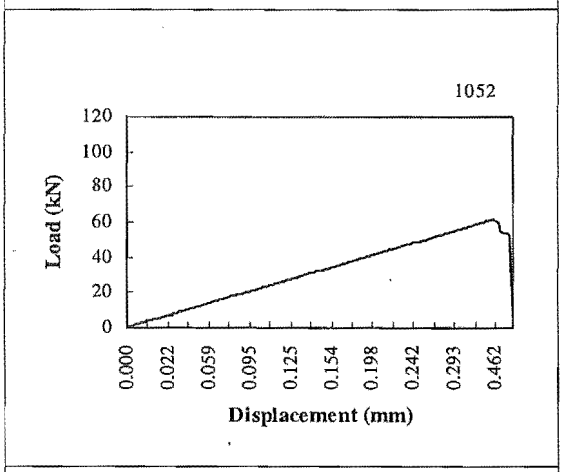

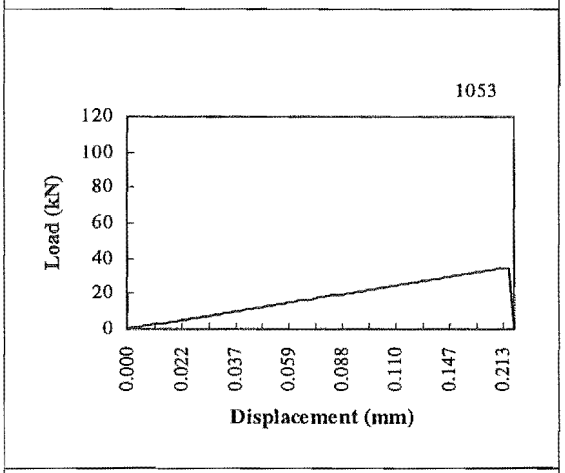

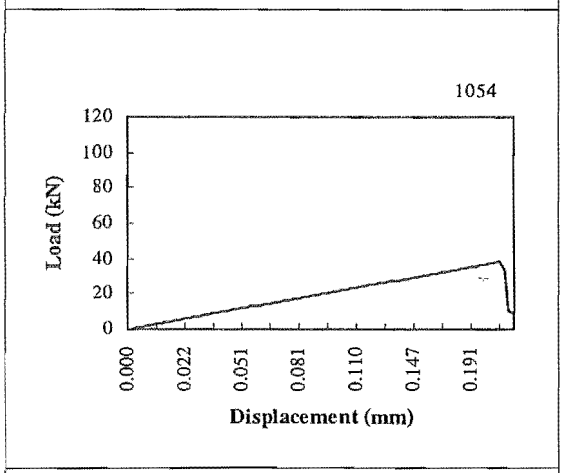

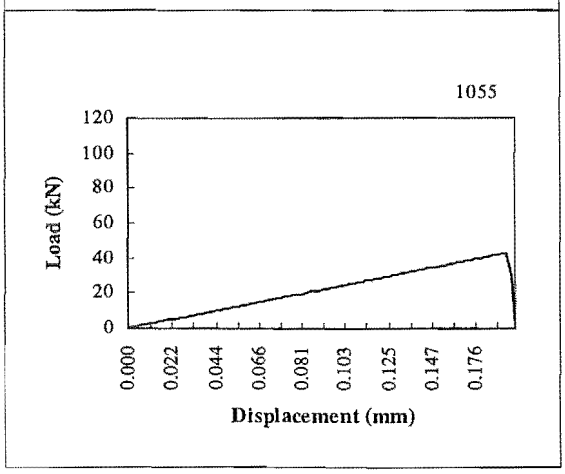

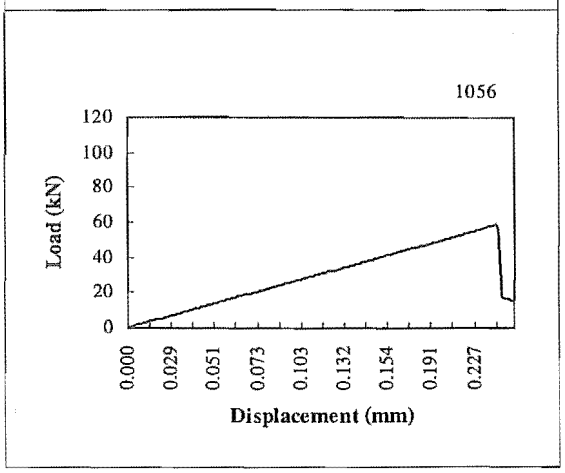

Appendix D (continued)

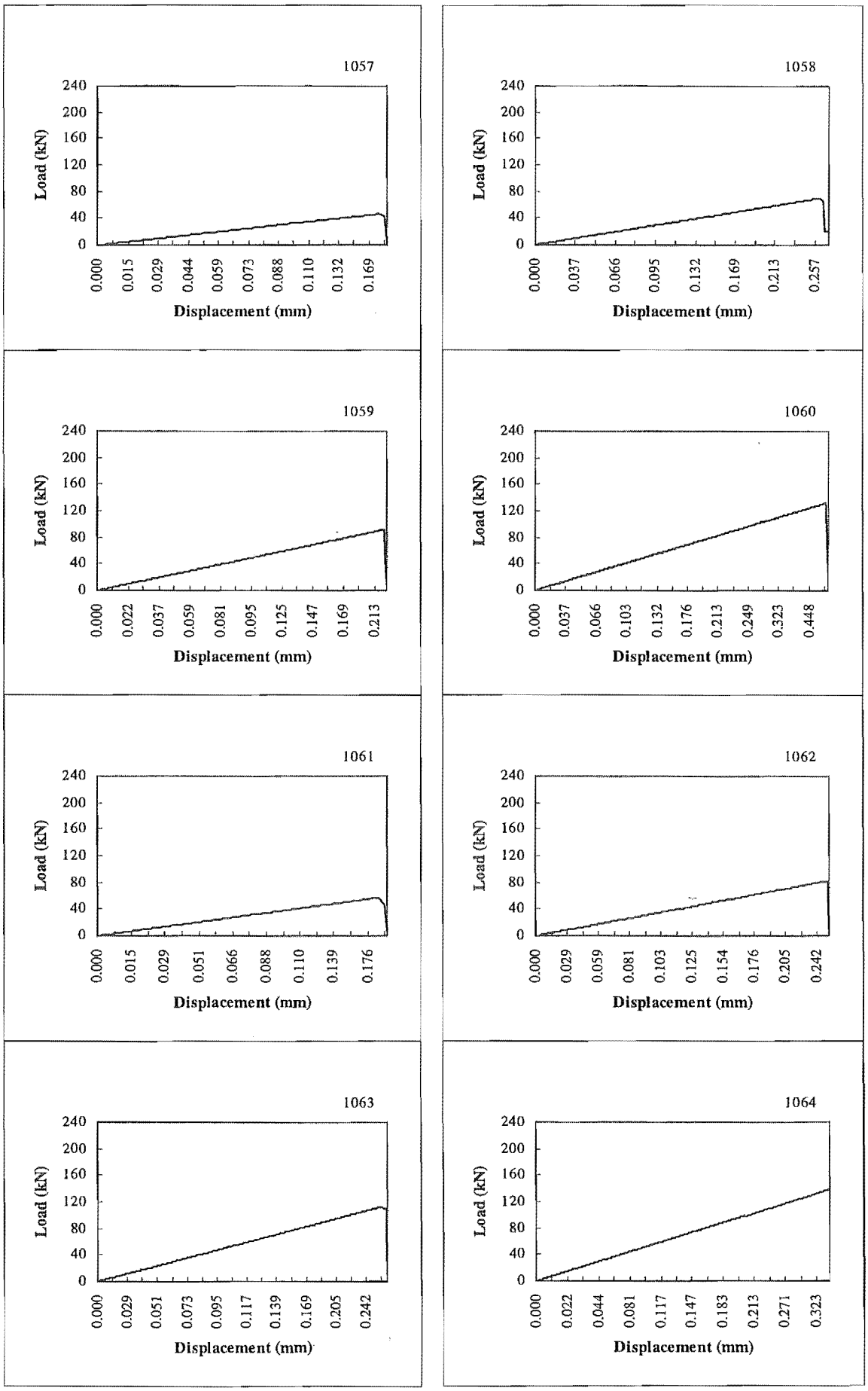

Appendix D (continued)

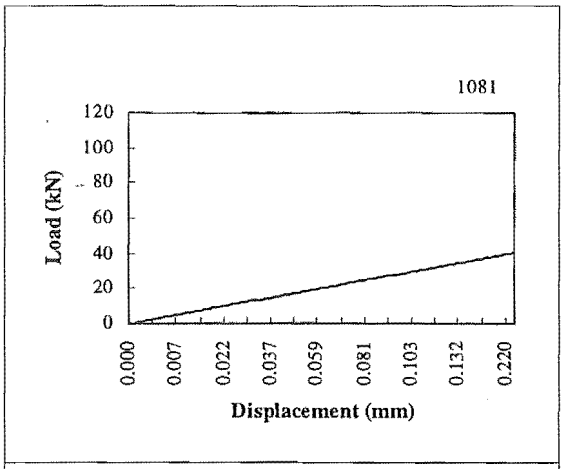

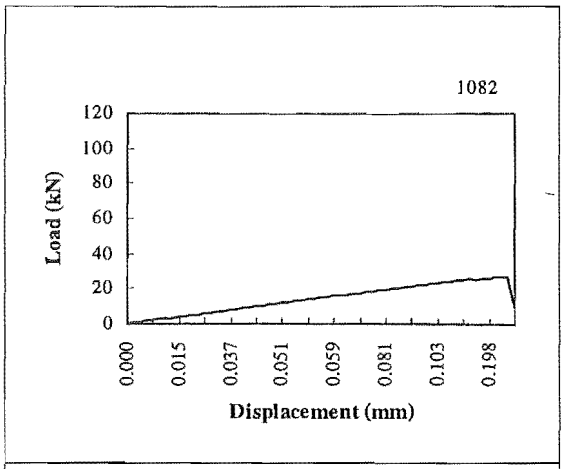

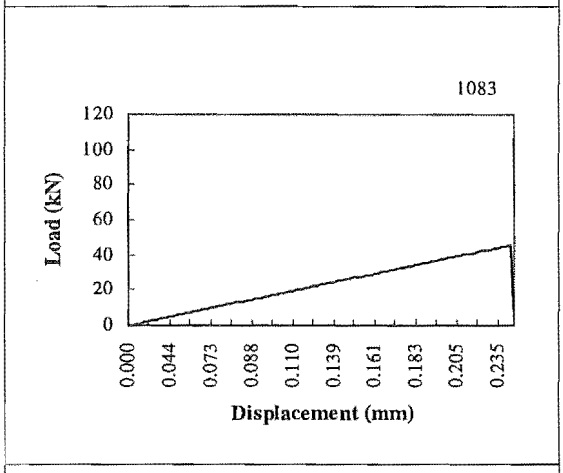

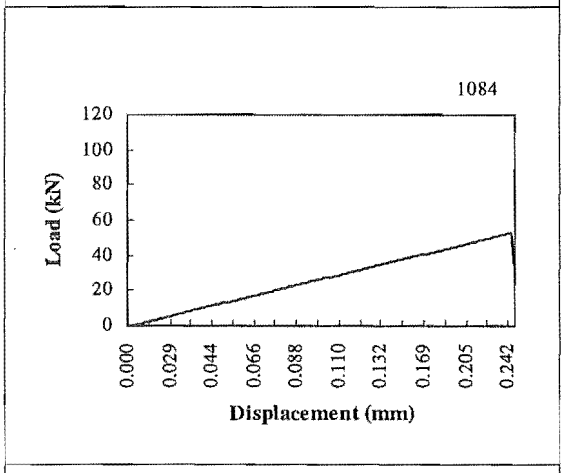

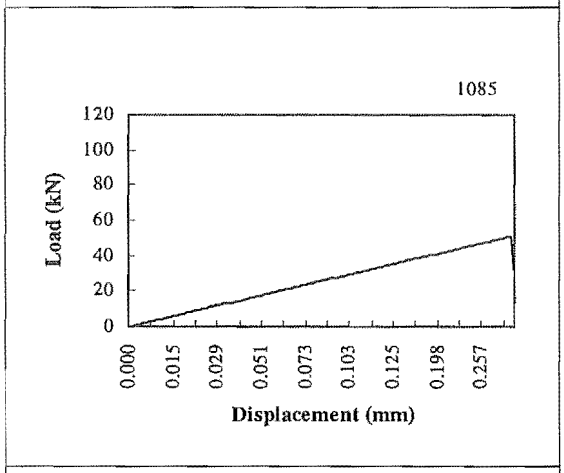

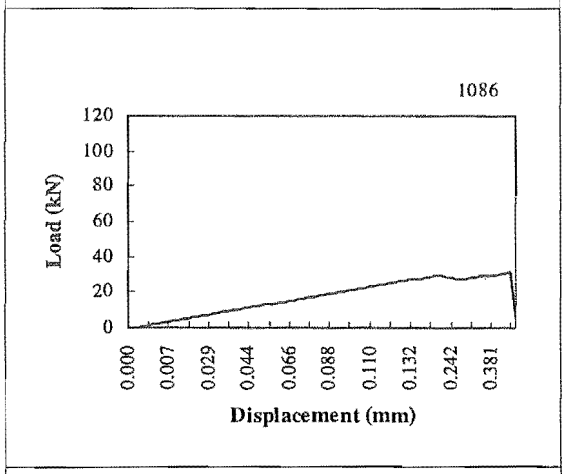

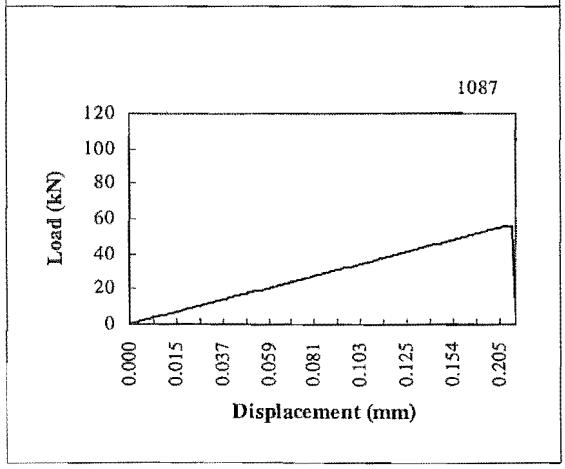

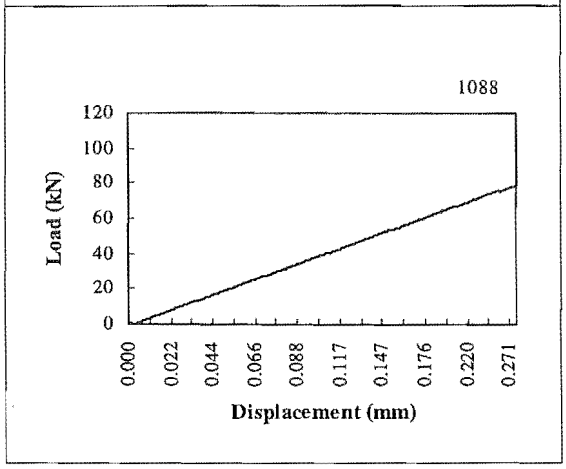

Appendix D (continued)

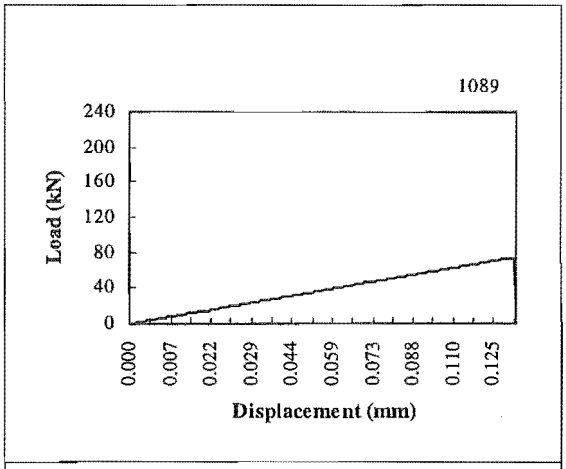

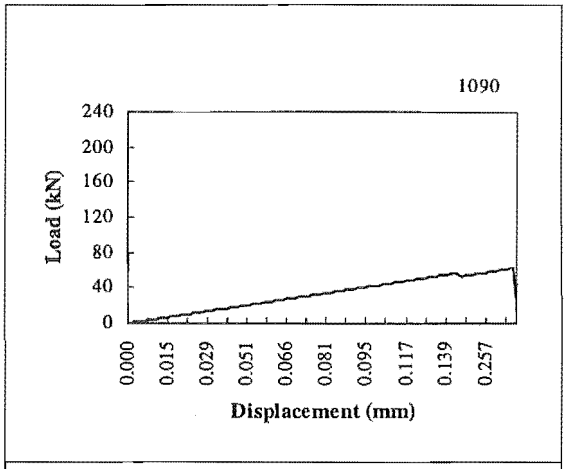

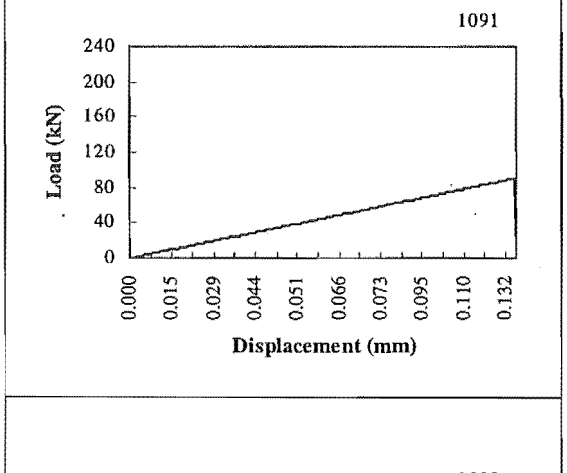

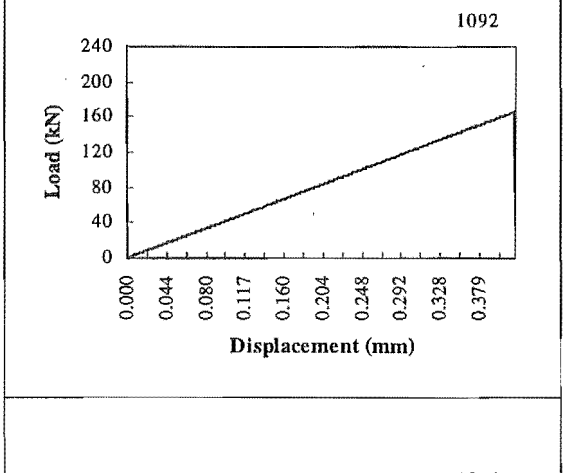

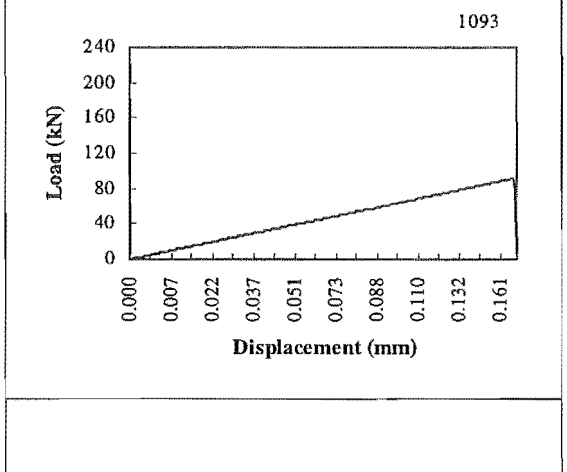

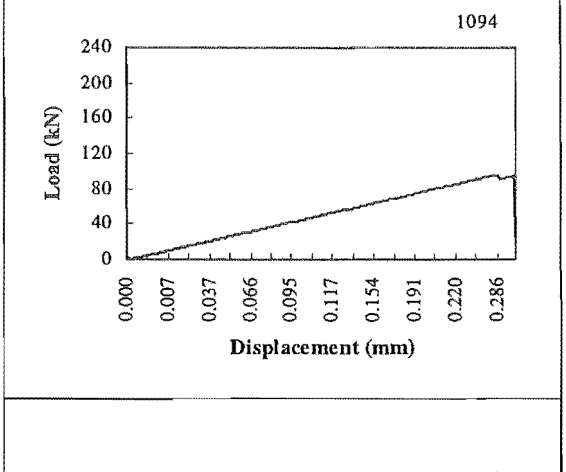

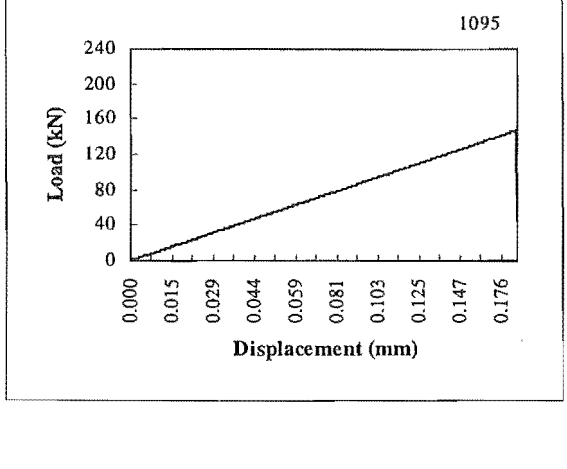

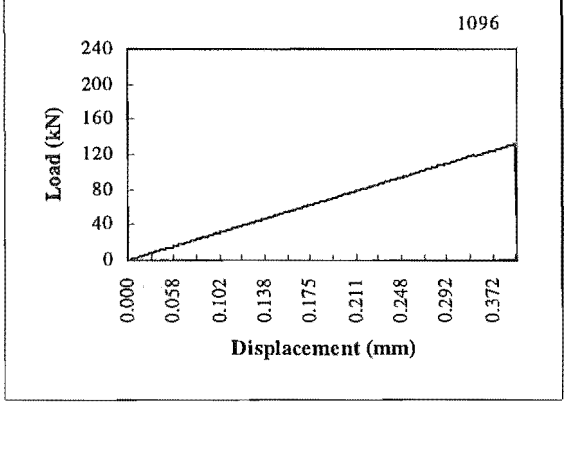

APPENDIX E STATISTICAL ANALYSIS OF THE SHORT DURATION EXPERIMENTS

1 Objectives

The statistical analysis was carried out by using a computer statistics software - Minitab (Minitab Inc., 1989). The purpose of the statistical analysis is:

(1) to test if specimens have different means in terms of ultimate tensile load among the different groups.
(2) to observe if the variation among the groups is significantly greater than the variation within groups.
(3) to see if there are any obvious interactions between two factors.[1]

2 Analysis of Experiment One

As we can see from Table E-1, the 95% confidence intervals and P-values are given to each factor. Each factor has two rows of data, which are obtained by different methods. The top row is produced supposing the experimental data are independent samples. The bottom row is calculated assuming that the data sets are paired data.

In both cases, the analysis was based on the assumption of random samples having normal distribution. In practice, the normality assumption is not particularly important and if a confidence interval is not based on a random sample, the real uncertainty is usually somewhat larger than that the values indicated by the confidence interval.

---

[1] When the effect of one factor depends on the level of another, the two factors interact.

Table E-1 The confidence interval of seven factors in Experiment One

Factors	95% Confidence Interval	P-values
bar diameter (d): ϕ24 - ϕ16	41.3, 62.6 (46.0, 57.9)	0.0000 (0.0000)
embedment length (l): 10d -5d	28.7, 52.8 (34.4, 47.1)	0.0000 (0.0000)
environment: dry - wet	5.6, 32.7 (14.5, 23.8)	0.0061 (0.0000)
bar type: threaded - deformed	1.6, 29.0 (10.0, 20.6)	0.029 (0.0000)
edge distance (e): 2.25d -1.5d	-0.3, 27.3 (8.0, 19.0)	0.055 (0.0000)
epoxy: K-80 - West System	-5.4, 22.4 (3.8, 13.1)	0.23 (0.0005)
hole diameter (h): 1.4d - 1.15d	-5.8, 22.0 (3.6, 12.6)	0.25 (0.0006)

Note:

1. The data from the top row of each factor is produced assuming the experiment data sets are independent samples.
2. The data from bottom row in bracket is calculated supposing the data sets are paired data.

2.1 Comparing Difference between Two Means of UTL: Independent Sampling

The top row data of each factor in Table E-1 was obtained in the following manner:

The ultimate tensile load of the specimens was classified into one of two groups according to the two levels of each factor separately, for example, for the factor of moisture condition in the specimens, the UTL values would be classified into two groups corresponding to either dry or wet specimens separately, regardless other factors. In this way, seven data sets were obtained and the confidence intervals calculated using the following formula:

$$(\overline{x_1} - \overline{x_2}) \pm t\sqrt{\frac{s_1^2}{n_1} + \frac{s_2^2}{n_2}} \qquad \text{(E-1)}$$

where,

$\overline{x}_1, s_1, n_1$ represent mean, standard deviation and number of observations in the first sample (the dry specimens) respectively.

$\overline{x}_2, s_2, n_2$ represent mean, standard deviation and number of observations in the second sample (the wet specimens) respectively.

t value from t-table corresponding to 95% confidence and number of degree of freedom.

With 95% significance level, the ultimate tensile load in dry specimens is higher than that in wet specimens. Since the values vary from 5.6 kN to 32.7 kN, it is implicit that the ultimate tensile load in dry specimens is at least 5.6 kN higher than that in wet specimens with 95% probability.

It is believed that 95% confidence interval is commonly used and is suitable for this study. In fact, four of seven factors have 95% confidence or more.

The P-value is a probability number that measures the extent to which the sample data are consistent with conclusion H_0 (null hypothesis of the test). In this case,

H_0: $\overline{X}_1 - \overline{X}_2 = 0$

H_1: $\overline{X}_1 - \overline{X}_2 \neq 0$

if P-value > α conclude H_0

if P-value < α conclude H_1

α is the probability of making a Type I error. A Type I error is the error which the hypothesis H_0 is true and it is rejected by the sample. For example, the p-value is 0.0061 for the difference between two means of UTL in term of dry or wet specimens. With such a small p-value, there is strong evidence that the mean value of ultimate tensile strength in dry test specimens is higher than that in wet test specimens; the null hypothesis H_0 would be rejected if $\alpha = 0.05$ or $\alpha = 0.01$ or any value of α down to 0.0061. In the same way, from the P-value in Table E-1, we can draw the conclusion with at least 99% significance level that: two means of UTL differ in terms of two embedment lengths, two bar diameters and two kinds of the environment condition for the specimens. the same conclusion could be drawn with 95% significance level for two different type of bars and with 90% significance level for edge distance. For epoxy type and hole diameter, their differences of two means are less significant.

2.2 Comparing the Difference between Two Means: Data as Paired Data

The bottom row data in bracket of each factor in Table E-1 was obtained as follows:

The UTL values are classified as above. It should be noticed that the two groups of data in each data set can be treated as paired data because Experiment One is a 2^7 factorial design, in which any specimen can be matched with the others with six exactly same factors and levels except one level difference from the "seventh" factor, e.g., to compare two different epoxies, a specimen with K-80 epoxy can be matched with a specimen using exactly same level of the factors except for being a West System epoxy. Suppose, a specimen with K-80 epoxy defined as K_i, the matched specimen as W_i, the difference is:

$$D_i = K_i - W_i \qquad (i = 1, 2, ..., 64) \qquad \text{(E-2)}$$

This is the data set used for testing the difference between two epoxies. Using the same method, the other six sets of data can be obtained. Now the analysis can be carried out and based on the difference of the paired data in term of two levels of each factor. The 95% confidence interval comes from:

$$\overline{D} \pm ts \qquad \text{(E-3)}$$

where, $$\overline{D} = \frac{\Sigma D_i}{64} \qquad \text{(E-4)}$$

t = value from t-table, corresponding to 95% confidence and number of degrees of freedom

$$s^2 = \frac{s_D^{\,2}}{64} \qquad \text{(E-5)}$$

$$s_D^{\,2} = \frac{\Sigma (D_i - \overline{D})^2}{n-1} \qquad \text{(E-6)}$$

n = sample size

D_i = the ith observation from the sample

$\overline{D}$ = mean of sample

The P- value has the same definition as in the previous section. As we can see from Table E-1 the 95% confidence interval from paired data sets are smaller than that from independent data sets and the difference between two levels in seven factors are all significant because P-values are all small. It seems likely that the inference about difference using matched samples would lead to a more precise estimate than by using independent samples. On the other hand, it tends to be conservative if independent samples are used. Considering the physical properties of wood and the connection, the paired samples could not be matched exactly, so that the data is still considered as independent in the further study and analysis.

3 Analysis of Experiment Two

3.1 One-way Analysis of Variance

The method used in Experiment One was not appropriate for Experiment Two because the experiment is 3^4 factorial design with more than two levels in each factor; the method of analysis of variance (ANOVA) was employed in Experiment Two. Results from the ANOVA analysis on the ultimate tensile load (UTL) are listed in Tables E-2.

Table E-2 (a) consists of two parts; the first is an ANOVA table and the second is a summary of the results for each level of the factor interested. The sample size, sample mean and standard deviation are given. The ANOVA notation and analytical approach are shown in Table E-3.

Table E-2 Analysis of variance on ultimate tensile load for each single factor

(a) Factor: embedment length

ANALYSIS OF VARIANCE ON UTL

SOURCE	DF	SS	MS	F	p
EMBED	2	101634	50817	89.70	0.000
ERROR	78	44189	567		
TOTAL	80	145824			

LEVEL	N	MEAN	STDEV
80	27	53.17	10.13
160	27	105.96	28.99
240	27	139.20	27.51

POOLED STDEV = 23.80

(b) Factor: epoxy

ANALYSIS OF VARIANCE ON UTL

SOURCE	DF	SS	MS	F	p
EPOXY	2	11892	5946	3.46	0.036
ERROR	78	133932	1717		
TOTAL	80	145824			

LEVEL	N	MEAN	STDEV
1	27	98.13	39.90
2	27	85.31	37.44
3	27	114.90	46.45

POOLED STDEV = 41.44

(c) Factor: edge distance

ANALYSIS OF VARIANCE ON UTL

SOURCE	DF	SS	MS	F	p
EDGE	2	9965	4982	2.86	0.063
ERROR	78	135859	1742		
TOTAL	80	145824			

LEVEL	N	MEAN	STDEV
1	27	87.40	37.08
2	27	96.77	38.13
3	27	114.17	48.96

POOLED STDEV = 41.73

(d) Factor: bar diameter

ANALYSIS OF VARIANCE ON UTL

SOURCE	DF	SS	MS	F	p
BARDIA	2	9492	4746	2.72	0.072
ERROR	78	136331	1748		
TOTAL	80	145824			

LEVEL	N	MEAN	STDEV
16	27	85.47	33.88
20	27	101.03	41.06
24	27	111.84	49.09

POOLED STDEV = 41.81

Table E-3 The notation and formula used in the one-way analysis of variance

SOURCE	DF	SS	MS	F
TREATMENT	a-1	$SSTR=S_i n_i(\bar{x}_i-\bar{x})^2$	MSTR = SSTR/(a-1)	$\frac{MSTR}{MSE}$
ERROR	n-a	$SSE = S_i S_j(x_{ij}-\bar{x}_i)^2$	MSE = SSE/(n-a)	
TOTAL	n-1	SSTR+SSE		

Note:

DF = degree of freedom

SS = sum of the squares

MS = mean square

F = F ratio

P = P - value

SSTR = sum of the squares for the treatment

SSE = sum of squares for the errors

MSTR = treatment mean square

MSE = error mean square

x_{ij} = the jth observation from level i

$\bar{x}_i$ = sample mean for the level i

a = number of levels

n = total number of observation

$\bar{x}$ = mean of all n observation

Table E-2 (a) indicates that the embedment length has a significant influence on the ultimate tensile strength. In fact, from the F-table, using $\alpha = 0.05$, F = 3.13, the given F-ratio from Table E-2 (a) is 89.7, which is much greater than the table value. That means MSTR is very much larger than MSE, viz. the variation among the different levels is much greater than the variation due to random error. Each confidence interval is calculated by the formula:

$$\overline{x_i} \pm \frac{ts_p}{n_i^{0.5}} \qquad \text{(E-7)}$$

where

$\bar{x}_i$ = sample mean for level i

n_i = sample size for level i

s_p = $(MSE)^{0.5}$, pooled standard deviation

t = value from t-table corresponding to 95% confidence and number of degrees of freedom

As can be seen the 3 intervals are quite apart from each other indicating that the mean UTL for different embedment length will differ. Table E-2 (b), (c), (d) can be obtained using the same method. They show that:

(1) With 95% significant, the mean UTL in different epoxies differs.

(2) With 90% significant, the mean UTL in different edge distances or bar diameters are different.

(3) The 95% confidence intervals and the means give us some idea of how the UTL means differ.

(4). For different epoxies, the specimens with Araldite 2005 epoxy have a highest mean value of UTL among these three epoxies, furthermore, mean of UTL with K-80 is higher than that with West System.

For different edge distances, the confidence interval between level one and level two seems closer than that between level two and level three. Furthermore, the difference of two means of UTL between level two and level three is higher than that between level one and level two. The reason for this is that fewer specimens failed due to wood failure in the specimens classified as level three of edge distance than in the other two levels (Table 4.1 (c)).

3.2 Two-way analysis of variance

The interaction between two factors can be investigated by using two-way analysis of variance. The interaction recognises the effect that one factor depends on the level of the other. Furthermore, using this method, one can discern whether the different levels of

the studied factor make any difference in ultimate tensile load. The analysis strategy is to use two factors out of four ignoring the others, i.e., only the epoxy and embedment length were considered when the interaction of these two factors was investigated ignoring bar diameter and edge distance effect. Only two-factor interaction was considered and presented in this appendix as from the nature of this experiment it is most unlikely that 3 or more factors interact if any two factors do not interact. Furthermore, in this way, a tedious presentation can be avoided. The layout of combination of the analysis is as follows:

epoxy - embedment length

epoxy - bar diameter

epoxy - edge distance

embedment length - bar diameter

embedment length - edge

bar diameter - edge

Table E-4 (a) Analysis of variance of UTL using bar diameter and embedment length as two factors

SOURCE	DF	SS	MS	F
BAR DIAMETER	2	9492	4746	10.59
EMBEDMENT	2	101634	50817	113.43
INTERACTION	4	2457	614	1.37
ERROR	72	32240	448	
TOTAL	80	145824		

Table E-4 (b) Analysis of variance of UTL using epoxy and bar diameter as two factors

SOURCE	DF	SS	MS	F
EPOXY	2	11892	5946	3.45
BAR DIAMETER	2	9492	4746	2.75
INTERACTION	4	412	103	0.06
ERROR	72	124027	1723	
TOTAL	80	145824		

Table E-4 (c) Analysis of variance of UTL using epoxy and embedment length as two factors

SOURCE	DF	SS	MS	F
EPOXY	2	11892	5946	13.86
EMBEDMENT	2	101634	50816	118.45
INTERACTION	4	1445	361	0.84
ERROR	72	30852	429	
TOTAL	80	145824		

Table E-4 (d) Analysis of variance of UTL using epoxy and edge distance as two factors

SOURCE	DF	SS	MS	F
EPOXY	2	11892	5946	3.48
EDGE	2	9965	4982	2.91
INTERACTION	4	769	192	0.112
ERROR	72	123197	1711	
TOTAL	80	145824		

Table E-4 (e) Analysis of variance of UTL using bar diameter and edge distance as two factors

SOURCE	DF	SS	MS	F
BAR DIAMETER	2	9492	4746	2.71
EDGE	2	9965	4982	2.85
INTERACTION	4	456	114	0.065
ERROR	72	125910	1749	
TOTAL	80	145824		

Table E-4 (f) Analysis of variance of UTL using embedment length and edge distance as two factors

SOURCE	DF	SS	MS	F
EMBEDMENT	2	101634	50817	117.36
EDGE	2	9965	4982	11.51
INTERACTION	4	3075	769	1.78
ERROR	72	31149	433	
TOTAL	80	145824		

All of these tables were calculated and set out in the same manner, so that only one of the table needs to be defined and explained. For example, Table E-4 (a) was formed as:

Source	DF	SS	MS
Factor 1	a-1	$bnS_i(\overline{x}_{i..} - \overline{x})^2$	$SS_{factor\ 1}/(a-1)$
Factor 2	b-1	$anS_j(\overline{x}_{.j.} - \overline{x})^2$	$SS_{factor\ 2}/(b-1)$
Interaction	(a-1)(b-1)	$nS_iS_j(\overline{x}_{ij.} - \overline{x}_{i..} - \overline{x}_{.j.} + \overline{x})^2$	$SS_{interaction}/((a-1)(b-1))$
Error	ab(n-1)	$S_iS_jS_k(x_{ijk} - \overline{x}_{ij.})$	$SS_{Error}/(ab(n-1))$
Total	abn-1	$S_iS_jS_k(x_{ijk} - \overline{x})$	

Note:

a = number of levels in factor 1

b = number of levels in factor 2

n = number of observations in each cell

x_{ijk} = kth observation in cell (i,j)

$\overline{x}_{ij}$ = mean of the n observations in cell (i,j)

$\overline{x}_{i..}$ = mean of the bn observations in row i

$\overline{x}_{.j.}$ = mean of an observations in column j

$\overline{x}$ = mean of all observations

The notations for F-ratio are the same as recorded in the last section. The table combines the results from the computer and hand calculated F-ratio values. In order to establish whether there is statistically significant evidence of interaction between the bar diameter and embedment length, the F-ratio has been calculated as: $(MS_{interaction})/(MS_{Error})$ = 614/448 = 1.37, and then this value was compared with the value from the F-table, with 4 degrees of freedom in the numerator and 72 in the denominator: the table values of 2.03, 2.5 and 3.62 correspond to $\alpha = 0.1$, $\alpha = 0.05$ and $\alpha = 0.01$ respectively. Since the calculated value of 1.37 is smaller than those value from the F-table, there is no statistical evidence of any interaction between bar diameter and embedment length. For bar diameter, F-ratio = $(MS_{Bardia})/(MS_{Error})$ = 10.59. The F-table value with 2 degrees of freedom in the numerator and 72 degrees of freedom in the denominator is 4.94 for $\alpha = 0.01$. This offers significant evidence of an overall effect of different bar. For embedment length, F-ratio = $(MS_{Embed})/(MS_{Error})$ = 113.43 is much larger than F-table value of 4.94 for $\alpha = 0.01$. The test indicates that there is highly significant evidence of a difference due to different embedment length.

The calculation was similar for all factors and analysis results including F-ratios are listed in Tables E-4. F-table values are also summarised in the Table E-5 for comparison. Only six values were employed due to same degrees of freedom for each factor.

Table E-5 Table values of F-ratio used in the analysis

Source	Numerator	Denominator	F values		
			$\alpha = 0.1$	$\alpha = 0.05$	$\alpha = 0.01$
Factor	2	72	2.38	3.12	4.94
Interaction	4	72	2.03	2.5	3.62

A conclusion drawn from the above analysis is that there is no significant evidence that any two factors interact. In general terms, there is statistical evidence of a difference among different levels of each factor.

APPENDIX F

COMPUTER PROGRAMME
FOR THE FINITE ELEMENT MODEL OF THE CONNECTION

Computer: DEC station 2100.

Software: ABAQUS (1993).

Input: All parameters for the reference model (Tables 5.1 and 5.2).

```
*HEADING
FILE NAME: 3DA-1.inp
WRITTEN BY XIXIAN DENG, 1994
ELEMENT: C3D6 & C3D8
MATERIALS: WOOD AS OTHOTROPIC, STEEL AND EPOXY
TENSILE LOAD = 50KN
EPOXY BOND WITH WOOD BUT STEEL AT BAR END
*RESTART,WRITE,FREQUENCY=1
*PREPRINT, ECHO=NO, HISTORY=NO
*NODE,NSET=CENEND1
1,0,0,0
2,0,0,0
3,0,0,0
4,0,0,0
*NODE,NSET=OUTEDGEA
51,5,0,0
101,9.5,0,0
151,10,0,0
201,10.5,0,0
251,11,0,0
301,11.5,0,0
351,12,0,0
401,12.5,0,0
451,13,0,0
*NODE
751,50,0,0
*NODE,NSET=A451
451
*NODE,NSET=A751
751
*NFILL,NSET=OUTEDGEB,BIAS=0.8
A451,A751,6,50
*NSET,NSET=OUTEDGE1
OUTEDGEA,OUTEDGEB
*NCOPY,CHANGE NUMBER=4,OLD SET=OUTEDGE1,REFLECT=LINE,NEW
SET=OUTEDGE2
0,0,0,40,40,0
*NGEN,NSET=ARC1,LINE=C
751,755,1,1
*NGEN,NSET=ARC2,LINE=C
701,705,1,1
*NGEN,NSET=ARC3,LINE=C
651,655,1,1
*NGEN,NSET=ARC4,LINE=C
601,605,1,1
```

```
*NGEN,NSET=ARC5,LINE=C
551,555,1,1
*NGEN,NSET=ARC6,LINE=C
501,505,1,1
*NGEN,NSET=ARC7,LINE=C
451,455,1,1
*NGEN,NSET=ARC8,LINE=C
401,405,1,1
*NGEN,NSET=ARC9,LINE=C
351,355,1,1
*NGEN,NSET=ARC10,LINE=C
301,305,1,1
*NGEN,NSET=AR11,LINE=C
251,255,1,1
*NGEN,NSET=ARC12,LINE=C
201,205,1,1
*NGEN,NSET=ARC13,LINE=C
151,155,1,1
*NGEN,NSET=ARC14,LINE=C
101,105,1,1
*NGEN,NSET=ARC15,LINE=C
51,55,1,1
*NSET,NSET=OUTFACE
CENEND1,ARC1,ARC2,ARC3
ARC4,ARC5,ARC6,ARC7,ARC8,ARC9
ARC10,ARC11,ARC12,ARC13,ARC14,ARC15
*NCOPY,CHANGE NUMBER=30000,OLD SET=OUTFACE,REFLECT=MIRROR,NEW
SET=BAREND
0,0,150,50,0,150
0,50,150
*NCOPY,CHANGE NUMBER=15000,OLD SET=OUTFACE,REFLECT=MIRROR,NEW
SET=BARMID
0,0,75,50,0,75
0,50,75
*NCOPY,CHANGE NUMBER=3000,OLD SET=BAREND,REFLECT=MIRROR,NEW
SET=EPOXYEND
0,0,301.5,50,0,301.5
0,50,301.5
*NCOPY,CHANGE NUMBER=4000,OLD SET=BAREND,REFLECT=MIRROR,NEW
SET=WOODEND
0,0,301.5,50,0,301.5
0,50,301.5
*NCOPY,CHANGE NUMBER=5000,OLD SET=BAREND,REFLECT=MIRROR,NEW
SET=FACE1
0,0,303,50,0,303
```

```
0,50,303
*NCOPY,CHANGE NUMBER=44000,OLD SET=OUTFACE,REFLECT=MIRROR,NEW
SET=MIDFACE
0,0,225,50,0,225
0,50,225
*NFILL,BIAS=0.8
OUTFACE,BARMID,15,1000
*NFILL,BIAS=1.25
BARMID,BAREND,15,1000
*NFILL
BAREND,EPOXYEND,3,1000
*NFILL
FACE1,MIDFACE,10,1000
*NSET,NSET=MIDEDGE1,GENERATE
44051,44751,50
*NSET,NSET=MIDEDGE2,GENERATE
44055,44755,50
*NSET,NSET=CENLIN1,GENERATE
1001,43001,1000
*NSET,NSET=CENLIN2,GENERATE
1002,43002,1000
*NSET,NSET=CENLIN3,GENERATE
1003,43003,1000
*NSET,NSET=CENLIN4,GENERATE
1004,43004,1000
*NSET,NSET=CENLIN
CENLIN1,CENLIN2,CENLIN3,CENLIN4
*NSET,NSET=V1,GENERATE
55,44055,1000
*NSET,NSET=V2,GENERATE
105,44105,1000
*NSET,NSET=V3,GENERATE
155,44155,1000
*NSET,NSET=V4,GENERATE
205,44205,1000
*NSET,NSET=V5,GENERATE
255,44255,1000
*NSET,NSET=V6,GENERATE
305,44305,1000
*NSET,NSET=V7,GENERATE
355,44355,1000
*NSET,NSET=V8,GENERATE
405,44405,1000
*NSET,NSET=V9,GENERATE
455,44455,1000
```

```
*NSET,NSET=V10,GENERATE
505,44505,1000
*NSET,NSET=V11,GENERATE
555,44555,1000
*NSET,NSET=V12,GENERATE
605,44605,1000
*NSET,NSET=V13,GENERATE
655,44655,1000
*NSET,NSET=V14,GENERATE
705,44705,1000
*NSET,NSET=V15,GENERATE
755,44755,1000
*NSET,NSET=H1,GENERATE
51,44051,1000
*NSET,NSET=H2,GENERATE
101,44101,1000
*NSET,NSET=H3,GENERATE
151,44151,1000
*NSET,NSET=H4,GENERATE
201,44201,1000
*NSET,NSET=H5,GENERATE
251,44251,1000
*NSET,NSET=H6,GENERATE
301,44301,1000
*NSET,NSET=H7,GENERATE
351,44351,1000
*NSET,NSET=H8,GENERATE
401,44401,1000
*NSET,NSET=H9,GENERATE
451,44451,1000
*NSET,NSET=H10,GENERATE
501,44501,1000
*NSET,NSET=H11,GENERATE
551,44551,1000
*NSET,NSET=H12,GENERATE
601,44601,1000
*NSET,NSET=H13,GENERATE
651,44651,1000
*NSET,NSET=H14,GENERATE
701,44701,1000
*NSET,NSET=H15,GENERATE
751,44751,1000
*NSET,NSET=HALL
H1,H2,H3,H4,H5,H6,H7,H8,H9
H10,H11,H12,H13,H14,H15
```

```
*NSET,NSET=VALL
V1,V2,V3,V4,V5,V6,V7,V8,V9
V10,V11,V12,V13,V14,V15
*NSET,NSET=CENEND2,GENERATE
44001,44004,1
*ELEMENT,TYPE=C3D6
1,1,51,52,1001,1051,1052
125,31001,31051,31052,32001,32051,32052
*ELEMENT,TYPE=C3D8
501,51,101,102,52,1051,1101,1102,1052
1001,101,151,152,102,1101,1151,1152,1102
625,31051,31101,31102,31052,32051,32101,32102,32052
1125,31101,31151,31152,31102,32101,32151,32152,32102
1501,151,201,202,152,1151,1201,1202,1152
*ELGEN
1,4,1,1,30,1000,4
*ELGEN
125,4,1,1,13,1000,4
*ELGEN
501,4,1,1,30,1000,4
*ELGEN
625,4,1,1,13,1000,4
*ELGEN
1001,4,1,1,30,1000,4
*ELGEN
1125,4,1,1,13,1000,4
*ELGEN
1501,4,1,1,44,1000,4,12,50,500
*ELSET,ELSET=STEEL,GENERATE
1,120,1
501,620,1
1001,1120,1
*ELSET,ELSET=EPOXY,GENERATE
125,136,1
625,636,1
1125,1136,1
1501,1636,1
2001,2136,1
2501,2636,1
3001,3136,1
3501,3636,1
4001,4136,1
*ELSET,ELSET=WOOD,GENERATE
137,176,1
637,676,1
```

```
1137,1176,1
1637,1676,1
2137,2176,1
2637,2676,1
3137,3176,1
3637,3676,1
4137,4176,1
4501,4676,1
5001,5176,1
5501,5676,1
6001,6176,1
6501,6676,1
7001,7176,1
*ELSET,ELSET=BAEND,GENERATE
1,4,1
501,504,1
1001,1004,1
*MATERIAL,NAME=STEEL
*ELASTIC
2E5,0.3
*MATERIAL,NAME=WOOD
*ELASTIC,TYPE=ENGINEERING CONSTANTS
.585E3,.585E3,9E3,.41,.037,.037,.06E3,.582E3
0.582E3
*MATERIAL,NAME=EPOXY
*ELASTIC
4E3,0.3
*SOLID SECTION,ELSET=STEEL,MATERIAL=STEEL
*SOLID SECTION,ELSET=WOOD,MATERIAL=WOOD
*SOLID SECTION,ELSET=EPOXY,MATERIAL=EPOXY
*BOUNDARY
MIDFACE,3,3
VALL,1,1
HALL,2,2
CENLIN,1,2
CENEND1,1,2
CENEND2,1,3
*PLOT,TRUE SCALE=0.02
*VIEWPOINT
0,0,1
*STEP,PERTURBATION
*STATIC
*DLOAD
BAEND,P1,-159.2
*END STEP
```